# Exploring the regulation of denitrification and NO and $N_2O$ kinetics in *Paracoccus denitrificans* using simulation modelling

*Paracoccus denitrificans*' regulering av denitrifikasjon, NO- og $N_2O$-kinetikk, en modell studie

Philosophiae Doctor (Ph.D.) Thesis

Junaid Hassan

Department of Environmental Sciences
Faculty of Environmental Science and Technology
Norwegian University of Life Sciences

Ås (2015)

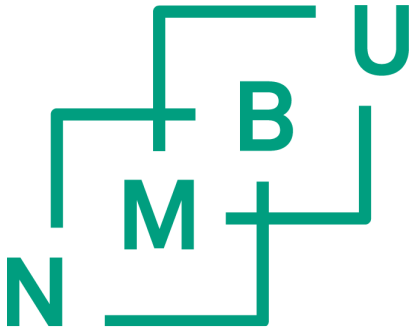


Thesis number 2015:59
ISSN 1894-6402
ISBN 978-82-575-1298-9

## Ph.D. Supervisors

**Prof. Lars R. Bakken** (Main supervisor)
Dept. of Environmental Sciences
Norwegian University of Life Sciences
1432 Ås, Norway
lars.bakken@nmbu.no

**Assoc. Prof. David Wheat** (Co-supervisor)
Dept. of Geography
University of Bergen
5020 Bergen, Norway
david.wheat@uib.no

**Prof. Stig W. Omholt** (Co-supervisor)
Dept. of Animal and Aquacultural Sciences
1432 Ås, Norway
stig.omholt@nmbu.no

## Thesis Evaluation Committee

**Prof. James Moir** (Opponent 1)
Dept. of Biology
University of York
Heslington, York, Y010 5DD, UK
james.moir@york.ac.uk

**Prof. Frank Bruggeman** (Opponent 2)
Systems Bioinformatics
Vrije Universiteit Amsterdam
De Boelelaan 1087, 1081 HV Amsterdam, Netherlands
f.j.bruggeman@vu.nl

**Prof. Trine A. Sogn** (Coordinator)
Dept. of Environmental Sciences
Norwegian University of Life Sciences
1432 Ås, Norway
trine.sogn@nmbu.no

***To the Father who modelled me in heavens and to my parents who have affectionately simulated me on the earth***

# Contents

# Acknowledgements

From left-to-right top-to-bottom: LARS BAKKEN; LARS MOLSTAD; LINDA BERGAUST; ZHI QU; DAVID WHEAT; SELINA KÖHR; JANINA REGUTZKI; MEMONA SARWAR; AHMED MUNIR & SAMAN AHMED; HAMAD HASSAN & KHADIJA HASSAN; MARIA SARFRAZ; SARFRAZ USMAN, SOPHIA & AMINA; ADAM; HANNA; EDEN; IMAAN; ZAMAD; AYAAN; AMBER AJAZ; MAHMOOD AJAZ; PIA & HERMANN KÖHR; ANGELINA; MUHAMMAD ABDULLAH; MARYAM & GHULAM SARWAR; AND CHAUDHARY ALI AKBAR

He started it, and he finished it. I was merely a raw tool, very fortunate to be picked, honed, and employed productively, yet cordially, by his proficient hands. Not just a dedicated scientist and a committed teacher, I have found him to be a devoted father, husband, friend, and a highly benevolent man, even toward strangers. If there is a God, I am sure He would be proud of this man. Surely one of my heroes; I cherish every moment I spent in his company, and I truly adore him. I know words cannot express my gratitude but thank you, thank you very much for being who you are, Lars Bakken!

Lars Molstad: I am grateful to you for being the 'Feynman' of our group, explaining complicated ideas simply and intuitively. I bothered you too much, but rather than frowning, you were eager to help throughout, considering my problems (and those of the other Nitrogen Group students) as your own and trying hard to come up with useful solutions. My modelling

work has benefitted enormously from your presence, and it would be correct in any sense of the word if I call you my co-supervisor for this work.

I am indebted to her persistent delightful smile and inspired by her punctuality, hard work, diligence (esp. regarding the NO experiments), ability to produce quality work within tight deadlines, careful and compact writing, and nerves to fulfil requests for prioritising tasks in the midst of a hectic schedule (where everything on-the-list seems equally important). Dear Linda Bergaust: accept my heartiest thanks for providing your immaculate hands for this project and being admirably affable at all times.

Zhi Qu: We shared the office for over two years but did not even have a single unpleasant incident between us – that says a lot! Thank you for being an easy-going and a warm-hearted friend. I must also appreciate your readily available explanations of experimental data, biology, and SigmaPlot along with reminders of deadlines and a number of suggestions that I practically benefitted from.

I am obliged to each member of the Nitrogen Group for creating an altruistic, amiable, and a productive family. I could not dream of a better environment to do science: tusen hjertelig takk, 非常感谢, vielen lieben Dank, tack så mycket, many thanks, hartelijk bedankt, dziękuję, asante, hvala, دلی مہربانی, አመሰግናለሁ, kiitos paljon. I would especially like to thank Daniel Mania & Kedir Jillo for useful discussions regarding the biochemistry of denitrification and Rannei Tjåland & Else Aasen for editing the Norwegian summary of this work.

Thank you David Wheat for believing in me, your much needed encouragement, and useful suggestions; Anne-Grethe Kolnes & Leif Martinsen for fulfilling all our hardware/software needs in the blink of an eye; and Anne Munkeby, Asbjørg Brean, Christel Nguyen & Mirian Wangen for your excellent administrative support.

This project could not have been realised without sacrifices, perseverance, and the ever-opened arms of my sweetheart Selina Köhr – the warmth of your embrace melts away glaciers of worries and sorrows! I feel guilty that you had to compromise your career, leave your homeland and the affectionate company of your parents for this project and, in addition, put up with not only demanding part-time jobs here but my mood swings too. I am looking forward to keep your wishes on the highest priority while bringing your way all the love and delight I possibly can, for I am deeply grateful to have you as my soulmate. I owe this feeling of gratitude to your parents Hermann Köhr & Pia Köhr, for it is their light shining within you.

I am much obliged for their priceless proactive advices, keeping me close to their hearts, and always owning my problems as theirs.

I am lucky to have sisters like Memona Sarwar & Maria Sarfraz: my life would have been lifeless without you! Thank you for your ever-surrounding love and appreciation, the laughter you bring my way and, not least, your financial support during the unpaid period of this project. My beloved brothers Sarfraz Usman, Ahmed Munir & Hamad Hassan: thank you for your financial support, reminding me to stay focused and work hard, and being my best friends. A special thank is also due to my cordial sisters-in-law Saman Ahmed, Khadija Hassan & Janina Regutzki and to the apples of my eyes Ayaan, Eden, Hanna, Zamad, Angelina, Amina, Imaan, Adam & Sophia for keeping the child in me alive and filling my life with so much love. This list would remain incomplete without acknowledging my 'Norwegian parents' Mahmood Ajaz & Amber Ajaz: the world would have been a difficult place to live without humans like you; thank you for your unconditional care, kindness, and support!

The one I miss the most on this occasion is Muhammad Abdullah (1925-2008), who fostered me with the love, attention, and protection of a mother and, like a father, taught me to stand for the right and fight the wrong. The earth must have been proud to have you on its chest as you lived and equally pleased to welcome you back into its womb. I also dearly miss my grandfather Chaudhary Ali Akbar (1916-2011) and wish that he were here to see his wish fulfilling as I graduate.

I can never be thankful enough to my parents Maryam Sarwar & Ghulam Sarwar for keeping my needs and wants far ahead of theirs, raising me up in the best way possible, discovering ways to help and support me even beyond their capacity, and for constantly remaining anxious and praying for my well-being and success. *'My Lord, bestow on them thy Mercy like they nurtured me in my childhood.'* (al-Qur'an: 17:23)

The ultimate praise, glory, and gratitude be to that Father who 'inspires' and nourishes a set of apparently worthless gametes to evolve into the flesh and bones of man, the intellectual being perfected to know Him through His myriad signs within himself and in the universe and appreciate His revealed plan. O Lord my God, open my breast for me to love you with all my heart, all my soul, all my strength, and all my intellect, and stir in me the same love for my neighbour as I keep for myself (Luke 10:27). Amen.

# Summary

In the environment, microbes frequently experience lack of oxygen. In response, certain microorganisms produce enzymes that enable them to respire molecules other than $O_2$ (anaerobic respiration). One such mode of anaerobic respiration is denitrification: the step-wise reduction[1] of nitrogen oxyanions ($NO_3^-$/$NO_2^-$, abbrev. $NO_x^-$) to nitrogen oxides (NO/$N_2O$, abbrev. $NO_x$) and, finally, to molecular nitrogen ($N_2$):

$$NO_3^- \xrightarrow{\text{Nar / Nap}} NO_2^- \xrightarrow{\text{NirS / NirK}} NO \xrightarrow{c\text{Nor / qNor}} N_2O \xrightarrow{\text{NosZ}} N_2$$

where Nar/Nap, NirS/NirK, and *c*Nor/qNor are the prominent variants of nitrate- ($NO_3^-$), nitrite- ($NO_2^-$), and nitric oxide (NO) reductase enzymes, respectively, and NosZ is nitrous oxide ($N_2O$) reductase. As an alternative mode of respiration, denitrification generates energy (ATP) to sustain the life processes in the absence of $O_2$. Denitrification is widespread in bacteria and also observed in archaea and fungi. Niches for denitrification are the sites where $O_2$ concentration fluctuates, such as biofilms, water columns, surface layers of sediments, wetlands, and drained soils.

Denitrification is of global significance being a key process in the nitrogen cycle (replenishing the atmosphere with $N_2$) and a major source of atmospheric NO and $N_2O$. NO plays a major role in producing the 'bad' (tropospheric) ozone, and $N_2O$, in addition to being a powerful greenhouse gas, depletes the 'good' (stratospheric) ozone. Robust strategies to mitigate NO and $N_2O$ emissions from denitrification (e.g., in agricultural soils) demands thorough understanding of the physiology and regulatory biology of denitrifiers. The present thesis contributes to this knowledge, utilising dynamic modelling to test various assumptions and experiment-based hypotheses regarding the physiology of a prominent soil bacterium, *Paracoccus denitrificans*. The organism is significant, for it is used as a model in denitrification research.

[1] Certain chemical reactions involve exchange of electrons ($e^-$); the reactant that loses $e^-$ is said to be 'oxidised', whereas the one that gains $e^-$ is termed 'reduced'. Thus, when $NO_3^-$ accepts $2e^-$ and, thereby, is converted to $NO_2^-$, the phenomenon is called the reduction of $NO_3^-$ to $NO_2^-$, and the enzyme that catalyses this transformation (Nar or Nap) is termed 'reductase'.

By modelling, we explored the regulation of **1)** NirS (controlling the $NO_2^-$- and $N_2$ kinetics[2]), **2)** NirS/*c*Nor (homeostatic control of NO by *Pa. denitrificans*), **3)** Nar, and **4)** *c*Nor/NosZ ($N_2O$ kinetics). The first two are the subject of Paper I & II, respectively, and the last two are addressed in Paper III.

For Paper I, we started with a simple model designed to match the conditions used to provide the empirical data to be analysed: recruitment of batch cultures from aerobic to anaerobic respiration in response to $O_2$ depletion, monitored by frequent sampling. We developed this model further to address more specialised problems in Paper II & III. Each model simulates the respiratory metabolism ($O_2$ reduction followed by that of $NO_x^-$/$NO_x$), growth, and gas transport between the experimental vial's liquid-phase and the headspace. The models also include estimation of gas loss and leaks due to sampling, so as to allow a direct comparison between experimental data and model simulations. The models use the Michaelis-Menten kinetics to simulate the activity of reductases involved, except that in the models for Papers II & III, the cooperative binding of two NO molecules with *c*Nor to form $N_2O$ is modelled by a dual substrate equation. All model parameters critical for our research questions were empirically determined under the same or similar experimental conditions as simulated. Each model is constructed in Vensim®, using techniques from the field of system dynamics.

## Paper I

It is commonly assumed that all cells in pure cultures of denitrifiers switch to denitrification in response to $O_2$ depletion. The assumption has been challenged based on crude inspections of *Pa. denitrificans* respiration kinetics during the transition from aerobic to anaerobic respiration, suggesting that only a minor fraction of the cells is able to switch to anaerobic respiration and growth. The reason, we hypothesise, is that the transcriptional initiation of genes necessary for the synthesis of $NO_2^-$ reductase (NirS, functional gene: *nirS*) is stochastic, which then becomes autocatalytic within the cell due to NO production. With this hypothesis built into our model, it effectively simulates the observed $N_2$ kinetics for a range of experimental conditions by assuming an extremely low probability of *nirS* transcription,

[2] $N_2$ kinetics are controlled by NirS since, in *Pa. denitrificans*, $NO_2^-$ reduction is the rate-determining step of denitrification.

0.005 $h^{-1}$. As a result, the model estimates that only 3.8–16.1% of the cells were recruited to denitrification prior to the complete depletion of $O_2$.

The phenomenon can be understood as a 'bet-hedging strategy': switching to denitrification is a gain if anoxic spell lasts long, but is a waste of energy (consumed in the synthesis of denitrification enzymes) if anoxia turns out to be a 'false alarm'. Certainly, not all denitrifiers are bet-hedgers; the exercise here indicates that distinct phenotypes exist in the regulatory biology of denitrifiers, which need to be taken into account for correctly interpreting experimental work on denitrification in general and *Pa. denitrificans* in particular.

## Paper II

Homeostatic control of NO at nanomolar concentrations appears common among denitrifying bacteria, ascribed to synchronised expression of nitrite- and nitric oxide reductase (Nir and Nor). But we questioned whether this is a sufficient explanation: using the reported substrate affinities for *c*Nor, our dynamic model of the enzyme activities in batch cultures of *Pa. denitrificans* predicted 1–3 orders of magnitude too high NO concentrations. A possible explanation for the low NO concentrations measured could be a negative feedback by NO on the activity of NirS. This was rejected, however, because the inclusion of such feedback resulted in too slow anaerobic growth and $N_2$ production. We proceeded by determining the kinetic parameters for *c*Nor *in vivo*, which is a non-trivial task. The experiments were carefully designed to allow estimation of the NO concentration at the cell surface while anoxic cultures, in a $NO_3^-$/$NO_2^-$-free medium, depleted low doses of NO. With the new parameters for *c*Nor[3]: $v_{max\mathrm{NO}}$ = 3.56 fmol NO $cell^{-1}$ $h^{-1}$, $K_{1\mathrm{NO}}$ < 1 nM, and $K_{2\mathrm{NO}}$ = 34 nM, the model predicted NO concentrations close to that measured.

This shows that the homeostatic control of NO at nanomolar concentrations can be understood as a result of the enzyme kinetics alone and that the high affinity of *c*Nor is essential. The

[3] Used in a dual substrate equation, developed by Girsch & de Vries (1997): $v_{\mathrm{NO}} = \frac{v_{max\mathrm{NO}}}{1 + K_{2\mathrm{NO}}\left(\frac{1}{[\mathrm{NO}]_{\mathrm{aq}}} + \frac{K_{1\mathrm{NO}}}{[\mathrm{NO}]_{\mathrm{aq}}^2}\right)}$,

where $v_{max\mathrm{NO}}$ (mol NO $cell^{-1}$ $h^{-1}$) is the maximum NO reduction rate, $[\mathrm{NO}]_{\mathrm{aq}}$ (mol $L^{-1}$) is the NO concentration in the aqueous medium, and $K_{1\mathrm{NO}}$ & $K_{2\mathrm{NO}}$ are the steady state dissociation constants for *c*Nor/NO- & *c*Nor/$(NO)_2$ complex, respectively.

result illustrates the importance of determining enzyme kinetic parameters *in vivo*, rather than *in vitro*, to understand and model denitrification phenotypes.

## Paper III

In this work, the regulation of all four reductases (Nar, NirS, *c*Nor and NosZ) was included in the model used to simulate batch cultivations supplemented with $NO_3^-$. The aim was to understand the observed $NO_2^-$ and $N_2O$ kinetics.

Like that for *nirS*, we assumed that the transcriptional activation of the *nar* genes (encoding Nar) is stochastic, with a positive feedback by $NO_2^-$ produced, thus quickly turning the cell into a full-fledge $NO_3^-$ reducer. By fitting the model to the observed $NO_2^-$ and $N_2$ kinetics, we found that *nar* transcription has a higher probability (0.035 $h^{-1}$) than that for *nirS* (0.004 $h^{-1}$), resulting in the production of Nar in 23–43.3% of all cells 'in time' (before depletion of $NO_3^-$).

For the $N_2O$ kinetics, the model assumes that transcription of the *nor* genes (encoding *c*Nor) is coordinated with that of *nirS* and that all cells produce NosZ, since the *nosZ* genes are readily induced in response to $O_2$ depletion. This implies that the majority of cells have only NosZ, and this sub-population (A) grows by respiring $N_2O$ produced by the sub-population with NirS and *c*Nor (B). Since B grows faster than A, B makes up an increasing fraction of the total population. As a result, the model predicts extremely low but gradually increasing $N_2O$ concentration throughout the anaerobic phase, exactly as observed.

In summary, the full-fledged model of *Pa. denitrificans*, which includes a rather complex cell diversification owing to the nature of the regulatory network, can adequately simulate essential characteristics of the regulatory phenotype, as observed in batch cultures.

Natural denitrifying communities are mixtures of organisms with widely different denitrification regulatory phenotypes. The regulatory response of such mixtures is not necessarily equal to the 'sum of its components' because there will be interactions, not the least via the intermediates NO and $NO_2^-$. Hence, it is probably a mission impossible to predict the regulatory responses of complex communities based on the phenotypes of their members. Nevertheless, investigations of the regulation and physiology of denitrification in model

organisms like *Pa. denitrificans* provide us with essential concepts, enhancing our ability to understand the regulatory responses of mixed communities and to generate meaningful hypotheses.

# Sammendrag (Norwegian Summary)

I naturlige miljø er det ofte mangel på oksygen i kortere eller lengre perioder. Noen organismer takler dette ved å respirere andre stoffer enn oksygen. Dette kalles anaerob respirasjon, og denitrifikasjon er en av flere varianter. Denitrifiserende bakterier respirerer ved en stegvis reduksjon av nitrogen oksy-anioner ($NO_3^-$/$NO_2^-$, forkortet til $NO_x^-$) via nitrogen oksider (NO/$N_2O$, forkortet til $NO_x$) til molekylært nitrogen ($N_2$):

$$NO_3^- \xrightarrow{\text{Nar / Nap}} NO_2^- \xrightarrow{\text{NirS / NirK}} NO \xrightarrow{c\text{Nor / qNor}} N_2O \xrightarrow{\text{NosZ}} N_2$$

hvor Nar/Nap, NirS/NirK, og *c*Nor/qNor er de viktigste variantene av henholdsvis nitrat-, nitritt-, and nitrogen monoksid reduktase, og NosZ er dinitrogen oksid reduktase. Prosessen (denitrifikasjon) genererer energi som organismene (denitrifikanter; bakterier, arker og sopp) kan bruke for å opprettholde liv (vedlikehold og vekst) på tross av fravær av oksygen.

Denitrifikasjon er en nøkkelprosess i det globale nitrogenkretsløpet; den tilbakefører nitrogenet til atmosfæren fra biosfæren, og den er en viktig kilde til atmosfærisk NO og $N_2O$. NO påvirker troposfærens kjemi og bidrar til dannelse av uønsket troposfærisk ozon. $N_2O$ bidrar til global oppvarming og ødeleggelse av stratosfærisk ozon. For å utvikle robuste tiltak for å redusere stadig økende utslipp av NO og $N_2O$ fra systemer skapt eller manipulert av menneskehånd, er det behov for god forståelse av denitrifiserende organismers fysiologi. Denne avhandlingen er et bidrag til slik forståelse. Hovedverktøyet har vært dynamisk modellering for å undersøke en rekke hypoteser vedrørende bakterien *Paracoccus denitrificans*, som i en årrekke har vært brukt som modellorganisme for undersøkelse av denitrifikasjons-fysiologi.

Utgangspunktet for studien var en rekke hypoteser, generert gjennom tidligere eksperimentelle arbeider, med vekt på fire regulatoriske og fysiologiske aspekter: **1)** NirS, **2)** NirS/*c*Nor (homeostatisk kontroll av NO), **3)** Nar, og **4)** *c*Nor/NosZ ($N_2O$ kinetikk). De første to står i fokus for artikkel nr. 1 og 2, mens de to siste er sentrale i artikkel 3.

Vi startet med å konstruere en forholdsvis enkel modell (artikkel 1) for simulering av oksisk og anoksisk respirasjon og vekst. Modellen ble tilpasset de spesielle eksperimentelle

betingelsene som ble brukt i de arbeidene som ligger til grunn for min modellering: «Batch-kulturer» som skifter fra oksisk til anoksisk respirasjon når bakteriene har brukt opp alt oksygenet. Kulturene ble overvåket ved hyppig prøvetaking fra gassfasen (headspace). Modellen ble så videreutviklet for å undersøke mer spesifikke problemer i artikkel 2 og 3. Felles for alle modellene er at de beregner respirasjon og vekst, reduksjon av $O_2$ og $NO_x^-/NO_x$, gasstransport mellom headspace og væskefase, og gasstapet via prøvetaking. Det siste er viktig for å tillate en direkte sammenligning mellom eksperimentelle data og simuleringer. Modellene benytter Michaelis-Menten kinetikk for alle enzymreaksjoner bortsett fra nitrogenmonoksid reduktase (*c*Nor), hvor utgangspunktet var en «dual substrate model». Modellene er laget med Vensim®, med teknikker hentet fra «system dynamics».

## Artikkel I

Det har hittil vært vanlig å anta at alle celler i en populasjon av denitrifiserende bakterier skifter til anoksisk respirasjon når oksygenkonsentrasjonen faller under et kritisk nivå. Denne oppfatningen ble utfordret, basert på inspeksjon av respirasjonskinetikken under overgangen fra oksisk til anoksisk respirasjon, som antyder at bare en marginal andel av populasjonen skifter til anoksisk respirasjon. Hypotesen, som ble bygget inn i modellen, var at dette skyldes stokastisk initiering av *nirS*-transkripsjon, som så blir autokatalytisk i den enkelte celle via NO produksjon. Modelltilpasning viste at data for en rekke ulike eksperimentelle betingelser kunne simuleres ved å anta en ekstremt lav sannsynlighet for initiering av nirS transkripsjon: 0.005 $t^{-1}$ (0.5 % pr time). Dette resulterte i at bare 3.6–16% av hele populasjonen skiftet til anoksisk respirasjon før oksygenet var fullstendig oppbrukt.

## Artikkel II

Mange denitrifiserende bakterier viser en fabelaktig evne til å holde NO konsentrasjonen på et ekstremt lavt nivå, og dette tilskrives vanligvis synkronisert ekspresjon av nitritt- og nitrogen monoksid-reduktase. Denne forklaringen ble trukket i tvil, og en første eksplisitt simulering av NO kinetikk basert på litteraturverdier for substrataffinitet resulterte i NO konsentrasjoner ~100 ganger høyere enn det som ble målt. En mulig forklaring som ble testet var at den homeostatiske kontrollen av NO på ekstremt lavt nivå kunne skyldes at NO inhiberer NirS (negativ feedback). Denne forklaringen ble forkastet, fordi en slik mekanisme

resulterte i at modellen predikerte alt for langsom anoksisk respirasjon. Det ble derfor besluttet å gjøre et forsøk på å bestemme kinetiske parametre for *c*Nor *in vivo*, hvilket er en ganske utfordrende oppgave. Eksperimentene ble utført slik at det var mulig å beregne NO-konsentrasjonen på celleoverflaten i en anoksisk batch med $NO_x^-$ -fritt medium tilført NO i headspace. Med de nye kinetikk-parametrene for *c*Nor ($v_{max\mathrm{NO}}$ = 3.56 fmol NO cell$^{-1}$ h$^{-1}$, $K_{1\mathrm{NO}}$ < 1 nM, and $K_{2\mathrm{NO}}$ = 34 nM) predikerte modellen NO konsentrasjoner i nærheten av det som ble målt.

Dette viser at homeostatisk kontroll av NO på ekstremt lave nivå kan forstås som et trivielt resultat av enzymkinetikk, og understreker at enzymkinetiske parameter må bestemmes *in vivo*, heller enn *in vitro*, for å forstå og modellere denitrifikasjonsfenotyper.

## Artikkel III

I dette arbeidet ble regulering av alle fire reduktaseenzymer (Nar, NirS, *c*Nor og NosZ) inkludert i modellen, som så ble brukt til å simulere batch-kulturer med $NO_3^-$ i mediet. Transkripsjonen av *nar* ble antatt å følge samme stokastisk-autokatalytiske mønster som *nirS:* lav sannsynlighet for initiering av *nar* transkripsjon, som så forsterkes via $NO_2^-$. Dette ble inkorporert i modellen, og tilpasning til observert $NO_2^-$ kinetikk tilsier en sannsynlighet på 0.035 t$^{-1}$ for initiering av *nar*-transkripsjon, og at 23–43 % av alle celler uttrykker Nar «i tide», dvs før alt $NO_3^-$ var redusert til $NO_2^-$.

Transkripsjonen av *nosZ* antas å skje i alle celler, dvs at alle celler har NosZ etter at oksygenet er brukt opp, men en marginal andel har NirS og *c*Nor. Dette betyr at majoriteten av celler bare har NosZ, og denne sub-populasjonen vokser anaerobt basert på reduksjon av $N_2O$ som leveres av sub-populasjonen som har NirS og *c*Nor. Siden den sistnevnte vokser raskest, vil dens andel av totalpopulasjonen øke gjennom den anoksiske fasen. Som et resultat av dette predikerer modellen svært lave $N_2O$ konsentrasjoner i tidlig anoksisk fase, men økende med tiden (siden andelen $N_2O$ produsenter øker). Dette er i overenstemmelse med observert $N_2O$.

Dette viser at den komplette modellen for *Pa. denitrificans*, som innebærer kompleks celledifferensiering på grunn av karakteristikker ved det genregulatoriske nettverket, kan gi

en adekvat simulering av de den regulatoriske fenotypen slik den kommer til uttrykk i en batchkultur.

Bakteriesamfunn i naturen inneholder en kompleks blanding av denitrifikasjonsbakterier. Den regulatoriske responsen av slike samfunn er ikke nødvendigvis lik «summen av delene». Grunnen til dette er at det vil forekomme utstrakt samspill, ikke minst via NO og $NO_2^-$. Derfor er det liten grunn til å tro at man noen gang skal kunne predikere bakteriesamfunns' regulatoriske respons ut fra de enkelte medlemmers regulatoriske fenotyper. Detaljerte undersøkelser av enkeltorganismer, som denne studien av *Pa. denitrificans,* er likevel meningsfulle fordi det frembringer nye konsepter og hypoteser, som øker våre muligheter til å forstå den regulatoriske responsen i bakteriesamfunn.

# Introduction

***Denitrification: a life-sustaining facultative trait.*** Many natural habitats have fluctuating $O_2$ availability, threatening the life functions and survival of microbes relying on respiration for energy (ATP). To adapt, certain microorganisms (facultative anaerobes) produce enzymes in response to impending anoxia, enabling them to respire molecules other than $O_2$ (anaerobic respiration). One such type of anaerobic respiration is denitrification[4]: the dissimilative reduction of nitrate ($NO_3^-$) to nitrite ($NO_2^-$) to gaseous nitric- and nitrous oxides (NO and $N_2O$) and finally to $N_2$, respectively (Zumft, 1997, p. 8).[5] Thus, denitrification also defends denitrifying organisms against toxic $NO_2^-$ and NO produced by themselves or by other organisms, such as ammonium- and ammonia oxidisers (emitting $NO_2^-$ and NO, respectively).

***Sites with fluctuating $O_2$: the niche for denitrification.*** Since permanently anoxic environments lack available nitrogen oxyanions/-oxides ($NO_x^-$/$NO_x$) and oxic environments provide bioenergetically the most preferable terminal electron ($e^-$) acceptor ($O_2$), the niche for denitrification are the sites where $O_2$ concentration ([$O_2$]) fluctuates, such as biofilms, surface layers of sediments, water columns, wetlands, and drained soils (which become anoxic in response to flooding). In oxic environments, denitrification can occur in anoxic micro-niches, where it is typically coupled with nitrification[6] (Bertrand et al., 2015, p. 576).

***Denitrifiers (bacteria, archaea, and fungi).*** The organisms capable of producing NO or $N_2O$ from $NO_3^-$ or $NO_2^-$ are considered denitrifiers, but not those that can only reduce $NO_3^-$ to $NO_2^-$ (Shapleigh, 2006). Denitrification is typically regarded as a prokaryotic trait, widespread

[4] However, simultaneous aerobic respiration and denitrification are also reported at high $O_2$ concentrations. (For a critical review of the evidence thereof, see Chen & Strous, 2013.)

[5] Although the process was discovered sometime in the middle of 1800s (Keeney & Hatfield, 2008), the first well-documented study of $NO_3^-$ conversion to gas was carried out by Gayoon and Dupetit in 1882, who were also the first to isolate denitrifying bacteria. Because of the loss of nitrate in the process, they termed it denitrification (Shapleigh, 2006). Synonymously, the terms dissimilatory $NO_3^-$ reduction and $NO_3^-$ respiration are also found in the literature.

[6] The microbial oxidation of ammonia to nitrate: $NH_3 \rightarrow NH_2OH \rightarrow NO_2^- \rightarrow NO_3^-$, where the first two steps are typically carried out by one group (e.g., *Nitrosomonas*) and the last one by another (e.g., *Nitrospira* or *Nitrobacter*). To conserve the energy produced, total $\Delta G° = -349$ kJ $mol^{-1}$ $NH_4^+$ (Muldera, van de Graafb, Robertsonb, & Kuenen, 1995), both the groups use an $e^-$-transport chain with $O_2$ as the terminal $e^-$-acceptor.

among bacteria (esp. within Proteobacteria) and also observed in halophilic and hyperthermophilic archaea (Zumft, 1997). However, many fungi (esp. within the genus *Fusarium*) are also denitrifiers (Arasimowicz-Jelonek & Floryszak-Wieczorek, 2013, p. 409; Shoun, Kim, Uchiyama, & Sugiyama, 1992).

Genetics and physiology of denitrification are largely identified through Proteobacteria: *Pseudomonas stutzeri*, *Pseudomonas aeruginosa*, *Ralstonia eutropha*, *Rhodobacter sphaeroides*, and *Paracoccus denitrificans*. Thus, these organisms are considered 'models' in denitrification research (Zumft, 1997).

***Moderating NO and $N_2O$ emissions: the 'end-point variables' for the present thesis.*** Although denitrification closes the loop of the N-cycle by replenishing the atmosphere with gaseous $N_2$, the process significantly emits NO and $N_2O$, both with serious consequences for the environment. Along with anthropogenic activities (esp. fossil fuel combustion), microbial nitrification and denitrification in soils are the main sources of NO emissions (Pilegaard, 2013). As for atmospheric $N_2O$, denitrification in soils is the most significant source thereof, and anthropogenic activities (esp. food production) contribute to accelerate denitrification rates, hence, $N_2O$ emissions therefrom (Signor & Cerri, 2013; Syakila & Kroeze, 2011). The present research explores the regulation and physiology of denitrification at a population-level by testing various hypotheses and assumptions through dynamic modelling. The aim is to contribute to denitrification knowledge so that vigorous strategies may be devised to control the end-point variables: NO and $N_2O$ emissions.

# 1. Biogeochemical role of denitrification

***Denitrification closes the loop of the N-cycle.*** Denitrification is one of the two main processes[7] that close the N-cycle by returning the fixed nitrogen (from the biosphere) to the atmosphere as relatively inert $N_2$ (see Fig. 1).

[7] The other being anammox (anaerobic ammonium oxidation): $NH_4^+ + NO_2^- \rightarrow N_2 + 2H_2O$. This energy yielding process ($\Delta G° = -357$ kj mol$^{-1}$ $NH_4^+$) is stepwise carried out by aquatic bacteria (Planctomycetes) and generates ATP most likely via proton-motive force (Kartal et al., 2011). Intriguingly, an intermediate product of anammox, hydrazine ($N_2H_4$), is used as a rocket-fuel and as a precursor for various pesticides and pharmaceuticals.

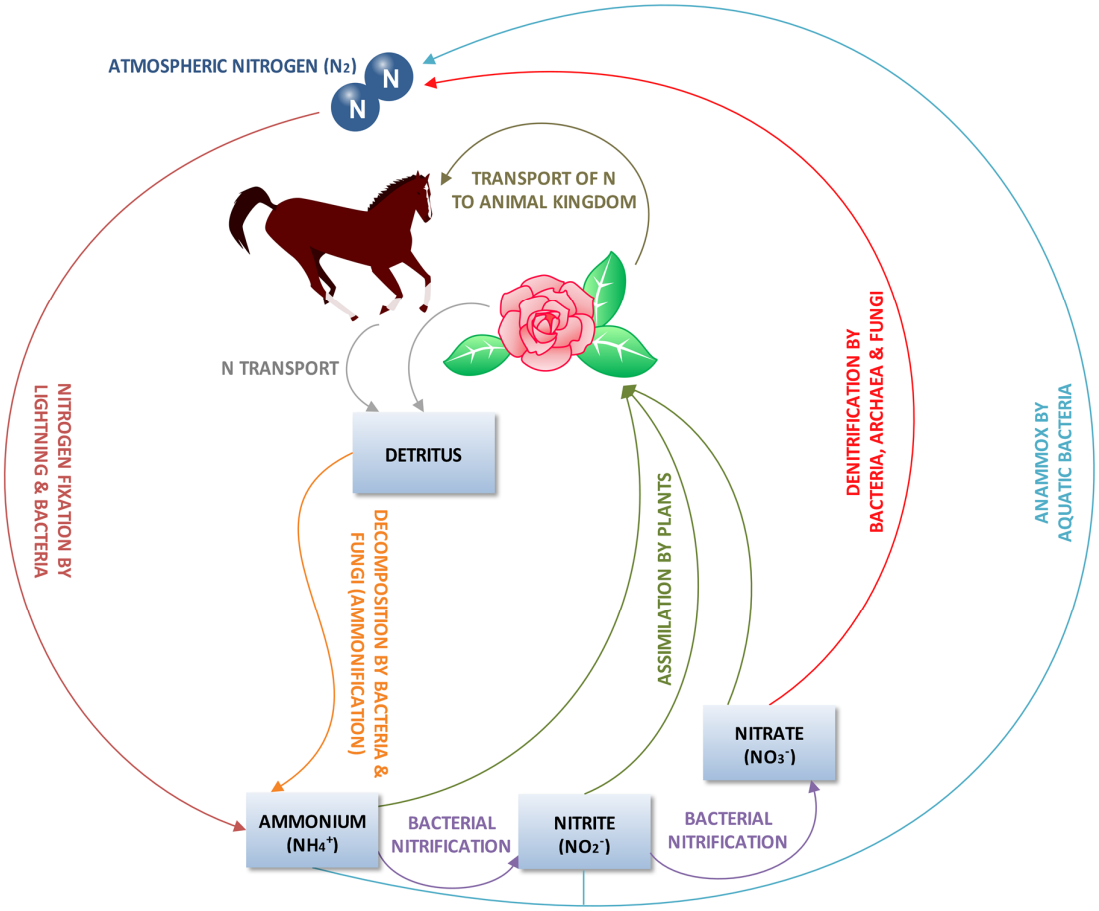


**Fig. 1. The N-cycle** (Based on Ward, 2012)**.** The earth is a closed system with a limited amount of the elements that are precursors for life. Nitrogen is one of them as a building block of amino acids (proteins), nucleotides (making up DNA), and various chemicals exploited by living organisms to generate energy (ATP) for survival and growth. The recycling of N between the atmosphere and living organisms is summarised here: Starting from the left, the atmospheric nitrogen ($N_2$) is converted to $NH_4^+$ by lightning and bacteria (nitrogen fixation), and the N contained within the fauna and flora is converted to $NH_4^+$ by detritus-decomposing bacteria and fungi (ammonification or mineralisation). $NH_4^+$ is further transformed to $NO_2^-$ and $NO_3^-$ mainly by bacteria (nitrification). The N as $NH_4^+$, $NO_2^-$, and $NO_3^-$ is **1)** absorbed back by the flora and, thereby, is also regained therefrom directly (herbivores) or indirectly (carnivores) by the fauna or **2)** returned to the atmosphere as $N_2$ mainly by bacteria (anammox and denitrification).

## 1.1. Removal of $NO_3^-$ and $NO_2^-$: a useful characteristic for the fauna, but not always for the flora

From an agricultural perspective, denitrification is unfavourable because $N_2$ released therefrom cannot be readily utilised by plants, as opposed to $NO_3^-$/ $NO_2^-$ (Madigan et al., 2014, pp. 412-413). However, removal of the excess nitrogen-oxyanions by denitrification is highly advantageous for humans and animals: $NO_3^-$ causes infant methemoglobinemia and a higher risk of birth defects (Knobeloch, Salna, Hogan, Postle, & Anderson, 2000; Sparacino-Watkins, Stolz, & Basua, 2014, respectively), and $NO_2^-$ is indirectly linked with carcinogenesis (Sparacino-Watkins et al., 2014). Therefore, the US Environmental Protection Agency (EPA, 2014) and the World Health Organisation (WHO, 2011) have set an upper limit of 10 and 50 mg $L^{-1}$ of $NO_3^-$, respectively, in the drinking water.[8] $NO_3^-$ and $NO_2^-$ are toxic for a wide variety of aquatic and terrestrial animals (Bruning-Fann & Kaneene, 1993; Camargo, Alonso, & Salamanca, 2005; Kroupova, Machova, & Svobodova, 2005). Furthermore, nutrients like $NO_3^-$ promote algal bloom in fresh waters, providing abundant substrates for bacteria. In turn, the bacteria proliferate so much as to critically decrease the dissolved oxygen in water, leading to the death of aquatic animals and plants. To remove $NO_3^-$/$NO_2^-$ from potable water and sewage, effluent, and industrial wastewater, biological denitrification is employed as an effective technique[9] (Jensen, Darby, Seidel, & Gorman, 2012, p. 8; Sapavatu & Setty, 2012).

## 1.2. NO and $N_2O$ emissions: the most alarming consequence of denitrification

***NO, substantially emitted by denitrification, plays a major role in producing 'bad' (tropospheric) ozone.*** NO is highly reactive and forms nitrogen dioxide ($NO_2$) in the

[8] Vegetables, fruits, grains, dairy products, and meat also contain $NO_3^-$, with vegetables being a major source thereof. $NO_3^-$/ $NO_2^-$ are required for the biosynthesis and regulation of NO, an important biological messenger. Therefore, it is clear that $NO_3^-$ is only harmful above a certain threshold. Interestingly, $NO_3^-$/ $NO_2^-$ have been recently reported to be useful in pulmonary hypertension, cardiovascular diseases, ischemia/reperfusion injury, and in mucus-production as part of immune system. (Sparacino-Watkins et al., 2014, pp. 4-6)

[9] However, as compared to denitrification, a less laborious and much more eco-friendly technique has been developed, known as the Sharon–anammox process (Madsen, 2008, pp. 383-384). The process is in use on the industrial scale in Europe.

troposphere, which is broken down by the sunlight to NO and O. The O then reacts with the atmospheric $O_2$ to produce most of $O_3$ (ozone) present in the troposphere (Wuebbles, 2010, pp. 201-202).[10] Ozone is unfavourable in the troposphere being a greenhouse gas (global warming) and a pollutant, known for its adverse effects on humans, animals, and plants (McKee, 1993). Reduced crop yield due to tropospheric ozone in the US alone is estimated to cost $500 million each year (EPA, 2011). Most of the global NO emissions are ascribed, more or less with equal importance, to nitrification and denitrification in soils[11]; however, non-enzymatic abiotic processes in soils are also likely to be an important source (Medinets, Skiba, Rennenberg, & Butterbach-Bahl, 2014).

***$N_2O$, substantially emitted by denitrification, is a powerful greenhouse gas and a dominant depleter of 'good' (stratospheric) ozone.*** Per molecule, nitrous oxide[12] has a global warming potential (heat-trapping capacity) 298 times that of carbon dioxide (Ussiri & Lal, 2013, p. 20); hence, although the atmosphere contains a thousand times less $N_2O$ than $CO_2$, still $N_2O$ is estimated to contribute ~10% to the anthropogenic climate forcing (Bryson Bates et al., 2008). Although ~80% of $N_2O$ reaching the stratosphere is photolysed to $N_2$, the rest by other reactions is converted to either $N_2$ or NO, where NO reacts with and depletes stratospheric ozone[13] (Schlesinger & Bernhardt, 2013, p. 81). Thus, $N_2O$ contributes to removing the natural umbrella that protects life on the earth from the radiation-induced DNA damage. $N_2O$ emissions are, and predicted to be throughout the 21$^{st}$ century, the most substantial anthropogenic source of ozone depletion (Ravishankara, Daniel, & Portmann, 2009). Data available since 1950s show an almost linear increase in the atmospheric $N_2O$; alarmingly, on average, an $N_2O$ molecule persists for ~120 years in the troposphere before undergoing photolysis in the stratosphere (Lassey & Harvey, 2007, p. 10). ~70% of global $N_2O$ emissions are tentatively attributed to microbial nitrification and denitrification in soils (Butterbach-Bahl, Baggs, Dannenmann, Kiese, & Zechmeister-Boltenstern, 2013, p. 2; Lassey & Harvey,

[10] The transportation of ozone from the stratosphere to the troposphere is also a major source of tropospheric ozone (ibid).

[11] Under oxic conditions (dry soils), nitrification is a more dominant source of NO (70%), whereas under anoxic conditions (wet soils), denitrification takes the lead (87%) (Medinets, Skiba, Rennenberg, & Butterbach-Bahl, 2014; Pilegaard, 2013).

[12] Commonly known as the laughing gas, since it induces euphoria (and hallucination) when inhaled.

[13] NO is highly reactive in the troposphere; hence, only traces of it reach the stratosphere. Almost all of the NO present in the stratosphere is produced via $N_2O$.

2007, p. 10), where denitrification, generally, is considered a more dominant source (Signor & Cerri, 2013; Syakila & Kroeze, 2011).

# 2. Exploring the physiology of denitrification with the ultimate aim to help mitigate global NO and $N_2O$ emissions

## 2.1. Physiology of denitrification is the 'boiling soup' with its 'steam' containing NO and $N_2O$.

***In devising any robust mitigation strategy for global NO and $N_2O$ emissions, we ought to consider genetics, physiology, and the regulatory biology of denitrifiers.*** A major task in NO and $N_2O$ research has been to develop strategies for reducing the fraction of N returned to the atmosphere as NO and $N_2O$. The emissions are orchestrated by **a)** physical and chemical conditions in the environment: soil's N- and organic C-content and water-holding capacity; copper (Cu) availability; and temperature, pH, and moisture ($[O_2]$) and **b)** the physiological response of nitrifying and denitrifying organisms to environmental conditions (Bakken, Bergaust, Liu, & Frostegård, 2012; D. Richardson, Felgate, Watmough, Thomson, & Baggs, 2009; Skiba, Fowler, & Smith, 1997). Any robust mitigation strategy must be based on understanding causalities, i.e., a thorough understanding of causes and effects within the network of factors controlling the emissions. Unfortunately, the biogeochemical research on NO and $N_2O$ emissions has been dominated by empirical approaches, i.e., emission measurements and attempts to correlate emissions with other factors. Further, the simulation models used in this research are rather crude imitations of the physiology of the organisms involved (Bakken & Dörsch, 2007). Perpetuating these efforts will probably not result in much progress, but amalgamating basic research on the biology with the studies of gas emissions may possibly pave the way for novel approaches.

***A natural denitrifying community comprises various denitrification regulatory phenotypes (DRPs) that require consideration.*** Generally, the biogeochemical models aiming at understanding NO and $N_2O$ emissions simplify away soil microbial communities as one homogeneous unit with certain characteristic responses to $O_2$ and $NO_3^-$ concentrations[14]

[14] Another typical shortcoming of such models is the use of relatively older, crude parametric values for enzyme and growth kinetics (ibid).

(Bakken et al., 2012; Bakken & Dörsch, 2007). However, denitrifying communities in soils are composed of a mixture of organisms with widely different denitrification regulatory phenotypes (DRPs): the [$O_2$] in response to which denitrification genes are expressed; accumulation and rates of $NO_2^-$, NO, and $N_2O$ reduction; relative growth and $e^-$-flow rates during aerobic and anaerobic respiration; cell yield from $NO_x^-$/$NO_x$-based respiration; effect of fluctuating [$O_2$] and [$NO_x^-$] and pH on denitrification; and the fraction of the population switching to denitrification in response to anoxic conditions (ibid; Bergaust, Bakken, & Frostegård, 2011; B. Liu, Mao, Bergaust, Bakken, & Frostegård, 2013). Therefore, in our search for mitigation strategies, it is of utmost importance to understand and appreciate DRPs, particularly the potential of ecologically relevant denitrifiers to produce and consume NO and $N_2O$ and the factors controlling that.

***The role of dynamic modelling in understanding DRPs.*** Dynamic models, from their development and testing to final simulations, improve the mechanistic understanding of the underlying processes governing the empirical data (e.g., gas kinetics), make it possible to test what is otherwise impossible or difficult to investigate in the laboratory, generate new hypotheses, guide the experimental work by highlighting discrepancies and deficiencies in our assumptions and theories and, thence, yield new knowledge. To understand DRPs, however, dynamic modelling has been employed rather scantly. Examples include the development of such models to analyse $NO_3^-$ and $NO_2^-$ reduction and gas-kinetic data for individual and a mixture of selected phenotypes (Betlach & Tiedje, 1981; Vasiliadou et al., 2006); to understand competition for electrons among $NO_x^-$/$NO_x$ by simulating the $NO_x^-$/$NO_x$ kinetics in pure cultures (Almeida, Reis, & Carrondo, 1997; Thomsen, Geest, & Cox, 1994); and to scrutinise the hypotheses that $O_2$ inactivates denitrification enzymes (affirmed) and NO inhibits cytochrome *c* oxidase and $NO_3^-$ reductase in *Agrobacterium tumefaciens* (affirmed and rejected, respectively) (Kampschreur et al., 2012). Recently, a simple model based on the Michaelis-Menten kinetics is developed for *Paracoccus denitrificans* to analyse negative correlation between the Cu availability and $N_2O$ emissions (Woolfenden et al., 2013).

***Using dynamic modelling, the present thesis contributes to the understanding of DRP of a prominent model organism, Paracoccus denitrificans.*** In the present thesis, we employ dynamic modelling to contribute to the DRP knowledge of the α-Proteobacterium *Paracoccus*

*denitrificans*[15], a prominent model organisms in denitrification research. By modelling and simulating the organism's growth and the $O_2$ and $NO_x^-$/$NO_x$ kinetics in batch cultures, we explicated our implicit mental model, assumptions, and hypotheses regarding the underlying DRP to test our knowledge, propose new testable hypotheses, and refine important parametric values for future simulations. The knowledge gained is also expected to help understand the physiology of denitrification in other ecologically important denitrifiers.

## 2.2. The significance of model organisms in denitrification research

In this section, we discuss reasons for proceeding with a model organism to explore the physiology of denitrification.

***Model organisms – the primary source of physiological knowledge of denitrification – allow stringent experimentation and robust modelling.*** Most of the physiological knowledge of denitrification is derived from the exploration of a few model organisms, particularly *Rhodobacter sphaeroides, Pseudomonas stutzeri, Pseudomonas aeruginosa, and Pa. denitrificans* (B. Liu et al., 2013). That is understandable because it takes years, if not decades any longer, of collective hard work to significantly unveil physiology of an organism; the progress would have been much slower had a simultaneous investigation of individual denitrifiers (a plethora of which is out there) was targeted. As compared to newly isolated strains, well-characterised model organisms lend themselves to stringent and more reliable experimentation. With most of their metabolic and transcriptional nuts and bolts unravelled, these organisms also allow us to construct robust mathematical models that help enhance the physiological understanding of denitrification and pave the way to specialised experiments for testing new hypotheses. The papers in the present thesis are an example thereof.

***A model organism is a source of new knowledge – a story of pH and $N_2O$ emissions.*** A model organism serves as a source of new knowledge that, to avoid the problem of induction, needs to be tested for its general applicability. For example, it has long been known that

[15] *Pa. denitrificans* is an interesting organism. Because of its extraordinary genomic, structural, and functional resemblance with the mitochondrion, it is hypothesised to be closely related to some α-proteobacterial ancestor of the mitochondrion (For a recent review of the story, see Gray, 2012). Another interesting aspect of *Pa. denitrificans* is recently discovered where the organism, along with *E. coli*, showed robust proliferation at extreme hypergravity, such as found on gigantic stars or in a supernova (Deguchi et al., 2011). The finding has positive implications for the panspermia hypothesis or the possibility of extra-terrestrial life.

denitrification in acidic soils emits more $N_2O$ than in alkaline ones, but reasons for that were poorly understood. Bergaust et al. (2010) shed some light on the phenomenon through batch culture experiments with *Pa. denitrificans*: the cultures accumulated miniscule transient $N_2O$ at the neutral pH but as pH was lowered, a negative correlation was observed, where $N_2O$ became the end product of denitrification at pH 6.0. Earlier, Thomsen et al. (1994) had demonstrated a similar inhibitory effect of low pH on $N_2O$ reductase (NosZ) in *Pa. denitrificans* and hypothesised that low pH interfered with NosZ at the functional level. Bergaust et al. (2010), however, showed that NosZ synthesised at pH 7.0 was fully functional at pH 6.0, but the cells were unable to make functional NosZ at this low pH, despite substantial transcription of the *nosZ* genes. This led them to hypothesise that low pH actually interfered with the enzyme assembly in the periplasm, where pH is not as controlled as in the cytoplasm. When tested on bacterial cells extracted from soils (Binbin Liu, Frostegård, & Bakken, 2014), the hypothesis was confirmed: the cells could not produce any appreciable amounts of functional Nos at pH $\leq$ 6.1 despite significant gene transcription, but the enzyme produced at pH 7.0 remained functional even at pH as low as 5.7. The story neatly demonstrates how insight provided by a model organism may be effectively utilised to gain new knowledge applicable to a wide range of organisms. The story has to offer a couple of other important lessons as well:

The undesirable effect of soil acidity on $N_2O$ emission has been known for over half a century (Nömmik, 1956; Wijler & Delwiche, 1954). Despite that, subsiding the acidity of soils through liming, as a mitigation option for $N_2O$ emissions, has largely been ignored in the global change research. A major reason for that seems to be the lack of insight into the underlying mechanisms governing the pH and $N_2O$ relationship (Binbin Liu et al., 2014). Most studies have focused on the short-term effects of liming, where it may actually boost $N_2O$ emissions. But that is temporary due to a surge in the denitrification rate as a result of liming transiently increasing the carbon and nitrogen mineralisation and nitrification (Baggs, Smales, & Bateman, 2010; Clough, Kelliher, Sherlock, & Ford, 2004). In the wake of the evidence suggesting that the Nos synthesis is strongly constricted by the soil acidity, maintaining the alkalinity of agricultural soils most likely would help minimise $N_2O$ emissions in the long run (Binbin Liu et al., 2014). The story, in contrast to a cursory understanding of denitrification, highlights the importance of mechanistic understanding, both at the environmental as well as at the microbial level. It also illustrates how insight gained through a model organism may help control the end-point variable: NO and $N_2O$ emissions.

***Model organisms provide insight into denitrification as a fitness trait.*** A detailed exploration of the model organisms is also fruitful since it provides clues to how the regulation of denitrification contributes to the prokaryotes' fitness for survival. For example, in Paper I we have demonstrated that in response to $O_2$ depletion, the measured denitrification may be achieved by only 4–16% of all cells switching to denitrification. In terms of fitness, this can be viewed as a 'bet-hedging' regulation 'strategy' (Veening, Smits, & Kuipers, 2008): the fraction switching to denitrification benefits if the anoxic spell is long-lasting and $NO_x^-/NO_x$ remains available, whereas the non-switching fraction benefits by saving energy required for synthesising denitrification enzymes if the anoxic spell is short.

To put the present thesis in context, the next three sections comprehensively introduce the apparatus, enzymology, bioenergetics, and the regulatory biology of denitrification.

# 3. The respiratory apparatus and functional enzymes of denitrification

## 3.1 The $e^-$-transport machinery of denitrification

***Aerobic respiration and denitrification utilise the same basic $e^-$-transport machinery.*** The machinery includes the two membrane bound enzyme-complexes NADH dehydrogenase (complex I) and the cytochrome $bc_1$ complex (complex III), the periplasmic cytochrome *c*, and the hydrophobic quinone/hydroquinone[16] ($Q/QH_2$) pool[17] present in the membrane (Fig. 2) (see Chen & Strous, 2013, pp. 136-140). Organic carbon catabolised through glycolysis and the TCA cycle provides strong $e^-$-donors, such as $C_4H_4O_4$ (succinate) and NADH. NADH is oxidised to $NAD^+$ by complex I, and succinate is oxidised to fumarate[18] by the membrane-bound succinate hydrogenase (complex II, not shown in Fig. 2). The $e^-$ scavenged therefrom are utilised by the same complexes to reduce Q to $QH_2$. In turn, $QH_2$ is oxidised to Q by nitrate

[16] Hydroquinone is also called quinol.

[17] There can be different types of hydroquinones involved (for example, menahydroquinones or ubihydroquinones). Here we simply use Q and $QH_2$ to represent the $e^-$-poor quinone and the $e^-$-rich hydroquinone, respectively. Interestingly, ubiquinone is the famous coenzyme $Q_{10}$ used as an anti-oxidant and an anti-ageing agent in dietary supplements and skin (cosmetic) products.

[18] $HO_2CCH=CHCO_2H$

reductase (Nar) and complex III[19]. Nar utilises the $e^-$ captured therefrom to reduce $NO_3^-$ to $NO_2^-$, and complex III further relays them to cytochrome *c* and/or some other copper-based $e^-$-transporter[20] (see Nicholls & Ferguson, 2013, pp. 108-146). From here, the aerobic respiration and denitrification pathways branch off to their own specific modules: for aerobic respiration, $e^-$ are drawn by a terminal oxidase(s) to reduce $O_2$ to $H_2O$ (complex IV, not shown), whereas for denitrification, $e^-$ are captured by $NO_x^-/NO_x$ reductases.

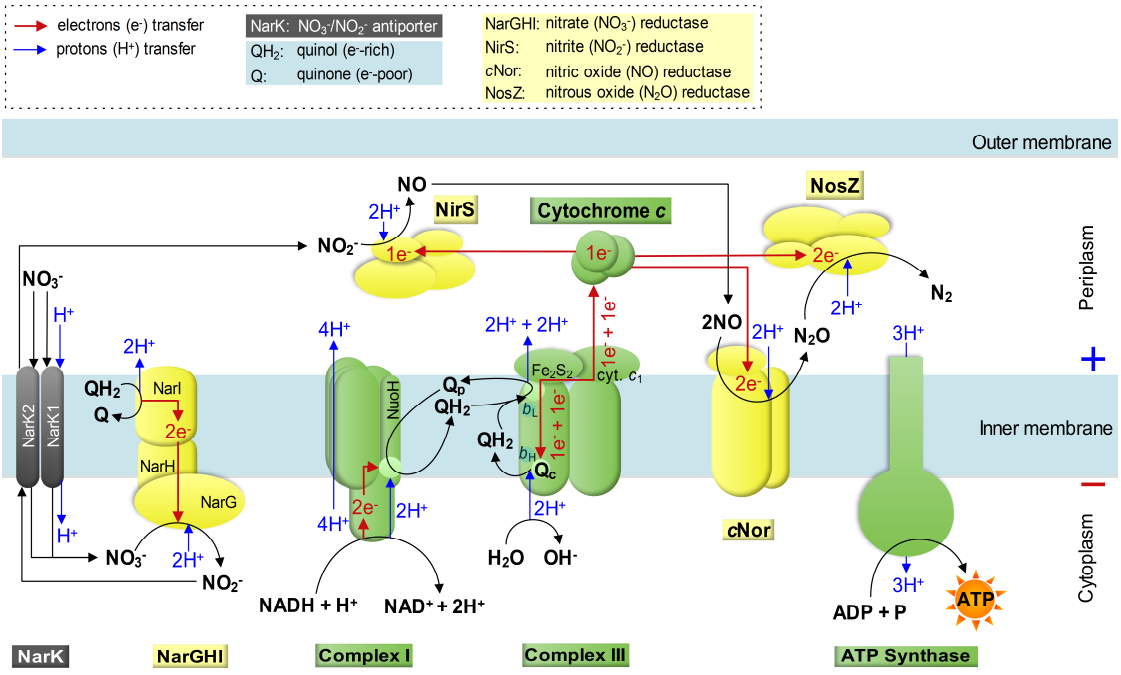


**Fig. 2. The $e^-$-transport model of denitrification** (Based on Chen & Strous, 2013; Nicholls & Ferguson, 2013, pp. 106-146; D. Richardson et al., 2009, p. 390; van Spanning, Richardson, & Ferguson, 2007, pp. 4-6, 7-9)**.** The figure and the text assume a gram-negative bacterium. A general $e^-$-transport model is difficult to present, since variants of each reductase exist, and denitrifiers harbour various combinations thereof. The model presented fits *Pa. denitrificans* except that complex II and Nap (periplasmic nitrate reductase) are omitted. The most energy-conserving $e^-$-pathway of this chain involves complex I, III, and any one of the three $NO_x^-/NO_x$ reductases: NirS, *c*Nor, or NosZ, where per $2e^-$ passing through the chain, $6H^+$ are translocated (by complex I and III) against the electrochemical gradient.

[19] Besides Nar and complex III, other proteins in the membrane (not discussed here) can also oxidise $QH_2$ to Q.

[20] In addition, complex III also utilises the $e^-$ to reduce Q back to $QH_2$, completing the so-called Q-cycle. The mechanism is discussed in Sec. 4.1.

***Electrogenic enzyme-complexes of the e⁻-transport chain.*** Complex I, III, IV, and Nar are electrogenic, for they harness the energy released by the redox reactions, as $e^-$ are relayed 'downhill'[21] from an initial $e^-$-donor ($NADH/C_4H_4O_4$) towards a final $e^-$-acceptor ($O_2/NO_x^-/NO_x$), to translocate $H^+$ from the cytoplasm to the periplasm[22] (see Chen & Strous, 2013, pp. 137-140). This develops an electrochemical potential difference ($\Delta pH + \Delta\psi$) between the cytoplasmic (-ve) and the periplasmic (+ve) vicinities of the membrane, which drives the diffusion of $H^+$ into the membrane (towards the cytoplasm)[23], for which the ATP synthase is the major gateway. Every ~$3.3H^+$ passing through the ATP synthase generate enough energy for the complex to produce one ATP molecule from ADP and P (D. Richardson et al., 2009, p. 390). To store energy as thus[24], aerobic respiration is more efficient than denitrification (see Sec. 4.2 for a detailed comparison).

## 3.2 Denitrification-specific enzyme complexes

The step-wise dissimilatory reduction of $NO_3^-$ to $N_2$ is carried out by four core enzyme-complexes:

$$NO_3^- \xrightarrow{\text{Nar/Nap}} NO_2^- \xrightarrow{\text{NirS/NirK}} NO \xrightarrow{c\text{Nor/qNor}} N_2O \xrightarrow{c\text{NosZ/NosZ}} N_2 \qquad \text{(R1)}$$

where Nar/Nap, NirS/NirK, *c*Nor/qNor, and *c*NosZ/NosZ are the most commonly discussed variants of nitrate reductase, nitrite reductase, nitric oxide reductase, and nitrous oxide reductase, respectively. Considering the diversity of organisms, many other variants are expected in nature; some others are mentioned below.

[21] I.e., the $e^-$ taking part in spontaneous reactions that produce usable energy, since the energy of reactants is greater than that of the products.

[22] And/or to move $e^-$ within the cell membrane in the opposite direction (see Nicholls & Ferguson, 2013, pp. 106-108).

[23] Generating the so-called proton-motive force: $\Delta pmf = \Delta\Psi - 61\Delta pH$, where $\Delta\Psi$ is the electrical potential- and $\Delta pH$ is the pH-difference across the membrane (Nicholls & Ferguson, 2013, p. 44).

[24] The mechanism is formally known as the chemiosmotic theory of oxidative phosphorylation.

### 3.2.1. Nitrate reductase

Denitrification begins with the reduction of nitrate to nitrite by nitrate reductase, a member of molybdopterin oxidoreductases with, at least, one 4Fe-4S cluster (Nicholls & Ferguson, 2013, pp. 139-140; D. J. Richardson, van Spanning, & Ferguson, 2007, p. 21):

$$NO_3^- + 2e^- + 2H^+ \xrightarrow{\text{NarGH / Nap}} NO_2^- + H_2O \quad \text{(R2)}$$

There are four known variants of nitrate reductase: prokaryotic Nar (NarGHI/NarGH), Nap (NapABC), Nas (NasBGC), and plant/fungal eukNR (see D. J. Richardson et al., 2007; Sparacino-Watkins et al., 2014). The cytoplasmic NasBGC system[25] and eukNR, however, are assimilatory nitrate reductases and, therefore, will not be discussed here.

***NarGH.*** The complex is membrane-bound with its nitrate-reducing site (NarG) in either the cytoplasm or the periplasm:

*NarGHI.* The cytoplasmic NarGHI[26] is an electrogenic complex, functioning according to the so-called redox loop model (see Nicholls & Ferguson, 2013, pp. 106-108): The complex acquires $2e^-$ and $2H^+$ when its NarI subunit oxidises $QH_2$ to Q near the periplasmic face of the membrane (Fig. 2). The $2H^+$ are thrust into the periplasm, whereas the $2e^-$ are transferred via NarH down to NarG, where they are utilised to reduce $NO_3^-$ to $NO_2^-$ in the cytoplasm (D. J. Richardson et al., 2007, pp. 23-25). The $2H^+$ required for the reaction (see Eq. R2) are drawn from the cytoplasm, which contribute to the charge separation (Chen & Strous, 2013, p. 139). The rest of the charge separation occurs mainly due to the inward movement of the $2e^-$ from the periplasmic end of the membrane to the active site in the cytoplasm, whereas a little contribution comes from the movement of the $2H^+$ (from $QH_2$) against the electrochemical gradient (Nicholls & Ferguson, 2013, pp. 108, 139).

[25] $NO_3^- \xrightarrow{\text{NasC}} NO_2^- \xrightarrow{\text{NasB}} NH_4^+$ (see Gates et al., 2011).

[26] Also called nNar, due to NarG being in the negatively charged (cytoplasmic) face of the membrane.

For NarGHI to function, the import of $NO_3^-$ into the cytoplasm is imperative, and the resulting $NO_2^-$ must be excreted to avoid toxicity. Both the functions are aptly performed by a membrane-bound protein, NarK, with two sub-units: NarK1 and NarK2. Genetics and biochemical studies indicate that NarK1 is an electroneutral $NO_3^-/H^+$ symporter, responsible for channelling the first molecules of $NO_3^-$ into the cytoplasm, while NarK2 is an electroneutral $NO_2^-/NO_3^-$ antiporter which, in the steady state, would excrete $NO_2^-$ produced in exchange for an equal amount of $NO_3^-$ into the cytoplasm (Goddard, Moir, Richardson, & Ferguson, 2008; van Spanning et al., 2007, pp. 4-5; Nicholas J. Wood, Alizadeh, Richardson, Ferguson, & Moir, 2002).

*NarGH.* The periplasmic NarGH is widespread in bacteria and takes part in fermentation, phototrophy, or denitrification (Chen & Strous, 2013, p. 139). Historically, however, the complex is considered a part of archaeal nitrate reductase system. The system indirectly contributes to the pmf with the reduction of NarGH coupled to an electrogenic complex (Martinez-Espinosa et al., 2007).

***NapABC.*** The enzyme-complex is membrane-bound with its nitrate-reducing site (NapA) in the periplasm[27]. It acquires the $2e^-$ required for reducing $NO_3^-$ (Eq. R2) by oxidising $QH_2$ to Q[28], plunging the $2H^+$ removed therefrom to the periplasm. It is likely that these $2H^+$ were, in the first place, pulled from the cytoplasm as, e.g., complex III reduced Q to $QH_2$.[29] In that case, a contribution to the pmf will be made; otherwise, NapABC itself is electroneutral. The complex, however, functions as part of energy-conserving denitrification and ammonification pathways (see D. J. Richardson et al., 2007, pp. 28-31). Many organisms containing Nar (including *Pa. denitrificans*) also contain NapABC, where the latter is active during aerobic respiration and is hypothesised to function as a scavenger of excess redox equivalents (Nicholls & Ferguson, 2013, pp. 139-140; ibid., p. 29).

[27] Hence, the complex is also referred to as pNar.

[28] Nap, Nir, Nor, and Nos extract the $2H^+$ required for the individual reactions they catalyse from the periplasm (Fig. 2). This, however, does not affect the pmf because these reductases consume almost equal number of $e^-$ from the periplasm (van Spanning et al., 2007). Another argument is that for a single cell, the environmental $H^+$ concentration is considered constant [Per. comm., Jianwei Chen, (Chen & Strous, 2013), Feb. 5, 2015]; hence, the periplasmic $H^+$ consumed by $NO_x$ reductases can be compensated from other sources, ready to diffuse into the membrane once its cytoplasmic side is made negative (by the $H^+$ uptake therefrom).

[29] That is likely but not guaranteed, since the $QH_2$ might have been formed by one of a few membrane-enzymes known to extract $2H^+$ from the periplasm (see Simon, van Spanning, & Richardson, 2008).

### 3.2.2. Nitrite reductase

The next step of denitrification is catalysed by nitrite reductase, which produces the first gaseous intermediate of denitrification by reducing nitrite to nitric oxide (Nicholls & Ferguson, 2013, pp. 140-141):

$$NO_2^- + 1e^- + 2H^+ \xrightarrow{\text{NirS / NirK}} NO + H_2O \qquad \text{(R3)}$$

***NirK vs. NirS.*** The dissimilatory enzymatic complex has two structurally divergent variants[30]: the copper-type NirK and the cytochrome $cd_1$-type NirS (see Rinaldo & Cutruzzolà, 2007). The latter is generally a homodimer, with each sub-unit containing a *c* heme and a $d_1$ heme. To our knowledge, only one bacterial strain has been identified so far containing both these variants together (Philippot & Hallin, 2006).

In the Gram-negative bacteria, NirK or NirS is generally found in the periplasm[31] (Fig. 2) and receives $e^-$ from cytochrome *c* (NirS: cytochrome $c_{550}$, $c_{551}$, or $c_{554}$; NirK: $c_2$ or $c_{553}$) and/or small copper-proteins, like azurin or pseudoazurin (Rinaldo & Cutruzzolà, 2007, pp. 39-42, 49, 51; van Spanning et al., 2007, pp. 4-7). In the Gram-positive bacteria, the reductase complex is membrane-bound but with its $NO_2^-$ reducing site in the periplasm-like space. In addition to a membrane-bound cytochrome $c_{550}$, the NirK of the Gram-positive bacterium *Bacillus azotoformans* has been proposed to receive $e^-$ by reducing menahydroquinone[32] ($MQH_2$) to menaquinone[33] (MQ) (Suharti & de Vries, 2005, pp. 132-133).

Both NirS and NirK are electroneutral but indirectly contribute to the pmf by drawing $e^-$ from cytochrome *c* and/or Cu-proteins, which are reduced by the electrogenic complex III (van Spanning et al., 2007, pp. 7-9). Furthermore, complex III itself is proposed to be reduced by $QH_2$ originating from the electrogenic complex I (Madigan et al., 2014, p. 92; Nicholls & Ferguson, 2013, pp. 56, 131-132). The NirK of *B. azotoformans* also indirectly contributes to

[30] Assimilatory plant and bacterial nitrite reductases are beyond the scope of this thesis.

[31] However, the Gram-negative bacterium *Thiobacillus denitrificans* contains both the periplasmic and the membrane-bound NirS (Hole et al., 1996).

[32] Also called menaquinol.

[33] Popularly known as vitamin $K_2$.

the charge separation by accepting $e^-$ from cytochrome $c_{550}$ and $MQH_2$: MQ is reduced to $MQH_2$ by complex I, which is then oxidised back by the electrogenic cytochrome $b_6f$ complex to reduce cytochrome $c_{550}$ (Suharti & de Vries, 2005, pp. 132-133).

### 3.2.3. Nitric oxide reductase

The haem-copper oxidase, with its catalytic site containing non-heme iron, reduces two molecules of nitric oxide to nitrous oxide (see de Vries, Suharti, & Pouvreau, 2007):

$$2NO + 2e^- + 2H^+ \xrightarrow{cNor\,/\,qNor\,/\,qCu_ANor} N_2O + H_2O \qquad \text{(R4)}$$

Since NO is a free radical and highly toxic, Nor (along with other such enzymes) is crucial for the fitness of an organism producing NO or encountering cytotoxic levels of environmental NO[34]. In archaea, detoxification seems to be the main function of Nor, rather than energy conservation (ibid., p. 57). Three main variants of this integral membrane-complex are known: *c*Nor, qNor, and $qCu_ANor$. In addition, a fungal NO reductase, cytochrome P450nor, is also proposed to be involved in denitrification and co-denitrification[35] (see Shoun, Fushinobu, Jiang, Kim, & Wakagi, 2012).

***cNor.*** This cytochrome *bc* complex is typical for Gram-negative denitrifying bacteria and is the most well-studied of the three (de Vries et al., 2007, pp. 58-60). As mentioned above, it is an integral membrane-complex (Fig. 2) and belongs to the haem-copper superfamily of the most commonly found bacterial terminal oxidases[36], which are electrogenic (see Sec. 3.3 and 4.2). Considering this and the reduction of NO being more energetic than that of $O_2$ (Berks, Ferguson, Moir, & Richardson, 1995, p. 101), one would expect *c*Nor to be electrogenic. But electrochemical, biochemical, and flow-flash experiments conducted over the last thirty years strongly suggest that the complex cannot pump $H^+$ across the membrane nor does it extract

[34] NO molecules can easily diffuse across the cell membrane.

[35] Simultaneous use of $NO_3^-$- and $O_2$-respiration, also known as aerobic denitrification or co-respiration (see Chen & Strous, 2013).

[36] Conspicuously similar to the $cbb_3$-type cytochrome *c* oxidase but with $Fe_B$ replacing the $Cu_B$ subunit (Forte et al., 2001, p. 6486). It is not surprising then that both can reduce NO as well as $O_2$ (de Vries et al., 2007, p. 58).

$2H^+$ required for the formation of $N_2O$ (see Eq. R4) from the cytoplasm (Berks et al., 1995, pp. 146-147; Blomberg & Siegbahn, 2013; Hino, Nagano, Sugimoto, Tosha, & Shiro, 2012, p. 681; Reimann, Flock, Lepp, Honigmann, & Ädelroth, 2007). Recent studies based on structural biochemistry are interesting in this regard: The crystal structure solved for *c*Nor in 2010 seemingly lacks the $H^+$-pathways identified in the haem-copper oxidases between their catalytic sites and the cytoplasm (Lee, Reimann, Huang, & Ädelroth, 2012). On the contrary, several periplasmic $H^+$-pathways have been proposed, and a specific one is confirmed to be used by *Pa. denitrificans* (ter Beek, Krause, Reimann, Lachmann, & Ädelroth, 2013). Molecular dynamic simulations of *c*Nor's crystal structure have also suggested two possible periplasmic $H^+$-pathways to the active site, but none from the cytoplasm (Pisliakov, Hino, Shiro, & Sugita, 2012). Interestingly, quantum chemical energy calculations have indicated that it is impossible for *c*Nor to be electrogenic (Blomberg & Siegbahn, 2013). Nonetheless, since *c*Nor most likely acquires $e^-$ either from cytochrome *c* ($c_{550}$)[37] or Cu-proteins (azurin, pseudoazurin), it indirectly contributes to the pmf for the same reasons as for Nir (de Vries et al., 2007, pp. 58-59; van Spanning et al., 2007, pp. 7-9).

***qNor*.** In contrast to *c* in *c*Nor, q in qNor indicates that this single-subunit variant utilises $QH_2$ or $MQH_2$ as the $e^-$-donor (de Vries et al., 2007, pp. 60-61). The structure-based mutagenesis and molecular dynamic simulations of the crystal structure solved for qNor in 2011 have suggested a water channel between the enzyme's active site and the cytoplasm (Matsumoto et al., 2012). The channel is hypothesised to serve as a $H^+$-pathway from the cytoplasm and, hence, has raised speculations about the electrogenicity of qNor; however, no pathway has yet been identified between the catalytic site and the periplasm for $H^+$ to permeate through the complex (ibid., , pp. 1911-1912). In addition to denitrifying bacteria and archaea, qNor is also found in non-denitrifying bacteria, including pathogens that invade mammalian cells. In these organisms, the primary function of the enzyme seems to be detoxification, which is crucial for pathogens to tackle the cytotoxic levels of NO produced by the defence system of the host (Hendriks et al., 2000).

***qCu$_A$Nor*.** To our knowledge, the two-subunit complex has only been found in *B. azotoformans* (de Vries et al., 2007, pp. 59, 62). qCu$_A$Nor is electroneutral but indirectly contributes to the pmf by accepting $e^-$ via a specific membrane-bound cytochrome $c_{551}$ and by

[37] Hence a *c* in the name *c*Nor.

oxidising $MQH_2$ to MQ: $MQH_2$ is formed by complex I, which in the process pumps $4H^+$ against the electrochemical gradient, and $c_{551}$ is reduced by the electrogenic cytochrome $b_6f$ complex (Suharti & de Vries, 2005, pp. 132-133). The main function of the $e^-$-pathway via $MQH_2$ is proposed to be a rapid NO detoxification, since the pathway's maximum $e^-$-delivery rate is found to be four times higher than that via $c_{551}$ (Suharti, Heering, & de Vries, 2004). Hence, *B. azotoformans* is more NO tolerant than, for instance, *Pa. denitrificans* that acquires $e^-$ from cytochrome $c_{550}$ or Cu-proteins for *c*Nor.

### 3.2.4. Nitrous oxide reductase

The enzyme-complex catalyses the last step of denitrification by reducing nitrous oxide to dinitrogen:

$$N_2O + 2e^- + 2H^+ \xrightarrow{\text{NosZ}/c\text{NosZ}} N_2 + H_2O \quad \text{(R5)}$$

Nos[38] is found in a wide variety of denitrifying and non-denitrifying archaea and bacteria, belonging to diverse taxonomic groups (see Zumft & Körner, 2007). Like Nir, the enzyme is either located in the periplasm as a water-soluble protein or is membrane-bound not only in Gram-positives but some Gram-negatives[39] as well (ibid., p. 77; Suharti & de Vries, 2005, p. 132). The catalytic-site of the reductase, however, is oriented towards the extracellular space (van Spanning et al., 2007, p. 6).

***Two variants and their potentially deceptive names.*** Two variants of the enzymatic complex are known: the so-called typical NosZ and atypical NosZ or, synonymously, Z-type Nos and *c*NosZ, respectively. First, both the set of names require some clarification: *c*NosZ, when first found in the non-denitrifying Epsilonproteobacterium *Wolinella succinogenes*[40], appeared to be atypical as compared to the typical NosZ known for denitrifiers (Simon, Einsle, Kroneck,

[38] Also known as $N_2OR$.

[39] *Flexibacter canadensis, Thiosphaera pantotropha, Pyrobaculum aerophilum,* and *Thiobacillus denitrificans.*

[40] The organism relies on $NO_3^-$ and $NO_2^-$ ammonification and $N_2O$ respiration, with each process depending on formate dehydrogenase for $e^-$.

& Zumft, 2004). However, in a recent study, 142 full-length prokaryotic *nosZ* gene sequences were examined[41], indicating that the genes encoding *c*NosZ is as abundant as that for the typical Z-type (Jones, Graf, Bru, Philippot, & Hallin, 2013). In another study, 126 bacterial and seven archaeal *nosZ*-carrying genomes were screened, revealing that 44% of the genomes with atypical *nosZ* clusters were denitrifiers (Sanford et al., 2012).

The names Z-type Nos and *c*NosZ (or sometimes simply *c*Nos) are also unintuitive: both the variants have copper-sulphide centres ($Cu_Z$) and a head-to-tail configuration (Fig. 3) for which the first is called Z-type[42] (as explained by Zumft & Körner, 2007, p. 68), and both may accept $e^-$ from cytochrome *c* for which the second has a *c* in its name. It may be argued that the *c* in *c*NosZ refers to an additional cytochrome *c* domain, covalently bound to the reductase. Genetic analyses, however, have revealed that such a domain, typical of *W. succinogenes*, is missing even in the two bacteria with their *c*NosZ sequences most similar to that of *W. succinogenes* (Simon et al., 2004, p. 10).

***Z-type Nos vs. cNosZ.*** Both the complexes have the same primary structure (Kern & Simon, 2009, pp. 652-653): a homodimer with its monomers bound together in a head-to-tail configuration, which is critical for the adequate functioning of the complex (see Fig. 3). Each monomer has a C-terminal with a copper centre ($Cu_A$), receiving and transporting $e^-$, and an N-terminal with a catalytic copper-sulphide centre ($Cu_Z$). The structure of *c*NosZ differs in that it typically[43] has an extended C-terminal with (e.g., *W. succinogenes*) or without (e.g., *Dechloromonas aromatica* and *M. magnetotacticum*) a covalently-bound monohaem cytochrome *c* domain[44] (Simon et al., 2004, p. 10).

The two variants differ in their translocation pathways from the cytoplasm to the periplasm: Z-type Nos, like Nap and periplasmic NarGH, is exported through Tat, whereas *c*NosZ, with

[41] Out of total 216 found in the NCBI microbes database. 216 – 142 = 74 *nosZ* sequences were disregarded as practically redundant.

[42] 'Z-type' may also mislead one to assume as if the variant is named after the *nosZ* gene, responsible for exclusively encoding this type. But *c*NosZ is also encoded by the gene called *nosZ*. [The two genes are evolutionarily related but not the same (Sanford et al., 2012, p. 1)].

[43] But not always [Per. comm., Jörg Simon (Simon et al., 2004), Mar. 3, 2015].

[44] The domain is thought to deliver $e^-$ to $Cu_A$ in *W. succinogenes.*

a few exceptions, is most likely transported through the Sec pathway (Jones et al., 2013, p. 420; Zumft & Körner, 2007, pp. 77-78).

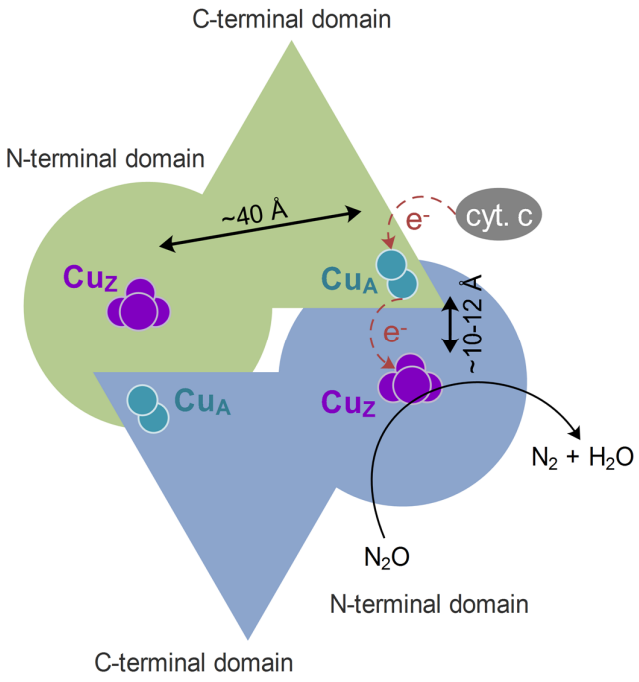


**Fig. 3. The NO reductase (Nos) Model** (Redrawn based on D. Richardson et al., 2009, p. 391). The homodimeric reductase complex has a C-terminal and an N-terminal domain. The C-terminal binds a binuclear copper centre ($Cu_A$), which accepts $e^-$ from cytochrome *c* (or another $e^-$-donor) and transfers them to the catalytic site. The N-terminal binds the catalytic site ($Cu_Z$) as a tetranuclear copper-sulphide centre. The distance between the $Cu_A$ and $Cu_Z$ of the same monomer is so much (~40 Å) that $e^-$ cannot be delivered efficiently enough to carry out the reduction of $N_2O$ at a useful rate. But because of the head-to-tail configuration of the two monomers, the $Cu_A$ of one comes in close proximity with the $Cu_Z$ of the other (~10-12 Å); hence, the $e^-$-transport and the reduction reaction adequately speeds up. The primary structure shown is the same for Z-type Nos and *c*NosZ; however, the latter typically contains an extended C-terminal (Jones et al., 2013).

Although the reduction of $N_2O$ to $N_2$ is highly exergonic ($\Delta G° = -339.5$ kJ $mol^{-1}$), both the catalytic variants are electroneutral. Nonetheless, since certain bacteria are known to grow via $N_2O$ respiration, the energy must somehow be conserved:

Regarding Z-type Nos, the energy is proposed to be conserved in the same way as for Nir and *c*Nor: the complex accepts $e^-$ from cytochrome *c* and/or Cu-proteins that, in turn, are reduced by electrogenic complexes III (directly) and, possibly, I (indirectly, see Fig. 2) (Nicholls & Ferguson, 2013, pp. 131-132, 140-141; Zumft & Körner, 2007, pp. 67-68). Similarly, the membrane-bound Z-type Nos of *P. aerophilum* and *B. azotoformans* is described to contribute indirectly to the pmf by oxidising $MQH_2$, which was reduced by complex I ($MQ \rightarrow MQH_2$)

with the pumping of $4H^+$ across the membrane (Suharti & de Vries, 2005, pp. 132-133). A Nos-specific membrane-bound protein, NosR, is also suggested to participate in the $e^-$-transport to Z-type Nos in *Pseudomonas stutzeri* (Wunsch & Zumft, 2005). It is, however, not clear how this pathway contributes to the charge separation.

On the other hand, a typical epsilonproteobacterial $N_2O$ respiration model is recently deduced from genetic studies (Kern & Simon, 2009, pp. 652-653). In this model, *c*NosZ is hypothesised to accept $e^-$ from a *c*NosZ-specific NosGH complex, directly or possibly via intermediary *c*-type cytochromes, NosC1 and NosC2. The membrane-bound NosGH acquires $e^-$ by oxidising $QH_2$ to Q and deposits the $2H^+$ extracted therefrom into the periplasm. Like for NapABC, the contribution to the pmf depends on whether the $QH_2$ oxidised was, in the first place, formed by the $2H^+$ originating from the cytoplasm.

## 3.3. Enzyme-complexes of *Pa. denitrificans* $e^-$-transport chain

***NarGHI, NapABC, NirS, cNor, and NosZ.*** The $e^-$-transport chain of *Pa. denitrificans* is as depicted in Fig. 2; however, in addition to NarGHI, NirS, *c*Nor, and NosZ, the organism also has NapABC (not shown). But the genes encoding Nap are predominantly expressed under oxic- rather than anoxic conditions, suggesting that Nar takes over the role of reducing $NO_3^-$ to $NO_2^-$ during anoxic conditions (Qu, Bergaust, & Bakken, 2014, Paper IV, p. 19). The function of Nap during aerobic respiration is hypothesised to be that of dissipating excess redox equivalents (Sears, Spiro, & Richardson, 1997). Hence, we did not consider the activity of Nap while modelling the reduction of $NO_3^-$ (Paper III).

***Complex II.*** In the core $e^-$-transport machinery, *Pa. denitrificans* also harbours the electroneutral succinate hydrogenase, feeding the machinery (by oxidising succinate to fumarate) with $2e^-$ (see Madigan et al., 2014, pp. 91-92), which are passed on to complex III. Since the $e^-$-pathway commencing from complex II bypasses the highly electrogenic complex I, a lower charge separation is achieved per $e^-$-pair, compared to the pathway involving complex I.

***Terminal oxidases (complex IV).*** *Pa. denitrificans* is a metabolically diverse organism with multiple haem-copper terminal oxidoreductases: cytochrome *c* oxidases[45] (*aa*$_3$, *cbb*$_3$, and *b*-containing) and hydroquinone oxidases (*ba*$_3$ or *bb*$_3$) (de Gier et al., 1994; Raitio & Wikström, 1994; Richter, Tao, Turba, & Ludwig, 1994). All these oxidases are proton pumps, at least, in *Pa. denitrificans* (de Gier et al., 1996; García-Horsman, Barquera, Rumbley, Ma, & Gennis, 1994, p. 5589). The role of *cbb*$_3$-type as a proton-pump long remained controversial, but recent studies suggest that this high-affinity oxidase, functional at low $O_2$ concentrations, does pump $H^+$ with a stoichiometry of 0.4–1$H^+$ translocation per $e^-$ received (Murali, Yildiz, Daldal, & Gennis, 2012; Rauhamäki, Bloch, & Wikström, 2012). This $H^+$-pumping efficiency, however, is much lower than that of a typical mitochondrial-type *aa*$_3$ oxidase of *Pa. denitrificans* (discussed below).

## 4. Bioenergetics of aerobic respiration vs. denitrification

As discussed above, the free energy released by redox reactions in the $e^-$-transport chain is coupled to the ATP generation through the proton-motive force (pmf). In conserving energy as such, aerobic respiration is more efficient than denitrification, since its $e^-$-transport machinery pumps 1.33–7.5 times more $H^+$ from the cytoplasm to the periplasm per $e^-$-pair (van Spanning et al., 2007, pp. 7-9). The number of $H^+$ translocation per $e^-$ depends on the enzyme-complexes involved.[46] Here, energetically the most favourable $e^-$-transport chain of aerobic respiration is compared with the counterpart from denitrification, both functioning under optimal conditions. Such chain for aerobic respiration involves NADH hydrogenase (complex I), cytochrome *bc*$_1$ complex (complex III), and *aa*$_3$-type cytochrome *c* oxidase as complex IV, whereas the denitrification counterpart involves complex I, complex III, NirS, *c*Nor, and NosZ[47]. Interestingly, *Pa. denitrificans* is diverse enough to harbour both these $e^-$-transport chains. We proceed by discussing complex I and III utilised by both the modes of respiration.

[45] Usually abbreviated as C*c*O.

[46] For the charge-separation capacity of various combinations of denitrification reductases versus aerobic respiration involving *aa*$_3$- or *ba*$_3$-type cytochrome *c* oxidases, see van Spanning et al., 2007, p. 8.

[47] A pathway including NirK, q$Cu_A$Nor, and *c*NosZ will be equally energetic. qNor is hypothesised to acquire 2$H^+$ to convert NO to $N_2O$ from the cytoplasm (Matsumoto et al., 2012), but further investigations are required to establish this.

## 4.1. Bioenergetics of complex I and III

***Complex I.*** The complex is peculiarly large, comprising up to 44 subunits in eukaryotes and 14 in bacteria. At the extreme-end of its cytoplasmic (hydrophilic) module, NADH + $H^+$ is oxidised to $NAD^+$ + $2H^+$ (Fig. 2). The oxidation induces conformational change in the complex, resulting in the translocation of $4H^+$ from the cytoplasm to the periplasm. The complex uses the $2H^+$ and $2e^-$ produced from the oxidation of NADH to reduce Q to $QH_2$, where the $2e^-$ reach the Q-reduction site via flavin mononucleotide (FMN) and Fe-S centres of the hydrophilic module.[48] The reduction of Q takes place at the NuoH subunit on the verge of the hydrophilic and hydrophobic modules, entailing that the $2e^-$ moving within complex I do not travel through the membrane, hence not having any implication for the charge separation. The $2H^+$ obtained by the oxidation of NADH in the cytoplasm are inconsequential for the charge separation since, in steady state, the production and uptake of such $H^+$ is equal.[49] Thus, overall, the electrogenic complex I deposits $\frac{4H^+}{2e^-}$ against the electrochemical gradient (Nicholls & Ferguson, 2013, pp. 56, 108-111, 131-132).

***Complex III (the Q-cycle).*** While performing its electrogenic function, the complex runs the so-called Q-cycle, which I describe here in two-steps (see Nicholls & Ferguson, 2013, pp. 118-125):

1) The complex binds a Q molecule ($Q_c$) near the cytoplasmic face and a $QH_2$ molecule near the periplasmic face of the membrane (Fig. 2). The $QH_2$ is oxidised to Q ($Q_p$), and the $2H^+$ therefrom are forced to the periplasm. One of the $2e^-$ from the $QH_2$ is relayed, via $Fe_2$-$S_2$ centre of the so-called Rieske protein, to the cytochrome $c_1$ subunit in the periplasm, which eventually reduces cytochrome *c*. The other $e^-$ is transferred, via cytochrome $b_L$ to $b_H$, against the electrochemical gradient to the bound $Q_c$,

[48] As mentioned in Sec. 3.3, $2e^-$ can also enter the $e^-$-transport chain by complex II (succinate dehydrogenase) or a few other reductases, bypassing complex I and directly delivering $e^-$ to the $Q/QH_2$ pool (Nicholls & Ferguson, 2013, p. 7).

[49] The cytoplasmic $H^+$ extracted by the $e^-$-transport complexes are either generated by the oxidation of NADH or dissociation of $H_2O$ into $H^+$ + $OH^-$ (Madigan et al., 2014, p. 91). The translocation of the latter $H^+$ to the periplasm will result in the build-up of negative charge ($OH^-$) in the cytoplasmic vicinity of the membrane, contributing to the electrochemical potential difference across the membrane.

reducing it to semiquinone ($Q_c^-$). $Q_p$ is released from the complex, whereas $Q_c^-$ remains tightly bound.

2) Complex III oxidises another $QH_2$ molecule near the periplasmic face. Like in step 1, the $2H^+$ therefrom are pushed to the periplasm, one of the $2e^-$ reduces cytochrome *c*, and the other reaches $b_H$ (via $b_L$). $b_H$ loses its $e^-$ to the free-radical $Q_c^-$ bound nearby, which is released by the complex as $QH_2$; the $2H^+$ required are drawn from the cytoplasm. $Q_p$ (produced by the oxidation of $QH_2$) is also released.

During the Q-cycle, complex III oxidises $2QH_2$ and reduces 1Q to $QH_2$, depositing $4H^+$ to the periplasm but extracting only $2H^+$ from the cytoplasm. If we look closely, however, there is no discrepancy in the $H^+$-stoichiometry here because one of the $2QH_2$ molecules oxidised by complex III was, in the first place, formed by complex I or II by extracting $2H^+$ from the cytoplasm (see Fig. 2). Regarding the $4e^-$ involved, $2e^-$ reach the periplasm whereas $2e^-$ are deposited back to the membrane through the reduction of Q to $QH_2$. Hence, per $2e^-$ delivered at the periplasmic side, complex III deposits $4H^+$ to the periplasm. But the net charge transfer is not equivalent to $4H^+$ because **a)** the effect of the $2H^+$ deposited to the periplasm will be cancelled out against the deposition of the $2e^-$ to the periplasm by complex III that eventually came from the cytoplasm (as complex I or II reduced Q to $QH_2$), and **b)** none of the $4H^+$ travel all the way as charged entities from the cytoplasmic- to the periplasmic side of the membrane. Most of the charge separation comes from the transfer of the $2e^-$ from $b_L$ at one hydrophobic end of the membrane to $b_H$ at the other; the effect is equivalent to the movement of $2H^+$ in the opposite direction. Thus, altogether, complex III's activity is equivalent to depositing $\frac{2H^+}{2e^-}$ against the electrochemical gradient (Nicholls & Ferguson, 2013, pp. 59-60, 122, 131-132).

## 4.2. Bioenergetics of complex IV vs. NirS/*c*Nor/NosZ

For aerobic respiration, $e^-$ are shuttled from complex III to IV ($aa_3$-type cytochrome *c* oxidase), whereas for denitrification, $e^-$ are transported from complex III to NirS, *c*Nor, and NosZ (Fig. 2, complex IV not shown).

***Complex IV.*** For reducing $O_2$ to $2H_2O$, complex IV picks up $4H^+$ from the cytoplasm and receives $4e^-$ from complex III via cytochrome *c* (periplasm) (Chen & Strous, 2013, p. 140).

The $4H^+$ and $4e^-$ move against the electrochemical gradient within the complex and meet half way through the membrane at the catalytic site of the complex, producing an effect equivalent to the translocation of $4H^+$ from the cytoplasm to the periplasm. In addition, the complex couples the energy released by the reduction of $O_2$ to pump $4H^+$ across the membrane. Thus, overall, complex IV's activity is equivalent to the translocation of $\frac{8H^+}{4e^-}$ or $\frac{4H^+}{2e^-}$ against the electrochemical gradient (Nicholls & Ferguson, 2013, pp. 126-132).

***Nir/cNor/NosZ***. In contrast, NirS, *c*Nor, and NosZ are electroneutral, extracting $e^-$ and $H^+$, required for their catalytic activity, from the periplasm (Fig. 2). Nonetheless, each indirectly contributes to the charge separation by accepting $e^-$ from the electrogenic complex III $\left(\frac{2H^+}{2e^-}\right)$, via cytochrome *c* or Cu-proteins (Nicholls & Ferguson, 2013, pp. 139-141).

***Nir/cNor/NosZ vs. NarGHI.*** If we compare the activity of NirS, *c*Nor, or NosZ with that of NarGHI (Fig. 2), the latter consumes $2H^+$ from the cytoplasm, deposits $2H^+$ to the periplasm, and relays $2e^-$ to the site of $NO_2^-$-formation against the electrochemical gradient, yielding a net stoichiometry equivalent to $\frac{2H^+}{2e^-}$ (Nicholls & Ferguson, 2013, pp. 106-108, 139-141). Therefore, although the reactions performed by Nor and Nos are much more exergonic than that catalysed by Nar (Berks et al., 1995, p. 101), the amount of energy conserved turns out to be the same. However, Nir, Nor, and Nos play a critical role as alternative $e^-$-sinks in the absence of $O_2$; without such sinks, complex I and III cannot function (Nicholls & Ferguson, 2013, p. 141).

***Aerobic respiration vs. denitrification.*** Overall, aerobic respiration, via complex I $\left(\frac{4H^+}{2e^-}\right)$, III $\left(\frac{2H^+}{2e^-}\right)$, and IV $\left(\frac{4H^+}{2e^-}\right)$, translocates $\frac{10H^+}{2e^-}$ across the membrane, whereas denitrification only $\frac{6H^+}{2e^-}$, via complex I and III. This provides energetic-basis to explain why all known denitrifiers down-regulate denitrification in the presence of $O_2$ (Chen & Strous, 2013, pp. 137-140; van Spanning et al., 2007, pp. 7-9).

# 5. Transcriptional regulation of denitrification genes

***$O_2$ controls denitrification at transcriptional as well as metabolic level.*** Typically, denitrifiers are facultative anaerobes, expressing the genes encoding denitrification-specific reductases in response to $O_2$ depletion. When a denitrifying population is exposed to full aeration, the typical response is **a)** an immediate transcriptional inactivation of denitrification genes and **b)** diversion of the $e^-$-route from $Q/QH_2$ pool–$NO_x^-/NO_x$ reductases to $Q/QH_2$–complex IV (van Spanning et al., 2007, p. 10). Thus, $O_2$ controls denitrification at transcriptional as well as metabolic level, and both have a plausible fitness value. The metabolic control maximises the ATP yield, since the ATP per mole $e^-$ transferred to complex IV is 1.33–7.5 times higher than to Nir, Nor, or Nos (van Spanning et al., 2007, p. 8). The transcriptional control, on the other hand, minimises the energy cost of producing denitrification enzymes.

***Denitrification proteome is diluted by aerobic growth and its re-synthesis costs ATP.*** The denitrification proteome produced in response to an anoxic spell is likely to linger within the cells under subsequent oxic conditions[50], ready to be used if $O_2$-limitation reoccurs. However, the proteome will be diluted by aerobic growth, since the transcription of denitrification genes is effectively inactivated by $O_2$. Hence, a population growing through many generations under fully oxic conditions will probably be dominated by the cells without intact denitrification proteome. When confronted with $O_2$ depletion, such a population will have to start from scratch, i.e., transcribe the relevant genes, translate mRNA into peptide chains (protein synthesis by ribosomes) and secure that these chains are correctly folded by the chaperones, transport the enzymes to their correct locations in the cell, and insert necessary co-factors (e.g., Cu, Fe, or Mo). In *E. coli* grown under optimal conditions, the entire process from the transcriptional activation to a functional enzyme takes ≤20 minutes (Proshkin, Rahmouni, Mironov, & Nudler, 2010) and is likely to cost significant ATP.

With a variety of $NO_x^-/NO_x$ reductases and $O_2$- and $NO_x^-/NO_x$-sensing mechanisms operating in various denitrifiers, there is no single apparatus of regulation of denitrification. Nonetheless, each regulatory network can be seen to function as to keep $NO_2^-$ and NO under

[50] This, however, has not been studied in detail.

cytotoxic levels (van Spanning et al., 2007, p. 11). Here we will confine our discussion to the regulatory network of *Pa. denitrificans.*

***Transcriptional regulation of denitrification genes in Pa. denitrificans.*** Nar, NirS, *c*Nor, and NosZ are encoded by *narKGHJI*, *nirSECF*, *norCBQDEF* and *nosRZDFYLX* gene clusters, respectively[51] (Spiro, 2012, p. 1222; van Spanning et al., 2007, pp. 9-10). Transcriptional regulation of these genes involves, at least, three FNR-type proteins acting as sensors for $O_2$, $NO_2^-$, and NO: FnrP, NarR, and NNR, respectively. FnrP contains a 4Fe-4S cluster for $O_2$-sensing, and NNR harbours a NO-sensing haem; NarR, however, is poorly characterised, and its role as a $NO_2^-$-sensor is hypothetical (Bouchal et al., 2010, pp. 1350-1351). All the three sensors remain completely inactive during aerobic growth conditions (ibid., pp. 1355-1356). NarR and FnrP self-regulate their concentrations by repressing their own synthesis (van Spanning et al., 2007, p. 16).

Low $O_2$ activates FnrP, which in an interplay with NarR induces *nar* transcription. NarR, most probably, is activated by $NO_2^-$; thus, once a cell starts producing traces of $NO_2^-$, *nar* expression becomes autocatalytic (Fig. 4, see $P_1$). Transcription of *nirS* is suppressed in the presence of $O_2$ (Bergaust et al., 2010; Qu et al., 2014, Paper III), but the exact inactivation mechanism in unknown. Probably, $O_2$ supresses NNR (Spiro, 2007, p. 198), required to induce *nirS* transcription. Nonetheless, under anoxic/micro-oxic conditions, the expression of *nirS* also becomes autocatalytic via positive feedback by NO-NNR (Fig. 4, $P_2$). In contrast, NO-NNR facilitate a substrate-induced transcription of *nor* (Fig. 4, see the negative feedback N) (Bouchal et al., 2010; van Spanning et al., 2007, pp. 10-16). Finally, *nosZ* is equally and independently induced by NNR and FnrP (Bergaust et al., 2012).

Increasing [NO] constraints *nar* transcription by inactivating FnrP (van Spanning et al., 2007, p. 16) and, like $O_2$, renders NosZ dysfunctional by inactivating the complex's CuZ subunit (D. Richardson et al., 2009, p. 391). These observations, however, are ignored for our modelling because *Pa. denitrificans* restricts [NO] to very low levels.

[51] For briefness, we will refer to these gene clusters as *nar*, *nirS*, *nor* and *nosZ*, respectively.

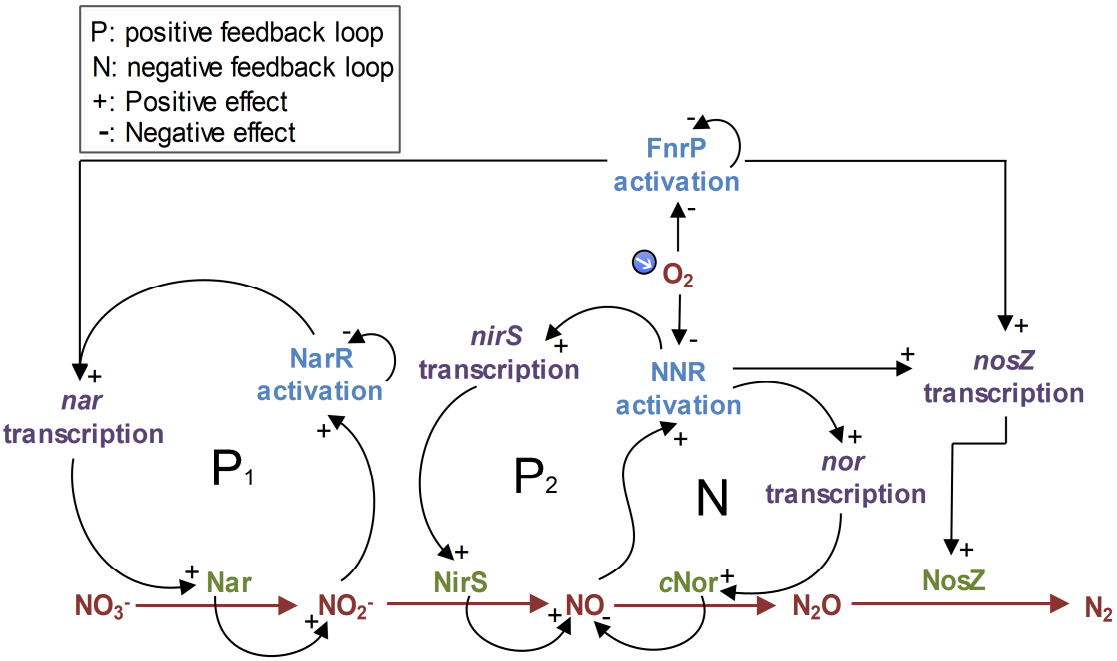


**Fig. 4. The regulatory network of denitrification in *Pa. denitrificans*** (Based on Bergaust, van Spanning, Frostegård, & Bakken, 2012; Bouchal et al., 2010; van Spanning et al., 2007, pp. 10-16; N. J. Wood et al., 2001, pp. 3611-3612)**.** Nar, NirS, *c*Nor, and NosZ are encoded by the *narG*, *nirS*, *norBC* and *nosZ* genes, respectively. Transcription of these genes is regulated by, at least, three FNR-type proteins, which are sensors for $O_2$ (FnrP), $NO_2^-$ (NarR), and NO (NNR). In response to $O_2$ depletion, FnrP in coaction with NarR facilitates a product-induced transcription of the *nar* genes (see the positive feedback $P_1$), and NNR activates a product-induced transcription of *nirS* ($P_2$).[52] NNR further induces *nor* transcription, thereby counteracting the NO accumulation (the negative-feedback N). Finally, NNR induces *nosZ* transcription, but that is also equally and independently induced by FnrP.[53]

## 6. Simulated experiments, research problems, modelling, and the outcome

The present thesis takes advantage of refined experiments with *Pa. denitrificans*, providing us with challenging datasets for testing whether we could simulate the observed denitrification

[52] NNR also controls transcription of the genes encoding NirI (not shown), a transmembrane protein required for a fine-tuned regulation of NirS concentration (Saunders et al., 1999; van Spanning et al., 2007).

[53] For *nosZ* expression, a transmembrane Fe-S flavoprotein, NosR (not shown), is also mandatory (Wunsch & Zumft, 2005).

phenotype based on existing knowledge of the regulatory network and enzymology of this organism. First, an overview of the simulated experiments is presented, followed by an introduction of each paper's research problem, model and, finally, the outcome and its implications.

## 6.1. A synopsis of the simulated experiments

***Batch incubation.*** *Pa. denitrificans* (DSM413) was incubated at 20 °C, using 50 mL Sistrom's (1960) medium in 120 mL gas-tight vials. Either succinate or butyrate (5 mM) was used as the main carbon source, enough to secure consumption of all available $e^-$-acceptors. After distribution of the medium, each vial was loaded with a magnetic stirring bar, sterilised through autoclaving, supplemented with 2 mM $KNO_3$ or $KNO_2$, and tightly sealed. To remove $O_2$ and $N_2$ from the headspace, the headspace air was evacuated and replaced by helium through several cycles of evacuation and He-filling (He-washing). Either 0, 1 or 7 headspace-vol.% $O_2$ was injected into the vials, where treatments pragmatically labelled as 0% contained detectable traces of $O_2$. All the vials were then equilibrated at 20 °C while being continuously stirred. Finally, the over-pressure was released, and each vial was inoculated with aerobically grown cells.

***Gas measurement.*** $O_2$ injected into the headspace diffused to the aqueous-phase, where it was consumed for aerobic respiration before the cells initiated denitrification. Gases diffused to the headspace, where $CO_2$, $O_2$, NO, $N_2O$, and $N_2$ were monitored by frequent sampling. For sampling of the headspace, an automated incubation system was used (see Molstad, Dörsch, & Bakken, 2007). The system sequentially takes samples through the rubber septa of the incubation vials, which were constantly stirred while being placed in a thermostatic water bath at 20 °C. The auto-sampler, connected to a gas chromatograph (GC) and a NO analyser, performs peristaltic pumping that removes a fraction of all headspace gases (3–3.4%) and replaces that fraction by an equal amount of He by reversing the pumping. The reverse pumping helps maintain ~1 atm pressure inside the vials. Each sampling also results in a marginal leakage of $O_2$ and $N_2$ through tubing and membranes of the injection system.

***$NO_2^-$ measurement*** *(Paper III).* To extract samples for measuring $NO_2^-$ without tampering the original vials, identical (parallel) vials were prepared for each treatment. Using sterile

syringes, samples of 0.1 mL were regularly drawn from the aqueous-phase of the parallel vials. From each extracted sample, 0.001 mL was injected into a vessel containing acetic acid with 1 vol.% sodium iodide, which converted the sampled $NO_2^-$ to NO. Using $N_2$, the NO produced was pumped from the vessel into a NO analyser, enabling us to infer the initial $NO_2^-$ concentration.

## 6.2. Research problems, modelling, and the outcome

By modelling, we explored the regulation of **1)** NirS (controlling the $NO_2^-$- and $N_2$ kinetics[54]), **2)** NirS/*c*Nor (homeostatic control of NO by *Pa. denitrificans*), **3)** Nar, and **4)** *c*Nor/NosZ ($N_2O$ kinetics). The first two are the subject of Paper I & II, respectively, and the last two are addressed in Paper III. We started with a simple model for Paper I and further developed it to address more specialised problems in Papers II & III. Each model simulates the respiratory metabolism ($O_2$ reduction followed by that of $NO_x^-$/$NO_x$), growth, and gas transport between the aqueous-phase and the headspace. The models also include estimation of gas loss and leaks due to sampling, so as to allow a direct comparison between experimental data and model simulations. The models use the Michaelis-Menten kinetics to simulate the activity of the reductases involved, except that in Models II & III the cooperative binding of the two NO molecules with *c*Nor to form $N_2O$ is modelled by an equation developed by Girsch & de Vries (1997, pp. 210-211). All model parameters critical for our research questions were empirically determined under the same or similar experimental conditions as simulated. Each model is constructed in Vensim® DSS 6.2 Double Precision[55] using techniques from the field of system dynamics (see Hannon & Ruth, 2014).

### PAPER I

#### 6.2.1. In response to anoxia, do all cells in batch cultures switch to denitrification?

***General assumption that the entire population switches to denitrification challenged by recent experiments.*** It is commonly assumed that in response to $O_2$ deprivation, all cells in a

[54] $N_2$ kinetics are controlled by NirS since, at least in *Pa. denitrificans*, $NO_2^-$ reduction is the rate-determining step in the denitrification pathway.

[55] Ventana Systems inc., http://vensim.com/

culture will switch to denitrification. But in recent batch culture experiments with *Pa. denitrificans*, as the cells transited from oxic to anoxic conditions, a severe depression was observed in the total $e^-$-flow rate (i.e., to $O_2$ + $NO_x^-$/$NO_x$) even in the presence of ample $NO_3^-$ or $NO_2^-$ (Bergaust et al., 2011, pp. 208-210; Bergaust et al., 2010, p. 6394; Nadeem, Dörsch, & Bakken, 2013, pp. 5-7). This was taken to indicate that a large fraction of the population did not switch to denitrification; otherwise, the total $e^-$-flow rate would have carried on increasing as $NO_x^-$/$NO_x$ replaced $O_2$ as the terminal $e^-$-acceptor. The depression was followed by an exponential increase in the $e^-$-flow rate, which was tentatively ascribed to anaerobic growth of a small fraction recruited to denitrification ($F_{den}$).

***Need of modelling.*** In the aforementioned empirical studies, the $e^-$-flow rate and $F_{den}$ were inferred from rates of consumption and production of gases ($O_2$, $NO_x$, and $N_2$), and a clear hypothesis as to the underlying cause of the low $F_{den}$ was also lacking. To fill these gaps, we formulated a refined hypothesis, addressing the regulatory mechanism responsible for cell diversification in response to $O_2$ depletion. On its basis, we constructed a dynamic model and explicitly simulated the kinetics of recruitment of cells to denitrification.

***Hypothesis.*** According to the formulated hypothesis, the low $F_{den}$ is due to a low probability of initiating *nirS* transcription, which in response to anoxia is possibly mediated through a minute pool of intact NNR, crosstalk with other factors (such as FnrP), unspecific reduction of $NO_2^-$ to NO by Nar, and/or through non-biologically formed traces of NO found in a $NO_2^-$-supplemented medium. Regardless of the exact mechanism(s), once *nirS* transcription is initiated, the positive feedback via NO-NNR (Fig. 4, see $P_2$) would allow the product of a single transcript of *nirS* to induce a subsequent burst of *nirS* transcription. The activated positive feedback will also help induce *nor* and *nosZ* transcription via NNR, facilitating the synthesis of a full-fledged denitrification proteome. We further hypothesised that such stochastic recruitment to denitrification will only be possible as long as a minimum of $O_2$ is available because, since *Pa. denitrificans* is non-fermentative, the synthesis of first molecules of NirS will depend on energy from aerobic respiration.

***Modelling.*** The above hypothesis is modelled by segregating the culture into two pools (subpopulations): one for the cells without and the other with denitrification enzymes ($N_{D-}$ & $N_{D+}$, respectively, see Fig. 5). Both are assumed to equally consume $O_2$ (if present), but

only $N_{D+}$ reduces $NO_2^-$ to $N_2$. Initially, only the $N_{D-}$ cells were present (inoculum), which grew by consuming $O_2$. As $O_2$ was depleted below a certain threshold, recruitment of the cells from $N_{D-}$ to $N_{D+}$ initiated as $N_{D-} \times r_{den}(O_2)$ (cells $h^{-1}$). $r_{den}(O_2)$ is a constant probability ($h^{-1}$) of initiating *nirS* transcription, triggering as $O_2$ is consumed below a critical threshold (empirically determined) and reinstating to zero as $O_2$ is completely exhausted (assuming the energy limitation for protein synthesis). Hence, the function assumes a limited time-window available for the recruitment to denitrification.

The recruitment is modelled ignoring the time-lag from the initiation of gene transcription till the cell is fully equipped with denitrification enzymes. That is because the lag observed between the emergence of denitrification gene transcripts and the subsequent gas products suggests that the synthesis of denitrification proteome takes less than half an hour (Bergaust et al., 2010; Qu et al., 2014), which is negligible for the purpose of this and the subsequent models (presented in Figs. 6 and 7).

***Outcome and implications.*** With a specific probability of recruitment to denitrification = 0.005 $h^{-1}$, the model robustly simulated the observed $N_2$ kinetics for a range of culture conditions (Bergaust et al., 2010), with the resulting fraction recruited to denitrification ($F_{den}$) = 3.8–16.1% (average = 8.2%). In contrast, as we forced our model to achieve $F_{den}$ = 100% within an hour, the simulated $N_2$ accumulation grossly overestimated that measured.

The phenomenon can be understood as a 'bet-hedging' regulation 'strategy' (Veening et al., 2008): the fraction switching to denitrification benefits if the anoxic spell is long-lasting and $NO_x^-/NO_x$ remains available, whereas the non-switching fraction benefits, by saving the energy required for producing denitrification proteome if the anoxic spell is short. The strategy has important implications for understanding the physiology of denitrification in general and that of *Pa. denitrificans* in particular and, not the least, for correctly interpreting various experiments on *Pa. denitrificans* and other denitrifying organisms (such as *Pseudomonas denitrificans*, see Paper I for details).

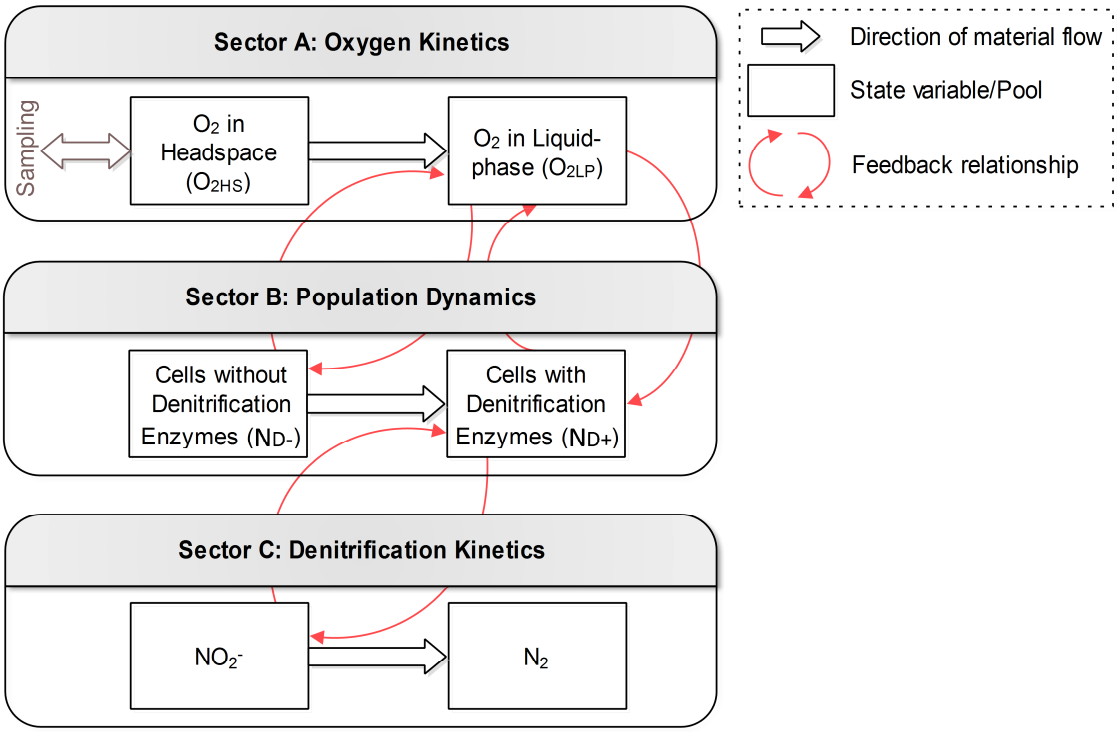


**Fig. 5. An overview of Model I.** *Initial Conditions.* $O_{2HS}$: 0, 1, or 7 headspace-vol.% (model units: mol); $N_{D-}$: inoculum (model units: cells); $NO_2^-$: 0.2, 1, or 2 mM (model units: mol). **A. $O_2$ Kinetics:** Transport of $O_2$ between the headspace and liquid is modelled as $k_t \times (K_{H(O_2)} \times P_{O_2} - [O_2]_{LP})$, where $k_t$ (L $h^{-1}$) is an empirically determined transport coefficient, $K_{H(O_2)}$ (mol $L^{-1}$ $atm^{-1}$) the solubility, $P_{O_2}$ (atm) the partial pressure in the headspace, and $[O_2]_{LP}$ (mol $L^{-1}$) is the $O_2$ concentration in the liquid-phase. The reduction of $O_{2LP}$ (mol $h^{-1}$) is modelled as a function of all cells ($N_{D-} + N_{D+}$) and a cell-specific velocity of $O_2$ reduction ($v_{O_2}$, mol $O_2$ $cell^{-1}$ $h^{-1}$), where $v_{O_2}$ is calculated as a Michaelis-Menten function of $[O_2]_{LP}$ with an empirically determined $v_{max}$ and an estimated $K_m$. Net effect of sampling (dilution and leakage) is included in the simulation of $O_{2HS}$ at the reported sampling times. **B. Population Dynamics:** Initially, $N_{D-}$ grows according to an empirically determined cell yield per mol $O_2$. As $[O_2]_{LP}$ is depleted below a certain threshold, $N_{D-}$ initiates recruitment to the pool of denitrifying cells ($N_{D+}$) with a constant specific probability ($h^{-1}$), and the recruitment continues until $O_2$ is exhausted (see the text for the underlying hypotheses). $N_{D-}$ grows by reducing $NO_2^-$ according to an empirically determined cell yield per mol $NO_2^-$ **C. Denitrification kinetics:** The reduction of $NO_2^-$ to $N_2$ (mol $h^{-1}$) is modelled as a product of $N_{D+}$ and a cell-specific velocity of $NO_2^-$ reduction ($v_{NO_2^-}$, mol $NO_2^-$ $cell^{-1}$ $h^{-1}$), where $v_{NO_2^-}$ is simulated as a Michaelis-Menten function of $[NO_2^-]$ with an empirically determined $v_{max}$ (mol $cell^{-1}$ $h^{-1}$) and a literature-based $K_m$.

**P A P E R  II**

### 6.2.2. How do denitrifying bacteria, like *Pa. denitrificans*, maintain homeostatic control of NO at nanomolar concentrations?

***Diverse phenotypes regarding NO emission.*** Denitrifying bacteria show diverse phenotypes with regard to NO production: *Agrobacterium tumefaciens* and strains within the genus *Bradyrhizobium* may produce detrimentally high (µM) NO concentrations when grown as pure cultures (Bergaust, Shapleigh, Frostegård, & Bakken, 2008; K. W. Jillo et al., unpublished, respectively). In contrast, the model organism *Paracoccus denitrificans* and various strains within the genus *Thauera* demonstrate a robust homeostatic control of NO ($[NO]_{ss}$) at *nM* concentrations (Bergaust et al., 2010; B. Liu et al., 2013, respectively). Thus, some denitrifiers have evolved the ability to restrict NO to extremely low concentrations, while others are clearly at risk of killing themselves by NO toxicity when grown in pure cultures.

***Discrepancy in the current understanding.*** Homeostatic control of NO would require a coordinated expression of *nir* and *nor* (van Spanning et al., 2007). Current understanding of the regulatory network of denitrification in *Pa. denitrificans* does indicate such a coordination, i.e., *nirS* and *nor* transcription via a common regulator, NNR (Fig. 4). But we were not convinced that this alone could explain the observed homeostasis of NO at nM levels because the reported half saturation constants ($K_m$) for *c*Nor are too high, i.e., in the µM range. This led us to consider a hypothesis that the homeostasis could be due to a negative feedback of NO on the activity of NirS (Kuňák, Kučera, & van Spanning, 2004). To explore this option and improve our overall understanding of the homeostatic control, we constructed a model and simulated the NO kinetics observed in batch cultures of *Pa. denitrificans* (Bergaust et al., 2010).

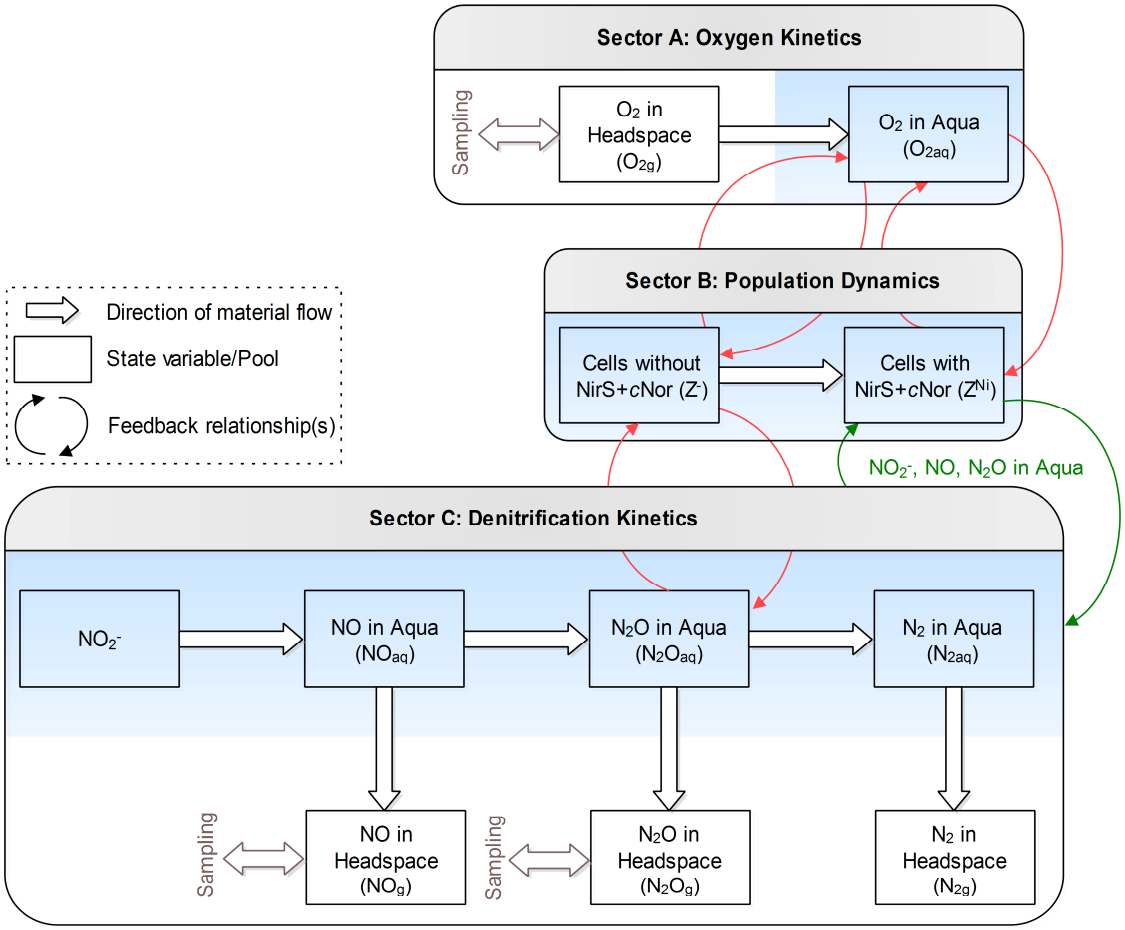


**Fig. 6. An overview of Model II.** *Initial Conditions.* $O_{2_g}$: 0, 1, or 7 headspace vol.% (model units: mol); $Z^{-}$: inoculum (model units: cells); $NO_2^-$: 0.2, 1, or 2 mM (model units: mol). The model is an extension of Model I (Fig. 5), with NO and $N_2O$ kinetics explicitly simulated here (Sector **C**). Like for $O_2$ in Model I, the transport of each gas between the aqueous-phase ($X_{aq}$) and headspace ($X_g$) along with the headspace sampling-losses are included (Sectors **A** and **C**). In Sector **B**, $Z^{-}$ & $Z^{Ni}$ are the counterparts of the Model I's sub-populations $N_{D-}$ & $N_{D+}$, respectively. Like in Model I, $Z^{-}$ first grows by aerobic respiration, but as $O_2$ is depleted below a critical concentration, the recruitment to $Z^{Ni}$ is initiated according to a low probabilistic function. The function represents the stochastic transcriptional activation of *nirS*, leading to the autocatalytic production of NirS and a coordinated expression of *nor* (Fig. 4). Once triggered, the recruitment continues as long as a minimum of respiratory metabolism is sustained by the $e^-$-flow to the available $e^-$-acceptors ($O_2$ + $N_2O$), assumed to generate a minimum of ATP required for synthesising denitrification enzymes. $N_2O$ is produced by $Z^{Ni}$ only but is assumed to be respired equally by all cells ($Z^{-}$ + $Z^{Ni}$) because the *nosZ* genes are readily expressed by the $O_2$-sensor FnrP (Bergaust et al., 2012) (Fig. 4). In Sector **C**, the

reduction of each $NO_{x_{aq}}$ (molN $h^{-1}$) is modelled as a function of $Z^{Ni}$ (cells) and a cell-specific rate of the individual $NO_{x_{aq}}$ reduction (molN $cell^{-1}$ $h^{-1}$), calculated using the Michaelis-Menten kinetics. However, the cell-specific reduction of $NO_{aq}$ is modelled according to a dual substrate kinetics equation (Girsch & de Vries, 1997) and, as indicated above, the reduction of $N_2O$ to $N_2$ is carried out by all cells ($Z^- + Z^{Ni}$).

***Modelling.*** Model I (Fig. 5) is extended here to incorporate the explicit modelling of the NO and $N_2O$ kinetics (Fig. 6). The reduction of $NO_2^-$ and $N_2O$ is simulated as a function of the cells with the relevant reductase and cell-specific rates of $NO_2^-$/$N_2O$ reduction (molN $cell^{-1}$ $h^{-1}$). The latter are modelled using the Michaelis-Menten kinetics with empirically determined maximum reduction velocities ($v_{max}$, molN $cell^{-1}$ $h^{-1}$), and a reported and an estimated half-saturation constant ($K_m$, mol $L^{-1}$) for $NO_2^-$- and $N_2O$ reduction, respectively. In the version of the model with a negative feedback by NO on NirS activity, the cell specific reduction of $NO_2^-$ is modelled using the Michaelis-Menten kinetics for non-competitive inhibition. As for NO, since two molecules participate in the production of $N_2O$, the cell-specific NO reduction is modelled according to a dual substrate kinetics equation (Girsch & de Vries, 1997):

$$v_{\mathrm{NO}} = \frac{v_{max\mathrm{NO}}}{1 + \mathrm{K}_{2\mathrm{NO}}\left(\frac{1}{[\mathrm{NO}]_{\mathrm{aq}}} + \frac{\mathrm{K}_{1\mathrm{NO}}}{[\mathrm{NO}]_{\mathrm{aq}}^2}\right)}$$

where $v_{max\mathrm{NO}}$ (mol $cell^{-1}$ $h^{-1}$) is the maximum velocity of NO reduction, $[\mathrm{NO}]_{\mathrm{aq}}$ (mol $L^{-1}$) is the NO concentration in the aqueous-phase, and $K_{1NO}$ & $K_{2NO}$ (mol $L^{-1}$) are the steady state dissociation constants for the binding of two NO molecules to *c*Nor.

***Outcome and implications.*** For the NO kinetics, critical parameters are the maximum velocities of $NO_2^-$ and NO reduction ($v_{max\mathrm{NO_2^-}}$ and $v_{max\mathrm{NO}}$)[56] and the two dissociation constants for *c*Nor ($K_{1NO}$ & $K_{2NO}$), determining the effective affinity for NO. $v_{max\mathrm{NO_2^-}}$ is estimated as 1.83 fmol $cell^{-1}$ $h^{-1}$, deduced from the empirically determined anaerobic growth rate (= 0.106 $h^{-1}$) and yield (= $5.79\times10^{13}$ cells $mol^{-1}$ $NO_2^-$) (Bergaust et al., 2010). Regarding

[56] Note that $v_{max\mathrm{NO_x}}$ (molN $cell^{-1}$ $h^{-1}$) = $ve^-_{max\mathrm{NO_x}}$ (mol electrons $cell^{-1}$ $h^{-1}$), since 1 $\frac{\mathrm{molN\ NO_x}}{\mathrm{mol\ e^-}}$, where $NO_x$ is $NO_2^-$, NO, and $N_2O$.

$v_{max\mathrm{NO}}$, however, no estimates were available. Unless assuming unrealistically high $v_{max\mathrm{NO}}$ or values for substrate-*c*Nor affinities ($K_{1\mathrm{NO}}$ & $K_{2\mathrm{NO}}$) much lower than reported in the literature, the model predicted $[\mathrm{NO}]_{ss}$ (the steady state [NO] in the liquid) much higher than that measured. Negative feedback by NO on NirS activity could effectively bring the predicted $[\mathrm{NO}]_{ss}$ down, but resulted in a much too slow anaerobic growth rate (hence, too slow $N_2$ production). We suspected that the reason for the failure of the model could be that the true substrate affinity of *c*Nor is much higher than commonly reported in the literature, where many parameters are based on *in vitro* measurements. We investigated this in detail by activity measurements *in vivo*, using chemiluminescence-based detection of NO in the headspace of anoxic batch cultures. The measurements were conducted with very low cell density to minimise headspace–liquid transport limitations, and the molecular diffusion from the bulk liquid to the cell surface was taken into account to calculate [NO] at the cell surface. With the new kinetic parameters for *c*Nor, $v_{max\mathrm{NO}}$ = $3.56\times10^{-15}$ mol cell$^{-1}$ h$^{-1}$, $K_{1\mathrm{NO}}$< 1 nM, and $K_{2\mathrm{NO}}$ = 34 nM, the model is able to simulate $[\mathrm{NO}]_{ss}$ in reasonable agreement with the measurements.[57]

Thus, the observed NO homeostasis can be understood as a result of simple enzyme kinetics, without any feedback inhibition. Such determinations of enzyme kinetic parameters *in vivo* appears essential to understand denitrification phenotypes and to adequately model the NO kinetics in soils and aquatic environments.

## PAPER III

Recently, a neat dataset was generated from $NO_3^-$-supplemented batch incubations of *Pa. denitrificans*, with frequently measured $NO_2^-$ and $N_2O$ (Qu et al., 2014). In the data-set previously available for comparison with simulations (Bergaust et al., 2010), the $NO_2^-$ kinetics were not measured, and $N_2O$ was measured by a thermal conductivity detector with a rather high detection limit. Qu et al. (2014), however, measured $N_2O$ by an electron capture detector, providing accurate measurements at very low concentrations. That encouraged us to extend Model II and simulate the cell diversification during transition from oxic to anoxic conditions,

[57] $v_{max\mathrm{NO}_2^-}$ was also empirically re-estimated, corroborating the value estimated by Bergaust et al. (2010) (= 1.83 fmol $NO_2^-$ cell$^{-1}$ h$^{-1}$).

focusing on the regulation of Nar ($NO_2^-$ production) (6.2.3) and *c*Nor/NosZ ($N_2O$ emission) (6.2.4).

### 6.2.3. Like for *nirS*, can the expression of *nar* be explained as an autocatalytic phenomenon in *Pa. denitrificans*, with a stochastic initiation of *nar* transcription?

It is commonly assumed that all cells in a batch culture produce Nar in response to impending anoxia. We investigated this by exploring whether, like for *nirS*, the initiation of *nar* transcription could also be explained as a probabilistic phenomenon. If so, we were interested to estimate what fraction of the cells is required to adequately simulate the measured $NO_2^-$ production.

***Modelling.*** To answer this question, we split the incubated population into four subpopulations (Fig. 7B):

1. $Z^-$: cells without Nar & NirS+*c*Nor
2. $Z^{Na}$: cells with Nar
3. $Z^{NaNi}$: cells with Nar & NirS+*c*Nor
4. $Z^{Ni}$: cells with NirS+*c*Nor

All the subpopulations are assumed to scavenge $O_2$ (if available) and produce NosZ likewise in response to impending anoxia. The latter because the *nosZ* genes are equally induced by NNR or FnrP (Bergaust et al., 2012), where, at least, FnrP is readily activated in response to $O_2$ depletion (van Spanning et al., 2007). $Z^-$ (Fig. 7) contains the inoculum that grows by aerobic respiration. As $[O_2]$ falls below a critical threshold (empirically determined, Qu et al., 2014, Paper IV), the cells within $Z^-$ are assumed to start synthesising Nar with a rate described by a probabilistic function: $Z^- \times r_{Na}(O_2, N_2O)$, where the second term is a constant conditional probability ($h^{-1}$), assumed to be that of the transcriptional activation of *nar*, quickly differentiating a cell into a full-fledge $NO_3^-$ scavenger through product ($NO_2^-$) induced transcription via NarR (Fig. 4, see $P_1$). $r_{Na}(O_2, N_2O)$ triggers when $[O_2]_{aq} < [O_2]_{na}$ **AND** $[ve_{O_2}^- + (0.5 \times ve_{N_2O}^-)] > ve_{min}^-$, where the first condition represents the depletion of $[O_2]$ in the aqueous-phase below a critical threshold ($[O_2]_{na}$), empirically determined as the $[O_2]_{aq}$ at the outset of $NO_2^-$ accumulation (Qu et al., 2014). The second condition is the velocity of

$e^-$-flow to $O_2$ + $N_2O$ (the two terminal $e^-$-acceptors $Z^-$ can utilise) above a critical minimum ($ve^-_{min}$). That is because the energy required to produce Nar is assumed to depend on a minimum of functional respiratory metabolism. $ve^-_{N_2O}$ in this comparison is weighted down by half because mole ATP per mole $e^-$ transferred to $NO_x^-$/$NO_x$ is lower for denitrification than for aerobic respiration (Bergaust et al., 2010; van Spanning et al., 2007).

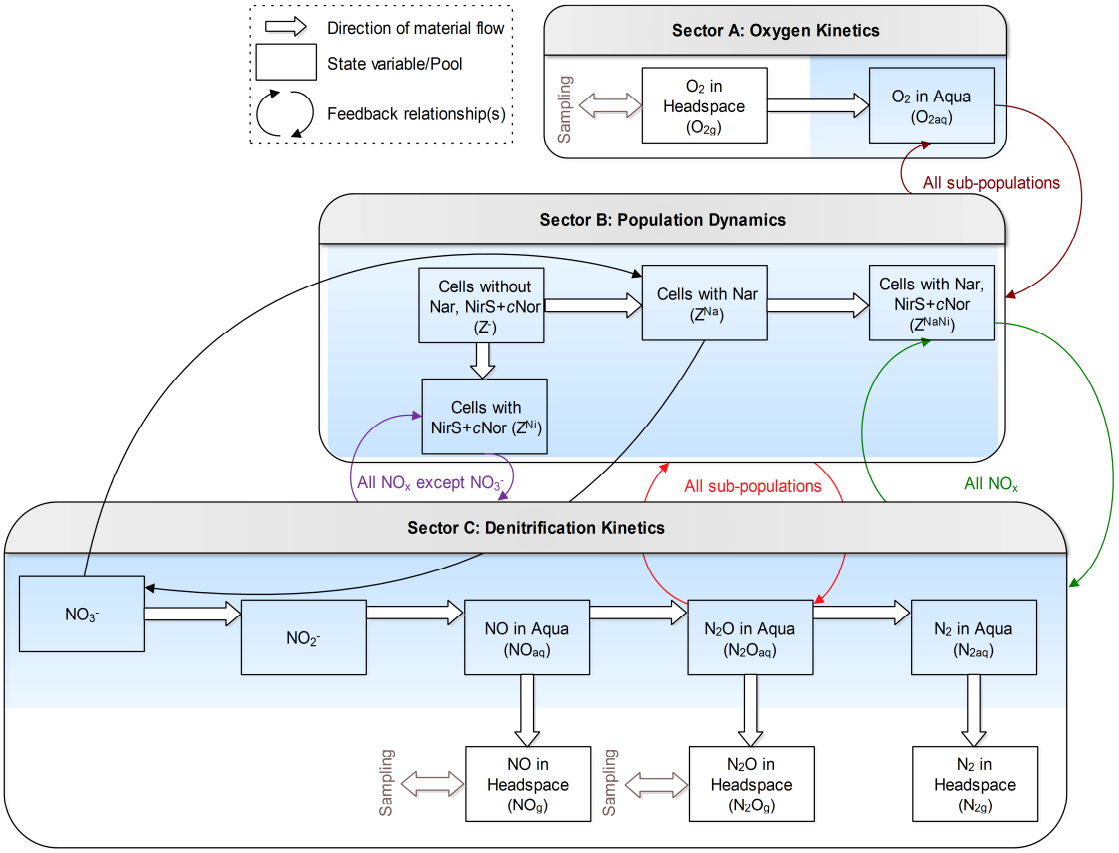


**Fig. 7. An overview of Model III.** *Initial Conditions.* $O_{2_g}$: 0 or 7 headspace-vol.% (model units: mol); $Z^-$: inoculum (model units: cells); $NO_3^-$: 2 mM (model units: mol). **A. $O_2$ Kinetics:** Transport of $O_2$ between the headspace ($O_{2_g}$) and aqueous-phase ($O_{2_{aq}}$) is modelled as in Model I (Fig. 5), and the reduction of $O_{2_{aq}}$ (mol $h^{-1}$) is modelled as a function of all cells ($Z^- + Z^{Na} + Z^{NaNi} + Z^{Ni}$) and a Michaelis-Menten based cell-specific rate of $O_2$ consumption (mol $cell^{-1}$ $h^{-1}$). Net effect of sampling (dilution and leakage) is included in the simulation of $O_{2_g}$. **B. Population Dynamics:** $Z^-$ contains the inoculum that grows according to an empirically estimated cell yield per mol $O_2$. As $[O_2]_{aq}$ is depleted below a certain threshold (empirically determined), $Z^-$ initiates recruitment to the pool of cells with Nar ($Z^{Na}$) with a constant specific-probability ($h^{-1}$, assumed to be that of the transcriptional activation

of *nar*). The recruitment continues as long as the velocity of $e^-$-flow to $O_2$ + $N_2O$ (the two terminal $e^-$-acceptors accessible to $Z^-$) remains above a critical minimum (assumed to sustain a minimum respiratory metabolism to provide energy for Nar production). Next, as $[O_2]_{aq}$ is further depleted below another critical concentration (empirically determined), the cells within $Z^{Na}$ and $Z^-$ are recruited to $Z^{NaNi}$ and $Z^{Ni}$, respectively, as they are assumed to stochastically initiate *nirS* transcription (paving the way for NO-NNR mediated expression of *nirS*+*nor*, Fig. 4). The recruitment to $Z^{NaNi}$ & $Z^{Ni}$ continues as long as a minimum of $e^-$-flow to the relevant terminal $e^-$-acceptor is possible, sustaining the respiratory metabolism to generate ATP for protein synthesis. After bulk of $O_2$ is depleted by $Z^-$, the cells within $Z^-$ (with NosZ), $Z^{Na}$ (with Nar & NosZ), $Z^{NaNi}$ (with Nar, NirS+*c*Nor & NosZ), and $Z^{Ni}$ (with NirS+*c*Nor & NosZ) grow by reducing the relevant $NO_x^-$/$NO_x$ according to an empirically determined cell yield per mol of $e^-$-flow to $NO_x^-$/$NO_x$. **C. Denitrification kinetics:** The reduction of each $NO_x^-$/$NO_x$ in aqua is modelled as a function of the relevant sup-population(s) and a per-cell $NO_x^-$/$NO_x$ consumption rate (molN $cell^{-1}$ $h^{-1}$), calculated using the Michaelis-Menten kinetics. However, as in Model II, the cell-specific reduction of NO is modelled according to Girsch & de Vries (1997). Like for $O_2$, the aqua/headspace transport of each gas and the headspace dilution (due to sampling) are taken into account.

***Outcome and implications.*** The $NO_2^-$ data of Qu et al. (2014, Paper IV), with various culture conditions, are adequately simulated by assuming a stochastic transcriptional activation of *nar* with an average probability = 0.035 $h^{-1}$, resulting in 23–43.3% of all cells with Nar. In contrast, simulations assuming ~100% of the population producing Nar within an hour grossly overestimate the measured $NO_2^-$ accumulation. Thus, our model corroborates the hypothesis that *nar* expression is autocatalytic in *Pa. denitrificans* with a low probability of transcriptional activation, albeit much higher than that for the transcriptional activation of *nirS* (0.004 $h^{-1}$, see Sec. 6.2.4).

The findings are important for understanding the regulation of denitrification in bacteria: product-induced transcription of denitrification genes is common (van Spanning et al., 2007, p. 15); thus, we surmise that diversification in response to anoxia is widespread.

### 6.2.4. Can $N_2O$ kinetics be explained by assuming $N_2O$ production by a sub-population but equal consumption by the entire population?

The aim was to explore whether the measured $N_2O$ kinetics could be explained assuming $N_2O$ production by $Z^{NaNi}$ (cells with Nar & NirS+*c*Nor) and $Z^{Ni}$ (cells with NirS+*c*Nor) but consumption by the entire population ($Z^- + Z^{Na} + Z^{NaNi} + Z^{Ni}$, Fig. 7), as suggested by Bergaust et al. (2011; 2010; 2012).

***Modelling.*** NirS+*c*Nor production (recruitment to $Z^{NaNi}$ & $Z^{Ni}$) is assumed to be **a)** coordinated because the transcription of both *nirS* and *nor* is induced by NO via the NO-sensor NNR (Fig. 4) and **b)** stochastic because the initial transcription of *nirS* (paving the way for the autocatalytic- and substrate-induced expression of NirS and *c*Nor, respectively) happens in the absence of NO or at too low [NO] to be sensed by NNR. Following these assumptions, the recruitments from $Z^{Na}$ to $Z^{NaNi}$ and from $Z^-$ to $Z^{Ni}$ are modelled as $Z^X \times r_{Ni}(O_2, NO_x)$, where $Z^X$ represents $Z^{Na}$ or $Z^-$, and $r_{Ni}(O_2, NO_x)$ is a constant conditional probability ($h^{-1}$, assumed to be that of transcriptional activation of *nirS*). $r_{Ni}(O_2, NO_x)$ triggers when $[O_2]_{aq} < [O_2]_{ni}$ **AND** $[ve^-_{O_2} + (0.5 \times ve^-_{NO_x})] > ve^-_{min}$, where the first condition represents the depletion of $[O_2]$ in the liquid below a critical threshold ($[O_2]_{ni}$), empirically determined as the $[O_2]_{aq}$ at the outset of NO accumulation (Qu et al., 2014). The second condition is the velocity of $e^-$-flow to $O_2$ and the relevant $NO_x^-/NO_x$ (for $Z^{Na}$: $NO_3^-$ & $N_2O$ and for $Z^-$: $N_2O$) above a critical minimum ($ve^-_{min}$), assumed to keep a minimum respiratory metabolism intact to provide energy for protein synthesis.

***Outcome and implications.*** The empirical data of Qu et al. (2014) ($NO_2^-$ depletion and $N_2$ production) are effectively simulated by assuming a very low probabilistic transcriptional-activation of *nirS* (= 0.004 $h^{-1}$), resulting in the recruitment of 7.7–22.1% of all cells to $Z^{NaNi}$ & $Z^{Ni}$ (i.e., the pools of NirS+*c*Nor positive cells, Fig. 7). The result corroborates the findings of Paper I, where we amply simulated Bergaust et al.'s (2010) experiments, assuming a similarly low probability of *nirS* transcription.

Assuming that 7.7–22.1% of the population producing $N_2O$ whereas the entire population equally consuming it, our model neatly simulates the peculiar shape of the measured $N_2O$ kinetics: **1)** abrupt initial accumulation to very low levels due to the recruitment of relatively

small numbers to the $N_2O$ producing pools ($Z^{NaNi}$ & $Z^{Ni}$) and **2)** increasing $N_2O$ concentration due to the recruitment and faster cell-specific growth of $Z^{NaNi} + Z^{Ni}$ (reducing $NO_2^-$, NO, and $N_2O$) than that of $N_2O$ consumers ($Z^- + Z^{Na} + Z^{NaNi} + Z^{Ni}$ with $N_2O$ being the only available $e^-$-acceptor for the majority: $Z^- + Z^{Na}$). On the other hand, if the model is simulated assuming that only the $N_2O$ producers ($Z^{NaNi}$ & $Z^{Ni}$) are able to consume it, the predicted $N_2O$ shows a quasi-equilibrium throughout the entire anoxic phase, which contradicts the available data. No parameterisation could force the model to reproduce the observed $N_2O$ kinetics other than the differential expression of *nirS+nor* and *nosZ.*

The modelling exercise sheds some light on the possible role of the regulatory biology of denitrification in controlling $N_2O$ emissions. If all cells in soils had the same regulatory phenotype as *Pa. denitrificans*, their emissions of $N_2O$ would probably be miniscule, and soils could easily become strong net sinks for $N_2O$ because the majority of cells would be 'truncated denitrifiers' with only $N_2O$ reductase expressed. It remains to be tested, however, if the regulatory phenotype of *Pa. denitrificans* is a rare or a common phenomenon among full-fledged denitrifiers. We foresee that further exploration of denitrification phenotypes will unravel a plethora of response patterns.

## 7. Concluding remarks

Models can only provide hypothetical explanations to observed phenomena or reasons to reject hypotheses/assumptions, if there is a notorious discrepancy between model and observations. Thus, the model exercises here provide strong reasons to reject the common assumption that all cells in a culture of *Pa. denitrificans* switch to denitrification in response to impending anoxia. A new hypothesis of cell diversification, based on the stochastic initiation of *nar* and *nirS* transcription, was built into the model, enabling it to robustly simulate $NO_2^-$, $N_2O$, and $N_2$ kinetics for a range of experimental conditions. This agreement between the simulations and observations is no proof for the validity of the model but simply a demonstration that we have no reasons to reject it. Verification is clearly needed by novel experiments that put the core assumptions to a stringent test. Measurement of Nar and NirS in single cells within a population would be one such approach; such experiments are in the making by the NMBU Nitrogen Group.

*Pa. denitrificans* is a model organism, used extensively for studying bioenergetics and regulatory biology of denitrification. Although originally isolated from soil, the organism is an unlikely representative for the denitrifying microbes in soils. Thus, phenomena observed in *Pa. denitrificans* cannot directly be projected onto natural ecosystems to explain observations therein. Nevertheless, model organisms represent a 'fast track' to new concepts and hypotheses, and experiments with model organisms can be much more stringent than those with natural populations. A good example is the studies regarding the effect of soil pH on $N_2O$ emission. More than 50 years of research with intact soils provided not more than a correlation (increasing $\frac{N_2O}{N_2}$ product ratio at low pH), whereas the experiments with *Pa. denitrificans* (Bergaust et al., 2010) indicated the mechanism involved, i.e., post translatoric problems with the assembly of Nos in the periplasm. Based on this, careful experiments with bacteria extracted from soils demonstrated the same phenomenon (Binbin Liu et al., 2014). Much biochemical research is needed to fully understand how low pH interferes with the making of Nos, and model organisms are expected to be our guides in this journey.

The present thesis provides a hypothetical explanation to the observed denitrification kinetics in *Pa. denitrificans*, and the kneejerk reaction of many microbial ecologists would be that this lacks ecological relevance. This may be true, if relevance is taken to depend on direct extrapolations. In fact, we do not know to which extent indigenous denitrifying prokaryotes display similar regulatory responses and apparent cell diversification as *Pa. denitrificans*. But it is worth a study, since it could have major implications for the interpretation of ecological observations. Microbial ecological research on denitrification and $N_2O$ emission is dominated by 'correlation research'; 'phenotypic phenomena' such as variations in denitrification and $N_2O$ emissions are tentatively explained by correlations with the denitrification community composition and the number of functional genes and their transcripts (a recent example is Jones et al., 2014). The present model-based analyses of *Pa. denitrificans* serves as a cautionary tale: a population of potentially full-fledged denitrifiers (such as *Pa. denitrificans*) may in reality be dominated by cells whose only denitrification enzyme is $N_2O$ reductase.

## References

Almeida, J. S., Reis, M. A. M., & Carrondo, M. J. T. (1997). A unifying kinetic model of denitrification. *J Theor Biol, 186*(2), 241-249.

Arasimowicz-Jelonek, M., & Floryszak-Wieczorek, J. (2013). Nitric oxide: an effective weapon of the plant or the pathogen? *Mol Plant Pathol, 15*(4), 406-416.

Baggs, E. M., Smales, C. L., & Bateman, E. J. (2010). Changing pH shifts the microbial source as well as the magnitude of $N_2O$ emission from soil. *Biol Fertil Soils, 46793-805* (8), 793-805.

Bakken, L. R., Bergaust, L., Liu, B., & Frostegård, Å. (2012). Regulation of denitrification at the cellular level – a clue to understanding of $N_2O$ emissions from soils. *Philos Trans R Soc Lond B Biol Sci, 367*, 1226-1234.

Bakken, L. R., & Dörsch, P. (2007). Nitrous oxide emission and global changes: modelling approaches. In H. Bothe, S. J. Ferguson & W. E. Newton (Eds.), *Biology of the Nitrogen Cycle* (pp. 382-395). Amsterdam: Elsevier B. V.

Bergaust, L., Bakken, L. R., & Frostegård, Å. (2011). Denitrification regulatory phenotype, a new term for the characterization of denitrifying bacteria. *Biochem Soc Trans, 39*, 207-212.

Bergaust, L., Mao, Y., Bakken, L. R., & Frostegård, Å. (2010). Denitrification response patterns during the transition to anoxic respiration and posttranscriptional effects of suboptimal pH on nitrogen oxide reductase in *Paracoccus denitrificans*. *Appl Environ Microbiol, 76*(19), 6387-6396.

Bergaust, L., Shapleigh, J., Frostegård, Å., & Bakken, L. R. (2008). Transcription and activities of $NO_x$ reductases in *Agrobacterium tumefaciens*: the influence of nitrate, nitrite and oxygen availability. *Environ Microbiol, 10*(11), 3070-3081.

Bergaust, L., van Spanning, R. J. M., Frostegård, Å., & Bakken, L. R. (2012). Expression of nitrous oxide reductase in *Paracoccus denitrificans* is regulated by oxygen and nitric oxide through FnrP and NNR. *Microbiology 158*, 826-834.

Berks, B. C., Ferguson, S. J., Moir, J. W. B., & Richardson, D. J. (1995). Enzymes and associated electron transport systems that catalyse the respiratory reduction of nitrogen oxides and oxyanions. *Biochim Biophys Acta, 1232*, 97-173.

Bertrand, J.-C., Bonin, P., Caumette, P., Gattuso, J.-P., Grégori, G., Guyoneaud, R., . . . Poly, F. (2015). Biogeochemical cycles In J.-C. Bertrand, P. Caumette, P. Lebaron, R. Matheron, P. Normand & T. Sime-Ngando (Eds.), *Environmental Microbiology: Fundamentals and Applications: Microbial Ecology*. Dordrecht: Springer.

Betlach, M. R., & Tiedje, J. M. (1981). Kinetic explanation for accumulation of nitrite, nitric oxide, and nitrous oxide during bacterial denitrification. *Appl Environ Microbiol, 42*(6), 1074-1084.

Blomberg, M. R. A., & Siegbahn, P. E. M. (2013). Why is the reduction of NO in cytochrome *c* dependent nitric oxide reductase (*c*NOR) not electrogenic? *Biochim Biophys Acta, 1827*, 826-833.

Bouchal, P., Struhárová, I., Budinská, E., Šedo, O., Vyhlídalová, T., Zdráhal, Z., . . . Kučera, I. (2010). Unraveling an FNR based regulatory circuit in *Paracoccus denitrificans* using a proteomics-based approach. *Biochim Biophys Acta, 1804*(6), 1350-1358.

Bruning-Fann, C. S., & Kaneene, J. B. (1993). The effects of nitrate, nitrite, and N-nitroso compounds on animal health. *Vet Hum Toxicol, 35*(3), 237-253.

Bryson Bates, Zbigniew W. Kundzewicz, Shaohong Wu, Nigel Arnell, Virginia Burkett, Petra Döll, . . . Wilbanks, T. (2008). Technical paper on climate change and water. Budapest: Intergovernmental Panel on Climate Change.

Butterbach-Bahl, K., Baggs, E. M., Dannenmann, M., Kiese, R., & Zechmeister-Boltenstern, S. (2013). Nitrous oxide emissions from soils: how well do we understand the processes and their controls? *Philos Trans R Soc Lond B Biol Sci, 368*, 20130122.

Camargo, J. A., Alonso, A., & Salamanca, A. (2005). Nitrate toxicity to aquatic animals: a review with new data for freshwater invertebrates. *Chemosphere, 58*(9), 1255-1267.

Chen, J., & Strous, M. (2013). Denitrification and aerobic respiration, hybrid electron transport chains and co-evolution. *Biochim Biophys Acta, 1827*(2), 136-144.

Clough, T. J., Kelliher, F. M., Sherlock, R. R., & Ford, C. D. (2004). Lime and soil moisture effects in nitrous oxide emissions from a urine patch. *Soil Sci Soc Am J, 68*(5), 1600-1609.

de Gier, J.-W. L., Lübben, M., Reijnders, W. N. M., Tipker, C. A., Slotboom, D.-J., van Spanning, R. J. M., . . . van der Oost, J. (1994). The terminal oxidases of *Paracoccus denitrificans*. *Mol Microbiol, 13*(2), 183-196.

de Gier, J.-W. L., Schepper, M., Reijnders, W. N. M., van Dyck, S. J., Slotboom, D. J., WarneI, A., . . . van der Oost, J. (1996). Structural and functional analysis of $aa_3$-type and $cbb_3$-type cytochrome *c* oxidases of *Paracoccus denitrificans* reveals significant differences in proton-pump design. *Mol Microbiol, 20*(6), 1247-1260.

de Vries, S., Suharti, & Pouvreau, L. A. M. (2007). Nitric oxide reductase: structural variations and catalytic mechanism. In H. Bothe, S. J. Ferguson & W. E. Newton (Eds.), *Biology of the Nitrogen Cycle* (pp. 57-66). Amsterdam: Elsevier B. V.

Deguchi, S., Shimoshige, H., Tsudome, M., Mukai, S.-a., Corkery, R. W., Ito, S., & Horikoshi, K. (2011). Microbial growth at hyperaccelerations up to 403,627 × *g*. *Proc Natl Acad Sci U S A, 108*(19), 7997-8002. doi: 10.1073/pnas.1018027108.

EPA, U. (2011). Ozone - good up high bad nearby. Retrieved June 2, 2014, 2014, from http://www.epa.gov/oar/oaqps/gooduphigh/bad.html

EPA, U. (2014). Basic information about nitrate in drinking water. Retrieved June 2, 2014, 2014, from http://water.epa.gov/drink/contaminants/basicinformation/nitrate.cfm

Forte, E., Urbani, A., Saraste, M., Sarti, P., Brunori, M., & Giuffrè, A. (2001). The cytochrome *cbb*$_3$ from *Pseudomonas stutzeri* displays nitric oxide reductase activity. *Eur J Biochem, 268*, 6486-6490.

García-Horsman, J. A., Barquera, B., Rumbley, J., Ma, J., & Gennis, R. B. (1994). The superfamily of heme-copper respiratory oxidases. *J Bacteriol, 176*(18), 5587-5600.

Gates, A. J., Luque-Almagro, V. M., Goddard, A. D., Ferguson, S. J., Roldán, M. D., & Richardson, D. J. (2011). A composite biochemical system for bacterial nitrate and nitrite assimilation as exemplified by *Paracoccus denitrificans. Biochem J, 435*(3), 743-753.

Girsch, P., & de Vries, S. (1997). Purification and initial kinetic and spectroscopic characterization of NO reductase from *Paracoccus denitrificans*. *Biochim Biophys Acta, 1318*, 202-216.

Goddard, A. D., Moir, J. W. B., Richardson, D. J., & Ferguson, S. J. (2008). Interdependence of two NarK domains in a fused nitrate/nitrite transporter. *Mol Microbiol, 70*(3), 667-681.

Gray, M. W. (2012). Mitochondrial evolution. *Cold Spring Harb Perspect Biol, 4*(9), a011403. doi: 10.1101/cshperspect.a011403.

Hannon, B., & Ruth, M. (2014). *Modeling Dynamic Biological Systems* (2nd ed.). New York: Springer.

Hendriks, J., Oubrie, A., Castresana, J., Urbani, A., Gemeinhardt, S., & Saraste, M. (2000). Nitric oxide reductases in bacteria. *Biochim Biophys Acta, 1459*, 266-273.

Hino, T., Nagano, S., Sugimoto, H., Tosha, T., & Shiro, Y. (2012). Molecular structure and function of bacterial nitric oxide reductase. *Biochim Biophys Acta, 1817*(4), 680-687.

Hole, U. H., Vollack, K.-U., Zumft, W. G., Eisenmann, E., Siddiqui, R. A., Friedrich, B., & Kroneck, P. M. H. (1996). Characterization of the membranous denitrification enzymes nitrite reductase (cytochrome *cd*$_1$) and copper-containing nitrous oxide reductase from *Thiobacillus denitrificans. Arch Microbiol, 165*(1), 55-61.

Jensen, V. B., Darby, J. L., Seidel, C., & Gorman, C. (2012). Drinking water treatment for nitrate *Addressing Nitrate in California's Drinking Water with a Focus on Tulare Lake Basin and Salinas Valley Groundwater. Report for the State Water Resources Control Board Report to the Legislature.* http://groundwaternitrate.ucdavis.edu/: Center for Watershed Sciences, University of California, Davis.

Jones, C. M., Graf, D. R. H., Bru, D., Philippot, L., & Hallin, S. (2013). The unaccounted yet abundant nitrous oxide-reducing microbial community: a potential nitrous oxide sink. *ISME J 7*, 417-426.

Jones, C. M., Spor, A., Brennan, F. P., Breuil, M.-C., Bru, D., Lemanceau, P., . . . Philippot, L. (2014). Recently identified microbial guild mediates soil $N_2O$ sink capacity. *Nat Clim Chang, 4*, 801-805 doi: 10.1038/nclimate2301.

Kampschreur, M. J., Kleerebezem, R., Picioreanu, C., Bakken, L., Bergaust, L., de Vries, S., . . . van Loosdrecht, M. C. M. (2012). Metabolic modeling of denitrification in *Agrobacterium tumefaciens*: a tool to study inhibiting and activating compounds for the denitrification pathway. *Front Microbiol, 3*. doi: 10.3389/fmicb.2012.00370.

Kartal, B., Maalcke, W. J., de Almeida, N. M., Cirpus, I., Gloerich, J., Geerts, W., . . . Strous, M. (2011). Molecular mechanism of anaerobic ammonium oxidation. *Nature, 479*(7371), 127-130.

Keeney, D. R., & Hatfield, J. L. (2008). The nitrogen cycle, historical perspective, and current and potential future concerns. In R. F. Follett & J. L. Hatfield (Eds.), *Nitrogen in the Environment: Sources, Problems and Management* (2nd ed., pp. 1-18). Oxford: Academic Press, Elsevier.

Kern, M., & Simon, J. (2009). Electron transport chains and bioenergetics of respiratory nitrogen metabolism in *Wolinella succinogenes* and other Epsilonproteobacteria. *Biochim Biophys Acta, 1787*, 646-656.

Knobeloch, L., Salna, B., Hogan, A., Postle, J., & Anderson, H. (2000). Blue babies and nitrate-contaminated well water. *Environ Health Perspect, 108*(7), 675-678.

Kroupova, H., Machova, J., & Svobodova, Z. (2005). Nitrite influence on fish: a review. *Vet Med (Praha), 50*(11), 461-471.

Kuňák, M., Kučera, I., & van Spanning, R. J. M. (2004). Nitric oxide oscillations in *Paracoccus denitrificans*: the effects of environmental factors and of segregating nitrite reductase and nitric oxide reductase into separate cells. *Arch Biochem Biophys, 429*(2), 237-243.

Lassey, K., & Harvey, M. (2007). Nitrous oxide: the serious side of laughing gas. *Water & Atmos, 15*(2), 10-11.

Lee, H. J., Reimann, J., Huang, Y., & Ädelroth, P. (2012). Functional proton transfer pathways in the heme–copper oxidase superfamily. *Biochim Biophys Acta, 1817*, 537-544.

Liu, B., Frostegård, Å., & Bakken, L. R. (2014). Impaired reduction of $N_2O$ to $N_2$ in acid soils is due to a posttranscriptional interference with the expression of *nosZ. MBio, 5*(3), e01383-01314.

Liu, B., Mao, Y., Bergaust, L., Bakken, L. R., & Frostegård, Å. (2013). Strains in the genus *Thauera* exhibit remarkably different denitrification regulatory phenotypes. *Environ Microbiol, 15*(10), 2816-2828.

Madigan, M. T., Martinko, J. M., Bender, K. S., Buckley, D. H., Stahl, D. A., & Brock, T. (2014). *Brock Biology of Microorganisms* (14th ed.). San Francisco: Pearson Benjamin Cummings.

Madsen, E. L. (2008). *Environmental Microbiology: From Genomes to Biogeochemistry* (1st ed.). Malden: Wiley-Blackwell.

Martinez-Espinosa, R. M., Dridge, E. J., Bonete, M. J., Butt, J. N., Butler, C. S., Sargent, F., & Richardson, D. J. (2007). Look on the positive side! The orientation, identification and bioenergetics of 'Archaeal' membrane-bound nitrate reductases. *FEMS Microbiol Lett, 276*(2), 129-139.

Matsumoto, Y., Tosha, T., Pisliakov, A. V., Hino, T., Sugimoto, H., Nagano, S., . . . Shiro, Y. (2012). Crystal structure of quinol-dependent nitric oxide reductase from *Geobacillus stearothermophilus*. *Nat Struct Mol Biol, 19*, 238-245.

McKee, D. J. (Ed.). (1993). *Tropospheric Ozone: Human Health and Agricultural Impacts* Florida: CRC Press.

Medinets, S., Skiba, U., Rennenberg, H., & Butterbach-Bahl, K. (2014). A review of soil NO transformation: associated processes and possible physiological significance on organisms. *Soil Biol Biochem, 80*, 92-117.

Muldera, A., van de Graafb, A. A., Robertsonb, L. A., & Kuenen, J. G. (1995). Anaerobic ammonium oxidation discovered in a denitrifying fluidized bed reactor. *FEMS Microbiol Ecol, 16*(3), 177-183.

Murali, R., Yildiz, G. G., Daldal, F., & Gennis, R. B. (2012). Stoichiometry of proton pumping by the $cbb_3$-type oxygen reductase in whole cells of *Rhodobacter capsulatus* at pH 7 is about 0.5 $H^+$ per electron. *Proc Natl Acad Sci U S A, 109*(32).

Nadeem, S., Dörsch, P., & Bakken, L. R. (2013). The significance of early accumulation of nanomolar concentrations of NO as an inducer of denitrification. *FEMS Microbiol Ecol, 83*(3), 672-684. doi: 10.1111/1574-6941.12024.

Nicholls, D. G., & Ferguson, S. J. (2013). *Bioenergetics* (4 ed.). London: Academic Press.

Nömmik, H. (1956). Investigations on denitrification in soil. *Acta Agric Scand, 6*(2), 195-228.

Philippot, L., & Hallin, S. (2006). Molecular analyses of soil denitrifying bacteria. In J. E. Cooper & J. R. Rao (Eds.), *Molecular approaches to soil, rhizosphere and plant microorganism analysis* (pp. 146-165). Oxford Cabi Publishing.

Pilegaard, K. (2013). Processes regulating nitric oxide emissions from soils. *Philos Trans R Soc Lond B Biol Sci, 368*, 20130126.

Pisliakov, A. V., Hino, T., Shiro, Y., & Sugita, Y. (2012). Molecular dynamics simulations reveal proton transfer pathways in cytochrome *c*-dependent nitric oxide reductase. *PLoS Comput Biol, 8*(8), e1002674.

Proshkin, S., Rahmouni, A. R., Mironov, A., & Nudler, E. (2010). Cooperation between translating ribosomes and RNA polymerase in transcription elongation. *Science 328*, 504-508.

Qu, Z., Bergaust, L. L., & Bakken, L. R. (2014). *Respiratory regulation in Paracoccus denitrificans and in soil, implications for $N_2O$ emissions* (Ph.D.), Norwegian University of Life Sciences, Ås.

Raitio, M., & Wikström, M. (1994). An alternative cytochrome oxidase of *Paracoccus denitrificans* functions as a proton pump. *Biochim Biophys Acta, 1186*(1-2), 100-106.

Rauhamäki, V., Bloch, D. A., & Wikström, M. (2012). Mechanistic stoichiometry of proton translocation by cytochrome *cbb*$_3$. *Proc Natl Acad Sci U S A, 109*(19), 7286-7291.

Ravishankara, A. R., Daniel, J. S., & Portmann, R. W. (2009). Nitrous oxide ($N_2O$): the dominant ozone-depleting substance emitted in the 21st century *Science, 326*(5949 ), 123-125.

Reimann, J., Flock, U., Lepp, H., Honigmann, A., & Ädelroth, P. (2007). A pathway for protons in nitric oxide reductase from *Paracoccus denitrificans. Biochim Biophys Acta, 1767*, 362-373.

Richardson, D., Felgate, H., Watmough, N., Thomson, A., & Baggs, E. (2009). Mitigating release of the potent greenhouse gas $N_2O$ from the nitrogen cycle – could enzymic regulation hold the key? *Trends Biotechnol, 27*(7), 388-397.

Richardson, D. J., van Spanning, R. J. M., & Ferguson, S. J. (2007). The prokaryotic nitrate reductases. In H. Bothe, S. J. Ferguson & W. E. Newton (Eds.), *Biology of the Nitrogen Cycle* (pp. 21-35). Amsterdam: Elsevier B. V.

Richter, O.-M. H., Tao, J.-s., Turba, A., & Ludwig, B. (1994). A cytochrome *ba*$_3$ functions as a quinol oxidase in *Paracoccus denitrificans*. *J Biol Chem, 269*, 23079-23086.

Rinaldo, S., & Cutruzzolà, F. (2007). Nitrite reductases in denitrification. In H. Bothe, S. J. Ferguson & W. E. Newton (Eds.), *Biology of the Nitrogen Cycle* (pp. 37-55). Amsterdam: Elsevier B. V.

Sanford, R. A., Wagner, D. D., Wu, Q., Chee-Sanford, J. C., Thomas, S. H., Cruz-García, C., . . . Löffler, F. E. (2012). Unexpected nondenitrifier nitrous oxide reductase gene diversity and abundance in soils *Proc Natl Acad Sci U S A, 109*(48), 19709-19714.

Sapavatu, S. N., & Setty, Y. P. (2012). *Biological denitrification of wastewater – a mini review on carbon source.* Paper presented at the International Conference on Chemical, Environmental Science and Engineering (ICEEBS-2012), Pattaya, Thailand.

Saunders, N. F. W., Houben, E. N. G., Koefoed, S., de Weert, S., Reijnders, W. N. M., Westerhoff, H. V., . . . van Spanning, R. J. M. (1999). Transcription regulation of the *nir* gene cluster encoding nitrite reductase of *Paracoccus denitrificans* involves NNR and NirI, a novel type of membrane protein. *Mol Microbiol, 34*(1), 24-36.

Schlesinger, W. H., & Bernhardt, E. S. (2013). *Biogeochemistry: An Analysis of Global Change* (3rd ed.). Oxford: Academic Press.

Sears, H. J., Spiro, S., & Richardson, D. J. (1997). Effect of carbon substrate and aeration on nitrate reduction and expression of the periplasmic and membrane-bound nitrate reductases in carbon-limited continuous cultures of *Paracoccus denitrificans* Pdl222. *Microbiology 143*, 3767-3774.

Shapleigh, J. P. (2006). The denitrifying prokaryotes. In M. Dworkin, S. Falkow, E. Rosenberg, K.-H. Schleifer & E. Stackebrandt (Eds.), *The Prokaryotes. A Handbook on the Biology of Bacteria: Ecophysiology and Biochemistry* (3rd ed., Vol. 2, pp. 769-792). New York: Springer.

Shoun, H., Fushinobu, S., Jiang, L., Kim, S.-W., & Wakagi, T. (2012). Fungal denitrification and nitric oxide reductase cytochrome P450nor. *Philos Trans R Soc Lond B Biol Sci, 367*, 1186-1194.

Shoun, H., Kim, D.-H., Uchiyama, H., & Sugiyama, J. (1992). Denitrification by fungi. *FEMS Microbiol Lett, 94*(3), 277-281.

Signor, D., & Cerri, C. E. P. (2013). Nitrous oxide emissions in agricultural soils: a review. *Pesq Agropec Trop, 43*(3), 322-338.

Simon, J., Einsle, O., Kroneck, P. M. H., & Zumft, W. G. (2004). The unprecedented *nos* gene cluster of *Wolinella succinogenes* encodes a novel respiratory electron transfer pathway to cytochrome *c* nitrous oxide reductase. *FEBS Lett, 569*, 7-12.

Simon, J., van Spanning, R. J. M., & Richardson, D. J. (2008). The organisation of proton motive and non-proton motive redox loops in prokaryotic respiratory systems. *Biochim Biophys Acta, 1777*, 1480-1490.

Skiba, U., Fowler, D., & Smith, K. A. (1997). Nitric oxide emissions from agricultural soils in temperate and tropical climates: sources, controls and mitigation options. *Nutr Cycl Agroecosys, 48*, 139-153.

Sparacino-Watkins, C., Stolz, J. F., & Basua, P. (2014). Nitrate and periplasmic nitrate reductases. *Chem Soc Rev, 43*(2), 676-706.

Spiro, S. (2007). Regulators of bacterial responses to nitric oxide. *FEMS Microbiol Rev, 31*, 193-211.

Spiro, S. (2012). Nitrous oxide production and consumption: regulation of gene expression by gas-sensitive transcription factors. *Philos Trans R Soc Lond B Biol Sci, 367*, 1213-1225.

Suharti, & de Vries, S. (2005). Membrane-bound denitrification in the Gram-positive bacterium *Bacillus azotoformans*. *Biochem Soc Trans, 33*, 130-133.

Suharti, Heering, H. A., & de Vries, S. (2004). NO reductase from *Bacillus azotoformans* is a bifunctional enzyme accepting electrons from menaquinol and a specific endogenous membrane-bound cytochrome $c_{551}$. *Biochemistry, 43*(42), 13487-13495.

Syakila, A., & Kroeze, C. (2011). The global nitrous oxide budget revisited. *Greenhouse Gas Meas Manage, 1*(1), 17-26.

ter Beek, J., Krause, N., Reimann, J., Lachmann, P., & Ädelroth, P. (2013). The nitric-oxide reductase from *Paracoccus denitrificans* uses a single specific proton pathway. *J Biol Chem, 288*(42), 30626-30635.

Thomsen, J. K., Geest, T., & Cox, R. P. (1994). Mass spectrometric studies of the effect of pH on the accumulation of intermediates in denitrification by *Paracoccus denitrificans*. *Appl Environ Microbiol, 60*(2), 536-541.

Ussiri, D., & Lal, R. (2013). *Soil Emission of Nitrous Oxide and its Mitigation*. Dordrecht: Springer.

van Spanning, R. J. M., Richardson, D. J., & Ferguson, S. J. (2007). Introduction to the biochemistry and molecular biology of denitrification. In H. Bothe, S. J. Ferguson & W. E. Newton (Eds.), *Biology of the Nitrogen Cycle* (pp. 3-20). Amsterdam: Elsevier B. V.

Vasiliadou, I. A., Siozios, S., Papadas, I. T., Bourtzis, K., Pavlou, S., & Vayenas, D. V. (2006). Kinetics of pure cultures of hydrogen-oxidizing denitrifying bacteria and modeling of the interactions among them in mixed cultures. *Biotechnol Bioeng, 95*(3), 513-525.

Veening, J.-W., Smits, W. K., & Kuipers, O. P. (2008). Bistability, epigenetics, and bet-hedging in bacteria. *Annu Rev Microbiol, 62*, 193-210.

Ward, B. (2012). The Global Nitrogen Cycle. In A. H. Knoll, D. E. Canfield & K. O. Konhauser (Eds.), *Fundamentals of Geobiology* (1 ed., pp. 36-47). West Sussex: Wiley-Blackwell.

WHO. (2011). Nitrate and nitrite in drinking-water. 2015.

Wijler, J., & Delwiche, C. C. (1954). Investigations on the denitrifying process in soil. *Plant Soil, 5*(2), 155-169.

Wood, N. J., Alizadeh, T., Bennett, S., Pearce, J., Ferguson, S. J., Richardson, D. J., & Moir, J. W. (2001). Maximal expression of membrane-bound nitrate reductase in *Paracoccus* is induced by nitrate via a third FNR-like regulator named NarR. *J Bacteriol, 183*(12), 3606-3613.

Wood, N. J., Alizadeh, T., Richardson, D. J., Ferguson, S. J., & Moir, J. W. B. (2002). Two domains of a dual-function NarK protein are required for nitrate uptake, the first step of denitrification in *Paracoccus pantotrophus*. *Mol Microbiol, 44*(1), 157-170.

Woolfenden, H. C., Gates, A. J., Bocking, C., Blyth, M. G., Richardson, D. J., & Moulton, V. (2013). Modeling the effect of copper availability on bacterial denitrification. *Microbiologyopen, 2*(5), 756-765.

Wuebbles, D. J. (2010). Oxygen Cycle. In S. E. Jørgensen (Ed.), *Global Ecology* (1 ed.). Amsterdam Academic Press.

Wunsch, P., & Zumft, W. G. (2005). Functional domains of NosR, a novel transmembrane iron-sulfur flavoprotein necessary for nitrous oxide respiration. *J Bacteriol, 187*(6).

Zumft, W. G. (1997). Cell biology and molecular basis of denitrification. *Microbiol Mol Biol Rev, 61*(4), 533-616.

Zumft, W. G., & Körner, H. (2007). Nitrous oxide reductases. In H. Bothe, S. J. Ferguson & W. E. Newton (Eds.), *Biology of the Nitrogen Cycle* (pp. 67-81). Amsterdam: Elsevier B. V.

# P A P E R I

**PLOS Computational Biology (2014)**

# Low Probability of Initiating *nirS* Transcription Explains Observed Gas Kinetics and Growth of Bacteria Switching from Aerobic Respiration to Denitrification

**Junaid Hassan, Linda L. Bergaust, I. David Wheat, Lars R. Bakken***

OPEN ACCESS Freely available online

PLOS | COMPUTATIONAL BIOLOGY

# Low Probability of Initiating *nirS* Transcription Explains Observed Gas Kinetics and Growth of Bacteria Switching from Aerobic Respiration to Denitrification

**Junaid Hassan[1], Linda L. Bergaust[1], I. David Wheat[2], Lars R. Bakken[1]***

**1** Department of Environmental Sciences, Norwegian University of Life Sciences, Ås, Norway, **2** Department of Geography, University of Bergen, Bergen, Norway

## Abstract

In response to impending anoxic conditions, denitrifying bacteria sustain respiratory metabolism by producing enzymes for reducing nitrogen oxyanions/-oxides ($NO_x$) to $N_2$ (denitrification). Since denitrifying bacteria are non-fermentative, the initial production of denitrification proteome depends on energy from aerobic respiration. Thus, if a cell fails to synthesise a minimum of denitrification proteome before $O_2$ is completely exhausted, it will be unable to produce it later due to energy-limitation. Such entrapment in anoxia is recently claimed to be a major phenomenon in batch cultures of the model organism *Paracoccus denitrificans* on the basis of measured $e^-$-flow rates to $O_2$ and $NO_x$. Here we constructed a dynamic model and explicitly simulated actual kinetics of recruitment of the cells to denitrification to directly and more accurately estimate the recruited fraction ($\mathbf{F_{den}}$). Transcription of *nirS* is pivotal for denitrification, for it triggers a cascade of events leading to the synthesis of a full-fledged denitrification proteome. The model is based on the hypothesis that *nirS* has a low probability ($\mathbf{r_{den}}$, $h^{-1}$) of initial transcription, but once initiated, the transcription is greatly enhanced through positive feedback by NO, resulting in the recruitment of the transcribing cell to denitrification. We assume that the recruitment is initiated as $[O_2]$ falls below a critical threshold and terminates (assuming energy-limitation) as $[O_2]$ exhausts. With $\mathbf{r_{den}} = 0.005\ h^{-1}$, the model robustly simulates observed denitrification kinetics for a range of culture conditions. The resulting $\mathbf{F_{den}}$ (fraction of the cells recruited to denitrification) falls within 0.038–0.161. In contrast, if the recruitment of the entire population is assumed, the simulated denitrification kinetics deviate grossly from those observed. The phenomenon can be understood as a 'bet-hedging strategy': switching to denitrification is a gain if anoxic spell lasts long but is a waste of energy if anoxia turns out to be a 'false alarm'.

**Citation:** Hassan J, Bergaust LL, Wheat ID, Bakken LR (2014) Low Probability of Initiating *nirS* Transcription Explains Observed Gas Kinetics and Growth of Bacteria Switching from Aerobic Respiration to Denitrification. PLoS Comput Biol 10(11): e1003933. doi:10.1371/journal.pcbi.1003933

**Editor:** Robinson Fulweiler, Boston University, United States of America

**Received** April 17, 2014; **Accepted** September 17, 2014; **Published** November 6, 2014



**Data Availability:** The authors confirm that all data underlying the findings are fully available without restriction. All relevant data are within the paper and its Supporting Information files.

**Funding:** This work is funded by Norwegian University of Life Sciences, financed by the Ministry of Education and Research, Norway. No institution has, in any way, influenced the outcome of this work. The funders had no role in study design, data collection and analysis, decision to publish, or preparation of the manuscript.

**Competing Interests:** The authors have declared that no competing interests exist.

* Email: lars.bakken@nmbu.no

## Introduction

A complete denitrification pathway includes the dissimilatory reduction of nitrate ($NO_3^-$) through nitrite ($NO_2^-$), nitric oxide (NO), and nitrous oxide ($N_2O$) to di-nitrogen ($N_2$). Typically, the genes encoding reductases for these nitrogen oxyanions/-oxides ($NO_x$) are not expressed constitutively but only in response to $O_2$ depletion, making denitrification a facultative trait [1]. Hence, during anoxic spells, the process enables denitrifying bacteria to sustain respiratory metabolism, replacing $O_2$ by $NO_x$ as the terminal electron ($e^-$) acceptors. Since permanently anoxic environments lack available $NO_x$, denitrification is confined to sites where $O_2$ concentration fluctuates, such as biofilms, surface layers of sediments, and drained soil (which turns anoxic in response to flooding).

### From modelling denitrifying communities as a homogenous unit to a model of regulation of denitrification in an individual strain

Denitrification is a key process in the global nitrogen cycle and is also a major source of atmospheric $N_2O$ [2]. A plethora of biogeochemical models have been developed for understanding the ecosystem controls of denitrification and $N_2O$ emissions [3]. A common feature of these models is that the denitrifying community of the system (primarily soils and sediments) in question is treated as one homogenous unit with certain characteristic responses to $O_2$ and $NO_3^-$ concentrations. This simplification is fully legitimate from a pragmatic point of view, but in reality any denitrifying community is composed of a mixture of organisms with widely different denitrification regulatory phenotypes [4]. Modelling has been used to a limited extent to analyse kinetic data for various phenotypes (See [5] and references therein) and for understanding the accumulation of intermediates [6]. To our knowledge, however, no attempts have been made to model the regulation during transition from aerobic to anaerobic respiration in individual strains, despite considerable progress in the understanding of their regulatory networks. It would be well worth the effort, since the regulatory phenomena at the cellular level provide clues as to how denitrification and NO and $N_2O$ emissions therefrom are regulated in intact soils [7]. Explicit modelling of the entire denitrification regulatory network,

## Author Summary

In response to oxygen-limiting conditions, denitrifying bacteria produce a set of enzymes to convert $NO_3^-/NO_2^-$ to $N_2$ via NO and $N_2O$. The process (denitrification) helps generate energy for survival and growth during anoxia. Denitrification is imperative for the nitrogen cycle and has far-reaching consequences including contribution to global warming and destruction of stratospheric ozone. Recent experiments provide circumstantial evidence for a previously unknown phenomenon in the model denitrifying bacterium *Paracoccus denitrificans:* as $O_2$ depletes, only a marginal fraction of its population appears to switch to denitrification. We hypothesise that the low success rate is due to ***a)*** low probability for the cells to initiate the transcription of genes (*nirS*) encoding a key denitrification enzyme (NirS), and ***b)*** a limited time-window in which NirS must be produced. Based on this hypothesis, we constructed a dynamic model of denitrification in *Pa. denitrificans*. The simulation results show that, within the limited time available, a probability of 0.005 $h^{-1}$ for each cell to initiate *nirS* transcription (resulting in the recruitment of 3.8–16.1% cells to denitrification) is sufficient to adequately simulate experimental data. The result challenges conventional outlook on the regulation of denitrification in general and that of *Pa. denitrificans* in particular.


however, would take us beyond available experimental evidence, with numerous parameters for which there are no empirical values. Considering this limitation, here we have constructed a simplified model to investigate if a stochastic transcriptional initiation of key denitrification genes (*nirS*) could possibly explain peculiar kinetics of $e^-$-flow as *Paracoccus denitrificans* switch from aerobic to anaerobic respiration [4,8].

Although denitrification is widespread among bacteria, the α-proteobacterium *Pa. denitrificans* is the 'paradigm' model organism in denitrification research. Recent studies [4,8,9] have indicated a previously unknown phenomenon in this species that, in response to $O_2$ depletion, only a marginal fraction ($F_{den}$) of its entire population appears to successfully switch to denitrification. In these studies, however, $F_{den}$ is inferred from rates of consumption and production of gases ($O_2$, $NO_x$, and $N_2$), and a clear hypothesis as to the underlying cause of the low $F_{den}$ is also lacking. To fill these gaps, we formulated a refined hypothesis addressing the underlying regulatory mechanism of the cell differentiation in response to $O_2$ depletion. On its basis, we constructed a dynamic model and explicitly simulated the actual kinetics of recruitment of the cells from aerobic respiration to denitrification. The model adequately matches batch cultivation data for a range of experimental conditions [4,8] and provides a direct and refined estimation of $F_{den}$. The exercise is important for understanding the physiology of denitrification in general and of *Pa. denitrificans* in particular and carries important implications for correctly interpreting various denitrification experiments.

## Regulation of denitrification in terms of relevance to fitness

Generally, the transcription of genes encoding denitrification enzymes is inactivated in the presence of $O_2$. A population undertaking denitrification typically responds to full aeration by completely shutting down denitrification and immediately initiating aerobic respiration [10]. Thus, $O_2$ controls denitrification at transcriptional as well as metabolic level, and both have a plausible fitness value. The transcriptional control minimises the energy cost of producing denitrification enzymes, and the metabolic control maximises ATP (per mole electrons transferred) because the mole ATP per mole electrons transferred to the terminal $e^-$-acceptor is ~50% higher for aerobic respiration than for denitrification [10].

Denitrification enzymes produced in response to an anoxic spell are likely to linger within the cells under subsequent oxic conditions (although, this has not been studied in detail), ready to be used if $O_2$ should become limiting later on. However, these enzymes will be diluted by aerobic growth, since the transcription of their genes is effectively inactivated by $O_2$. Hence, a population growing through many generations under fully oxic conditions will probably be dominated by the cells without intact denitrification proteome. When confronted with $O_2$ depletion, such a population will have to start from scratch, i.e., transcribe the relevant genes, translate mRNA into peptide chains (protein synthesis by ribosomes) and secure that these chains are correctly folded by the chaperones, transport the enzymes to their correct locations in the cell, and insert necessary co-factors (e.g., Cu, Fe, or Mo). In *E. coli* grown under optimal conditions, the whole process from the transcriptional activation to a functional enzyme takes ≤20 minutes [11] and costs significant amount of energy (ATP).

Synthesis of denitrification enzymes is rewarding if anoxia lasts long and $NO_x$ remains available, but it is a waste of energy if anoxia is brief. Since the organisms cannot sense how long an impending anoxic spell will last, a 'bet-hedging strategy' [12] where one fraction of a population synthesises denitrification enzymes while the other does not may increase overall fitness.

## A delayed response to $O_2$ depletion may lead to entrapment in anoxia

Most, if not all, denitrifying bacteria are non-fermentative and completely rely on respiration to generate energy [13,14]. This implies that their metabolic machinery will run out of energy whenever deprived of terminal $e^-$-acceptors. When [$O_2$] falls below some critical threshold, the cells will 'sense' this and start synthesising denitrification proteome, utilising energy from aerobic respiration [10]. However, if $O_2$ is suddenly exhausted or removed, the lack of a terminal $e^-$-acceptor will create energy limitation, restraining the cells from enzyme synthesis, hence, entrapping them in anoxia. This was clearly demonstrated by Højberg *et al.* [15], who used silicone immobilised cells to transfer them from a completely oxic to a completely anoxic environment. Such a rapid transition is unlikely to occur in nature; however, the experiment illustrates one of the apparent perils in the regulation of denitrification: the cells that respond too late to $O_2$ depletion will be entrapped in anoxia, unable to utilise alternative electron acceptors for energy conservation and growth.

Højberg *et al.*'s [15] observations have largely been ignored in the research on the regulation of denitrification, and it is implicitly assumed that, in response to $O_2$ depletion, all cells in cultures of denitrifying bacteria will switch to denitrification. Contrary to this, however, Bergaust *et al.* [4,8,16] followed by Nadeem *et al.* [9] proposed that in batch cultures of *Pa. denitrificans*, only a small fraction of all cells is able to switch to denitrification. During transition from oxic to anoxic conditions, they observed a severe depression in the total $e^-$-flow rate (i.e., to $O_2$+$NO_x$, see Fig. 1), which was estimated on the basis of measured gas kinetics. Had all of the cells switched to denitrification as $O_2$ exhausted, the total $e^-$-flow rate would have carried on increasing, without such a depression. The depression was followed by an exponential increase in the $e^-$-flow rate, which was tentatively ascribed to anaerobic growth of a small $F_{den}$ (fraction recruited to denitrification). It was postulated that this fraction escaped entrapment in

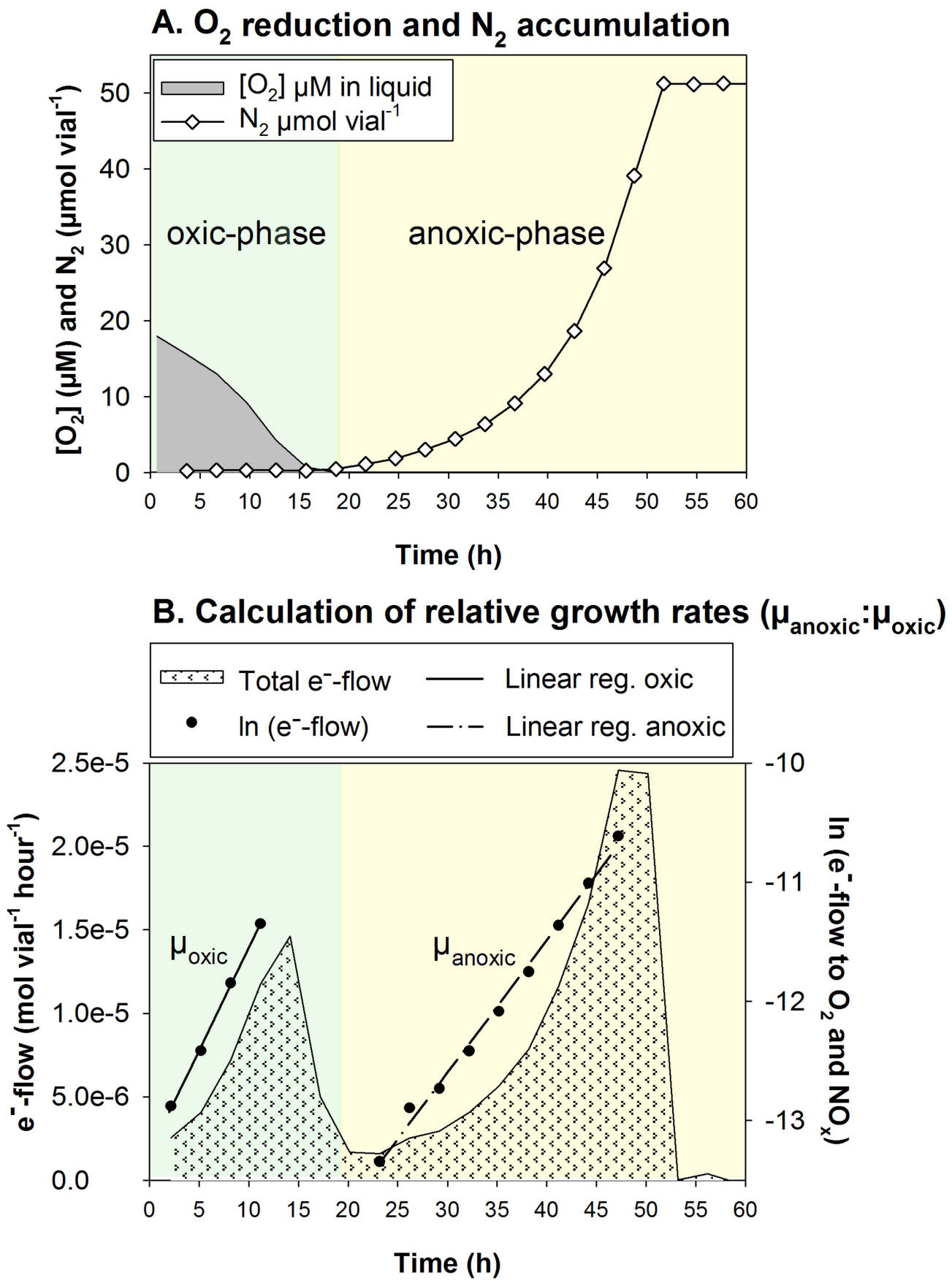
A. O2 reduction and N2 accumulation
[O2] µM in liquid
N2 µmol vial-1
oxic-phase
anoxic-phase
[O2] (µM) and N2 (µmol vial-1)
Time (h)
B. Calculation of relative growth rates (µanoxic:µoxic)
Total e--flow
ln (e--flow)
Linear reg. oxic
Linear reg. anoxic
µoxic
µanoxic
e--flow (mol vial-1 hour-1)
ln (e--flow to O2 and NOx)
Time (h)

**Figure 1. Data generated by batch cultivation of *Pa. denitrificans* [4] (redrawn).** As the cells transited from oxic to anoxic conditions (Panel A), Bergaust *et al.* [4] observed a severe depression in the total $e^-$-flow rate (i.e., to $O_2$+$NO_x$, Panel B), which was taken to indicate that only a fraction of the cells switched to anaerobic respiration (denitrification). Had all of the cells switched, the total $e^-$-flow would have carried on increasing without such a depression. The depression was followed by an exponential increase in the $e^-$-flow rate, which was ascribed to anaerobic growth of a small fraction ($F_{den}$) of the cells that escaped entrapment in anoxia and carried on growing by denitrification.
doi:10.1371/journal.pcbi.1003933.g001

anoxia by synthesising initial denitrification proteins within the time-window when $O_2$ was still present, whereas the majority of the cells ($1-F_{den}$) failed to do so, thus remained unable to utilise $NO_x$.

## The core hypothesis: A low probability of initiating *nirS* transcription seems to drive the cell differentiation

**Autocatalytic transcription of denitrification genes.** In *Pa. denitrificans*, denitrification is driven by four core enzymes: Nar (membrane-bound nitrate reductase), NirS (cytochrome $cd_1$ nitrite reductase), cNor (nitric oxide reductase), and NosZ (nitrous oxide reductase, see Fig. 2). The transcriptional regulation of genes encoding these enzymes (*nar*, *nirS*, *nor* and *nosZ*, respectively) involves, at least, three FNR-type proteins acting as sensors for $O_2$ (FnrP), $NO_3^-/NO_2^-$ (NarR), and NO (NNR) [10,17,18]. NarR and NNR facilitate product-induced transcription of the *nar* and *nirS* genes: When anoxia is imminent, the low [$O_2$] is sensed by FnrP, which in interplay with NarR induces *nar* transcription. NarR is activated by $NO_2^-$ (and/or probably by $NO_3^-$); thus once a cell starts producing traces of $NO_2^-$, *nar* expression becomes autocatalytic. The transcription of *nirS* is induced by NNR, which requires NO for activation; thus once traces of NO are produced, the expression of *nirS* also becomes autocatalytic. In contrast, the transcription of *nor* is substrate (NO) induced via NNR, while *nosZ* is equally but independently induced by NNR and FnrP [19]. Here we are concerned with the dynamics that start with the transcription of *nirS*, since the experimental treatments that we simulated were not supplemented with $NO_3^-$ but various concentrations of $NO_2^-$ only (Table 1).

**Low probability of initiating *nirS* transcription.** The transcription of *nirS* is known to be suppressed by $O_2$ [4,8], but the exact mechanism remains unclear. Circumstantial evidence suggests that it is due to $O_2$ inactivating NNR [20] (dashed link in Fig. 2), but this is not necessary to explain the repression of NirS. There are several mechanisms through which high $O_2$ concentrations may restrain NirS activity, i.e., through post-transcriptional regulation, direct interaction with the enzyme, or due to competition for electrons. Regardless of the exact mechanism(s),

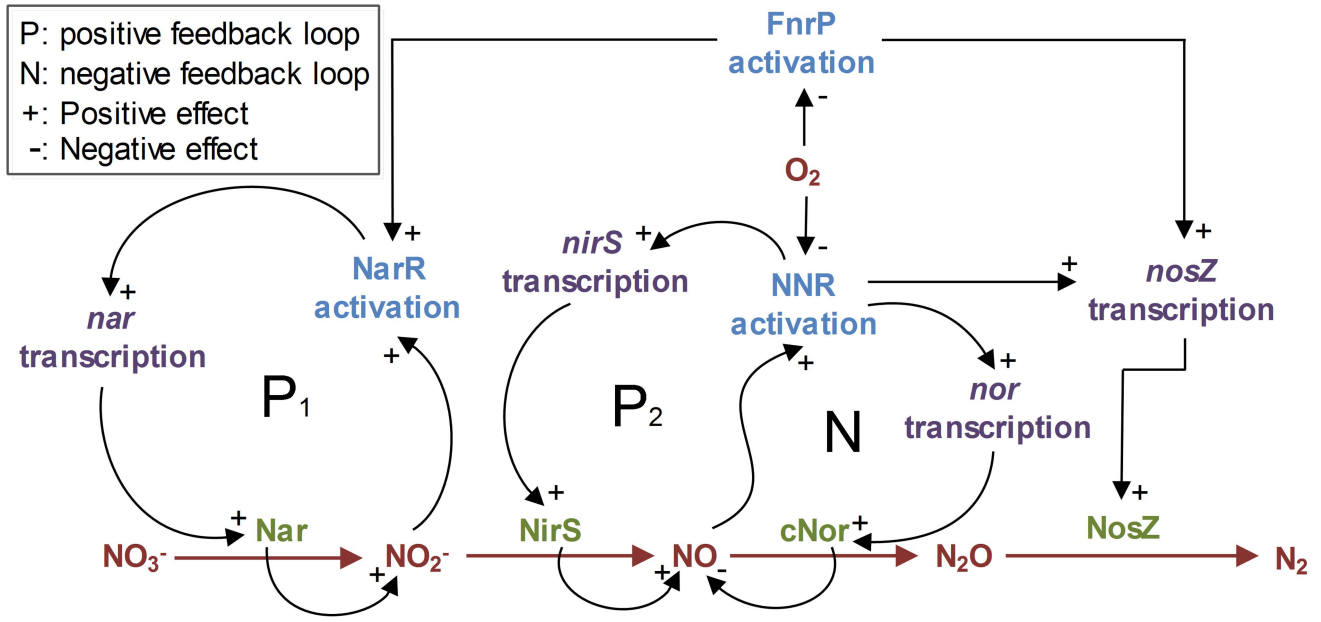


**Figure 2. The regulatory network of denitrification in *Pa. denitrificans*.** In *Pa. denitrificans*, denitrification is driven by four core enzymes: Nar (nitrate reductase encoded by the *nar* genes), NirS (nitrite reductase encoded by *nirS*), cNor (NO reductase encoded by *nor*), and NosZ ($N_2O$ reductase encoded by *nosZ*). The transcription of these genes is regulated by, at least, three FNR-type proteins, which are sensors for $O_2$ (FnrP), $NO_3^-/NO_2^-$ (NarR), and NO (NNR). NarR and NNR facilitate product-induced transcription of the *nar* and *nirS* genes (see positive-feedback loops), where NNR also counteracts the NO accumulation (negative-feedback loop) [10,17,18]. Circumstantial evidence suggests that $O_2$ inactivates NNR (grey dashed link) [20], and NirS is also unlikely to be functional in the presence of high $O_2$ concentrations. Hence, for our modelling we hypothesise that the probability of an autocatalytic transcriptional activation of *nirS* is zero until $O_2$ falls below a critical concentration $\left([O_2]_{trigger}\right)$. When $O_2$ falls below $[O_2]_{trigger}$, the initial *nirS* transcription is possibly mediated through a minute pool of intact NNR, crosstalk with other factors, or through non-biological traces of NO found in an $NO_2^-$-supplemented medium. Regardless of the exact mechanism(s), once *nirS* transcription is initiated, it will be substantially enhanced by spikes of internal NO emitted from the first molecules of NirS (the positive-feedback loop). The activated positive-feedback will also induce *nor* and *nosZ* transcription via NNR (although, the latter can also be induced independently by FnrP [19]), facilitating the synthesis of a full-fledged denitrification proteome. Our model assumes that such recruitment to denitrification will occur with a low probability. We further assume that the recruitment will only be possible as long as a minimum of $O_2$ $\left([O_2]_{min}\right)$ is available because the production of the first molecules of NirS will depend on energy from aerobic respiration.
doi:10.1371/journal.pcbi.1003933.g002

**Table 1.** The simulated experiment of Bergaust *et al* [4,8].

| Batch No. | $O_{2HS}$ ($t_0$) (vol. %)* | $NO_2^-$ ($t_0$) (mM) |
|---|---|---|
| 1 | ~0 | 0.2 |
| 2 | ~0 | 1 |
| 3 | ~0 | 2 |
| 4 | 1 | 0.2 |
| 5 | 1 | 1 |
| 6 | 1 | 2 |
| 7 | 7 | 0.2 |
| 8 | 7 | 1 |
| 9 | 7 | 2 |

*Targeted values for initial $O_2$ in the headspace (where the headspace vol. = 70 mL). The actual initial $O_2$ measured in the 0, 1, and 7% treatments was 0.012–0.19, 1.2–1.66, 6.6–6.8 vol.%, respectively. The $O_2$ present in the ~0% treatments was due to traces of $O_2$ left behind despite various cycles of evacuation of the headspace air and subsequent flushing of the vials with helium (He-washing).

doi:10.1371/journal.pcbi.1003933.t001

the ultimate consequence is the elimination of the positive feedback via NO and NNR. When $O_2$ falls below a critical threshold, facilitating NirS activity, this positive feedback would allow the product of a single transcript of *nirS* to induce a subsequent burst of *nirS* transcription in response to NO. Such 'switches' in gene expression by positive-feedback loops are not uncommon in prokaryotes, and they have been found to result in cell differentiation because the initial transcription is stochastic with a relatively low probability [21].

Our model assumes such stochastic recruitment to denitrification, triggered by an initial *nirS* transcription occurring with a low probability. This initial transcription is possibly mediated by a minute pool of intact NNR and/or through crosstalk with other factors, such as FnrP. A $NO_2^-$-supplemented medium contains non-biologically formed traces of NO which, once diffused into the cells while $O_2$ is low, will activate background levels of NNR and, thereby, may also increase the probability of triggering *nirS* transcription.

For this modelling exercise, we do not need a full clarification of the mechanisms involved but only to assume that the probability of an autocatalytic transcriptional activation of *nirS* would be practically zero as long as $O_2$ concentration is above a certain threshold. This assumption is backed by empirical data indicating that NO is not produced to detectable levels before $O_2$ concentration falls below a critical threshold [8,22]. For $O_2$ concentrations below this threshold, the model assumes a low (but unknown) probability for each cell to initiate the autocatalytic transcription of *nirS*, paving the way for the rest of the denitrification proteome.

**$O_2$ is required for the initial production of NirS.** We further assume that the recruitment to denitrification will only be possible as long as a minimum of $O_2$ is available because the synthesis of first molecules of NirS will depend on energy from aerobic respiration.

**Can NO produced within one cell help activate the autocatalytic transcription of *nirS* in the neighbouring cells?** It is perhaps less obvious that the autocatalytic transcriptional activation of *nirS* takes place only within the NO-producing cell because NO diffuses easily across membranes [23]. However, the average distance between the cells in a culture with $10^9$ cells $mL^{-1}$ (roughly the numbers that we are dealing with) is ~10 μm, which is ~10 times the diameter of a cell. This implies that an NO molecule produced by a cell has a much higher probability to react with and activate the NNR inside the same cell than to do so in another one.

## Modelling the cell differentiation

To represent the batch cultivation conducted by Bergaust *et al*. [4,8], the model explicitly simulates growth of two sub-populations, one *with* denitrification enzymes ($N_{D+}$) and the other *without* ($N_{D-}$); both equally consume $O_2$, but $N_{D-}$ cannot reduce $NO_x$ to $N_2$. Once oxygen concentration in the liquid $\left([O_2]_{LP}\right)$ falls below a critical level $\left([O_2]_{trigger}\right)$ [22], the cells within $N_{D-}$ are assumed to initiate *nirS* transcription (and thereby ensure recruitment to $N_{D+}$) with a rate described by a probabilistic function: $N_{D-} \times r_{den}(O_2)$ (cells $h^{-1}$), where $r_{den}(O_2)$ is assumed to be an $[O_2]_{LP}$ dependent probability ($h^{-1}$) for any cell within $N_{D-}$ to initiate *nirS* transcription (leading to a full denitrification capacity). When $[O_2]_{LP}$ falls below $[O_2]_{trigger}$, $r_{den}(O_2)$ triggers and holds a constant value as long as $[O_2]_{LP}$ is above a critical minimum $\left([O_2]_{min}\right)$. For $[O_2]_{LP} > [O_2]_{trigger}$, $r_{den}(O_2)$ is zero (assuming the inactivation of NNR by $O_2$); $r_{den}(O_2)$ is also zero for $[O_2]_{LP} < [O_2]_{min}$ (assuming the lack of energy for protein synthesis).

The recruitment of $N_{D-}$ to $N_{D+}$ is simulated as an instantaneous event; thus, the model does not take into account the time-lag between the initiation of *nirS* transcription and the time when the transcribing cell has become a fully functional denitrifier. This simplification is based on the evidence that this lag is rather short. Experiments with *E. coli* [11] under optimal conditions suggest lags of ~20 minutes between the onset of transcription and the emergence of a functional enzyme. In *Pa. denitrificans* [8,22], the lag observed between the emergence of denitrification gene transcripts and the subsequent gas products suggests that the time required for synthesising the enzymes is within the same range.

## Employing the model to understand 'diauxic lags' between the aerobic and anaerobic growth-phases

In a series of experiments with denitrifying bacteria (*Pseudomonas denitrificans*, *Pseudomonas fluorescens*, *Alcaligenes eutrophus* and *Paracoccus pantotrophus*) [24–26], oxic cultures were sparged with $N_2$ to remove $O_2$ and were monitored by measuring optical density ($OD_{550}$). All the strains except *Ps. fluorescens* went through a conspicuous *'diauxic lag: a period of little or no growth'* [26]; the OD remained practically constant during the lag period, lasting 4–30 hours, which was eventually followed by anaerobic growth.

To understand the diauxic lag, Liu *et al*. [24] used the common assumption that *all* cells would eventually switch to denitrification. They constructed a simulation model based on the assumption that all the cells contained a minimum of denitrification proteome (even after many generations under oxic conditions). This minimum would allow them to produce more denitrification enzymes when deprived of $O_2$, albeit very slowly due to energy limitation. The time taken to effectively produce adequate amounts of denitrification enzymes (= the diauxic lag) was taken to be a function of the initial amounts of these enzymes per cell. Although their model may possibly explain short time-lags, it appears unrealistic for lag phases as long as 10–30 hours [25] because to produce such long lags, conceivably, the initial enzyme concentration would be less than one enzyme molecule per cell, which is mathematically possible but biologically meaningless.

The model presented in this paper provides an alternative explanation for the apparent diauxic lags: a sudden shift from fully oxic to near anoxic conditions (by sparging with $N_2$) would leave the medium with only traces of $O_2$, which would be quickly depleted due to aerobic respiration. As a consequence, the available time for initiating the synthesis of denitrification proteome would be marginal, allowing only a tiny fraction ($F_{den}$) of the cells to switch to denitrification. This marginal fraction would grow exponentially from the very onset of anoxic conditions, but it would remain practically undetectable as measured (OD) for a long time, creating the apparent 4–30 h lag. The length of the lag depends on the fraction of the cells switching to denitrification. To demonstrate this alternative explanation, we adjusted our model to the reported conditions and simulated the experiment of Liu *et al* [24]. The model produced qualitatively similar 'diauxic lags' in the simulated cell density (OD), although the time length of the lag could be anything (depending on assumptions regarding the residual $O_2$ after sparging, which was not measured).

## Materials and Methods

### An overview of the modelled experiment: Batch incubations in gas-tight vials

Bergaust *et al.* [4,8] studied aerobic and anaerobic respiration rates in *Paracoccus denitrificans* (DSM413). The cells were incubated (at 20°C) as stirred batches in 120 mL gastight vials, containing 50 mL Sistrom's medium [27] (Fig. 3). The medium was supplemented with various concentrations of $KNO_3$ or $KNO_2$. Prior to inoculation, air in the headspace was replaced with He to remove $O_2$ and $N_2$ (He-washing), followed by the injection of no, 1, or 7 headspace-vol.% $O_2$. Finally, each vial was inoculated with $\sim 3\times10^8$ aerobically grown cells.

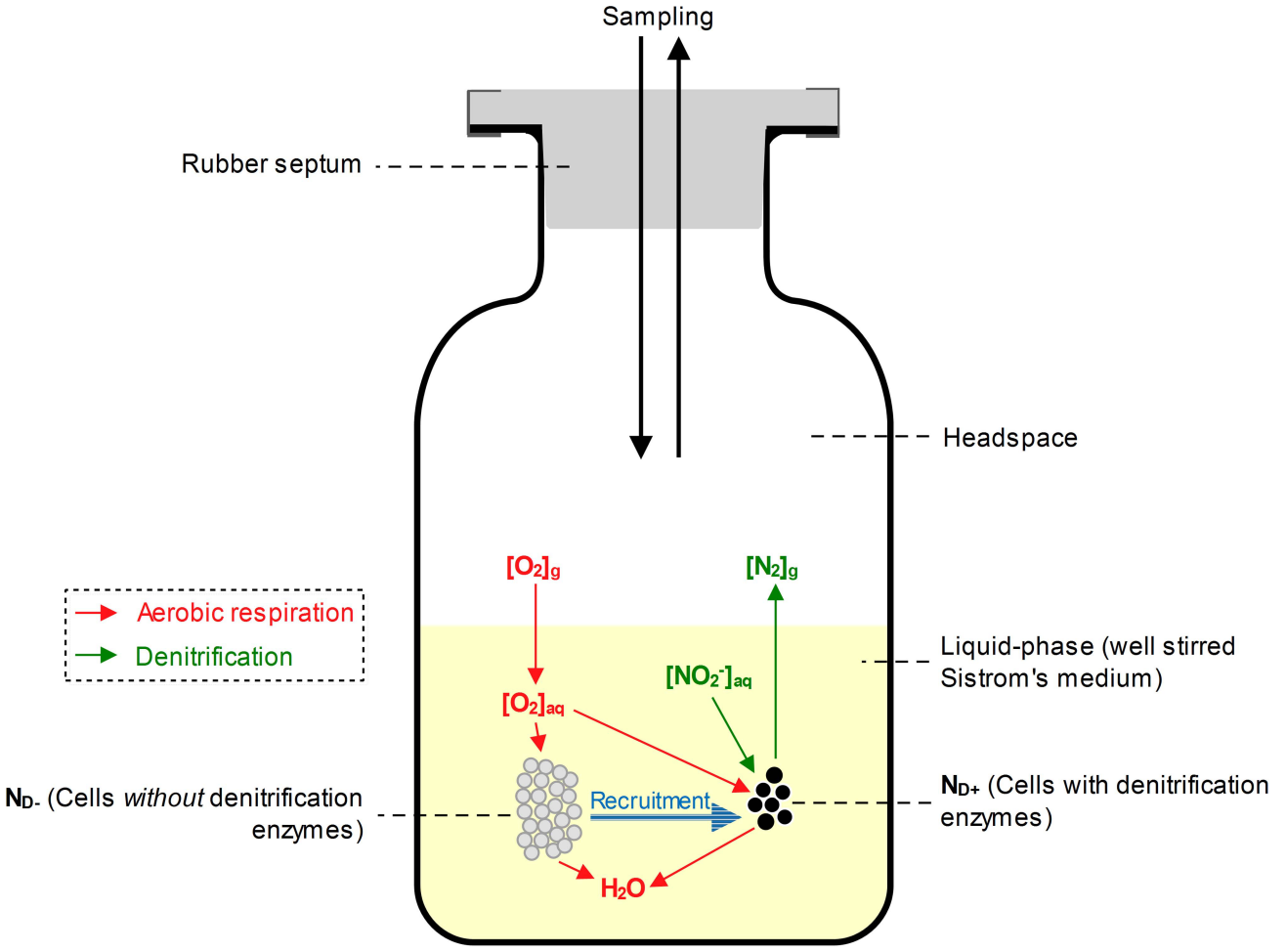


**Figure 3. An overview of the modelled system: batch incubation in a gas-tight vial.** The experiment: The stirred Sistrom's medium [27] was inoculated with aerobically grown *Pa. denitrificans* cells, which were provided with different concentrations of $O_2$ and $NO_2^-$ (g or aq with a chemical species-name represents gaseous or aqueous, respectively). $O_2$ is consumed by respiration, driving its transport from the headspace to the liquid. Once the aerobic respiration becomes limited, the cells may switch to denitrification (recruitment), reducing $NO_2^-$ to $N_2$ via the intermediates NO and $N_2O$ (not shown). For monitoring $O_2$, $CO_2$, $N_2$, NO and $N_2O$, a robotised incubation system [28] was used, which automatically takes samples from the headspace by piercing the rubber septum. Each sampling removes a fraction (3–3.4%) of all gases in the headspace, but it also involves a marginal leakage of $O_2$ and $N_2$ into the vial (as indicated by the two-way arrows at the top of the figure). The model: The model operates with two sub-populations: one without and the other with denitrification enzymes ($N_{D-}$ and $N_{D+}$, respectively). Both consume $O_2$ if present, but $N_{D-}$ cannot reduce $NO_x$. The $N_{D-}$ cells may be recruited to the $N_{D+}$ pool as $[O_2]_{aq}$ falls below a critical threshold. The rate of recruitment ($R_{rec}$) is modelled as a probabilistic function: $R_{rec} = N_{D-} \times r_{den}(O_2)$ (cells $h^{-1}$), where $r_{den}(O_2)$ represents an $O_2$ dependent specific-probability ($h^{-1}$) for any $N_{D-}$ cell to initiate *nirS* transcription (leading to the synthesis of a full-fledged denitrification proteome).
doi:10.1371/journal.pcbi.1003933.g003

**Treatments selected for simulation.** Only $NO_2^-$-supplemented treatments (Table 1) were selected for this modelling exercise for two reasons. First, $NO_2^-$ was not monitored; hence, results of the $NO_3^-$-supplemented treatments could not provide exact estimates of anaerobic respiration rates (due to an unknown transient accumulation of $NO_2^-$). Second, by excluding the treatments requiring Nar, we could single out and focus on the regulation of the other key enzyme NirS.

**Aerobic respiration followed by denitrification.** $O_2$ diffused from the headspace to the liquid (Fig. 3), where the cells consumed it before switching to denitrification: the stepwise reduction of $NO_2^-$ to $N_2$ via the intermediates NO and $N_2O$ (not shown). Headspace concentrations of gases were monitored by frequent sampling (every 3 hours). A typical result is shown in Fig. 1A, illustrating the increasing rate of $O_2$ consumption until depletion, followed by transition to denitrification. The denitrification rate increased exponentially till all the $NO_2^-$ present in the medium was recovered as $N_2$. The medium contained ample amounts of carbon substrate (34 mM succinate) to support the consumption of all available electron acceptors.

**Sampling procedure.** To monitor $O_2$, $CO_2$, NO, $N_2O$, and $N_2$ in the headspace for respiring cultures, Bergaust *et al.* [4,8] used a robotised incubation system, which automatically takes samples from the headspace by piercing the rubber septum (Fig. 3). The auto-sampler is connected to a gas chromatograph (GC) and an NO analyser (For details, see [28]). The system uses peristaltic pumping, which removes a fraction (3–3.4%) of all the gases in the headspace and then reverses the pumping to inject an equal amount of He into the headspace, thus maintaining ~1 atmosphere pressure inside the vial. Sampling also involves a marginal leakage of $O_2$ and $N_2$ into the headspace (~22 and ~60 nmol per sampling, respectively) through tubing and membranes of the injection system.

**Calculation of gases in the liquid.** Concentrations of gases in the liquid were calculated using solubility of each gas at the given temperature (20°C), assuming equilibrium between the headspace and the liquid. However, the $O_2$ consumption rate was so high that to calculate $[O_2]$ in the liquid, its transport rate (from the headspace to the liquid) had to be taken into account.

## An overview of the model

The model effectively represents the physical phenomena mentioned above, so as to ensure that the simulation results match the measured data for the right reasons. Net effect of sampling (dilution and leakage) is included in the simulation of $O_2$ kinetics at the reported sampling times. Transport of $O_2$ between the headspace and the liquid is modelled using an empirically determined transport coefficient and the solubility of $O_2$ in water at 20°C. To simulate the metabolic activity ($O_2$ consumption and $N_2$ production) and growth, the model divides the cells into two sub-populations: one without and the other with denitrification enzymes ($N_{D-}$ and $N_{D+}$ pools, respectively, see Fig. 3). Both equally consume $O_2$ if present, but $N_{D-}$ cannot reduce $NO_2^-$ to $N_2$. Those $N_{D-}$ cells that, in response to $O_2$ depletion, are able to initiate *nirS* transcription (see Fig. 2) are recruited to the $N_{D+}$ pool, where $N_{D+} = 0$ prior to the recruitment. The recruitment rate ($R_{rec}$) is modelled according to a probabilistic function described below (Eqs. 7–8).

The model ignores sampling effect on $N_2$ (leakage and loss), thus calculating the cumulative $N_2$ production as if no sampling took place. That is because the experimentally determined $N_2$ accumulation (which is to be compared with the model predictions) was already corrected for the net sampling effect.

The model is developed in Vensim DSS 6.2 Double Precision (Ventana Systems, Inc. http://vensim.com/) using techniques from the field of system dynamics [29]. The model is divided into three sectors: I. $O_2$ kinetics, II. Population dynamics of $N_{D-}$ and $N_{D+}$, and III. Denitrification kinetics (Fig. 4).

## Sector I: $O_2$ kinetics

Structural-basis for the $O_2$ kinetics is mapped in Fig. 4A: the squares represent the state variables, the circles the rate of change in the state variables, the shaded ovals the auxiliary variables, the arrows mutual dependencies between the variables, and the edges represent flows into or out of the state variables. Briefly, Fig. 4A (left to right) shows that $O_2$ in the vial's headspace ($O_{2HS}$) is transported ($Tr_{O_2}$) to the liquid-phase ($O_{2LP}$), where it is consumed ($Cr_{O_2}$) by both the $N_{D-}$ and $N_{D+}$ populations (lacking and carrying denitrification enzymes, respectively) in proportion to an identical cell-specific velocity of $O_2$ consumption ($v_{O_2}$). $\Delta O_{2(S)}$ represents net marginal changes in $O_{2HS}$ due to sampling. Below we present equations and a detailed explanation of the structural components shown for this sector.

**$O_2$ in the headspace.** ($O_{2HS}$, mol vial$^{-1}$) is initialised by measured initial concentrations (Table 1) and modelled as a function of transport ($Tr_{O_2}$) between the headspace and the liquid [28]:

$$Tr_{O_2} = k_t \times \left(k_{H(O_2)} \times P_{O_2} - [O_2]_{LP}\right) \quad (1)$$

Units: *mol vial$^{-1}$ h$^{-1}$*

where $k_t$ (L vial$^{-1}$ h$^{-1}$) is the empirically determined coefficient for the transport of $O_2$ between the headspace and the liquid (See Table 2 for parametric values and their sources), $k_{H(O_2)}$ (mol L$^{-1}$ atm$^{-1}$) is the solubility of $O_2$ in water at 20°C, $P_{O_2}$ (atm) is the partial pressure of $O_2$ in the headspace, and $[O_2]_{LP}$ (mol L$^{-1}$) is the $O_2$ concentration in the liquid-phase $\left([O_2]_{LP} = \frac{O_{2LP}}{Vol_{LP}}\right)$.

In addition, changes in $O_{2HS}$ due to sampling are included at the reported sampling times. The robotised incubation system [28] used in the experiment monitors gas concentrations by sampling the headspace, where each sampling alters the concentrations in a predictable manner: a fraction of $O_{2HS}$ is removed and replaced by He (dilution), but the sampling also results in a marginal leakage of $O_2$ through the tubing and membranes of the injection system. Eq. 2 shows how the model calculates the *net* change in $O_{2HS}$ $(\Delta O_{2(S)})$ as a result of each sampling:

$$\Delta O_{2(S)} = \frac{(O_{2leak} - O_{2HS} \times D)}{t_s} \quad (2)$$

*mol vial$^{-1}$ h$^{-1}$*

where $O_{2leak}$ (mol vial$^{-1}$) is the $O_2$ leakage into the headspace, D (dilution) is the fraction of $O_{2HS}$ replaced by He, and $t_s$ (h) is the time taken to complete each sampling. $\Delta O_{2(S)}$ is negative if $O_{2HS}$ is greater than 0.58 µmol vial$^{-1}$ and marginally positive if it is less than that.

**$O_2$ in the liquid-phase.** ($O_{2LP}$, mol vial$^{-1}$, see Fig. 4A) is initialised by assuming equilibrium with $O_{2HS}$ at the time of inoculation $\left(O_{2LP}(t_0) = P_{O_2} \times k_{H(O_2)} \times Vol_{LP}\right)$. $O_{2LP}$ is modelled as a function of its transport into the liquid ($Tr_{O_2}$, Eq. 1) and consumption rate ($Cr_{O_2}$, mol vial$^{-1}$ h$^{-1}$), where the latter is

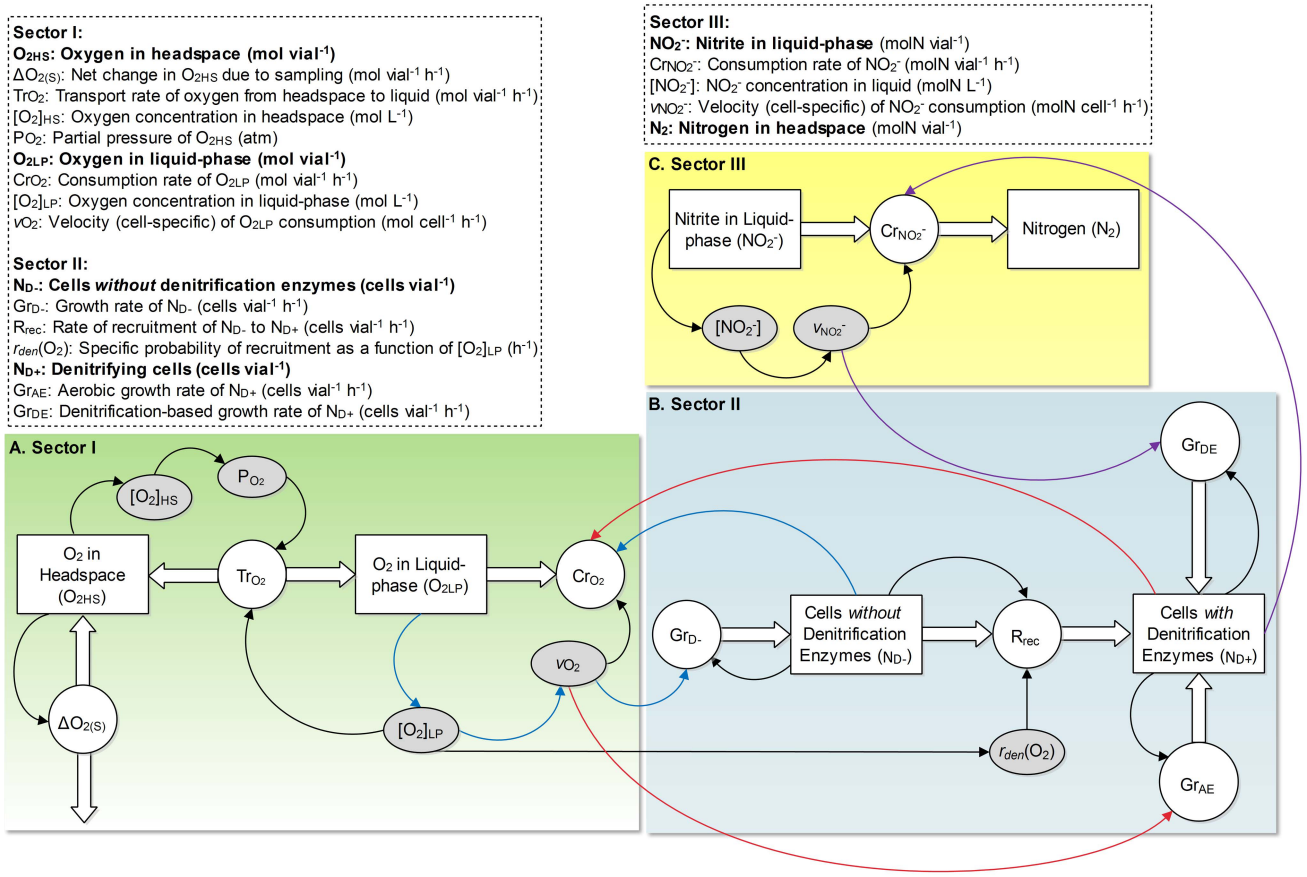


**Figure 4. A stock and flow diagram of the model's structure.** The squares represent the state variables, the circles the rate of change in the state variables, the shaded ovals the auxiliary variables, the arrows dependencies between the variables, and the edges represent flows into or out of the state variables. **A.** The panel represents the structure that governs the $O_2$ kinetics. Briefly, it shows that $O_2$ in the vial's headspace ($O_{2HS}$) is transported ($Tr_{O_2}$) to the liquid-phase ($O_{2LP}$), where it is consumed ($Cr_{O_2}$) by both $N_{D-}$ and $N_{D+}$ populations with an identical cell-specific velocity of $O_2$ consumption ($v_{O_2}$). $\Delta O_{2(S)}$ represents net marginal changes in $O_{2HS}$ due to sampling. **B.** The panel represents the structural basis for population dynamics of the cells without ($N_{D-}$) and with ($N_{D+}$) denitrification enzymes. Briefly, it shows that both the populations are able to grow by aerobic respiration ($Gr_{D-}$ and $Gr_{AE}$, respectively). The growth rate of $N_{D+}$, however, is primarily based on denitrification ($Gr_{DE}$). Initially, $N_{D+}=0$ and is populated through recruitment ($R_{rec}$) of the cells from $N_{D-}$, where the recruitment is a function of $N_{D-}$ and an $[O_2]$ dependent specific-probability of the recruitment ($r_{den}(O_2)$) for any $N_{D-}$ cell. **C.** The panel represents the structural basis for the $NO_2^-/N_2$ kinetics. Briefly, it illustrates that $N_{D+}$ control the consumption rate of $NO_2^-$ ($Cr_{NO_2^-}$), recovered as $N_2$, in proportion to a cell-specific velocity of $NO_2^-$ consumption ($v_{NO_2^-}$).
doi:10.1371/journal.pcbi.1003933.g004

modelled as a function of total cell numbers and the cell-specific velocity of $O_2$ consumption:

$$\frac{d(O_{2LP})}{dt} = Tr_{O_2} - Cr_{O_2} = Tr_{O_2} - (N_{D-} + N_{D+}) \times v_{O_2} \quad (3)$$

$$mol\ vial^{-1}\ h^{-1}$$

where $N_{D-}$ and $N_{D+}$ (cells $vial^{-1}$, see Sector II for details) are the cells without and with denitrification enzymes, respectively, and $v_{O_2}$ (mol $cell^{-1}$ $h^{-1}$) is the cell-specific velocity of $O_2$ consumption. Thus, we assume that the $N_{D+}$ and $N_{D-}$ cells have the same potential to consume $O_2$.

$v_{O_2}$ is modelled as a Michaelis-Menten function of $O_2$ concentration:

$$v_{O_2} = \frac{v_{max(O_2)} \times [O_2]_{LP}}{\left(K_{m(O_2)} + [O_2]_{LP}\right)} \quad (4)$$

$$mol\ cell^{-1}\ h^{-1}$$

where $v_{max(O_2)}$ (mol $cell^{-1}$ $h^{-1}$) is the maximum cell-specific velocity of $O_2$ consumption (determined under the actual experimental conditions), $[O_2]_{LP}$ (mol $L^{-1}$) is the $O_2$ concentration in the liquid-phase, and $K_{m(O_2)}$ (mol $L^{-1}$) is the half saturation constant for $O_2$ reduction.

## Sector II: Population dynamics of the cells without ($N_{D-}$) and with ($N_{D+}$) denitrification proteome

Fig. 4B represents the structure governing the population dynamics of $N_{D-}$ and $N_{D+}$. Briefly, the figure shows that both the populations are able to grow by aerobic respiration ($Gr_{D-}$ and $Gr_{AE}$, respectively). Initially, $N_{D+}=0$ and is populated through recruitment ($R_{rec}$) of the cells from the $N_{D-}$ pool, where the recruitment is a product of $N_{D-}$ and an $[O_2]$ dependent specific-probability ($h^{-1}$) of the recruitment ($r_{den}(O_2)$, see Eqs. 7–8). The growth rate of $N_{D+}$ is primarily based on denitrification ($Gr_{DE}$), but the $N_{D+}$ cells that are recruited before $O_2$ is completely exhausted also grow by consuming the remaining traces of $O_2$. Below we present equations and a detailed explanation of the structural components shown for this sector.

**Table 2.** Model parameters.

| | Description | Value | Units | Reference |
|---|---|---|---|---|
| **Sector I: $O_2$ Kinetics** | | | | |
| D | Dilution: the fraction of $O_2$ replaced by He during sampling | 0.035 | Unitless | [28] |
| $k_{H(O_2)}$ | Solubility of $O_2$ in water (20°C) | 0.00139 | mol $L^{-1}$ $atm^{-1}$ | [37] |
| $k_t$ | The $O_2$ transport coefficient between headspace and liquid | 1.62 | L $vial^{-1}$ $h^{-1}$ | [28] |
| $O_{2leak}$ | $O_2$ leakage into the vial during each sampling | $2.04\times10^{-8}$ | mol $vial^{-1}$ | [28] |
| $t_s$ | The time taken to complete each sampling | 0.017 | h | [28] |
| $K_{m(O_2)}$ | The half saturation constant for $O_2$ consumption | $2.5\times10^{-7}$ | mol $L^{-1}$ | Model-based estimation |
| $v_{max(O_2)}$ | The maximum cell-specific velocity of $O_2$ consumption | $1.33\times10^{-15}$ | mol $cell^{-1}$ $h^{-1}$ | [4,8] |
| **Sector II: Population dynamics of the cells without ($N_{D-}$) and with ($N_{D+}$) denitrification proteome** | | | | |
| $[O_2]_{min}$ | $[O_2]$ in the liquid below which the recruitment to $N_{D+}$ halts | $1\times10^{-9}$ | mol $L^{-1}$ | Assumption |
| $[O_2]_{trigger}$ | $[O_2]$ below which the recruitment to $N_{D+}$ triggers | $9.75\times10^{-6}$ | mol $L^{-1}$ | [22] |
| $r_{den}$ | The specific-probability of recruitment of a cell to $N_{D+}$ | 0.0052 | $h^{-1}$ | Model-based estimation |
| $Y_{NO_2^-}$ | The growth yield per molN $NO_2^-$ | $5.79\times10^{13}$ | cells $molN^{-1}$ | [4,8] |
| $Y_{O_2}$ | The growth yield per mol $O_2$ | $15\times10^{13}$ | cells $mol^{-1}$ | [4,8] |
| **Sector III: Denitrification Kinetics** | | | | |
| $K_{m(NO_2^-)}$ | The half saturation constant for $NO_2^-$ reduction | $4\times10^{-6}$ | molN $L^{-1}$ | [33,34] |
| $v_{max(NO_2^-)}$ | The maximum cell-specific velocity of $NO_2^-$ reduction | $1.83\times10^{-15}$ | molN $cell^{-1}$ $h^{-1}$ | [4,8] |
| **General** | | | | |
| R | Universal gas constant | 0.083 | L atm $K^{-1}$ $mol^{-1}$ | – |
| T | Temperature | 293.1 | K | [4,8] |
| $Vol_{HS}$ | Headspace volume | 0.07 | L $vial^{-1}$ | [4,8] |
| $Vol_{LP}$ | Liquid-phase volume | 0.05 | L $vial^{-1}$ | [4,8] |

doi:10.1371/journal.pcbi.1003933.t002

**The pool of the cells lacking denitrification proteome.** The pool of the cells lacking denitrification proteome ($N_{D-}$) is initialised with $3\times10^8$ cells $vial^{-1}$. The population dynamics of $N_{D-}$ are modelled as:

$$\frac{d(N_{D-})}{dt} = Gr_{D-} - R_{rec} \quad (5)$$

$$cells\ vial^{-1}\ h^{-1}$$

where $Gr_{D-}$ (cells $vial^{-1}$ $h^{-1}$) is the (aerobic) growth rate, and $R_{rec}$ (cells $vial^{-1}$ $h^{-1}$, Eq. 7) is the rate of recruitment of $N_{D-}$ to the $N_{D+}$ pool.

$Gr_{D-}$ is modelled as:

$$Gr_{D-} = N_{D-} \times v_{O_2} \times Y_{O_2} \quad (6)$$

$$cells\ vial^{-1}\ h^{-1}$$

where $v_{O_2}$ (mol $cell^{-1}$ $h^{-1}$, Eq. 4) is the cell-specific velocity of $O_2$ consumption, and $Y_{O_2}$ (cells $mol^{-1}$) is the cell yield per mole of $O_2$ (determined under the actual experimental conditions).

**The rate of recruitment.** The rate of recruitment ($R_{rec}$, see Fig. 4B) of the cells from $N_{D-}$ to $N_{D+}$ is modelled as:

$$R_{rec} = N_{D-} \times r_{den}(O_2) \quad (7)$$

$$cells\ vial^{-1}\ h^{-1}$$

where $r_{den}(O_2)$ ($h^{-1}$) represents the conditional specific-probability for any $N_{D-}$ cell to be recruited to denitrification, modelled as a function of $O_2$ concentration in the liquid-phase ($[O_2]_{LP}$, see Fig. 5):

$$r_{den}(O_2) = \begin{cases} 0 & for \quad [O_2]_{LP} > [O_2]_{trigger} \\ r_{den} & for \quad [O_2]_{min} < [O_2]_{LP} < [O_2]_{trigger} \\ 0 & for \quad [O_2]_{LP} < [O_2]_{min} \end{cases} \quad (8)$$

$$h^{-1}$$

where $r_{den}$ ($h^{-1}$) is a constant representing the specific-probability of the recruitment, $[O_2]_{trigger}$ is the $O_2$ concentration above which the transcription of *nirS* is effectively suppressed by $O_2$, and $[O_2]_{min}$ is the $O_2$ concentration assumed to provide minimum energy for the initial transcription to result in functional NirS. Once the first molecules of NirS are produced while $[O_2]_{min} < [O_2]_{LP} < [O_2]_{trigger}$, the transcription of *nirS* will be greatly enhanced through positive feedback by NO, paving the way for a full-scale production of denitrification proteome [10] (See Introduction and Fig. 2 for details).

$[O_2]_{trigger}$ ($= 9.75\times10^{-6}$ mol $L^{-1}$) is the empirically determined $[O_2]_{LP}$ at the outset of NO accumulation: Bergaust *et al.* [8] estimated $[O_2]_{trigger}$ between 0.1–12 μM, but recent *Pa. denitrificans* batch incubation data have provided a more precise estimate between 8.8–10.7 μM (average = 9.75 μM) [22].

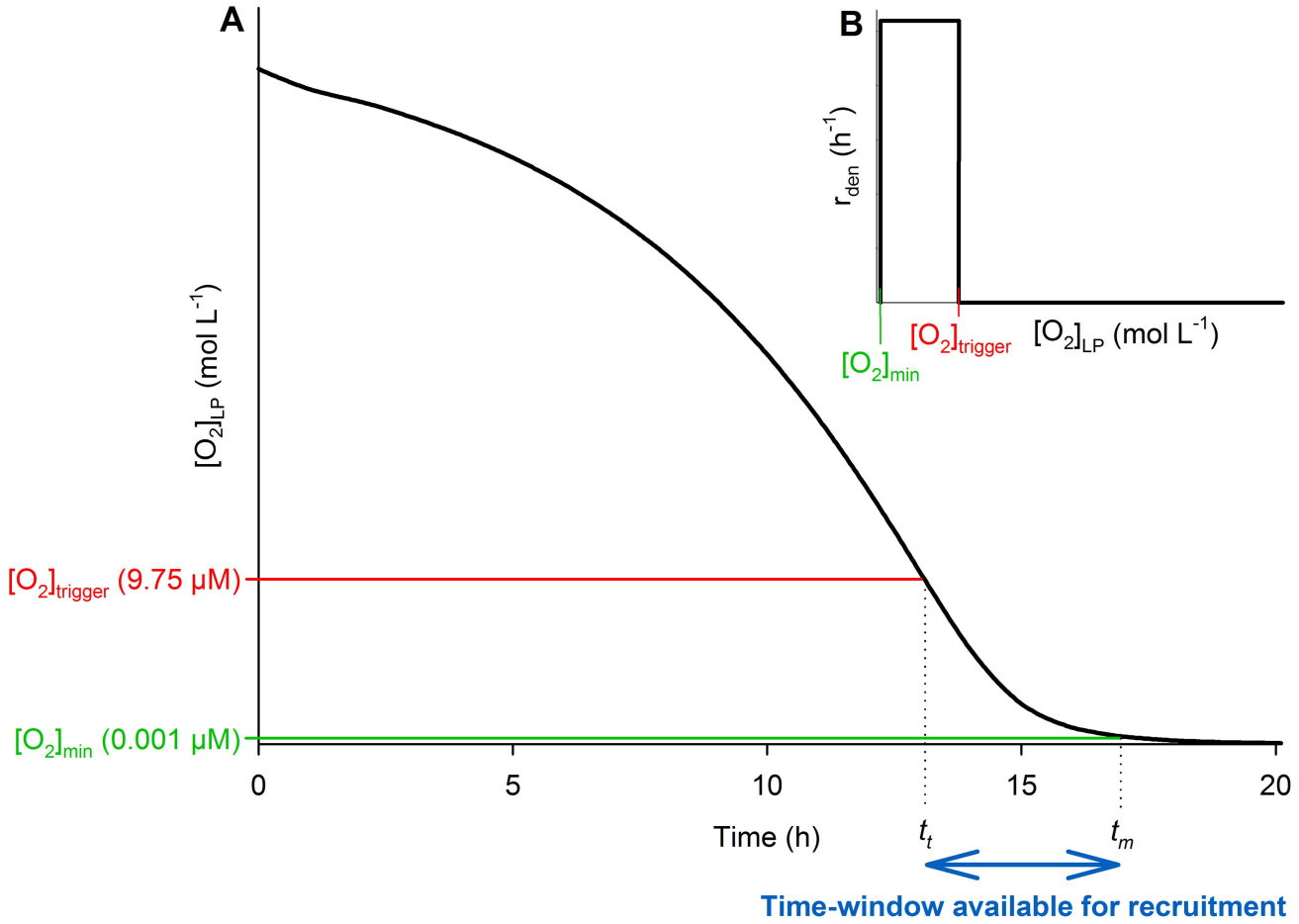


**Figure 5. Modelling of $r_{den}(h^{-1})$ as a function of $[O_2]_{LP}$. A.** The panel shows the $O_2$ concentration in the liquid-phase ($[O_2]_{LP}$) falling as a result of aerobic respiration. **B.** The panel shows the probability for a cell to switch to denitrification ($r_{den}$, $h^{-1}$) modelled as a function of $[O_2]_{LP}$. $[O_2]_{trigger}$ (Panels A & B) is the concentration below which $r_{den}$ is assumed to trigger (due to withdrawal of the transcriptional control of $O_2$ on denitrification [22]), whereas $[O_2]_{min}$ is assumed to be the concentration below which $r_{den}$ terminates (due to lack of energy for enzyme synthesis). The double-headed arrow (at the bottom of Panel A) illustrates the limited time-window ($t_m - t_t$) available for the cells to switch to denitrification.
doi:10.1371/journal.pcbi.1003933.g005

As for $[O_2]_{min}$, we lack empirical basis for determining the parameter value, but sensitivity of the model to this parameter was tested (See Results/Discussion). Our simulations were run with $[O_2]_{min} = 1 \times 10^{-9}$ mol $L^{-1}$, which would sustain an aerobic respiration rate equivalent to 0.4% of the empirically determined $v_{max(O_2)}$ (assuming our estimated $K_{m(O_2)} = 2.5 \times 10^{-7}$ mol $L^{-1}$, Table 2).

As modelled, the time-window for the recruitment to denitrification depends on the time taken to deplete $[O_2]_{LP}$ from $[O_2]_{trigger}$ to $[O_2]_{min}$ (Fig. 5); for obvious reasons, the length of this time-window depends on the cell density.

The lag observed between the emergence of denitrification gene transcripts and the subsequent gas products is as short as 20 minutes [8,22], which is insignificant in the sense that the estimations of $r_{den}$ and $F_{den}$ will not be affected by including it in the model. Therefore, the recruitment (Eq. 7) is modelled as an instantaneous event.

**Calculation of $F_{den}$: The fraction of the cells recruited to denitrification.** $F_{den}$ is calculated based on the integral of the recruitment (Eq. 7):

$$F_{den} = 1 - e^{-r_{den} \times (t_m - t_t)} \qquad (9)$$

*Dimensionless*

where $r_{den}$ ($h^{-1}$, see Eqs. 7–8 and Fig. 5) is the specific-probability for the recruitment of a cell to denitrification, $t_t$ is the time when $[O_2]$ in the liquid falls below $[O_2]_{trigger}$ (the concentration below which $r_{den}$ triggers), and $t_m$ is the time when $[O_2]$ in the liquid falls below $[O_2]_{min}$ (the concentration below which $r_{den}$ is assumed to be zero). Hence, effectively, $F_{den}$ expresses the probability for any cell to switch to denitrification within the time-frame $t_m - t_t$.

**The pool of the cells carrying denitrification proteome.** The pool of the cells carrying denitrification proteome ($N_{D+}$, see Fig. 4B) is initialised with zero cells, and its population dynamics are modelled as:

$$\frac{d(N_{D+})}{dt} = R_{rec} + Gr_{DE} + Gr_{AE} \qquad (10)$$

*cells $vial^{-1}$ $h^{-1}$*

where $R_{rec}$ (cells $vial^{-1}$ $h^{-1}$, Eq. 7) is the recruitment rate, $Gr_{DE}$ (cells $vial^{-1}$ $h^{-1}$) the denitrification-based growth and $Gr_{AE}$ (cells $vial^{-1}$ $h^{-1}$) the aerobic growth rate.

$Gr_{DE}$ is modelled as:

$$Gr_{DE} = N_{D+} \times v_{NO_2^-} \times Y_{NO_2^-} \quad (11)$$

$$cells\ vial^{-1}\ h^{-1}$$

where $v_{NO_2^-}$ (molN cell$^{-1}$ h$^{-1}$, see Eq. 15) is the cell-specific velocity of $NO_2^-$ reduction, and $Y_{NO_2^-}$ (cells molN$^{-1}$) is the growth yield per molN of $NO_2^-$ as the $e^-$-acceptor (determined under the actual experimental conditions).

The $N_{D+}$ cells are assumed to have the same ability as $N_{D-}$ to grow by aerobic respiration; their aerobic growth rate is formulated as:

$$Gr_{AE} = N_{D+} \times v_{O_2} \times Y_{O_2} \quad (12)$$

$$cells\ vial^{-1}\ h^{-1}$$

where $v_{O_2}$ (mol cell$^{-1}$ h$^{-1}$, see Eq. 4) is the cell-specific velocity of $O_2$ consumption, and $Y_{O_2}$ (cells mol$^{-1}$) is the growth yield per mole of $O_2$ as the $e^-$-acceptor.

## Sector III: Denitrification kinetics

The structure controlling the denitrification kinetics is mapped in Fig. 4C. Briefly, the figure shows that the cells with denitrification proteome ($N_{D+}$) control the consumption rate of $NO_2^-$ ($Cr_{NO_2^-}$), recovered as $N_2$, in proportion to a cell-specific velocity of $NO_2^-$ consumption ($v_{NO_2^-}$). The denitrification intermediates NO and $N_2O$ are not explicitly modelled, as they accumulated to miniscule concentrations only [4,8].

**$NO_2^-$ and $N_2$.** The $NO_2^-$ pool (molN vial$^{-1}$) is initialised by measured initial concentrations (Table 1), and the $N_2$ pool is initialised with zero molN vial$^{-1}$. $NO_2^-$ and $N_2$ kinetics are modelled as:

$$\frac{d(NO_2^-)}{dt} = -Cr_{NO_2^-} \quad (13)$$

$$molN\ vial^{-1}\ h^{-1}$$

where $Cr_{NO_2^-}$ is the consumption rate of $NO_2^-$:

$$Cr_{NO_2^-} = N_{D+} \times v_{NO_2^-} \quad (14)$$

$$molN\ vial^{-1}\ h^{-1}$$

where $N_{D+}$ (cells vial$^{-1}$) represents the denitrifying cells, and $v_{NO_2^-}$ (molN cell$^{-1}$ h$^{-1}$) is the cell-specific velocity of $NO_2^-$ reduction, which is modelled as a function of $NO_2^-$ using the Michaelis-Menten equation:

$$v_{NO_2^-} = \frac{v_{max(NO_2^-)} \times [NO_2^-]}{\left(K_{m(NO_2^-)} + [NO_2^-]\right)} \quad (15)$$

$$molN\ cell^{-1}\ h^{-1}$$

where $v_{max(NO_2^-)}$ (molN cell$^{-1}$ h$^{-1}$) is the maximum cell-specific velocity of $NO_2^-$ consumption (determined under the actual experimental conditions), $[NO_2^-]$ (molN L$^{-1}$) is the $NO_2^-$ concentration in the liquid-phase, and $K_{m(NO_2^-)}$ (molN L$^{-1}$) is the half saturation constant for $NO_2^-$ reduction.

See Table 2 for a summary of the parametric values and their sources and Table 3 for the initial values assigned to the state variables.

## Parameterisation

Most of the parameter values used in the model are well established in the literature (See Table 2). However, somewhat uncertain parameters include $K_{m(O_2)}$, $K_{m(NO_2^-)}$, $[O_2]_{trigger}$, and the assumed parameter $[O_2]_{min}$:

**$K_{m(O_2)}$.** *Pa. denitrificans* has three alternative terminal oxidases [30] with $K_{m(O_2)}$ ranging from nM to μM [31,32], so we decided to estimate $K_{m(O_2)}$ by fitting our model to the data. Unfortunately, Bergaust *et al.'s* [4,8] ~0% $O_2$ treatments data, for which $K_{m(O_2)}$ is relevant, has technical problems (needle clogging and/or high $O_2$ leakage during sampling). Therefore, we estimated $K_{m(O_2)}$ ($=2.5\times10^{-7}$ mol L$^{-1}$) by aptly simulating our model against another ~0% $O_2$ data-set produced by batch cultivations of *Pa. denitrificans* under similar experimental conditions [22].

**$K_{m(NO_2^-)}$** is given in the literature as 4–5 μM [33,34]. The model, however, does not show any considerable sensitivity to this parameter even within a range as wide as 0.1–10 μM because the simulated experiments were operating with much higher $[NO_2^-]$.

**$[O_2]_{trigger}$** ($=9.75\times10^{-6}$ mol L$^{-1}$) is empirically determined as the $[O_2]_{LP}$ at the outset of NO accumulation: Bergaust *et al.* [8]

**Table 3.** Initial values for the state variables.

| | Symbol | Value | Units | Reference |
|---|---|---|---|---|
| **Sector 1: O2 Kinetics** | | | | |
| Initial $O_2$ in the headspace | $O_{2HS}(t_0)$ | See Table 5 | mol vial$^{-1}$ | [4,8] |
| Initial $O_2$ in the liquid-phase | $O_{2LP}(t_0)$ | Equilibrium with $O_{2HS}(t_0)$ | mol vial$^{-1}$ | Assumption |
| **Sector II: Population dynamics of the cells without ($N_{D-}$) and with ($N_{D+}$)denitrification proteome** | | | | |
| The initial number of cells | $N_{D-}(t_0)$ | $3\times10^8$ | cells vial$^{-1}$ | [4,8] |
| The initial number of denitrifying cells | $N_{D+}(t_0)$ | 0 | cells vial$^{-1}$ | Assumption |
| **Sector III: Denitrification Kinetics** | | | | |
| Initial $NO_2^-$ in the liquid-phase | $NO_2^-(t_0)$ | See Table 5 | molN vial$^{-1}$ | [4,8] |
| Initial $N_2$ in the headspace | $N_2(t_0)$ | 0 | molN vial$^{-1}$ | [4,8] |

doi:10.1371/journal.pcbi.1003933.t003

estimated $[O_2]_{trigger}$ between 0.1–12 μM, but recent batch incubation data from *Pa. denitrificans* have provided a more precise estimate in the range 8.8–10.7 μM (average = 9.75 μM) [22]. The model, however, is not sensitive to $[O_2]_{trigger}$ within the latter range because of a high velocity of $O_2$ depletion.

$[\mathbf{O_2}]_{\mathbf{min}}$ ($=1\times10^{-9}$ mol $L^{-1}$) is assigned an arbitrary low value, since we lack any empirical estimation/data to support it. To compensate for the uncertainty, we conducted a sensitivity analysis exploring the consequences of increasing or decreasing $[O_2]_{min}$ by one order of magnitude (See Results/Discussion).

## Results/Discussion

### The specific-probability ($r_{den}$, $h^{-1}$) of recruitment of a cell to denitrification

To test the assumption of a single homogeneous population, we forced our model to achieve 100% recruitment to denitrification by setting $r_{den} = 1\ h^{-1}$. In consequence, the simulated $N_2$ accumulation (molN $vial^{-1}$) showed gross overestimation as compared to the measured for all the treatments (as illustrated for some randomly selected ones in Fig. 6).

To find a more adequate value, $r_{den}$ was calibrated to produce the best possible match between the simulated and measured $N_2$ through optimisation. (The optimisation was carried out in Vensim DSS 6.2 Double Precision, http://vensim.com/). Table 4 presents the optimal $r_{den}$ for each treatment; no consistent effect of initial $[O_2]$ and $[NO_2^-]$ was found on the optimal results. The average for all the treatments = 0.0052, which appears to give reasonable fit between the simulated and measured $N_2$ (See Figs. 7, 8, and 9). This indicates that the simulations with $r_{den} = 0.0052$ should provide a reasonable approximation of $F_{den}$ (the fraction recruited to denitrification) during the actual experiment.

**Sensitivity analysis.** $[\mathbf{O_2}]_{\mathbf{min}}$ (the $O_2$ concentration below which the recruitment is arrested) was arbitrarily chosen to be $1\times10^{-9}$ mol $L^{-1}$. In order to evaluate the sensitivity of the model to this parameter, we tested the model performance by increasing and decreasing $[O_2]_{min}$ by one order of magnitude. For each parameter value, we estimated $r_{den}$ for the individual vials by optimisation (as outlined in the foregoing paragraph). A good fit was obtained for both the $[O_2]_{min}$ values, but the optimisation resulted in slightly different $r_{den}$ values. Increasing $[O_2]_{min}$ by a

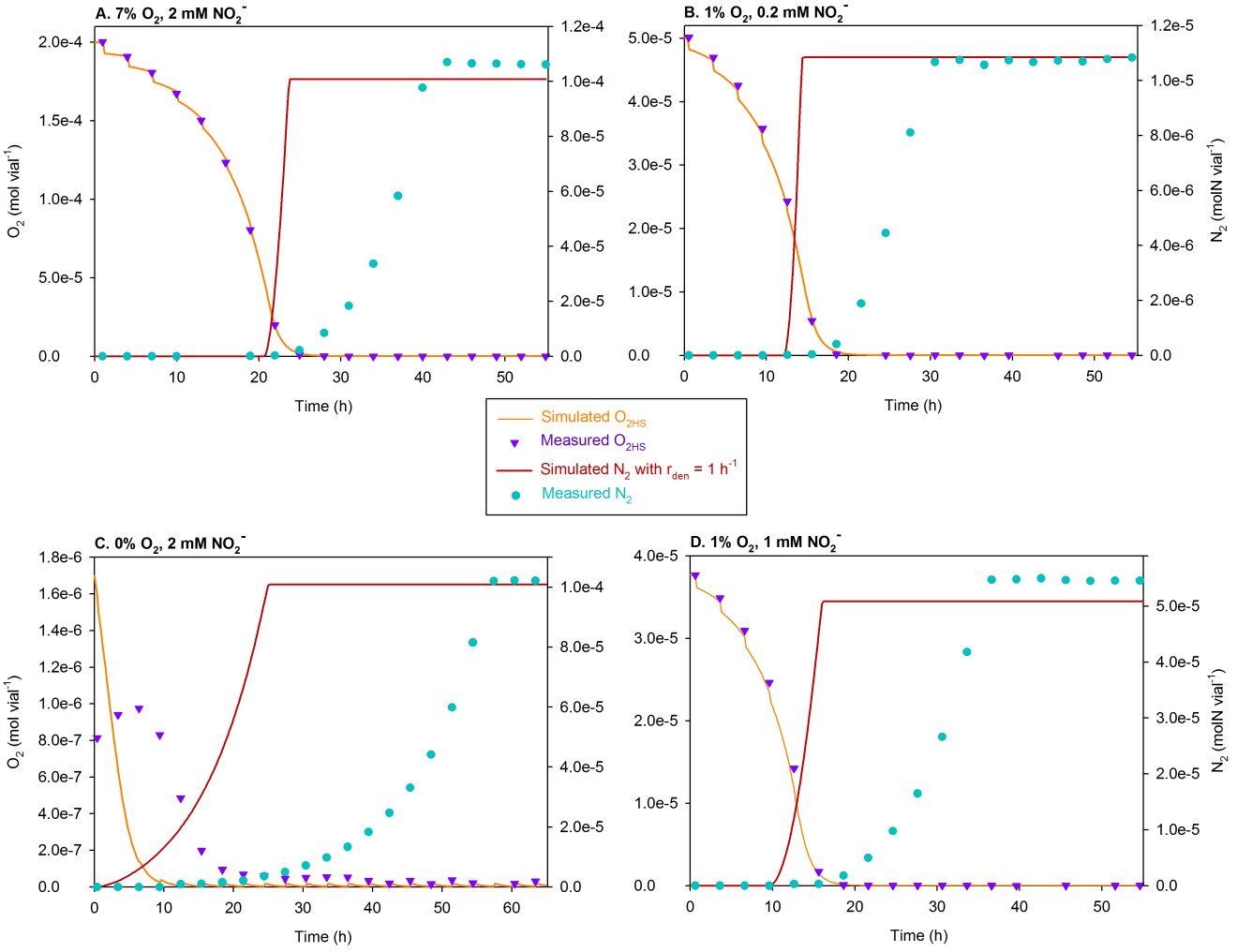


**Figure 6. Comparison of the measured [4,8] and simulated data assuming $r_{den} = 1\ h^{-1}$.** Assuming a single homogeneous population, as we forced our model to achieve 100% recruitment to denitrification by setting the specific-probability of recruitment ($r_{den}$) to 1 $h^{-1}$, the simulated $N_2$ accumulation (molN $vial^{-1}$) showed considerable overestimation as compared to that measured. To illustrate this, the simulated and measured data are compared here for some randomly chosen treatments. Initial vol.% $O_2$ in the headspace and initial $NO_2^-$ is shown above each panel.
doi:10.1371/journal.pcbi.1003933.g006

**Table 4.** Specific-probability of recruitment of a cell to denitrification ($r_{den}$) estimated for each batch culture by optimisation (best match between the simulated and measured $N_2$ kinetics).

| Batch No. | Treatment*: $O_{2HS}(t_0)$ (vol.%) $NO_2^-(t_0)$ (mM) | Optimal $r_{den}$ ($h^{-1}$) |
|---|---|---|
| 1 | ~0, 0.2 | 0.0066 |
| 2 | ~0, 1 | 0.0059 |
| 3 | ~0, 2 | 0.0029 |
| 4 | 1, 0.2 | 0.0033 |
| 5 | 1, 1 | 0.0062 |
| 6 | 1, 2 | 0.0020 |
| 7 | 7, 0.2 | 0.0018 |
| 8 | 7, 1 | 0.0117 |
| 9 | 7, 2 | 0.0066 |
| | | **Avg. = 0.0052** |

*Treatment refers to the initial concentration of $O_2$ in the headspace (measured as headspace vol.%) and the initial concentration of $NO_2^-$ in the medium (mM).
doi:10.1371/journal.pcbi.1003933.t004

factor of 10 (to $1\times10^{-8}$ mol $L^{-1}$) resulted in 18–38% higher $r_{den}$ estimates (average = 28% ±stdev 10). Decreasing $[O_2]_{min}$ by a factor of 0.1 (to $1\times10^{-10}$ mol $L^{-1}$) resulted in 5–17% lower $r_{den}$ estimates (average = 11% ±stdev 6).

## The fraction recruited to denitrification ($F_{den}$)

**A refined estimation with the presented model.** Bergaust *et al.* [8,16] and Nadeem *et al.* [9] used data from batch cultivations of *Pa. denitrificans*, as illustrated in Fig. 1, to assess $F_{den}$. Their estimation was effectively $F_{den} = \frac{N_{D+}(t_{ex})}{N(t_{ex})}$, where $t_{ex}$ is the time when $O_2$ is exhausted, $N_{D+}$ (cells $vial^{-1}$) is the number of actively denitrifying cells estimated by the measured rate of denitrification (molN $h^{-1}$) divided by the cell-specific denitrification (molN $cell^{-1}$ $h^{-1}$), and N is the total number of cells estimated on the basis of $O_2$ consumption. Although this equation indisputably estimates the fraction of the cells that was actively denitrifying at the time $t_{ex}$, it is a biased estimate of the 'true' $F_{den}$ because the number of cells does not remain constant through the recruitment phase: $N_{D-}$ (the cells without denitrification enzymes) and $N_{D+}$ will both grow until $O_2$ is depleted, but $N_{D+}$ will grow faster because their growth is supported by both $O_2$ and $NO_x$. As a result, the estimation of $F_{den}$ by this equation might be too high.

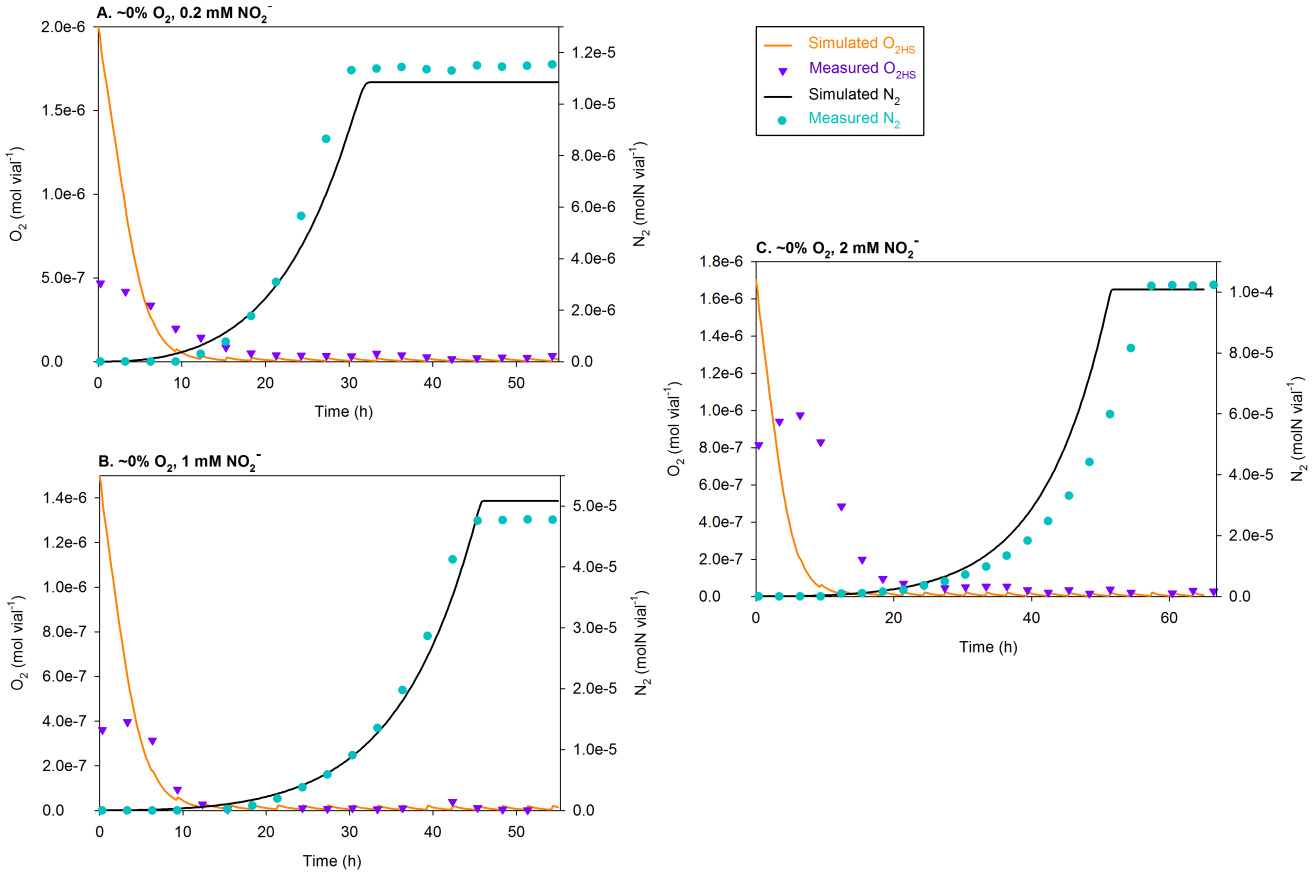


**Figure 7. Simulations of the treatments with ~0 vol.% $O_{2HS}$ using $r_{den} = 0.0052\ h^{-1}$.** The figure compares the measured and simulated $O_2$ depletion (mol $vial^{-1}$) and $N_2$ accumulation (molN $vial^{-1}$) for the ~0 vol.% $O_2$ treatments of Bergaust *et al.* [4,8], i.e., the vials with near-zero $O_2$ in the headspace ($O_{2HS}$) at the time of inoculation. Separate plots are shown for each initial concentration of $NO_2^-$ (0.2, 1, and 2 mM). The measured initial $O_2$ was somewhat erratic due to episodes of needle clogging and/or high $O_2$ leakage during sampling, so the initial $O_{2HS}$ used in the simulations is chosen somewhat *ad lib* so that the simulated $O_2$ depletion coincides with that measured. The discrepancy compared to the measured $O_2$ seems to be significant for 2 mM $NO_2^-$ treatment. That is most likely due to the inhibitory effect of nitrite on aerobic respiration, which is not taken into account; all simulations are run with an identical $K_{m(O_2)}$. Near exhaustion, the simulated $O_2$ increases slightly at each sampling time; that is due to the leakage of $O_2$ via the injection system exceeding dilution of the headspace (with He) during each sampling.
doi:10.1371/journal.pcbi.1003933.g007

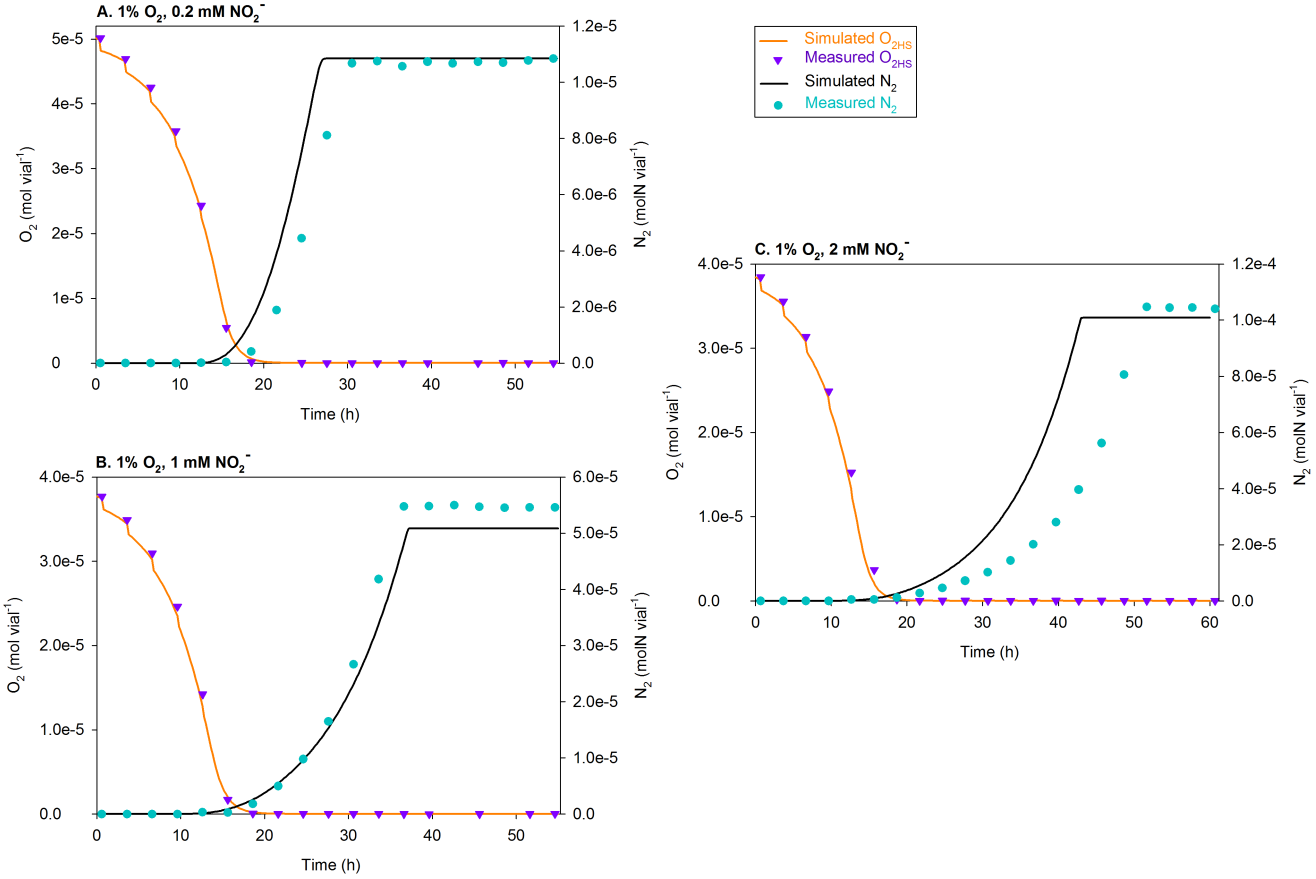


**Figure 8. Simulations of the treatments with 1 vol.% $O_{2HS}$ using $r_{den} = 0.0052\ h^{-1}$.** The figure compares the measured and simulated $O_2$ depletion (mol $vial^{-1}$) and $N_2$ accumulation (molN $vial^{-1}$) for the treatments with 1 vol.% $O_2$ in the headspace ($O_{2HS}$) at the time of inoculation; separate plots are shown for each initial concentration of $NO_2^-$ (0.2, 1, and 2 mM). At each sampling time, the simulated $O_2$ is visibly reduced; that is because sampling implies 3.4% dilution of the headspace (with He). This contrasts with the simulations of the treatments with low $O_2$ (Fig. 7), where the leakage of $O_2$ into the system is more dominant.
doi:10.1371/journal.pcbi.1003933.g008

Besides, the experimental estimation is prone to error because of infrequent sampling, since the sampling time does not necessarily coincide with $t_{ex}$.

In contrast, our model directly and more precisely calculates $F_{den}$ (Eq. 9) by ***a)*** explicitly simulating the actual kinetics of the recruitment of the cells to denitrification (in contrast to estimating total and denitrifying cell numbers from gas kinetics) and ***b)*** avoiding aerobic and anaerobic growth of the cells. Table 5 shows the model's estimations of $F_{den}$ and the time-span of the recruitment ($t_m - t_l$) along with the $F_{den}$ estimations of Bergaust *et al* [8,16].

**In the ~0% $O_2$ treatments, $F_{den}$ is supported by the sampling leaks of $O_2$.** Due to low cell density in the ~0% $O_2$ treatments (initial $O_2$ = 1.5–2 µmol), the $O_2$ leakage into the vial during sampling (every 3 hours) caused oxygen concentrations to exceed $[O_2]_{min}$ for 0.1–2.4 hours. This resulted in various spikes of recruitment after the initial $O_2$ was depleted. The recruitment through these spikes amounted to, on average, ~19% of $F_{den}$ in the ~0% $O_2$ treatments.

**$F_{den}$<<100%.** The model's estimations of $F_{den}$ (Table 5) corroborate the suggestion of Bergaust *et al.* [8,16] and Nadeem *et al.* [9] that in batch cultures of *Pa. denitrificans* $F_{den}$ remains far below 100%. According to Bergaust *et al.* [8,16], $F_{den}$ was 2–21% (average = 10%), whereas the model estimated it between 3.8–16.1% (average = 8.2%).

**$F_{den}$ is inversely related to cell density.** Bergaust *et al.* [16] argued that as the velocity of $O_2$ depletion is proportional to cell density, the time-frame available for the cells to produce (necessary initial) denitrification proteome would be inversely related to the cell density at the time of $O_2$ depletion. Simulation results (Table 5) support this: high initial $O_2$ concentrations resulted in high cell densities at the time of $O_2$ depletion, shortening the time-span for the recruitment to denitrification, hence resulting in the low $F_{den}$.

**Underlying cause of the low $F_{den}$.** $F_{den}$ remains low because of ***a)*** the limited time-window available to the cells for the recruitment and ***b)*** the low $r_{den}$ (specific-probability of the recruitment), presumably due to a low probability of initiating *nirS* transcription (subsequently reinforced through positive feedback by NO).

## Simulation of the 'diauxic lag'

To investigate whether the recruitment of a small fraction of the cells to denitrification could explain the 'diauxic lag' observed by Liu *et al.* [24], we used our model to simulate the conditions they reported for their experiment. In short, Liu *et al.* [24] incubated *Ps. denitrificans* (ATCC 13867) in oxic batch cultures, which were sparged with $N_2$ as the cultures had reached different cell densities ($OD_{550}$ = 0.05–0.17). The sparging resulted in apparent diauxic lags, i.e., periods with little or no detectable growth. The length of

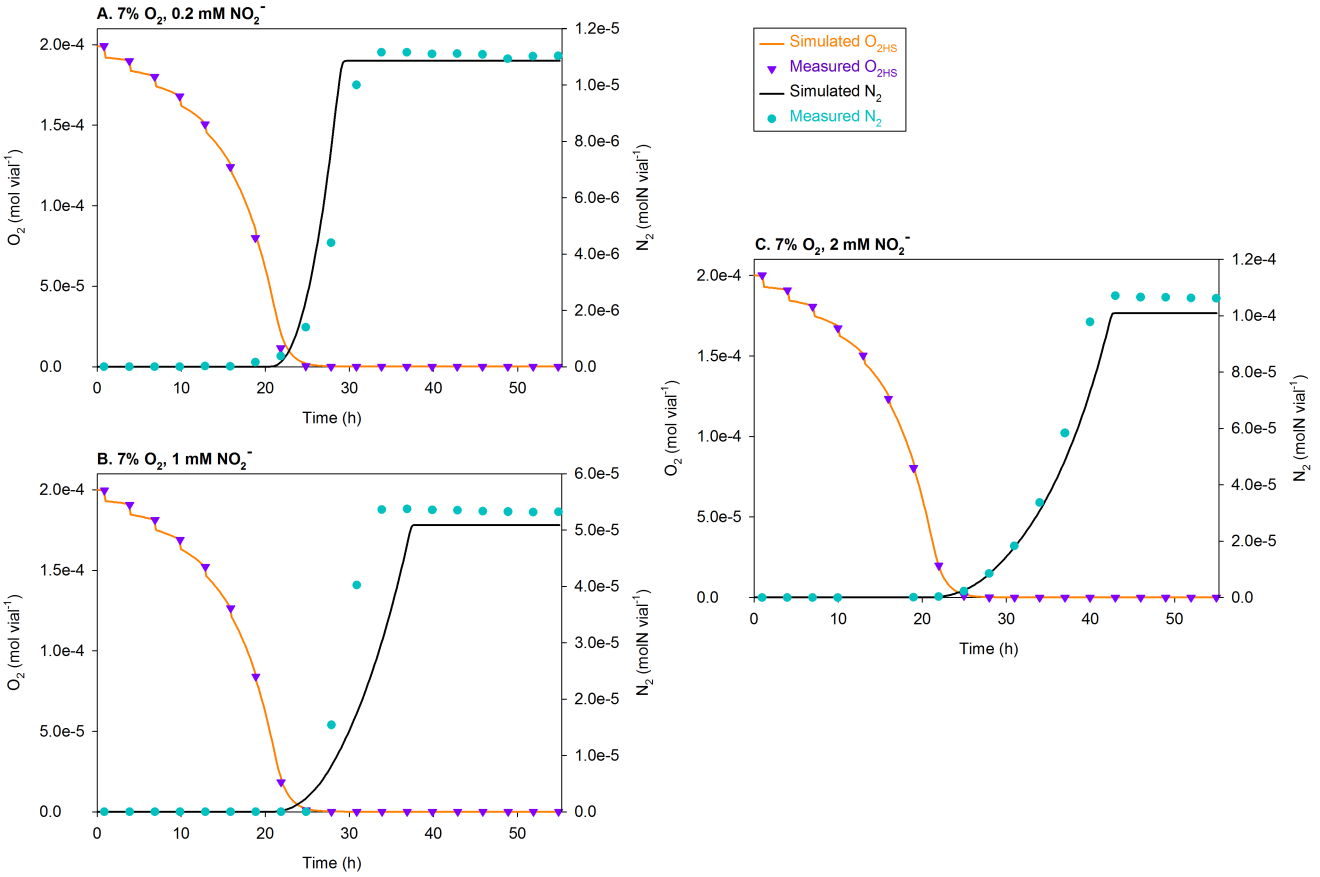


**Figure 9. Simulations of the treatments with 7 vol.% $O_{2HS}$ using $r_{den} = 0.0052\ h^{-1}$.** The figure compares the measured and simulated $O_2$ depletion (mol vial$^{-1}$) and $N_2$ production (molN vial$^{-1}$) for the treatments with 7 vol.% $O_2$ in the headspace ($O_{2HS}$) at the time of inoculation; separate plots are shown for each initial concentration of nitrite (0.2, 1, and 2 mM). At each sampling time, the simulated $O_2$ is visibly reduced because of sampling, which results in 3.4% dilution of the headspace (with He).
doi:10.1371/journal.pcbi.1003933.g009

**Table 5.** The model's and Bergaust *et al.'s* [16] estimations of the fraction recruited to denitrification ($F_{den}$).

| Batch No. | $O_{2HS}(t_0)$ (vol.%) $NO_2^-(t_0)$ (mM) | $O_{2HS}(t_0)$ (μmol)* | Model-based Estimations | | Estimations of [16] |
|---|---|---|---|---|---|
| | | | $t_m - t_t$** | $F_{den}$ | $F_{den}$ |
| 1 | 0, 0.2 | 2 | 25.8 | 0.141 | 0.19 |
| 2 | 0, 1 | 1.5 | 29.2 | 0.161 | 0.21 |
| 3 | 0, 2 | 1.7 | 27.2 | 0.156 | 0.19 |
| 4 | 1, 0.2 | 50.1 | 10.1 | 0.052 | 0.03 |
| 5 | 1, 1 | 37.8 | 11.1 | 0.056 | 0.07 |
| 6 | 1, 2 | 38.4 | 11.3 | 0.057 | 0.04 |
| 7 | 7, 0.2 | 199 | 7.4 | 0.038 | 0.02 |
| 8 | 7, 1 | 200 | 7.4 | 0.038 | 0.07 |
| 9 | 7, 2 | 200 | 7.4 | 0.038 | 0.08 |
| | | | | **Avg. = 0.082** | **Avg. = 0.1** |

*Refers to the initial values of $O_2$ in the headspace ($O_{2HS}$) used in the simulations. The values show some inconsistency for the treatments corresponding to the same vol.% because of traces of $O_2$ left behind after He-washing.
**$t_t$ is the time when $[O_2]$ in the liquid falls below $[O_2]_{trigger}$ (= 9.75 μM [22], the concentration below which recruitment of the cells to denitrification is assumed to trigger), and $t_m$ is the time when $[O_2]$ in the liquid falls below $[O_2]_{min}$ (= 1 nM, a practically zero concentration below which the recruitment is assumed to terminate). Due to low cell density in the ~0% $O_2$ treatments, the $O_2$ leakage into the vial during sampling (every 3 hours) caused oxygen concentration to exceed $[O_2]_{min}$ for 0.1–2.4 hours. This resulted in various recruitment spikes after the initial $O_2$ was depleted. If such recruitment is omitted, $F_{den}$ = 0.126, 0.142, and 0.133 for the treatments 1, 2, and 3, respectively.
doi:10.1371/journal.pcbi.1003933.t005

such lags increased with the cell density present at the time of sparging.

**Structural amendments and parameterisation of the model.** To tentatively simulate their experiment, two changes were made in the $O_2$ kinetics sector (Fig. 4A). Firstly, the net sampling loss of $O_{2HS}$ ($\Delta O_{2(S)}$) was omitted, since it was specifically set up for the robotised incubation system [28] used by Bergaust *et al* [4,8]. Secondly, a sparging event was introduced, which immediately takes $O_{2HS}$ down to very low levels ($=1\times10^{-9}$ mol vial$^{-1}$). Since we lack information about the exact concentration of $O_2$ immediately after the sparging, the present exercise is only qualitative.

Liu *et al.* [24] inoculated the culture to have an initial $OD_{550}=0.07$, which would correspond to $\sim6.5\times10^{9}$ cells vial$^{-1}$ [4,8]. We used this number to initialise the $N_{D-}$ pool (shown in Fig. 4B). They used $NO_3^-$ ($=157$ µmolN vial$^{-1}$) instead of $NO_2^-$, so we replaced the $NO_2^-$ pool (Fig. 4C) by the $NO_3^-$ pool, initialised it accordingly, and adjusted Eqs. 11 and 15: In Eq. 11, $Y_{NO_2^-}$ was replaced with the cell yield per molN of $NO_3^-$ as the $e^-$-acceptor ($Y_{NO_3^-}=9.65\times10^{13}$ cells molN$^{-1}$ [4,8]). In Eq. 15, $v_{max(NO_2^-)}$ was replaced with the maximum cell-specific velocity of $NO_3^-$ consumption ($v_{max(NO_3^-)}=2\times10^{-15}$ molN cell$^{-1}$ h$^{-1}$), calculated using the maximum specific $NO_x$-based growth rate ($=0.322$ h$^{-1}$) reported for their experiment. Finally, in Eq. 4, $v_{max(O_2)}$ was calibrated ($=2.28\times10^{-15}$ mol cell$^{-1}$ h$^{-1}$) with the reported maximum specific aerobic growth rate ($=0.342$ h$^{-1}$).

**The 'diauxic lag' is plausibly the initial growth phase of a minute $F_{den}$ (fraction recruited to denitrification).** As the experiment of Liu *et al.* [24] was simulated with the model's estimated $r_{den}=0.0052$ h$^{-1}$ (specific-probability of recruitment), $F_{den}$ turned out to be 1.1% for the treatment sparged at h = 1.1 and 0.2% for the one sparged at h = 2.55. Simulations of the total cell density ($N_{D-}+N_{D+}$) for these cases (Fig. 10A) showed long apparent lags comparable to 10–30 h lag phases observed in their later experiments [25]. However, lags in the range that Liu *et al.* [24] observed ($=3$ and 6 h for sparging at h = 1.1 and 2.55, respectively) could be achieved by our model by assuming higher residual $O_2$ concentrations after sparging (resulting in a higher $F_{den}$). Fig. 10B isolates the OD of $N_{D+}$ for the simulated treatments and shows them on a logarithmic scale so that their exponential growth, right from the onset of anoxic conditions, becomes apparent. The figure initially shows a quick recruitment of the cells from the $N_{D-}$ to the $N_{D+}$ pool, followed by the exponential growth-phase of $N_{D+}$.

This exercise serves to illustrate that the 'diauxic lags' observed [24–26] may simply be a result of low recruitment to denitrification in response to sudden removal of $O_2$. This is possibly a more plausible explanation than suggested by the authors and further elaborated by Hamilton *et al.* [35], claiming that there is a true lag caused by extremely slow production of denitrification enzymes due to energy limitation. Our explanation of the apparent diauxic lag is corroborated by a chemostat culturing experiment conducted by Bauman *et al* [36]: A steady state carbon (acetate) limited continuous culture with *Pa. denitrificans* was made anoxic and monitored for denitrification gene transcription, N-gas production, and acetate concentrations. A transient (8–10 h) peak of acetate accumulation after $O_2$ depletion suggested an apparent diauxic lag in the metabolic activity, but denitrification started immediately and increased gradually throughout the entire 'lag' period. They further observed that the number of denitrification gene transcripts peaked sharply during the first 1–2 hours. These observations are in good agreement with our model.

The aforestated observation of Liu *et al.* [24] that the length of the apparent lags increased with the aeration period (or the cell density at the time of sparging) is also in agreement with our model demonstrating that the time available for the cells to switch to denitrification is inversely related to the cell density at the time of $O_2$ depletion.

## Model-based hypothesis: Initial $O_2$ determines the timespan to denitrify all $NO_2^-$ to $N_2$ in a batch

Two sensitivity analyses were run to investigate the system's response to initial $O_2$ in the headspace, $O_{2HS}(t_0)$: one corresponding

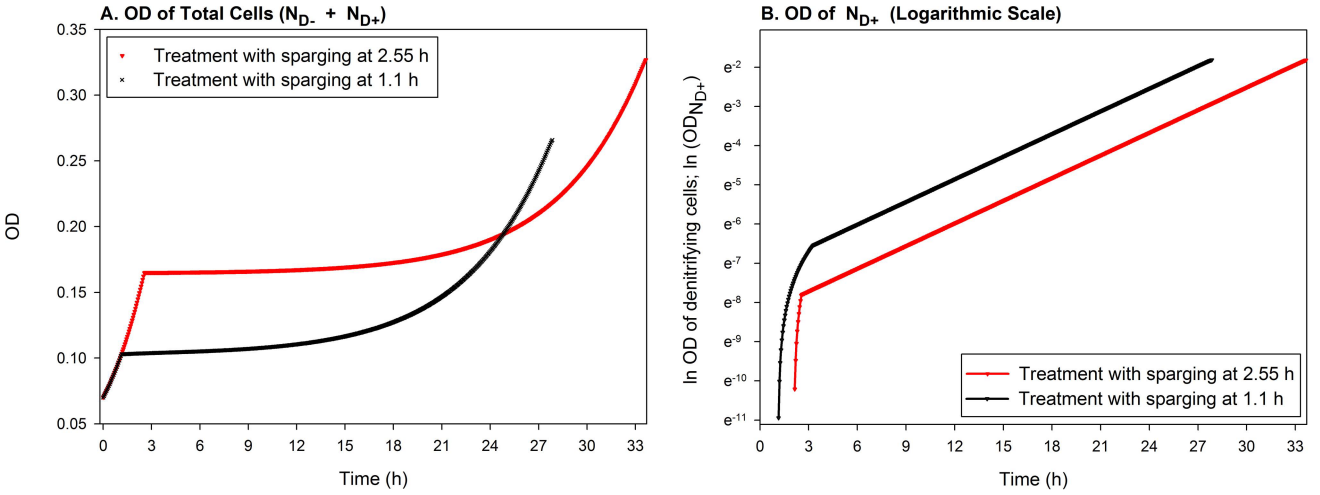


**Figure 10. Simulation of the 'diauxic lags' observed by Liu *et al* [24].** A. The panel shows cumulated OD (optical density) of the cells without ($N_{D-}$) and with ($N_{D+}$) denitrification enzymes for the simulated experiment of Liu *et al.* [24], where one treatment was sparged at time = 2.55 h and the other at 1.1 h. The simulations show, qualitatively, similar 'lags' in the two ODs as observed by the experimenters. These apparent lags are due to exponential growth of a minute fraction of the cells that successfully switched to denitrification. The growth of this fraction remains practically undetectable (the "lag" phase) until it reaches a level comparable to the large population trapped in anoxia. B. This panel isolates the ODs of $N_{D+}$ and show them on a logarithmic scale so that the exponential growth of $N_{D+}$, right from the onset of anoxic conditions, becomes visible. The graph initially shows a quick recruitment of the cells from the $N_{D-}$ to the $N_{D+}$ pool, followed by the exponential growth-phase.
doi:10.1371/journal.pcbi.1003933.g010

to a range of initial $[O_2]$ in the liquid-phase $\left([O_2]_{LP}(t_0)\right)$ below $[O_2]_{trigger}$ (see Eqs. 7–8) and the other for a range much higher than $[O_2]_{trigger}$. All other model parameters and initial values remained as listed in Tables 2 and 3, respectively. The exercise helps illustrate the relative importance of aerobic growth versus the recruitment ($F_{den}$) in determining the time taken to deplete the $NO_2^-$ pool.

**Sensitivity analysis (1).** Sensitivity analysis (1) was run with three $[O_2]_{LP}(t_0)$ within a very low range, starting from a concentration marginally below $[O_2]_{trigger}$:

1) $O_{2HS}(t_0) = 2.02\times10^{-5}$ mol vial$^{-1}$ $\left([O_2]_{LP} = 9.75\,\mu M\right)$,
2) $O_{2HS}(t_0) = 1.01\times10^{-5}$ mol vial$^{-1}$ $\left([O_2]_{LP} = 4.88\,\mu M\right)$,
3) $O_{2HS}(t_0) = 5.04\times10^{-6}$ mol vial$^{-1}$ $\left([O_2]_{LP} = 2.44\,\mu M\right)$

This is rather a simple case demonstrating that increasing $[O_2]_{LP}(t_0)$ within this low range (Fig. 11A) will result in increasing rates of denitrification (Fig. 11D) by increasing the number of aerobically grown cells ($N_{D-}$, Fig. 11B) and, thus, the rate of recruitment ($R_{rec}$, Fig. 11C).

**Sensitivity analysis (2).** Sensitivity analysis (2) was run with three initial $O_2$ concentrations much higher than $[O_2]_{trigger}$:

1) $O_{2HS}(t_0) = 2\times10^{-4}$ mol vial$^{-1}$ $\left([O_2]_{LP} = 93\,\mu M\right)$,
2) $O_{2HS}(t_0) = 1.19\times10^{-4}$ mol vial$^{-1}$ $\left([O_2]_{LP} = 55\,\mu M\right)$,
3) $O_{2HS}(t_0) = 3.84\times10^{-5}$ mol vial$^{-1}$ $\left([O_2]_{LP} = 18\,\mu M\right)$

In this case, the cumulated $N_2$ reached stable plateaus at nearly the same time for all the runs (Fig. 12E), despite that the time taken to deplete $O_2$ below $[O_2]_{trigger}$ decreased with increasing

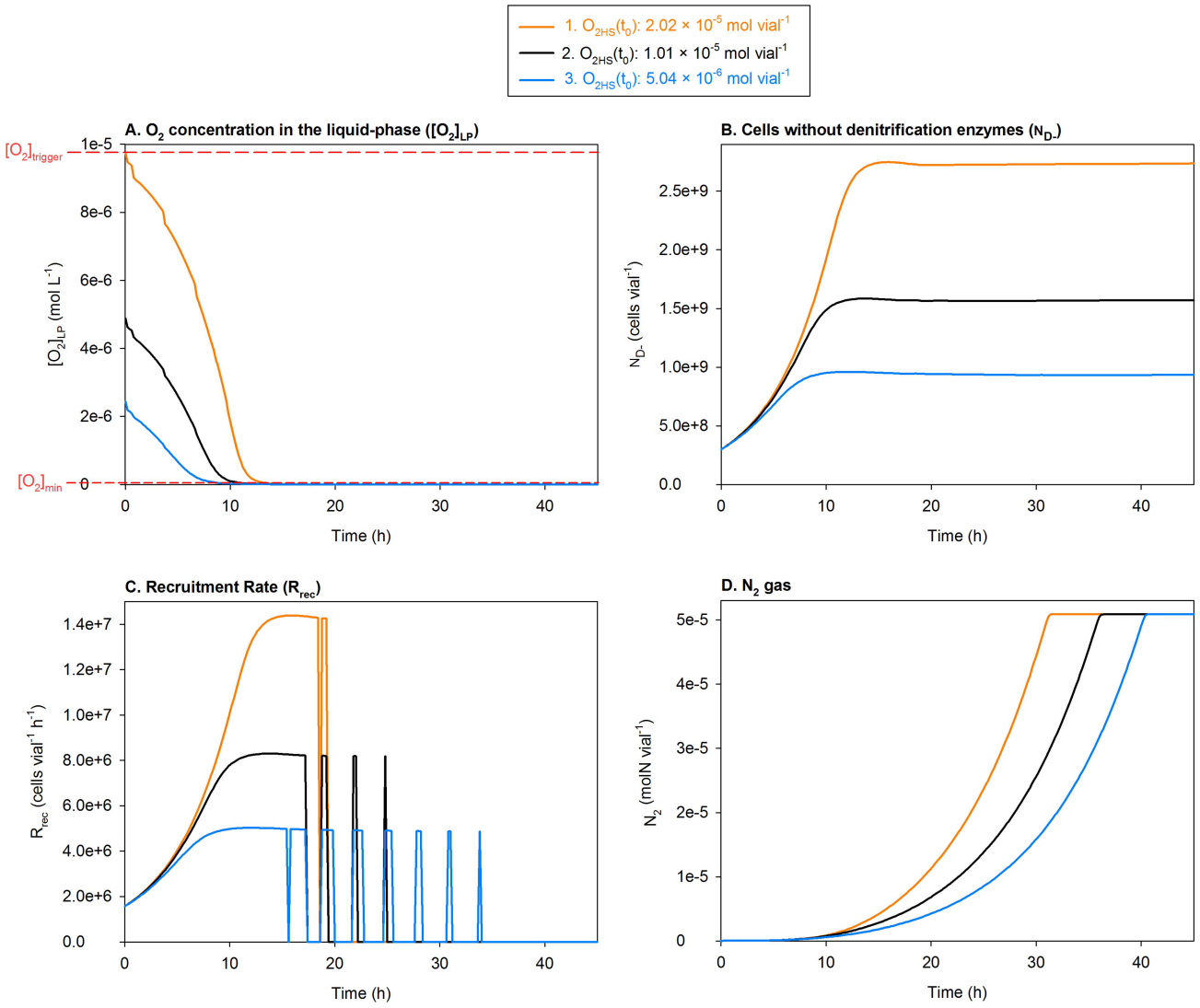


**Figure 11. Sensitivity analysis (1): Varying initial $O_2$ in the headspace $(O_{2HS}(t_0))$ within a low range.** The figure shows the impact of varying $O_{2HS}(t_0)$ within a low range on: **A.** $O_2$ concentration in the liquid-phase $([O_2]_{LP})$, **B.** The number of aerobically growing cells ($N_{D-}$), which do not possess denitrification enzymes, **C.** The rate of recruitment of $N_{D-}$ to denitrification ($R_{rec}$), and **D.** $N_2$ accumulation. Marked in Panel A, $[O_2]_{trigger}$ is the $[O_2]_{LP}$ below which $R_{rec}$ triggers, and $[O_2]_{min}$ is the $[O_2]_{LP}$ below which $R_{rec}$ terminates. In Panel C, the spikes of recruitment (following the initial recruitment) are due to spikes of $O_2$ by sampling, causing $[O_2]_{LP}$ to transiently exceed $[O_2]_{min}$. The model predicts that reducing $[O_2]_{LP}(t_0)$ within a low range (Panel A) will lower the number of aerobically grown cells (Panel B) and, thereby, the recruitment rate (Panel C), thus increasing the time taken to deplete $NO_2^-$ (slower $N_2$ accumulation, Panel D).
doi:10.1371/journal.pcbi.1003933.g011

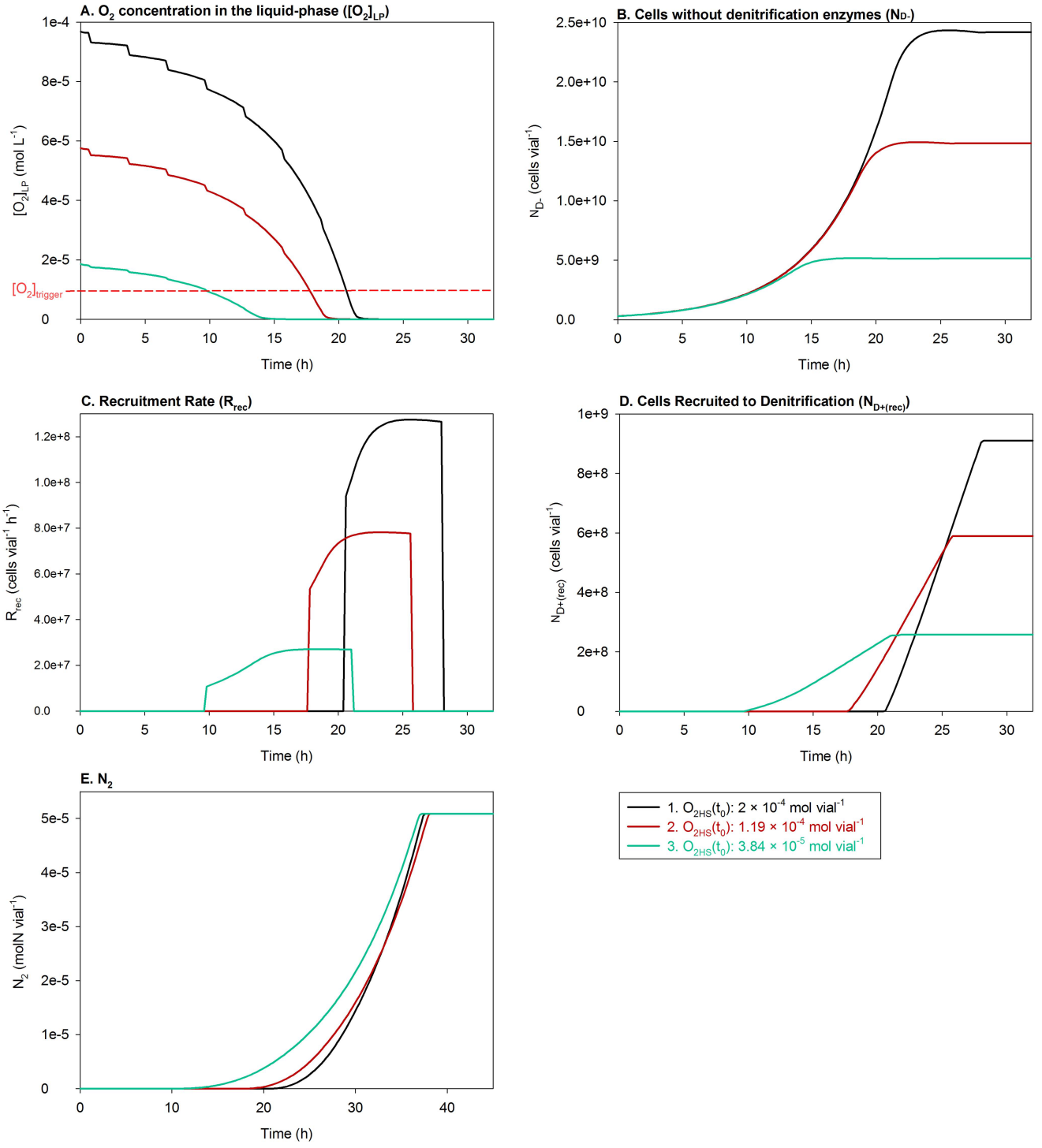


**Figure 12. Sensitivity analysis (2): Varying initial $O_2$ in the headspace ($O_{2HS}(t_0)$) within a high range.** The figure shows the impact of varying $O_{2HS}(t_0)$ within a range much higher than $[O_2]_{trigger}$ (the $[O_2]$ below which recruitment of the cells to denitrification is assumed to trigger) on: **A.** $O_2$ concentration in the liquid-phase ($[O_2]_{LP}$), **B.** The number of aerobically growing cells ($N_{D-}$), which do not possess denitrification enzymes, **C.** The rate of recruitment of $N_{D-}$ to denitrification ($R_{rec}$), **D.** The number of cells as a result of the recruitment alone ($N_{D+(rec)}$), i.e., the denitrifying cells ($N_{D+}$) but without aerobic and $NO_x$-based growth, and **E.** Cumulated $N_2$. The cumulated $N_2$ reached stable plateaus at nearly the same time for all the runs (Panel E), despite the fact that the time taken to deplete $O_2$ below $[O_2]_{trigger}$ decreased with increasing $[O_2]_{LP}(t_0)$ (Panel A). Thus, once denitrification was initiated, the rates increased with increasing initial $[O_2]_{LP}$ due to an increasing population of oxygen-grown cells (Panels B–D). The fraction of the cells recruited to denitrification ($F_{den}$) declined with increasing initial $O_2$ concentration (not shown), but this was not sufficient to compensate for the increasing number of oxygen-raised cells.
doi:10.1371/journal.pcbi.1003933.g012

$[O_2]_{LP}(t_0)$ (Fig. 12A), reducing the time available to the cells for switching to denitrification (See Fig. 5). Thus, once denitrification was initiated, the rates increased with increasing $[O_2]_{LP}(t_0)$ due to an increasing population of oxygen-grown cells (Fig. 12B–D). $F_{den}$ (Eq. 9) declined with increasing $[O_2]_{LP}(t_0)$ ($F_{den} = 0.058$, 0.041 and 0.028 for runs 3, 2 and 1, respectively), but this was not sufficient to compensate for the increasing number of oxygen-raised cells.

If the model is run without any initial $O_2$, there would be no recruitment and, hence, no denitrification. Verification of this in batch cultures is difficult because traces of $O_2$ remain after He-washing of the batches. However, we (Bergaust *et al.*, unpublished data) have been able to demonstrate that the aerobically grown *Pa. denitrificans* cells are indeed entrapped in anoxia if transferred to anoxic conditions as instantaneously as in the experiments conducted by Højberg *et al.* [15].

## Conclusion

The prevailing wisdom in denitrification research is that, under impending anoxic conditions, *all* cells in a batch culture of denitrifying bacteria will switch to denitrification. However, recent experiments with batch cultures of *Pa. denitrificans* have provided evidence that, in response to $O_2$ depletion, only a small fraction ($F_{den}$) of the entire population is able to switch to denitrification [4,8,9]. The evidence is based on indirect analyses of $e^-$-flow rates to $O_2$ and $NO_x$ during the transition of the cells from aerobic to anaerobic respiration. To provide a direct and refined estimation of $F_{den}$, we constructed a dynamic model and directly simulated kinetics of recruitment of the cells to denitrification. We first formulated a hypothesis as to the underlying regulatory mechanism of cell differentiation under approaching anoxia. Briefly, it is that the low $F_{den}$ is due to a low probability of initiating transcription of the *nirS* genes, but once initiated, the transcription is greatly enhanced through autocatalytic positive feedback by NO, resulting in the recruitment of the transcribing cell to denitrification. Then, as we implemented this hypothesis in the model, the simulation results showed that the specific-probability ($F_{den}$) of 0.0052 ($h^{-1}$) for a cell to switch to denitrification is sufficient to robustly simulate the measured denitrification gas kinetics. The model estimated the resultant $F_{den}$ between 3.8–16.1% only (average = 8.2%). The phenomenon may be considered as a 'bet-hedging' regulation 'strategy' [12]: the fraction switching to denitrification benefits if the anoxic spell is long and $NO_x$ remains available, whereas the non-switching fraction benefits, by saving energy required for the protein synthesis, if the anoxic spell is short. The strategy has important implications for the interpretation of numerous experiments on *Pa. denitrificans* and other denitrifying organisms, as this study has illustrated by presenting a more plausible explanation of the apparent diauxic lags [24] on the basis of the low $F_{den}$.

## Supporting Information

**Dataset S1** contains a Vensim simulation model (Hassan_et_al_2014.mdl) used in this study along with two files (7%_Oxygen_2mM_Nitrite.vdf and Measured_Data) containing simulated and measured data, respectively.
(ZIP)

## Acknowledgments

We wish to thank Lars Molstad, Senior Engineer, Norwegian University of Life Sciences, for his useful suggestions and assistance with mathematical formulations of the model.

## Author Contributions

Conceived and designed the experiments: LLB LRB. Performed the experiments: LLB. Analyzed the data: JH LLB LRB. Contributed reagents/materials/analysis tools: IDW. Wrote the paper: JH LLB LRB. Constructed the model: JH IDW LRB. Analysed the simulation results: JH LRB. Edited and revised the text: JH LLB IDW LRB.

## References

1. Zumft WG (1997) Cell biology and molecular basis of denitrification. Microbiol Mol Biol Rev 61: 533–616.
2. Schlesinger WH (2009) On the fate of anthropogenic nitrogen. Proc Natl Acad Sci U S A 106: 203–208.
3. Bakken LR, Dörsch P (2007) Nitrous oxide emission and global changes: modelling approaches. In: Bothe H, Ferguson SJ, Newton WE, editors. Biology of the Nitrogen Cycle Amsterdam: Elsevier B. V. pp. 382–395.
4. Bergaust L, Bakken LR, Frostegård Å (2011) Denitrification regulatory phenotype, a new term for the characterization of denitrifying bacteria. Biochem Soc Trans 39: 207–212.
5. Vasiliadou IA, Siozios S, Papadas IT, Bourtzis K, Pavlou S, et al. (2006) Kinetics of pure cultures of hydrogen-oxidizing denitrifying bacteria and modeling of the interactions among them in mixed cultures. Biotechnol Bioeng 95: 513–525.
6. Woolfenden HC, Gates AJ, Bocking C, Blyth MG, Richardson DJ, et al. (2013) Modeling the effect of copper availability on bacterial denitrification. Microbiologyopen 2: 756–765.
7. Bakken LR, Bergaust L, Liu B, Frostegård Å (2012) Regulation of denitrification at the cellular level – a clue to understanding of $N_2O$ emissions from soils. Philos Trans R Soc Lond B Biol Sci 367: 1226–1234.
8. Bergaust L, Mao Y, Bakken LR, Frostegård Å (2010) Denitrification response patterns during the transition to anoxic respiration and posttranscriptional effects of suboptimal pH on nitrogen oxide reductase in *Paracoccus denitrificans*. Appl Environ Microbiol 76: 6387–6396.
9. Nadeem S, Dörsch P, Bakken LR (2013) The significance of early accumulation of nanomolar concentrations of NO as an inducer of denitrification. FEMS Microbiol Ecol 83: 672–684.
10. van Spanning RJM, Richardson DJ, Ferguson SJ (2007) Introduction to the biochemistry and molecular biology of denitrification. In: Bothe H, Ferguson SJ, Newton WE, editors. Biology of the Nitrogen Cycle Amsterdam: Elsevier B. V. pp. 3–20.
11. Proshkin S, Rahmouni AR, Mironov A, Nudler E (2010) Cooperation between translating ribosomes and RNA polymerase in transcription elongation. Science 328: 504–508.
12. Veening J-W, Smits WK, Kuipers OP (2008) Bistability, epigenetics, and bet-hedging in bacteria. Annu Rev Microbiol 62: 193–210.
13. Shieh W, Lin Y, Jean W (2004) Pseudovibrio denitrificans gen. nov., sp. nov., a marine, facultatively anaerobic, fermentative bacterium capable of denitrification. Int J Syst Evol Microbiol 54: 2307–2312.
14. Zumft WG, Kroneck PMH (1997) Respiratory transformation of nitrous oxide ($N_2O$) to dinitrogen by bacteria and archaea. Adv Microb Physiol 52: 107–227.
15. Højberg O, Binnerup SJ, Sørensen J (1997) Growth of silicone-immobilized bacteria cells on polycarbonate membrane filters, a technique to study microcolony formation under anaerobic conditions. Appl Environ Microbiol 63: 2920–2924.
16. Bergaust L (2009) Regulatory biology of denitrification in *Agrobacterium tumefaciens* and *Paracoccus denitrificans*; responses to environmental controllers. Ås: Norwegian University of Life Sciences.
17. Bouchal P, Struhárová I, Budinská E, Šedo O, Vyhlídalová T, et al. (2010) Unraveling an FNR based regulatory circuit in *Paracoccus denitrificans* using a proteomics-based approach. Biochimica et Biophysica Acta (BBA) - Proteins and Proteomics 1804: 1350–1358.
18. Wood NJ, Alizadeh T, Bennett S, Pearce J, Ferguson SJ, et al. (2001) Maximal expression of membrane-bound nitrate reductase in *Paracoccus* is induced by nitrate via a third FNR-like regulator named NarR. J Bacteriol 183: 3606–3613.
19. Bergaust L, van Spanning RJM, Frostegård Å, Bakken LR (2012) Expression of nitrous oxide reductase in *Paracoccus denitrificans* is regulated by oxygen and nitric oxide through FnrP and NNR. Microbiology 158: 826–834.
20. Spiro S (2007) Regulators of bacterial responses to nitricoxide. FEMS Microbiol Rev 31: 193–211.
21. Raj A, van Oudenaarden A (2008) Nature, nurture, or chance: stochastic gene expression and its consequences. Cell 135: 216–226.
22. Qu Z (2014) Respiratory regulation in Paracoccus denitrificans and in soil, implications for $N_2O$ emissions. Ås, Norway: Norwegian University of Life Sciences.
23. Beckman JS, Koppenol WH (1996) Nitric oxide, superoxide, and peroxynitrite: the good, the bad, and ugly. Am J Physiol 271: C1424–C1437.

24. Liu P-H, Svoronos SA, Koopman B (1998) Experimental and modeling study of diauxic lag of *Pseudomonas denitrificans* switching from oxic to anoxic conditions. Biotechnol Bioeng 60: 649–655.
25. Lee D-U, Woo S-H, Svoronos S, Koopman B (2009) Influence of alternating oxic/anoxic conditions on growth of denitrifying bacteria. Water Res 44: 1819–1824.
26. Durvasula K, Jantama K, Fischer K, Vega A, Koopman B, Svoronos SA (2009) Effect of periplasmic nitrate reductase on diauxic lag of *Paracoccus pantotrophus*. Biotechnol Prog 25: 973–979.
27. Lueking DR, Fraley RT, Kaplan S (1978) Intracytoplasmic membrane synthesis in synchronous cell populations of *Rhodopseudomonas sphaeroides*. Fate of "old" and "new" membrane. The Journal of Biological Chemistry 253: 451–457.
28. Molstad L, Dörsch P, Bakken LR (2007) Robotized incubation system for monitoring gases ($O_2$, NO, $N_2O$, $N_2$) in denitrifying cultures. J Microbiol Methods 71: 202–211.
29. Hannon B, Ruth M (2014) Modeling Dynamic Biological Systems; Ruth M, Hannon B, editors. New York: Springer
30. de Gier J-WL, Lübben M, Reijnders WNM, Tipker CA, Slotboom D-J, et al. (1994) The terminal oxidases of *Paracoccus denitrificans*. Molecular Microbiology 13: 183–196.
31. Pitcher RS, Watmough NJ (2004) The bacterial cytochrome *cbb3* oxidases. Biochim Biophys Acta 1655: 388–399.
32. Fukumori Y, Yamanaka T (1984) Two $K_m$ values for cytochrome *c* of $aa_3$-type two-subunit cytochrome c oxidase from *Nitrobacter agilis*. FEBS Lett 170: 301–304.
33. Gates AJ, Luque-Almagro VM, Goddard AD, Ferguson SJ, Roldán MD, et al. (2011) A composite biochemical system for bacterial nitrate and nitrite assimilation as exemplified by Paracoccus denitrificans. Biochem J 435: 743–753.
34. Pan Y, Ni B-J, Yuan Z (2013) Modeling electron competition among nitrogen oxides reduction and N2O accumulation in denitrification. Environ Sci Technol Lett 47: 11083–11091.
35. Hamilton R, Casasu A, Rasche M, Narang A, Svoronos SA, et al. (2005) Structured model for denitrifier diauxic growth. Biotechnol Bioeng 90: 501–508.
36. Baumann B, Snozzi M, Zehnder AJB, van der Meer JR (1996) Dynamics of denitrification activity of Paracoccus denitrificans in continuous culture during aerobic-anaerobic changes. J Bacteriol 178: 4367–4374.
37. Wilhelm E, Battino R, Wilcock RJ (1977) Low-pressure solubility of gases in liquid water. Chem Rev 77: 219–262.

# P A P E R  II

**To be submitted to Environmental Microbiology**

# Homeostatic control of NO at nanomolar concentrations in denitrifying bacteria – modelling and *in vivo* experimental determination of nitric oxide reductase kinetics in the model organism *Paracoccus denitrificans*

**Junaid Hassan, Linda L. Bergaust, Lars Molstad, Simon de Vries, Lars R. Bakken***

# Homeostatic control of NO at *nanomolar* concentrations in denitrifying bacteria – modelling and *in vivo* experimental determination of nitric oxide reductase kinetics in the model organism *Paracoccus denitrificans*

**Junaid Hassan[1], Linda L. Bergaust[2], Lars Molstad[1], Simon de Vries[3], Lars R. Bakken[1]**
[1] Department of Environmental Sciences, Norwegian University of Life Sciences, Ås, Norway
[2] Chemistry, Biotechnology and Food Science, Norwegian University of Life Sciences, Ås, Norway
[3] Department of Biotechnology, Delft University of Technology, The Netherlands

**Lars R. Bakken**
NMBU, Box 5003, 1432 Ås, Norway
(+47) 6496 5530
lars.bakken@nmbu.no

## Abstract

Homeostatic control of NO at *nanomolar* concentrations appears common among denitrifying bacteria, often ascribed to synchronised expression of nitrite- and nitric oxide reductase (Nir and Nor). But we questioned whether this is a sufficient explanation: using the reported substrate affinities for *c*Nor, our dynamic model of the enzyme activities in batch cultures of *Paracoccus denitrificans* predicted 1–3 orders of magnitude too high NO concentrations. We rejected a hypothesis that the homeostatic control is due to a negative feedback by NO on the activity of NirS because the inclusion of such feedback resulted in too slow anaerobic growth and $N_2$ production. We proceeded by determining the kinetic parameters for *c*Nor *in vivo* by a carefully designed experiment, allowing the estimation of NO concentration at the cell surface while anoxic cultures in a $NO_3^-$/$NO_2^-$-free medium depleted low headspace-doses of NO. With the new parameters for *c*Nor ($v_{max\mathrm{NO}}$ = 3.56 *fmol NO cell$^{-1}$ h$^{-1}$*, $K_{1\mathrm{NO}}$ < 1 *nM*, $K_{2\mathrm{NO}}$ = 34 *nM*), the model predicted NO concentrations close to that measured. Such determinations of enzyme kinetic parameters *in vivo* appears essential to understand denitrification phenotypes and for adequate modelling of the NO kinetics in soils and aquatic environments.

# Introduction

Nitric oxide (NO) is a toxic intermediate product of denitrification and is also produced by organisms reducing nitrite ($NO_2^-$) to ammonium (Mania et al., 2014) and by nitric oxide synthase (NOS) in both eukaryotic and prokaryotic organisms (Bowman et al., 2011). In eukaryotic organisms, NO plays vital roles as a signalling molecule and a pathogen-killing agent; many prokaryotes appear to protect themselves against NO by enzymes which either oxidise it to $NO_2^-$ or reduce it to $N_2O$ (Poole and Hughes, 2000). In soils, NO is produced and consumed by a plethora of microorganisms, and soils emit significant amounts of NO (Medinets et al., 2014), which contribute to the formation of tropospheric ozone (Ludwig et al., 2001; Schlesinger and Bernhardt, 2013). Denitrifying bacteria and archaea are thought to protect themselves from their own NO production by delicately balancing the activity of the two enzymes Nir and Nor, responsible for the production and reduction of NO, respectively (van Spanning et al., 2007). However, their capacity to achieve this varies grossly between strains: *Agrobacterium tumefaciens* is shown to accumulate detrimentally high ($\mu M$) concentrations of NO during rapid transition from oxic to anoxic conditions (Bergaust et al., 2008). Similar phenomena have been observed in a number of strains within the genus *Bradyrhizobium* (K. W. Jillo et al., unpublished). In contrast, *Paracoccus denitrificans* – a model organism used for decades in research on the biochemistry of denitrification – demonstrates a robust homeostatic control of NO at 10–30 *nM* ($[NO]_{ss}$) under a variety of experimental conditions (Bergaust et al., 2010). Similar $[NO]_{ss}$ were observed for eight strains within the genus *Thauera* (Liu et al., 2013). Thus, some denitrifiers have evolved the ability to robustly restrict NO to extremely low concentrations, while others are clearly at risk of killing themselves by NO when grown in pure cultures.

Homeostatic control of NO would require a coordinated expression of genes encoding nitrite- and nitric oxide reductase, *nir* and *nor*, respectively (van Spanning et al., 2007). Current understanding of the regulatory network of denitrification in *Pa. denitrificans* is summarised in Fig. 1, showing that there is indeed a coordination of *nirS* and *nor* transcription via a common regulator, NNR. But we were not convinced that such transcriptional coordination alone could explain the observed homeostasis of NO at *nM* levels. That is primarily because the reported apparent half-saturation constants ($K_m$) for *c*Nor are in the $\mu M$ range, which we found intuitively incompatible with the

low $[NO]_{ss}$ observed (a typical result for *Pa. denitrificans* is shown in Fig. 2C). This led us to consider a hypothesis that the homeostasis could be due to a negative feedback of NO on the activity of NirS (Kuňák et al., 2004), as indicated by the dashed red arrow in Fig. 1. To explore this option and enhance our overall understanding of the homeostatic control, we constructed a model and simulated the NO kinetics observed in batch cultures of *Pa. denitrificans*:

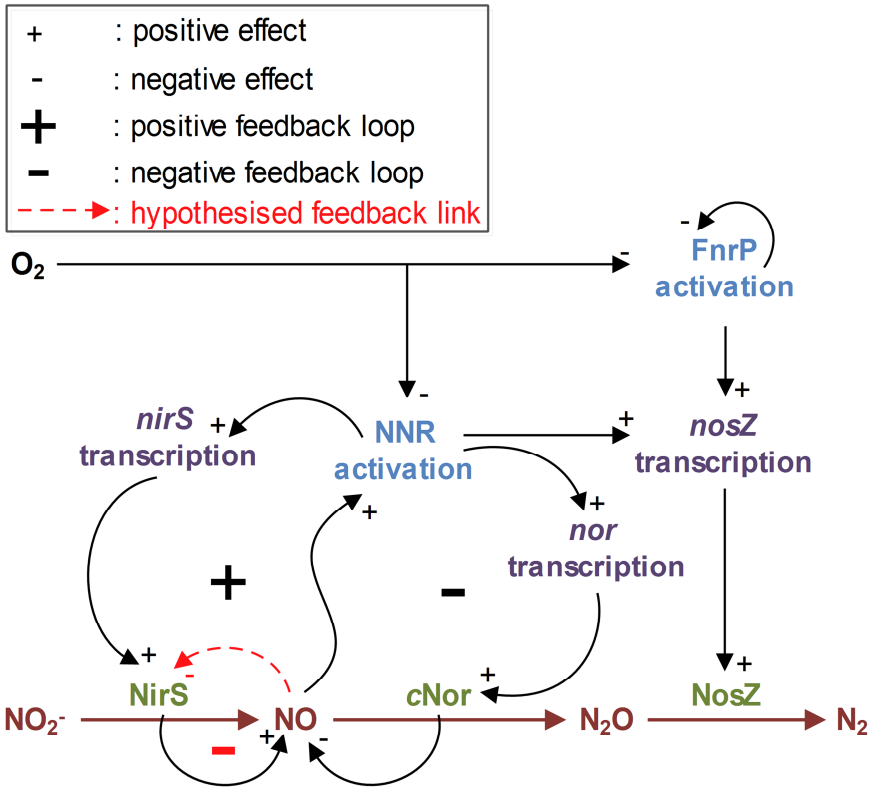


**Figure 1. Regulatory network for the stepwise reduction of $NO_2^-$ to $N_2$ in *Pa. denitrificans*.** The reduction is driven by three enzymes: NirS (cytochrome $cd_1$ nitrite reductase), *c*Nor (cytochrome *c* dependent nitric oxide reductase), and NosZ (typical Z-type nitrous oxide reductase), encoded by *nirS*, *norBC*, and *nosZ*, respectively. Transcription of *nirS* and *nor* is orchestrated by an FNR-type NO-sensor, NNR, which is apparently inhibited by $O_2$ (Spiro, 2007, 2012). Under micro-oxic or anoxic conditions, NO binds to and activates NNR, triggering the product-induced transcription of *nirS*. Thus, once a cell starts producing traces of NO, *nirS* transcription becomes autocatalytic via NNR (van Spanning et al., 2007; Bouchal et al., 2010). As for *c*Nor and NosZ, *nor* transcription is substrate (NO) induced via NNR, while *nosZ* is equally and independently induced by both NNR and the self-regulatory FnrP protein (Bergaust et al., 2012). The dashed red arrow (low left) closes the loop of our hypothetical negative feedback by NO on the activity of NirS.

The model here is an elaboration of our previous model (Hassan et al., 2014), used to simulate $O_2$ consumption and $N_2$ production in $NO_2^-$-supplemented batch culture experiments with *Pa. denitrificans*. The model explicitly simulated aerobic and anaerobic growth, the kinetics of $O_2$ consumption and denitrification (using the Michaelis-Menten kinetics), and the transport of gases between the headspace and the liquid. The activities of *c*Nor and NosZ, however, were not explicitly simulated, thus lumping the reduction of $NO_2^-$ directly to $N_2$ without taking into account [NO] and [$N_2O$]. We could afford this simplification because the main purpose was to assess denitrification kinetics ($N_2$ production) as a function of stochastic transition to denitrification, where $N_2$ production is essentially orchestrated by NirS activity (the rate limiting-step in the pathway). The simulations corroborated the hypothesis that the measured rates of $N_2$ production could be explained by a low probabilistic initiation of *nirS* transcription (= 0.005 $h^{-1}$), which then becomes autocatalytic via NO-NNR (Fig. 1). This implies that in such batch cultivations, only a small fraction of the cells (with activated *nirS* transcription) sustains respiratory metabolism and growth once $O_2$ is depleted.

The present model explicitly simulates NO production and consumption, using enzyme kinetic parameters taken from the literature, with and without a negative feedback by NO on NirS activity. Unless assuming unrealistically high $v_{max}$ values for *c*Nor or much lower $K_{mNO}$ than reported in the literature, the model predicted $[NO]_{ss}$ (the steady state [NO] in the liquid) much higher than that measured. Negative feedback by NO on NirS activity could effectively bring the predicted NO concentrations down, but this resulted in a much too slow denitrification rate ($N_2$ production). We suspected that the reason for the failure of the model could be that the true substrate affinity of *c*Nor is much higher than commonly reported in the literature, where parameters are generally based on *in vitro* measurements, employing detergent solubilised enzyme. We investigated this in detail by activity measurements *in vivo*, using chemiluminescence-based detection of NO in the headspace of anoxic batch cultures. The measurements were conducted with very low cell density to minimise headspace–liquid diffusion limitations, and the molecular diffusion from the bulk liquid to the cell surface was taken into account when calculating the NO concentration at the cell surface. With the new kinetic parameters for *c*Nor, the model is able to simulate $[NO]_{ss}$ in reasonable agreement with the measurements. Thus, the observed NO homeostasis can be understood as a result of simple enzyme kinetics, without any feedback inhibition.

# Results and Discussion

## *In vitro* affinity constants estimated for *c*Nor fail to explain the measured homeostatic control of NO.

We first simulated the model without feedback inhibition of NirS by NO. For the NO kinetics, critical parameters are the maximum velocities of $NO_2^-$ and NO reduction ($v_{max\mathrm{NO}_2^-}$ and $v_{max\mathrm{NO}}$) and the two dissociation constants for *c*Nor ($K_{1\mathrm{NO}}$ and $K_{2\mathrm{NO}}$), determining the effective affinity for NO. Since *c*Nor requires two molecules of NO to make one molecule of $N_2O$, the default kinetics is not a regular Michaelis-Menten equation, but a 'dual substrate kinetics' model with two dissociation constants $K_{1\mathrm{NO}}$ and $K_{2\mathrm{NO}}$ (see Eq. 3). $v_{max\mathrm{NO}_2^-}$ was estimated to be 1.83 *fmol cell*$^{-1}$ *h*$^{-1}$, deduced from empirically obtained parameters [growth rate = 0.106 *h*$^{-1}$ and yield = $5.79\times10^{13}$ *cells mol*$^{-1}$ $NO_2^-$ (Bergaust et al., 2010)]. For $v_{max\mathrm{NO}}$, however, no estimates were available. Regarding the literature values for the affinity of *c*Nor in *Pa. denitrificans*, Girsch and de Vries (1997) reported $K_{1\mathrm{NO}}$ and $K_{2\mathrm{NO}}$ = 6 and 0.55 $\mu M$, respectively. The other available papers with *in vitro* determinations of the affinity have fitted a simple Michaelis-Menten function to their data, reporting $K_{m\mathrm{NO}}$ values from 0.25–27 $\mu M$: $K_{m\mathrm{NO}}$ < 17 $\mu M$ (Hoglen and Hollocher, 1989), < 10 (Carr and Ferguson, 1990), < 1 (Dermastia et al., 1991), = 0.25 (Fujiwara and Fukumori, 1996), and = 27 $\mu M$ (Thorndycroft et al., 2007). To evaluate the model performance using the reported *c*Nor-affinities, we tested the model's predicted steady state NO concentrations ($[\mathrm{NO}]_{\mathrm{ss}}$) for a range of $v_{max\mathrm{NO}}$ values (as multiples of $v_{max\mathrm{NO}_2^-}$).

When we adopted Girsh and de Vries (1997) parameters ($K_{1\mathrm{NO}}$ = 6 and $K_{2\mathrm{NO}}$ 0.55 $\mu M$), the model predicted $[\mathrm{NO}]_{\mathrm{ss}}$ = 2 $\mu M$ for $v_{max\mathrm{NO}} = 2 \times v_{max\mathrm{NO}_2^-}$ (= 3.7 *fmol NO cell*$^{-1}$ *h*$^{-1}$). This is two orders of magnitude higher than the target value (measured $[\mathrm{NO}]_{\mathrm{ss}}$ = 10–30 *nM*). We had to increase $v_{max\mathrm{NO}}$ to $60 \times v_{max\mathrm{NO}_2^-}$ for $[\mathrm{NO}]_{\mathrm{ss}}$ to reach 25 *nM*. Such high $v_{max\mathrm{NO}}$ values seem unrealistic: $v_{max\mathrm{NO}} = 60 \times 1.83$ *fmol cell*$^{-1}$ *h*$^{-1}$ is equivalent to $18.5\times10^6$ *NO molecules cell*$^{-1}$ *s*$^{-1}$, i.e., $9.3\times10^6$ *$N_2O$ molecules cell*$^{-1}$ *s*$^{-1}$. If we consider that each cell has 3200–4800 *c*Nor molecules (see Supporting Information), this implies a turnover number ($k_{cat}$) = 1940–2900 *s*$^{-1}$ (i.e., *mol $N_2O$ mol*$^{-1}$ *cNor s*$^{-1}$). Such high $k_{cat}$ values are very unusual (Bar-Even et al., 2011); the values are 48–

73 times higher than the $k_{cat}$ ($\approx 40\ s^{-1}$) estimated for *Pa. denitrificans* *c*Nor, produced in *E. coli* (Thorndycroft et al., 2007) and 24–35 times higher than the $k_{cat}$ ($\approx 82\ s^{-1}$) determined by Al-Attar and de Vries (2015).

To test the other affinity estimates, we set $K_{1NO} = 0$, which turns Eq. 3 into a simple Michaelis-Menten function with $K_{mNO} = K_{2NO}$. For $K_{mNO} = 1\ \mu M$ (i.e., $K_{1NO} = 0$ and $K_{2NO} = 1$), the model predicted $[NO]_{ss} \approx 1\ \mu M$ for $v_{maxNO} = 2 \times v_{maxNO_2^-}$, as illustrated in Fig. 2. We had to increase $v_{maxNO}$ to $40 \times v_{maxNO_2^-}$ for $[NO]_{ss}$ to reach 25 *nM*. If we adopt the lowest $K_{mNO}$ value reported, i.e., 0.25 $\mu M$ (Fujiwara and Fukumori, 1996), $[NO]_{ss}$ reaches 250 *nM* for $v_{maxNO} = 2 \times v_{maxNO_2^-}$; for $[NO]_{ss}$ to reach 25 *nM*, we had to increase $v_{maxNO}$ to $11 \times v_{maxNO_2^-}$.

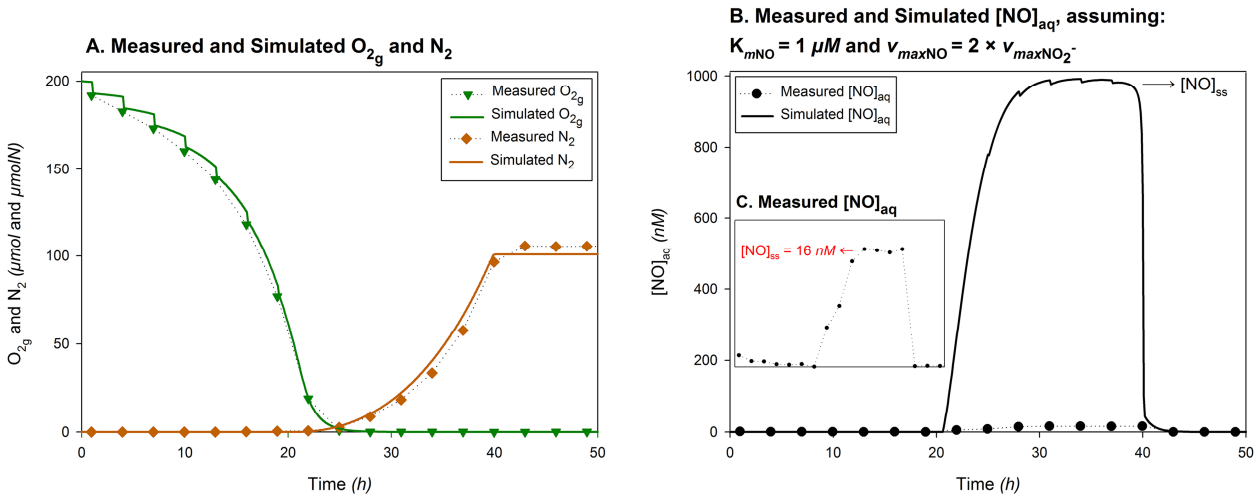


**Figure 2. Comparison of measured and simulated data.** Treatment with initially 7% $O_2$ in headspace and 2 *mM* $NO_2^-$ (Bergaust et al., 2010) is shown as a representative for all. **A.** A good-fit between the measured and simulated $O_2$ depletion in the headspace ($O_{2_g}$) and cumulated $N_2$-N $vial^{-1}$. **B.** Measured data vs. simulation of transient NO accumulation in the aqueous phase ($[NO]_{aq}$) is shown. Assuming $K_{mNO} = 1\ \mu M$ and $v_{maxNO} = 2 \times v_{maxNO_2^-}$, the simulated $[NO]_{aq}$ at steady state ($[NO]_{ss}$) ≈ 60 times higher than that measured. [At each sampling time, the simulated $O_{2_g}$ and $[NO]_{aq}$ is visibly reduced because of sampling loss.] **C** (inserted panel)**.** Measured $[NO]_{aq}$ appropriately scaled to illustrate the measured $[NO]_{ss}$.

Assuming a simple Michaelis-Menten function ($K_{1NO}$ = 0 and $K_{2NO}$ = $K_{mNO}$), $[NO]_{ss}$ can also be calculated as $[NO]_{ss} = \frac{v_{max NO_2^-} \times K_{mNO}}{V_{max NO} - v_{max NO_2^-}}$. Thus, dynamic modelling is not necessary to calculate $[NO]_{ss}$ as a function of the kinetics of NO reduction, but consideration of other variables requires a dynamic model (see below).

## Negative feedback of NO on NirS activity?

By introducing a non-competitive inhibition of NirS by NO (Eq. 5), we easily forced the model to predict $[NO]_{ss}$ to the measured range (15–30 *nM*) with any of the reported affinities for *c*Nor, using dissociation constants ($K_{iNO}$) within the range 15–50 *nM*. If a time-lag is assumed in such inhibition, it is also possible to reproduce the NO oscillations (frequency = 3–10 $h^{-1}$) observed by Kuňák et al. (2004) in anoxic cultures of *Pa. denitrificans* (results not reported). However, the inclusion of inhibition appears spurious because its effect is equivalent to curtailing $v_{max NO_2^-}$, resulting in too slow growth rates and $N_2$ production compared to measurements. This poor overall fit of the model could be patched by increasing $v_{max NO_2^-}$ to compensate for the inhibition, but that would bring us back to square one regarding $[NO]_{ss}$.

## Experimental determination of enzyme kinetics *in vivo*.

The model exercises so far suggested that we needed experimental data on NO reduction kinetics ($v_{max NO}$, $K_{1NO}$ and $K_{2NO}$) *in vivo*. To obtain that, we monitored the depletion of NO injected into the headspace of vials with low cell density in a medium without nitrogen oxyanions. The low cell density was necessary to secure reasonably accurate estimation of NO in the bulk liquid ($[NO]_{aq}$). Further, the measured rates of NO reduction per cell ($v_{NO}$) were used to estimate the NO concentration at the cell surface.

The approach was first to raise cultures of *Pa. denitrificans* by anaerobic growth in Sistrom's (1960) medium, with 2 *mM* $NO_2^-$ in three consecutive batches (the first used to inoculate the second and so on). The consecutive batches were necessary to secure a culture with 100% denitrifying cells. The last batch was monitored for growth ($OD_{660}$) and gas kinetics, and the results were used

to estimate $v_{\mathrm{NO_2^-}}$ (cell-specific rates of $\mathrm{NO_2^-}$ reduction) throughout the incubation. $[\mathrm{NO}]_{\mathrm{aq}}$ in these cultures reached stable levels after 1–2 *h*, average ≈ 33 *nM*, until all $\mathrm{NO_2^-}$ was recovered as $N_2$ after 10 *h*. The calculated realised $v_{max\mathrm{NO_2^-}}$ fluctuated between 1.5 and 2 *fmol cell*$^{-1}$ *h*$^{-1}$ until $\mathrm{NO_2^-}$ depletion, average = 1.78 *fmol cell*$^{-1}$ *h*$^{-1}$ (Supporting Information, Fig. S1). The value corroborates the realised $v_{max\mathrm{NO_2^-}}$ = 1.83 *fmol cell*$^{-1}$ *h*$^{-1}$ (Bergaust et al., 2010) used for simulations.

These cultures were then used to inoculate new vials with He-atmosphere and N-oxyanion free medium (initial cell density was $1.8\times10^6$ *cell mL*$^{-1}$). The cultures were first allowed to deplete residual $O_2$ (124–272 *ppmv in the headspace* = 0.37–0.8 *μmol O*$_2$ *vial*$^{-1}$) during a 7 *h* preincubation, resulting in some aerobic growth and final cell densities reaching $2.8–4\times10^6$ *cells mL*$^{-1}$. NO was then injected into the headspace to monitor its depletion. The results for a single vial are presented in Fig. 3, showing the depletion of consecutive headspace doses (*ppmv NO*$_g$, right axis) and the aqueous concentration ($[\mathrm{NO}]_{\mathrm{aq}}$, left axis, estimated by Eq. 10). The 'equilibrium concentration' shown, $[\mathrm{NO}]_{\mathrm{aq}\Downarrow\Uparrow} = \mathrm{P_{NO}} \times \mathrm{k_{H(NO)}}$ (left axis), is what $[\mathrm{NO}]_{\mathrm{aq}}$ would have been if in equilibrium with the measured concentration in the headspace. The ratio $\frac{[\mathrm{NO}]_{\mathrm{aq}}}{[\mathrm{NO}]_{\mathrm{aq}\Downarrow\Uparrow}}$ was 0.27–0.85 throughout the entire incubation, average = 0.45 ±0.16 (stdev). The experiment was done in three replicate vials, where the other two replicates were very similar with respect to $\frac{[\mathrm{NO}]_{\mathrm{aq}}}{[\mathrm{NO}]_{\mathrm{aq}\Downarrow\Uparrow}}$ (average = 0.34 and 0.45, respectively). This is important because it implies that the estimated $[\mathrm{NO}]_{\mathrm{aq}}$ is sufficiently accurate to use for further analyses, despite a somewhat uncertain transport coefficient for NO transport between the headspace and liquid (see Experimental Procedures).

The concentrations of $N_2O$ remained low (0–12 *ppmv*) throughout the entire incubation, with transient peaks after each injection, amounting to 2–4% of the injected NO-N, and the cumulative $N_2$ production closely matched the cumulative NO reduction (Fig. S2).

Preliminary experiments were run with much higher final doses than shown in Fig. 3. These experiments showed that *micromolar* $[\mathrm{NO}]_{\mathrm{aq}}$ resulted in permanent damage to the cells (Supporting Information, Fig. S3). In the final experiment (Fig. 3), the final density was measured ($OD_{660}$; = $1.25\times10^9$ *OD*$^{-1}$ *mL*$^{-1}$) to check the growth in relation to the cumulated NO- and $O_2$-

reduction (each sampling caused an input of 6 *nmol* $O_2$). Based on the cumulated NO (3 $\mu mol$) and $O_2$ (0.48 $\mu mol$) reduction, the OD should increase from the initial 0.0022 to 0.0052, according to the previously measured yield ($3.75\times10^{13}$ *cells* $mol^{-1}$ $e^-$ *to* $O_2$ and $1.9\times10^{13}$ *cells* $mol^{-1}$ $e^-$ *to* $NO_x$) (Bergaust et al., 2010). In comparison, the measured final OD was 0.006, which is only 15% higher than that predicted. For the two other vials, the measured final OD was 36 and 7% higher than that predicted by cumulated $O_2$- and NO-reduction. This shows that the calculation of the cell density based on the cumulative NO and $O_2$-reduction is fairly accurate.

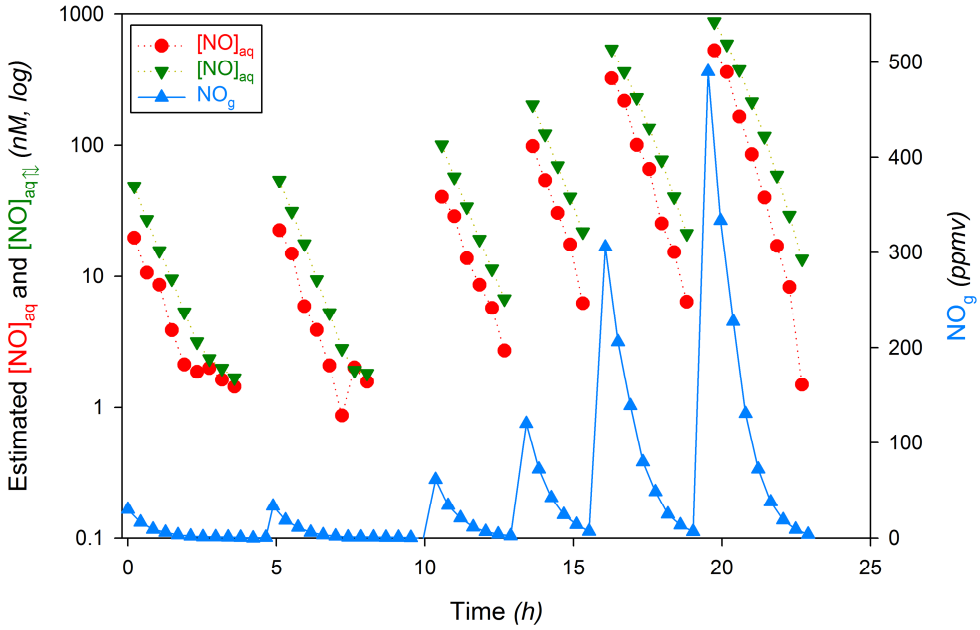


**Figure 3. Estimation of aqueous NO concentration ($[NO]_{aq}$) based on measurements in the gas-phase ($NO_g$).** $[NO]_{aq}$ is the estimated NO concentration for each time increment between two samplings, and $[NO]_{aq\downarrow\uparrow} = P_{NO} \times k_{H(NO)}$ is the $[NO]_{aq}$ if in equilibrium with the average partial pressure ($P_{NO}$, *atm)* for the time increment. ($k_{H(NO)}$ is the solubility of NO, *mol* $L^{-1}$ $atm^{-1}$). The result is for a single vial (n = 3), which received six doses of NO.

The cell density throughout the incubation of each vial was estimated by the cumulative reduction of NO to $N_2$. These numbers were used to calculate the cell specific rate of NO reduction, $v_{NO}$ (*fmol NO* $cell^{-1}$ $h^{-1}$), for each time increment. The estimates were variable, which is hardly surprising, since they are based on short time intervals between two samplings (10 *min*).

Nevertheless, $v_{\mathrm{NO}}$ showed a strong relationship with the NO concentration and a satisfactory agreement between individual vials (Supporting Information, Fig. S3).

Based on the estimated $[\mathrm{NO}]_{\mathrm{aq}}$ and $v_{\mathrm{NO}}$, we estimated the NO concentration at the cell surface ($[\mathrm{NO}]_{\mathrm{cell}}$), using the function of molecular diffusion towards a sphere with radius 0.4 $\mu m$ (see Eq. 17). The ratio between estimated cell surface- and bulk concentration $\left(\frac{[\mathrm{NO}]_{\mathrm{cell}}}{[\mathrm{NO}]_{\mathrm{aq}}}\right)$ for single time increments varied grossly due to experimental noise, especially for the low concentration range. But for $[\mathrm{NO}]_{\mathrm{aq}}$ > 20 *nM*, there was a general agreement between the empirical data and the theoretical model (Supporting Information, Fig. S4): $\frac{[\mathrm{NO}]_{\mathrm{cell}}}{[\mathrm{NO}]_{\mathrm{aq}}} \approx 0.5$ for $[\mathrm{NO}]_{\mathrm{aq}}$ = 100 *nM* and increases towards 1 with increasing $[\mathrm{NO}]_{\mathrm{aq}}$ . The theoretical $\frac{[\mathrm{NO}]_{\mathrm{cell}}}{[\mathrm{NO}]_{\mathrm{aq}}} \approx 0.25$ for $[\mathrm{NO}]_{\mathrm{aq}}$ < 20 *nM*.

Although we used lower NO concentrations in the final experiment than in the preliminary ones, the highest final dose (≈ 881 *ppmv*) apparently resulted in some inhibition (Supporting Information, Fig. S3B), and the estimated rates for $[\mathrm{NO}]_{\mathrm{aq}}$ > 300 *nM* were more variable than at lower concentrations (Supporting Information, Fig. S5). We, therefore, decided to use only the data for $[\mathrm{NO}]_{\mathrm{aq}}$ < 300 *nM* to estimate the kinetic parameters.

The data for $v_{\mathrm{NO}}$, which was taken as an estimate of the flux of NO towards the cell (J, *mol* $s^{-1}$), and $[\mathrm{NO}]_{\mathrm{cell}}$ were used to estimate the parameters $v_{max\mathrm{NO}}$, $\mathrm{K}_{1\mathrm{NO}}$, $\mathrm{K}_{2\mathrm{NO}}$, and $\mathrm{K}_{i\mathrm{NO}}$ (Eq. 18) by nonlinear least-squares regression. The estimated $\mathrm{K}_{i\mathrm{NO}}$ reached extremely high values (1 *M*), probably reflecting that the dataset does not include concentrations at which inhibition was significant. Further, $\mathrm{K}_{1\mathrm{NO}}$ approached zero, $\mathrm{K}_{2\mathrm{NO}}$ = 49 *nM*, and $v_{max\mathrm{NO}}$ = 3.9 *fmol* $cell^{-1}$ $h^{-1}$. The model performed equally well by forcing $\mathrm{K}_{1\mathrm{NO}}$ to 1 *nM*, indicating that $\mathrm{K}_{1\mathrm{NO}} << \mathrm{K}_{2\mathrm{NO}}$ and, thus, a simple Michaelis-Menten model would adequately describe the data.

Due to the uncertainties in the estimates of $[\mathrm{NO}]_{\mathrm{cell}}$, we suspected a bias in the parameter estimates with this approach (for 23% of the time increment, the estimated $[\mathrm{NO}]_{\mathrm{cell}}$ was negative, Fig. 4A). Thus, we tried an alternative approach, using a simple Michaelis-Menten function (Eq. 19) combined with the function for molecular diffusion towards the cell surface (Eq. 16) to find flux

(J, *mol NO* $s^{-1}$) as an explicit function of the aqueous concentration ($[NO]_{aq}$, Eq. 20). By fitting this function to the empirical data ($v_{NO}$ and $[NO]_{aq}$), we estimated $v_{maxNO}$ = 3.56 ±0.2 *fmol cell*$^{-1}$ $h^{-1}$ and $K_{mNO}$ = 34 ±4 *nM* using Levenberg Marquardt algorithm (Fig. 4B and 4C).

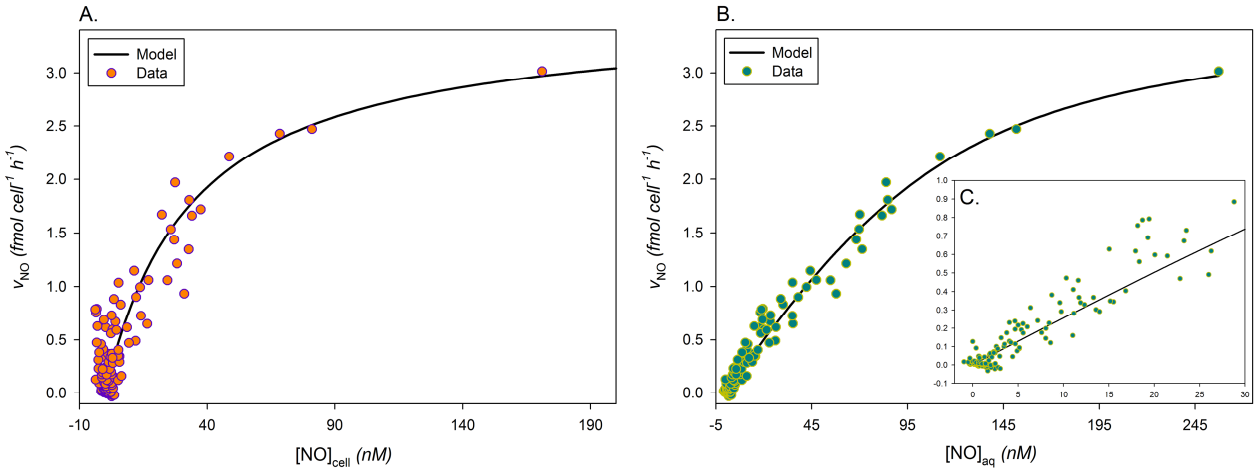


**Figure 4. Rates of NO reduction depending on concentrations, data vs. model with $v_{maxNO}$ = 3.56 *fmol cell*$^{-1}$ $h^{-1}$ and $K_{mNO}$ = 34 *nM*. A.** The empirically determined cell-specific rate of NO reduction ($v_{NO}$, *fmol cell*$^{-1}$ $h^{-1}$) plotted against the measured NO concentration at the cell surface ($[NO]_{cell}$) for single time increments, together with model predictions. **B.** The empirical $v_{NO}$ plotted against the measured bulk aqueous concentration ($[NO]_{aq}$), together with model predictions using Eq. 20. **C** (inserted panel)**.** $v_{NO}$ versus $[NO]_{aq}$ for the low concentration range (0–30 *nM*). Due to the uncertainties in the estimates of $[NO]_{cell}$, we suspected a bias in the $v_{maxNO}$ and $K_{mNO}$ estimates with the approach shown in **A**: for 23% of the time increment, the estimated $[NO]_{cell}$ is negative. Thus, an alternative approach was adopted (**B** and **C**), using a simple Michaelis-Menten function combined with the function for NO diffusion towards the cell surface to find flux (J, *mol NO* $s^{-1}$) as an explicit function of the aqueous concentration ($[NO]_{aq}$, Eq. 20). By fitting this function to the empirical data ($v_{NO}$ and $[NO]_{aq}$), $v_{maxNO}$ = 3.56 ±0.2 *fmol cell*$^{-1}$ $h^{-1}$ and $K_{mNO}$ = 34 ±4 *nM* was estimated using Levenberg Marquardt algorithm.

The $v_{maxNO}$ estimated is probably not reflecting the upper limit of *c*Nor, since the cultures receiving $[NO]_{aq}$ > 1 $\mu M$ did indeed show higher $v_{NO}$ (> 5 *fmol cell*$^{-1}$ $h^{-1}$). But the $v_{NO}$ in response to high $[NO]_{aq}$ was highly variable; growth was inhibited, and the cells exposed to *micromolar*

$[NO]_{aq}$ were apparently permanently offended, as judged by their poor *c*Nor-performance (compared to the unoffended cells) once $[NO]_{aq}$ reached below 300 *nM* (Supporting Information, Fig. S3). It appears that the upper limit for $v_{NO}$ is rather determined by the delivery of electrons than by the enzyme (*c*Nor) itself: a reduction rate of 3.56 *fmol NO cell$^{-1}$ h$^{-1}$* is equivalent to 7.1 *fmol electrons cell$^{-1}$ h$^{-1}$* (2 *electrons per NO reduced to $N_2$*). In comparison, the electron flow to denitrification during unrestricted growth with $NO_2^-$ is 5.34 *fmol electrons cell$^{-1}$ h$^{-1}$* (= 1.78 *fmol $NO_2^-$ cell$^{-1}$ h$^{-1}$*, 3 *e$^-$ per $NO_2^-$*), and for unrestricted aerobic growth it is 5.33 *fmol electrons cell$^{-1}$ h$^{-1}$* (Bergaust et al., 2010).

A $v_{max\mathrm{NO}}$ = 3.56 *fmol cell$^{-1}$ h$^{-1}$* is equivalent to $0.6\times10^6$ *NO-molecules cell$^{-1}$ s$^{-1}$* or $0.3\times10^6$ *$N_2O$ molecules cell$^{-1}$ s$^{-1}$*. If we assume that each cell contains 3200–4800 *c*Nor molecules (see Supporting Information), we arrive at $k_{cat}$ values ranging from 62 to 94 $N_2O$ *s$^{-1}$*, which are higher than that determined for *c*Nor expressed in *E. coli* ≈ 40 $N_2O$ *s$^{-1}$* (Thorndycroft et al., 2007), but encompass the recently measured turnover rates for purified *c*Nor reconstituted in liposomes ≈ 82 $N_2O$ *s$^{-1}$* (Al-Attar and de Vries, 2015). Given that $K_{1NO} << K_{2NO}$ under steady state conditions, the reduced *c*Nor contains a permanently bound molecule of NO. Only when the second NO molecule comes in ($K_{2NO}$ = 34 *nM*), the enzyme turns over to produce $N_2O$.

## Simulations of Bergaust et al's. (2010) data with $v_{max\mathrm{NO}}$ = 3.56 *fmol cell$^{-1}$ h$^{-1}$* and $K_{m\mathrm{NO}}$ = 34 *nM*

With these parameters and $v_{max\mathrm{NO_2^-}}$ = 1.8 *fmol cell$^{-1}$ h$^{-1}$*, the predicted steady state NO aqueous-concentration ($[NO]_{ss}$) for an actively denitrifying population is 35 *nM*, which closely matches the range measured in the batches used for the experimental determination of $v_{NO_2^-}$ ($[NO]_{ss}$ = 30–35 *nM*, see Supporting Information, Fig. S1). Since these cultures were raised by many generations of anaerobic growth, they were all actively denitrifying. In contrast, the major fraction of the cells in the batch cultures of Bergaust *et al*. (2010) was without NirS ($Z^-$, see Experimental Procedures). Our dynamic model assumes that these cells neither have *c*Nor, but this is not known. It might be that a fraction of the $Z^-$ cells actually has some *c*Nor activity. If so, this could explain the low $[NO]_{ss}$ in batch cultures switching from aerobic to anaerobic respiration, compared to that in

cultures with 100% denitrifying cells. Model simulations of the batch cultures by Bergaust *et al.* (2010) are shown in Fig. 5.

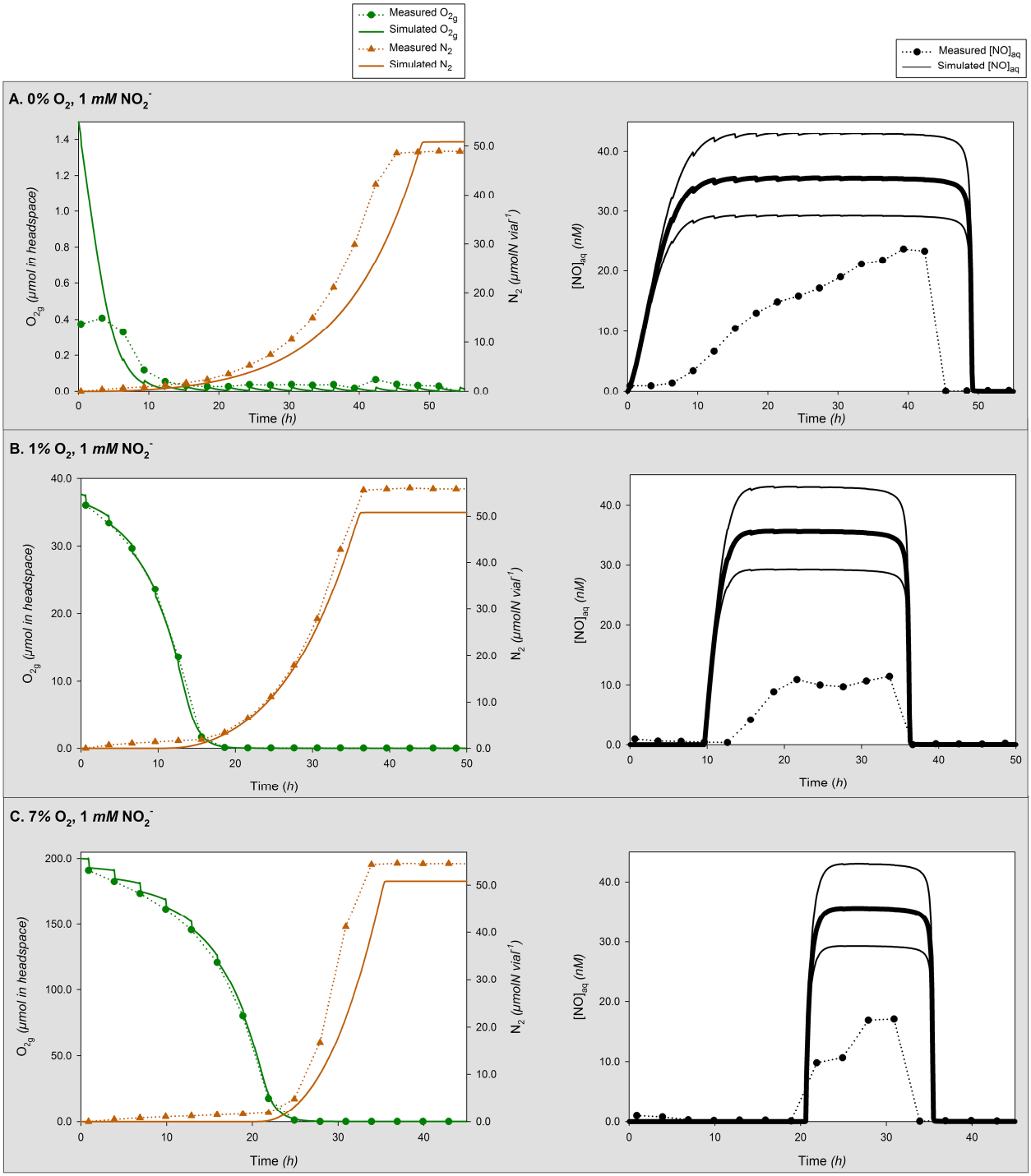


**Figure 5. Comparison of measured and simulated $O_2$ in headspace ($O_{2_g}$), $N_2$-N vial$^{-1}$ (liquid + headspace), and NO concentration in aqua ($[NO]_{aq}$).** The NO kinetics are simulated assuming

no feedback inhibition of NirS by NO and with the empirically estimated parameters for *c*NOR: $v_{max\mathrm{NO}}$ = 3.56 *fmol NO cell*$^{-1}$ *h*$^{-1}$ (SD = 0.2) and $\mathrm{K}_{m\mathrm{NO}}$ = 34 *nM* (SD = 4). The bold line is the result with the estimated values (3.56 *fmol NO cell*$^{-1}$ *h*$^{-1}$ and 34 *nM*) and the two thin lines are the results for the two extreme combinations of parameter estimates ± SD (worst-case: $v_{max\mathrm{NO}} - \mathrm{SD}$, $\mathrm{K}_{m\mathrm{NO}} + \mathrm{SD}$; best-case: $v_{max\mathrm{NO}} + \mathrm{SD}$, $\mathrm{K}_{m\mathrm{NO}} - \mathrm{SD}$). Out of nine treatments simulated, three are shown here as representative for all.

There are speculations in the literature for *in vivo* $\mathrm{K}_{m\mathrm{NO}}$ to be around 10 *nM* (de Vries et al., 2007; Pan et al., 2013), but the present exercise shows that this is not needed to explain the perfomance of *Pa. denitrificans*.

# Experimental Procedures

## A synopsis of the simulated experiment

Bergaust et al. (2010) incubated *Paracoccus denitrificans* (DSM413) as stirred batches (20 $^{o}C$) in 120 *mL* gastight vials with 50 *mL* Sistrom's medium (Lueking et al., 1978). The medium was supplemented with 0.2, 1, or 2 *mM* $\mathrm{KNO_2^-}$ and 34 *mM* succinate as the main carbon source. Prior to inoculation, the headspace atmosphere was replaced by He + $O_2$ (initial concentrations ≈ 0.1, 1 and 7 *vol.%* $O_2$). The vials were inoculated with $3\times10^8$ cells of *Pa. denitrificans* (raised by aerobic growth) and monitored for $O_2$, NO, $N_2O$ and $N_2$ concentration in the headspace while the cultures depleted $O_2$ and switched to anoxic respiration, thus reducing the available $\mathrm{NO_2^-}$ to $N_2$. Monitoring of the headspace was done with a robotised incubator, described by Molstad et al. (2007), which takes frequent gas samples by peristaltic pumping, returning equal amounts of He after each sampling so as to sustain 1 *atm* pressure. NO is analysed by chemiluminescence, while the other gases ($O_2$, $N_2O$ and $N_2$) are analysed by gas chromatography. By taking sampling loss and marginal leakage of $N_2$ into account, the system allows an accurate determination of $N_2$ production. The monitoring of NO aqueous concentrations ($[\mathrm{NO}]_{\mathrm{aq}}$) in these cultures demonstrated, irrespective of

the treatments, that the steady state concentration $[NO]_{ss}$ is 10–30 *nM* in the liquid during active denitrification.

## Model

The model is an elaborated version of our previous model (Hassan et al., 2014), designed to analyse a depression in the $e^-$-flow during the transition from aerobic to anaerobic respiration in batch cultures of *Pa. denitrificans* (Bergaust et al., 2010). The depression was hypothesised to be due to a large fraction of the population not being able to produce denitrification enzymes. The model was designed to enable a direct comparison with measurements of headspace gas concentration as measured with a robotised incubation system (Bergaust et al., 2010), thus simulating not only the enzymatic reactions and growth but also the gas loss by sampling and the gas transport between the headspace and the liquid. The model successfully simulated the $O_2$ and $NO_2^-$ reduction ($N_2$ accumulation); the latter assuming a stochastic initiation of *nirS* transcription in each cell (Fig. 1), with a very low probability (0.005 $h^{-1}$). Thus, the model corroborated our hypothesis, predicting that only a small fraction of the population ($F_{den}$) was able to express *nirS* prior to $O_2$ depletion and that the major fraction ($1 - F_{den}$) was entrapped in anoxia, without enough energy to produce NirS (the medium contained only $NO_2^-$; hence, the energy from nitrate reduction was no option). The model did not explicitly simulate the intermediates NO and $N_2O$ kinetics, since *Pa. denitrificans* accumulated only miniscule amounts thereof under the experimental conditions used.

The present model is identical to the original regarding the simulation of gas transport between the liquid and headspace, gas losses by sampling, and the probabilistic initiation of *nirS* transcription. The new element is the explicit simulation of NO and $N_2O$ transformations (production and consumption). In response to anoxia, *nosZ* is assumed to be expressed in all cells, whereas the initiation of *nirS*- and *nor*-transcription is stochastic (and synchronised), as in the previous model. The explicit simulation of $N_2O$ kinetics allowed us to include a new feature: after $O_2$ depletion, the cells without NirS could still sustain a minimum of respiration by reducing the miniscule amounts of $N_2O$ produced by the cells with NirS (and *c*Nor); hence, they may have indeed had the energy required to produce denitrification enzymes (NirS and *c*Nor) despite the complete exhaustion of $O_2$. The model is visualised in Fig 6.

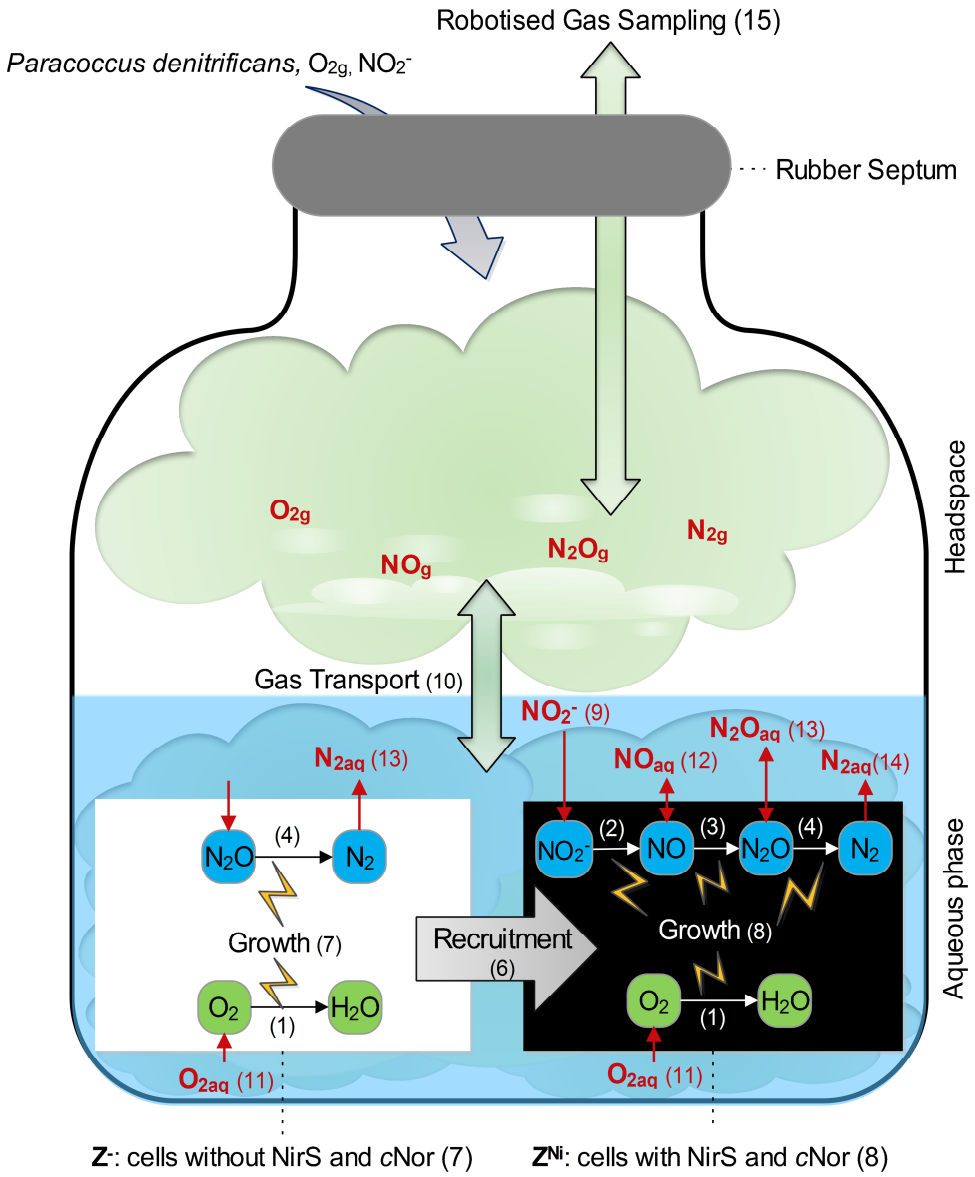


**Figure 6. Model overview.** The model assumes two sub-populations $Z^{-}$ (white box) and $Z^{Ni}$ (black box), differentiated according to their enzymes. $Z^{-}$ contains the inoculum that grows by aerobic respiration. As $O_2$ is depleted below a critical concentration, $Z^{-}$ initiates recruitment to $Z^{Ni}$, according to a low probabilistic function. The function represents the stochastic initiation of *nirS* transcription, leading to the autocatalytic NirS production and coordinated expression of *nor* (Fig. 1). $Z^{Ni}$ can reduce $O_2$ and $Z^{-}$ can respire traces of $N_2O$ produced by $Z^{Ni}$. The latter because, in response to $O_2$ depletion, *nosZ* is expressed in all cells via FnrP (Bergaust et al., 2012). The kinetics of $e^{-}$-flow by $Z^{-}$ and $Z^{Ni}$ are controlled by the $e^{-}$-acceptors in the liquid ($X_{aq}$), and the amounts of gases in the liquid are controlled by the rate of consumption/production and the

concentration-dependent transport between the aqueous phase and the headspace. The headspace amounts ($X_g$) are disturbed at each sampling (dilution and leakage). All these phenomena are included in the model, and the numbers in the figure refer to equation numbers in the text.

**Respiration and cell diversification**

The cell-specific respiration rate drives the concentration dependent rates of $e^-$-flow to the available electron acceptors:

$$ve^-_{O_2} = \frac{ve^-_{max O_2} \times [O_2]_{aq}}{K_{mO_2} + [O_2]_{aq}} \qquad (mol\ e^-\ cell^{-1}\ h^{-1}) \qquad (1)$$

$$ve^-_{NO_2^-} = \frac{ve^-_{max NO_2^-} \times [NO_2^-]}{K_{mNO_2^-} + [NO_2^-]} \qquad (mol\ e^-\ cell^{-1}\ h^{-1}) \qquad (2)$$

$$ve^-_{NO} = \frac{ve^-_{max NO}}{1 + K_{2NO}\left(\frac{1}{[NO]_{aq}} + \frac{K_{1NO}}{[NO]^2_{aq}}\right)} \qquad (mol\ e^-\ cell^{-1}\ h^{-1}) \qquad (3)$$

$$ve^-_{N_2O} = \frac{ve^-_{max N_2O} \times [N_2O]_{aq}}{K_{mNO_2^-} + [N_2O]_{aq}} \qquad (mol\ e^-\ cell^{-1}\ h^{-1}) \qquad (4)$$

where $ve^-_{max X}$ (*mol e⁻ cell⁻¹ h⁻¹*) is the maximum $e^-$-flow to the acceptor X (see Table 1 for parametric values and sources thereof), $K_{mX}$ (*mol O₂ L⁻¹* or *mol N L⁻¹*) is the half saturation concentration, [X] (*mol O₂ L⁻¹* or *mol N L⁻¹*) is the concentration in the aqueous-phase, specified as $[X]_{aq}$ for the gases, and $K_{1NO}$ & $K_{2NO}$ (*mol N L⁻¹*) are the dissociation constants for NO binding to *c*Nor (Girsch and de Vries, 1997).

In the version of the model with a negative feedback by NO on NirS activity, Eq. 2 was modified according to the Michaelis-Menten kinetics for non-competitive inhibition:

$$ve^-_{NO_2^-} = \frac{ve^-_{max NO_2^-} \times [NO_2^-]}{(K_{mNO_2^-} + [NO_2^-]) \times \left(1 + \frac{[NO]_{aq}}{K_{iNO_2^-}}\right)} \qquad (mol\ e^-\ cell^{-1}\ h^{-1}) \qquad (5)$$

where $K_{iNO_2^-}$ (*mol N L*$^{-1}$) is the dissociation constant.

The model has two populations, defined according to their reductases:

1. $Z^-$ (*cells*): cells without NirS and *c*Nor
2. $Z^{Ni}$ (*cells*): cells with NirS and *c*Nor

**Table 1. Model parameters.**

| | Description | Value | Units | Source |
|---|---|---|---|---|
| $[O_2]_{ni}$ | $[O_2]_{aq}$ below which recruitment from $Z^-$ to $Z^{Ni}$ triggers | $9.75\times10^{-6}$ | *mol L*$^{-1}$ | (Qu, 2014) |
| $D_g$ | Dilution: the fraction of gas replaced by He during sampling | 0.035 | *Unitless* | Measured |
| $k_{H(O_2)}$ | Solubility of $O_2$ in water at 20 °*C* | 0.00139 | *mol L*$^{-1}$ *atm*$^{-1}$ | (Wilhelm et al., 1977) |
| $k_{H(NO)}$ | Solubility of NO at 20 °*C* | 0.0021 | *mol N L*$^{-1}$ *atm*$^{-1}$ | (Molstad et al., 2007) |
| $k_{H(N_2O)}$ | Solubility of $N_2O$ at 20 °*C* | 0.056 | *mol N L*$^{-1}$ *atm*$^{-1}$ | (Wilhelm et al., 1977) |
| $k_{H(N_2)}$ | Solubility of $N_2$ at 20 °*C* | 0.0014 | *mol N L*$^{-1}$ *atm*$^{-1}$ | (Wilhelm et al., 1977) |
| $K_{mO_2}$ | The half saturation constant for $O_2$ reduction | $2.5\times10^{-7}$ | *mol L*$^{-1}$ | Model-based estimation |
| $K_{mNO_2^-}$ | The half saturation constant for $NO_2^-$ reduction | $4.13\times10^{-6}$ | *mol N L*$^{-1}$ | (Gates et al., 2011; Pan et al., 2013) |
| $K_{iNO_2^-}$ | The dissociation constant for Nir/$NO_2^-$ complex | $4\times10^{-8}$ | *mol N L*$^{-1}$ | Assumption |
| $K_{1NO}$ | The steady state dissociation constant for *c*Nor/NO complex | $8.07\times10^{-14}$ | *mol N L*$^{-1}$ | Estimated based on experiments |
| $K_{2NO}$ | The steady state dissociation constant for *c*Nor/$(NO)_2$ complex | $34\times10^{-9}$ | *mol N L*$^{-1}$ | Estimated based on experiments |
| $K_{mN_2O}$ | The half saturation constant for $N_2O$ reduction | $8.82\times10^{-7}$ | *mol N L*$^{-1}$ | Model-based estimation |
| $k_t$ | The $O_2$ transport coefficient between the headspace and liquid | 0.001 | *L s*$^{-1}$ | Measured |
| $L_{O_2}$ | $O_2$ leakage into the vial during each sampling | $2.04\times10^{-8}$ | *mol* | (Bergaust et al., 2010) |
| $r_{Ni}$ | The specific-probability of recruitment from $Z^-$ to $Z^{Ni}$ | 0.0072 | *h*$^{-1}$ | Model-based estimation |
| $t_s$ | The time taken to complete a sampling procedure | 0.017 | *h* | (Molstad et al., 2007) |
| T | Temperature | 293.15 | °*K* | (Bergaust et al., 2010) |
| $ve^-_{maxO_2}$ | The maximum cell-specific velocity of e$^-$-flow to $O_2$ | $5.32\times10^{-15}$ | *mol e*$^-$ *cell*$^{-1}$ *h*$^{-1}$ | (Bergaust et al., 2010) |
| $ve^-_{maxNO_2^-}$ | The maximum cell-specific velocity of e$^-$-flow to $NO_2^-$ | $1.83\times10^{-15}$ | *mol e*$^-$ *cell*$^{-1}$ *h*$^{-1}$ | (Bergaust et al., 2010) & measured |
| $ve^-_{maxNO}$ | The maximum cell-specific velocity of e$^-$-flow to NO | $3.56\times10^{-15}$ | *mol e*$^-$ *cell*$^{-1}$ *h*$^{-1}$ | Measured |
| $ve^-_{maxN_2O}$ | The maximum cell-specific velocity of e$^-$-flow to $N_2O$ | $5.50\times10^{-15}$ | *mol e*$^-$ *cell*$^{-1}$ *h*$^{-1}$ | (Bergaust et al., 2012) |

| | | | | |
|---|---|---|---|---|
| $ve^-_{min}$ | The minimum e$^-$-flow required for protein synthesis (ATP) | $5.30\times10^{-18}$ | *mol e$^-$ cell$^{-1}$ h$^{-1}$* | Assumption |
| $Ye^-_{O_2}$ | The growth yield for e$^-$-flow to $O_2$ | $3.75\times10^{13}$ | *cells mol$^{-1}$ e$^-$* | (Bergaust et al., 2010) |
| $Ye^-_{NO_x}$ | The growth yield for e$^-$-flow to $NO_x$ | $1.93\times10^{13}$ | *cells mol$^{-1}$ e$^-$* | (Bergaust et al., 2010) |
| $Vol_g$ | Headspace volume | 0.07 | *L* | (Bergaust et al., 2010) |
| $Vol_{aq}$ | Aqueous-phase volume | 0.05 | *L* | (Bergaust et al., 2010) |

The model is initiated with all cells in $Z^-$, which then express NirS + *c*Nor, thus recruiting to $Z^{Ni}$ in response to $O_2$ depletion. The NirS and *c*Nor expression is assumed to be coordinated because they are both enhanced by NO (via the NO-sensor NNR, Fig. 1), and the initiation of *nirS* transcription is stochastic because it happens in the absence of NO (or at too low concentrations to be sensed by NNR, see Hassan et al., 2014). All cells ($Z^-$ + $Z^{Ni}$) are assumed to be able to respire $O_2$ and express NosZ in response to impending anoxia (see Bergaust *et al*. 2012).

The kinetics of NirS + *c*Nor expression (i.e., recruitment to $Z^{Ni}$) are modelled as instantaneous recruitment events (i.e., ignoring the time from the initiation of the gene expression till the cell is fully equipped with the reductases in question). The simplification is based on the observations that the lag between the emergence of denitrification gene transcripts and the subsequent gas products is practically insignificant (≈ 20 minutes, Bergaust et al., 2010; Qu, 2014). The rate of recruitment from $Z^-$to $Z^{Ni}$ is given by:

$$R_{Ni} = \begin{cases} Z^- \times r_{Ni} & \textbf{IF } [O_2]_{aq} < [O_2]_{Ni} \textbf{ AND } [ve^-_{O_2} + (0.5 \times ve^-_{N_2O})] > ve^-_{min} \\ 0 & \textbf{OTHERWISE} \end{cases} \quad (cells\ h^{-1}) \quad (6)$$

where $Z^-$ (*cells*) is the population without NirS and *c*Nor, $r_{Ni}$ ($h^{-1}$) is the probability for a $Z^-$ cell to initiate *nirS* transcription once the aqueous oxygen concentration ($[O_2]_{aq}$) reaches below a critical limit $[O_2]_{ni}$, empirically determined as the $[O_2]_{aq}$ at the outset of NO accumulation (Qu, 2014). The second condition for the cell to express NirS is a minimum of e$^-$-flow to other e$^-$-acceptors, expressed as $ve^-_{min}$ (*mol e$^-$ cell$^{-1}$ h$^{-1}$*). The idea is that a minimum of energy required for protein synthesis must be available by the reduction of an accessible e$^-$-acceptor(s). The e$^-$-flow to $N_2O$ ($ve^-_{N_2O}$) is assumed to count only 50% of the e$^-$-flow to $O_2$ because of the lower ATP production per e$^-$ to $NO_x$ (van Spanning et al., 2007).

**Growth**

The number of cells within each population ( $Z^-$ and $Z^{Ni}$) change as a function of growth and recruitment. The growth is a direct function of the rates of $e^-$-flow to the various $e^-$-acceptors:

$$\frac{d(Z^-)}{dt} = Z^- \times \left(ve^-_{O_2} \times Ye^-_{O_2} + ve^-_{N_2O} \times Ye^-_{NO_x}\right) - R_{Ni} \qquad (cells\ h^{-1}) \qquad (7)$$

where $Z^-$ (*cells*) is the population size, $ve^-_{O_2}$ (*mol e⁻ cell⁻¹ h⁻¹*, Eq. 1) is the cell-specific rate of $e^-$-flow to $O_2$, $Ye^-_{O_2}$ (*cells mol⁻¹ e⁻ to O₂*) is the growth yield for aerobic respiration, $ve^-_{N_2O}$ is the cell-specific rate of $e^-$-flow to $N_2O$, $Ye^-_{NO_x}$ is the growth yield for the $e^-$-flow to $NO_x$ (identical for all N species), and $R_{Ni}$ (*cells h⁻¹*) is the recruitment from $Z^-$ to $Z^{Ni}$ in response to $O_2$ depletion (Eq. 6).

Likewise:

$$\frac{d(Z^{Ni})}{dt} = Z^{Ni} \times \left[ve^-_{O_2} \times Ye^-_{O_2} + \left(ve^-_{NO_2^-} + ve^-_{NO} + ve^-_{N_2O}\right) \times Ye^-_{NO_x}\right] + R_{Ni}\,(cells\ h^{-1}) \qquad (8)$$

**Kinetics of $O_2$ and $NO_x$**

The $O_2$ and $NO_x$ kinetics in the aqueous-phase are simulated as a net result of consumption and production as well as the transport between the liquid and the headspace (for gases).

The nitrite depletion rate is a simple function (no gaseous phase required):

$$\frac{d(NO_2^-)}{dt} = -Z^{Ni} \times v_{NO_2^-} \qquad (mol\ N\ h^{-1}) \qquad (9)$$

where $v_{NO_2^-}$ (*mol N cell⁻¹ h⁻¹*) is the cell-specific velocity of $NO_2^-$ consumption, obtained by the velocity of $e^-$-flow to $NO_2^-$ (see Eq. 2, 1 $\frac{molN}{mol\ e^-}$).

The gas consumption and production takes place in the aqueous phase, but the gases are transported between the aqueous phase and the headspace depending on their concentrations in the two phases. The transport is modelled according to Molstad et al. (2007):

$$\mathrm{Tr_X} = \mathrm{k_t} \times \left(\mathrm{P_X} \times \mathrm{k_{H(X)}} - [\mathrm{X}]_{\mathrm{aq}}\right) \qquad (mol\ O_2\ h^{-1} \text{ or } mol\ N\text{-}NO_x\ h^{-1}) \qquad (10)$$

where $\mathrm{Tr_X}$ is the transport of gas X, $\mathrm{k_t}$ ($L\ h^{-1}$) is the transport coefficient, $\mathrm{P_X}$ ($atm$) is the partial pressure of the gas in the headspace, $\mathrm{k_{H(X)}}$ ($mol\ O_2\ L^{-1}\ atm^{-1}$ or $mol\ N\text{-}NO_x\ L^{-1}\ atm^{-1}$) is the solubility of the gas, and $[\mathrm{X}]_{\mathrm{aq}}$ ($mol\ L^{-1}$) is the aqueous gas concentration. $\mathrm{Tr_X}$ is positive for the net transport from the headspace to the aqueous phase (i.e., $[\mathrm{X}]_{\mathrm{aq}} < \mathrm{P_X} \times \mathrm{k_{H(X)}}$).

The production and consumption of the various gases in the liquid are proportional to the $e^-$-flow rates; thus, the amounts of each gas in the aqueous-phase are modelled as:

$$\frac{\mathrm{d}(\mathrm{O_{2aq}})}{\mathrm{dt}} = \mathrm{Tr_{O_2}} - (\mathrm{Z^-} + \mathrm{Z^{Ni}}) \times v_{O_2} \qquad (mol\ O_2\ h^{-1}) \qquad (11)$$

$$\frac{\mathrm{d}(\mathrm{NO_{aq}})}{\mathrm{dt}} = \mathrm{Tr_{NO}} + \mathrm{Z^{Ni}} \times (v_{\mathrm{NO_2^-}} - v_{\mathrm{NO}}) \qquad (mol\ N\ h^{-1}) \qquad (12)$$

$$\frac{\mathrm{d}(\mathrm{N_2O_{aq}})}{\mathrm{dt}} = \mathrm{Tr_{N_2O}} + \mathrm{Z^{Ni}} \times v_{\mathrm{NO}} - \left(\mathrm{Z^-} + \mathrm{Z^{Ni}}\right) \times v_{\mathrm{N_2O}} \qquad (mol\ N\ h^{-1}) \qquad (13)$$

$$\frac{\mathrm{d}(\mathrm{N_2}_{\mathrm{aq}})}{\mathrm{dt}} = \mathrm{Tr_{N_2}} + \left(\mathrm{Z^-} + \mathrm{Z^{Ni}}\right) \times v_{\mathrm{N_2O}} \qquad (mol\ N\ h^{-1}) \qquad (14)$$

where $\mathrm{Tr_X}$ (Eq. 10) is the transport rate of the relevant gas from the headspace to the liquid, and $v_{\mathrm{X}}$ is the cell-specific velocity of the X's consumption, obtained by the velocity of $e^-$-flow to X (Eqs. 1–4; $v_{\mathrm{O_2}} = \frac{1}{4} \times v\mathrm{e^-_{O_2}}$ and $v_{\mathrm{NO_x}} = v\mathrm{e^-_{NO_x}}$).

**Gases in the headspace affected by gas sampling**

Gases in the headspace ($X_g$, *mol* $O_2$ or *molN* $NO_x$) is a function of transport (Eq. 10) and the net sampling loss. The gas sampling removes a fraction of the headspace (replaced by He), but it also involves a leakage of $O_2$ and $N_2$ via tubing and valves in the injection system (Molstad et al., 2007). To simulate the experiments conducted, the sampling disturbance is simulated as discrete events, at time points given as input to the model (equivalent to the sampling times in the simulated experiment):

$$\Delta X_s = \frac{L_X - X_g \times D_g}{t_s} \qquad (mol\ O_2\ h^{-1} \text{ or } mol\ N\text{-}NO_x\ h^{-1}) \tag{15}$$

where $\Delta X_s$ is the net change in the amount of gas X in the headspace, $L_X$ (*mol* $O_2$ or *mol N-*$NO_x$) is the leakage of X into the system via the sampling operation, $X_g$ (*mol* $O_2$ or *mol N-*$NO_x$) is the amount of gas, and $D_g$ is the fraction of the headspace volume replaced by He. The sampling disturbance is simulated as a continuous process over a short time period ($t_s$), equivalent to the time taken to complete each sampling.

For all other gases than $O_2$, $L_X$ is negligible and is not included in the model. $\Delta O_{2_s}$ is negative (outflow) at high $O_2$ concentrations and turns positive (inflow) only at very low $O_{2_{aq}}$, depending on the value of $L_{O_2}$ and D. For the simulated experiment, $L_{O_2}$ = $4\times10^{-9}$ *mol* $O_2$, and D = 0.013; hence, $\Delta O_{2_s}$ turns positive when $O_{2_{aq}} < 0.3\ \mu mol$, equivalent to 100 *ppmv* in the headspace or 0.13 $\mu M$ in the liquid if in equilibrium.

For $N_2$, the model ignores the sampling disturbance because the experimental data on $N_2$ production to be compared with the model output are already corrected for the sampling disturbance (Molstad et al., 2007).

## Determination of NirS and *c*Nor kinetics *in vivo*

All experiments were done in gas-tight 120 *mL* serum vials containing 50 *mL* Sistrom's (1960) medium with 34 *mM* succinate, stirred at 650 *rpm* (3.5 *cm* long magnetic stirrers) at 20 $^{o}C$. The vials were placed in a robotic incubation system for monitoring the gas concentrations in the headspace (Molstad et al., 2007). Sistrom's medium contains $K_2HPO_4$: 3.48, $NH_4Cl$: 0.195, succinic acid: 4.00, L-glutamic acid: 0.10, L-aspartic acid: 0.04, NaCl: 0.50, nitrilotriacetic acid: 0.20, $MgSO_4 \times 7H_2O$: 0.30, $CaCl_2 \times 7H_2O$: 0.015, and $FeSO_2 \times 7H2O$: 0.007 $g\ L^{-1}$. In addition, trace elements and vitamins were added as EDTA (triplex 3): 0.001765, $ZnSO_4 \times 7H_2O$: 0.01095, $FeSO_4 \times 7H_2O$: 0.005, $MnSO_4 \times H_2O$: 0.00154, $CuSO_4 \times 5H_2O$: 0.00039, $CoCl_2 \times 6H_2O$: 0.0002 g, $H_3BO_3$: 0.000114, nicotinic acid: 0.0010, thiamine HCl: 0.0005, biotin: 0.00001 ($g\ L^{-1}$). pH was brought to 7.0 with 1 M KOH, and the medium was autoclaved for sterility.

### Inoculum preparation

To determine the enzyme kinetic parameters for NirS and *c*Nor *in vivo*, we needed an inoculum with all cells actively denitrifying. This was obtained by three sequential batch cultivations under anoxic conditions: 120 *mL* vials, with He atmosphere containing 50 *mL* Sistrom's medium with 2 *mM* $NO_2^-$, were inoculated to an initial cell density of $\approx 10^6$ *cells* $mL^{-1}$ and incubated at 20 $^{o}C$ (stirred) in the incubation robot. When $NO_2^-$ had been depleted (recovered as $N_2$), 1 *mL* of the culture ($\approx 1 \times 10^8$ *cells*) was used to inoculate a second equivalent batch culture, which was then used to inoculate a third batch. The culture was allowed to deplete $NO_2^-$ (final cell density = $1.8 \times 10^8$ *cells* $mL^{-1}$) before 0.5 *mL* therefrom was used to inoculate vials for the two enzyme kinetic assays:

### Nitrite reductase (NirS) assay

For determination of the cell-specific rate of nitrite reductase ($v_{NO_2^-}$), we inoculated vials (n=3) with 50 *mL* Sistroms containing 1 *mM* $NO_2^-$ and He atmosphere. Once $NO_2^-$ had been depleted (recovered as $N_2$), a second dose of $NO_2^-$ was added (2 *mM*), and the gas production (NO, $N_2O$ and $N_2$) was monitored by frequent sampling (every 25 *min*) until all the $NO_2^-$ was recovered as $N_2$ (10

*h*). In order to estimate $v_{NO_2^-}$ throughout this incubation, we needed an estimate of cell density for each time increment. The cell density was measured only at the beginning and at the end of the incubation, but we could use the cumulative $e^-$-flow to $NO_x$ (based on measured NO, $N_2O$ and $N_2$) to estimate the cell density throughout, assuming a growth yield of $1.79\times10^{13}$ *cells mol*$^{-1}$ *e*$^-$ during anaerobic growth on $NO_2^-$ (Bergaust et al., 2010, Supplementary Material). The validity of this growth yield was confirmed in the present experiment: the net increase in cell density by reducing 2 *mM* $NO_2^-$ to $N_2$ (= 100 $\mu$*mol* $NO_2^-$ *vial*$^{-1}$; 300 $\mu$*mol e*$^-$ *vial*$^{-1}$) was $5.1\times10^9$ *cells vial*$^{-1}$ (stdev = $0.1\times10^9$, n=3), giving yield = $1.7\times10^{13}$ *cells mol*$^{-1}$ *e*$^-$ (which is only 5% lower than that obtained by Bergaust et al., 2010).

**Nitric oxide reductase (*c*Nor) assay**

For this assay, we needed a medium completely free of N-oxyanions, which is not the case for the standard Sistrom's medium (Bergaust et al., 2008). The oxyanion concentration was reduced by using $CoCl_2$ instead of $Co(NO_3)_2$, but we still found traces of $NO_2^-$, possibly due to impurities of the medium components, water, or glassware. This appears to be a common problem for microbiological media (Xu et al., 2000). To remove the residual $NO_2^-$, *Paracoccus denitrificans* was grown anaerobically overnight in 50 *mL* stirred batches at 30 $^0C$ (final cell density < $2\times10^7$ *cells mL*$^{-1}$). The cells were then removed by filtering, and the medium was distributed back to the same vials and re-autoclaved (for details, see Bergaust et al., 2012).

We inoculated vials with 50 *mL* N-oxyanion stripped medium and He atmosphere and monitored the NO depletion kinetics after injections of NO into the headspace. The NO injected was produced in separate vials with He atmosphere, containing acetic acid and NaI (saturated) to which a small dose of $KNO_2^-$ was added while stirring (with magnetic bars). Once $NO_2^-$ was converted to NO (which is practically instantaneous), 1 *M* NaOH was injected to ensure pH > 8, so as to minimise the vapour pressure of acetic acid in the headspace. Small doses of the headspace were then transferred to the culture vials.

To estimate NO concentrations in the liquid ($[NO]_{aq}$), we used the transport function (see Eq. 10). For each time increment between two measurements, $[NO]_{aq}$ was estimated by solving Eq. 10 for

$[NO]_{aq} = k_{H(NO)} \times P_{NO} - \frac{Tr_{NO}}{k_t}$, where $P_{NO}$ is the average partial pressure of NO in the headspace ($NO_g$) for the time increment, and $Tr_{NO}$ is the estimated transport of NO from the headspace to the liquid, which is corrected for a significant loss by each sampling, as explained by Molstad et al. (2007).

The estimated $[NO]_{aq}$ depends on accurate determination of the transport coefficient ($k_t$), and this becomes critical if $[NO]_{aq} << P_{NO} \times k_{H(NO)}$ (Eq. 10), i.e., if the NO reduction rate is so high that $[NO]_{aq}$ is much lower than the 'equilibrium concentration' = $P_{NO} \times k_{H(NO)}$. For instance, if $\frac{[NO]_{aq}}{k_{H(NO)} \times P_{NO}} = 0.1$, a 10% error in $k_t$ results in 90–100% error in the estimate of $[NO]_{aq}$. On the other hand, if $\frac{[NO]_{aq}}{k_{H(NO)} \times P_{NO}} > 0.5$, the $[NO]_{aq}$ estimate is less than 10% off-target by a 10% error in the determination of $k_t$. Thus, our target was to achieve $\frac{[NO]_{aq}}{k_{H(NO)} \times P_{NO}} > 0.5$ throughout the NO reductase assay by low cell density and high transport coefficient ($k_t$).

Initial experiments were done with relatively high initial cell densities ($\approx 6\times10^7$ *cells mL*$^{-1}$) and the same magnetic stirrers (2.5 *cm*) as used by Molstad et al (2007). The results were found to be useless at low NO concentrations in the headspace (0–50 *ppmv*): the estimated $\frac{[NO]_{aq}}{k_{H(NO)} \times P_{NO}}$-ratio was close to zero, resulting in very inaccurate determinations of $[NO]_{aq}$. To improve the experiments, we switched to longer magnetic bars (3.5 *cm*), thus increasing $k_t$. We determined $k_t$ with the new 3.5 *cm* magnetic bars for seven individual vials with 50 *mL* distilled water. The measurements were done by first injecting NO into the headspace ($\approx$ 0.1 *vol.%*), which was allowed to equilibrate with the liquid by stirring for 5 *min*. Then the stirring was stopped, and the headspace was purged by He-flow for 5 *min* (via needles through the septa). Finally, stirring was restarted (650 *rpm*), and the NO concentration was monitored by frequent sampling. The average $k_t$ for the seven vials was 0.87 *mL s*$^{-1}$ (stdev = 0.1 *mL s*$^{-1}$). The value is substantially higher than the $k_t$ = 0.28 *mL s*$^{-1}$ with the 2.5 *cm* magnetic bars, determined by Molstad et al. (2007).

Further, we reduced the number of cells inoculated to an initial cell density of $1.8\times10^6$ *cells* $mL^{-1}$ in order to secure $\frac{[NO]_{aq}}{k_{H(NO)} \times P_{NO}} > 0.5$ throughout the entire experiment. Although the target of 0.5 was not sustained throughout (see Results and Discussion), the combination of high transport rates and low cell densities secured a reasonably high $\frac{[NO]_{aq}}{k_{H(NO)} \times P_{NO}}$ ratio.

**NO concentration at the cell surface ($[NO]_{cell}$)**

During the NO reductase assay, there is a net flux of NO towards the cells (J, *mol* $s^{-1}$), driven by molecular diffusion. This implies that the NO concentration at the cell surface ($[NO]_{cell}$) is lower than the bulk concentration of NO in the liquid ($[NO]_{aq}$). To estimate $[NO]_{cell}$ for each time increment, we used the equation for molecular diffusion towards a sphere (Berg, 1983):

$$J = 4\,\pi\,D\,r\,([NO]_{aq} - [NO]_{cell}) \qquad (mol\ s^{-1}) \tag{16}$$

where J is the area integrated flux of NO towards the cell, D (= $1.93\times10^{-5}$ $cm^2\ s^{-1}$) is the diffusion coefficient for NO in water, r (= $4\times10^{-5}cm$) is the radius of the sphere, $[NO]_{aq}$ (*mol* $cm^{-3}$) is the bulk concentration of NO, and $[NO]_{cell}$ (*mol* $cm^{-3}$) is the NO concentration at the cell surface. Zacharia and Deen (2005) found identical diffusion coefficients for NO in water and phosphate buffer solution at 25 $^oC$ (D = $2.21\times10^{-5}$ $cm^2\ s^{-1}$). Extrapolation to our temperature of 20 $^oC$, using the Stokes-Einstein equation (Poling et al., 2000), gives D = $1.93\times10^{-5}$ $cm^2\ s^{-1}$.

Solving Eq. 16 for $[NO]_{cell}$ gives:

$$[NO]_{cell} = [NO]_{aq} - \frac{J}{4\,\pi\,D\,r} \qquad (mol\ cm^{-3}) \tag{17}$$

which was used to estimate $[NO]_{cell}$ for each time increment; J (*mol* $s^{-1}$) is estimated by the measured rate of NO reduction (per cell) divided by cell numbers, and $[NO]_{aq}$ (*mol* $cm^{-3}$) is the bulk concentration estimated as described above.

**Enzyme kinetics**

Since *c*Nor requires the participation of two molecules of NO to make one molecule of $N_2O$, the default kinetics is not a regular Michaelis-Menten equation, but rather a 'dual substrate kinetics' model. Further, analysis of *in vitro* kinetics of *c*Nor has shown that the enzyme reaction is inhibited by high (*micromolar*) NO concentrations. To take these phenomena into account, we adopted the model by Girsch and de Vries (1997):

$$v_{\mathrm{NO}} = \frac{v_{max\mathrm{NO}}}{1+\frac{\mathrm{K_{2NO}}}{[\mathrm{NO}]_{\mathrm{cell}}}+\frac{\mathrm{K_{1NO}}\times\mathrm{K_{2NO}}}{[\mathrm{NO}]^2_{\mathrm{cell}}}+\frac{[\mathrm{NO}]_{\mathrm{cell}}}{\mathrm{K}_{i\mathrm{NO}}}} \quad (mol\ cell^{-1}\ h^{-1}) \tag{18}$$

where $v_{max\mathrm{NO}}$ ($mol\ cell^{-1}\ h^{-1}$) is the maximum reduction rate, $\mathrm{K_{1NO}}$ and $\mathrm{K_{2NO}}$ ($mol\ L^{-1}$) are the apparent half-saturation constants for the two active sites, $\mathrm{K}_{i\mathrm{NO}}$ ($mol\ L^{-1}$) is the inhibition dissociation constant, and $[\mathrm{NO}]_{\mathrm{cell}}$ ($mol\ L^{-1}$) is the NO concentration at the cell surface.

Using the data for $v_{\mathrm{NO}}$ and $[\mathrm{NO}]_{\mathrm{cell}}$, we estimated the parameters $\mathrm{K_{1NO}}$, $\mathrm{K_{2NO}}$, $\mathrm{K}_{i\mathrm{NO}}$, and $v_{max\mathrm{NO}}$ by least-squares regression, using the Levenberg-Marquardt algorithm and Metropolis Markov chain Monte Carlo (Tarantola, 2005; Müller et al., 2007). Both the methods predicted extremely high values for $\mathrm{K}_{i\mathrm{NO}}$ (> 100 $\mu M$) and $\mathrm{K_{1NO}}$ approaching zero. This suggested that the dataset contains no information about these two parameters, apart from indicating that $\mathrm{K_{1NO}}$ is too low to affect the model predictions significantly within the measured range and that $\mathrm{K}_{i\mathrm{NO}}$ is too high to affect the predictions within the concentration range used. The latter agrees well with the apparent $\mathrm{K}_{i\mathrm{NO}}$ = 13 $\mu M$ determined *in vitro* (Girsch and de Vries, 1997).

On this basis, we decided to fit a regular Michaelis-Menten function to our data (Eq. 18 becomes a Michaelis-Menten function if we eliminate the inhibition term and assume $\mathrm{K_{1NO}} = 0$):

$$v_{\mathrm{NO}} = \frac{v_{max\mathrm{NO}} \times [\mathrm{NO}]_{\mathrm{cell}}}{(\mathrm{K}_{m\mathrm{NO}} + [\mathrm{NO}]_{\mathrm{cell}})} \quad (mol\ cell^{-1}\ h^{-1}) \tag{19}$$

Combining Eq. 16 and 19 ($\mathrm{J} = v_{\mathrm{NO}}$), we can find J (flux of NO towards the cell) as an explicit function of $[\mathrm{NO}]_{\mathrm{aq}}$ (Bailey et al., 1986):

$$J = -\frac{b}{2} - \frac{1}{2}\sqrt{b^2 - 16\, v_{max\mathrm{NO}}\, \pi\, D\, r\, [NO]_{aq}} \quad (mol\ s^{-1}) \tag{20}$$

where $b = -4\, \pi\, D\, r\, \left(K_{m\mathrm{NO}} + [NO]_{aq}\right) - v_{max\mathrm{NO}}$

The parameters $v_{max\mathrm{NO}}$ and $K_{m\mathrm{NO}}$ were then estimated by fitting Eq. 20 to the measured rate of NO reduction ($J = v_{\mathrm{NO}}$) and estimated $[NO]_{aq}$ (Fig. 4B), using the least squares regression (Levenberg-Marquardt and Metropolis MCMC).

Once the enzyme kinetic parameters for *c*Nor are known, the steady state NO concentrations ($[NO]_{ss}$) in a culture can be explicitly calculated, since at steady state: $\frac{d(NO_{aq})_{ss}}{dt} = v_{NO_2^-} - v_{\mathrm{NO}} = 0$, and we can assume $v_{NO_2^-}$ to be nearly constant (since $[NO_2^-] >> K_{mNO_2^-}$); hence, we get:

$$\frac{d(NO_{aq})_{ss}}{dt} = v_{NO_2^-} - \frac{v_{max\mathrm{NO}}}{1 + K_{2\mathrm{NO}}\left(\frac{1}{[NO]_{cell}} + \frac{K_{1\mathrm{NO}}}{[NO]_{cell}^2}\right) + \frac{[NO]_{cell}}{K_{i\mathrm{NO}}}} = 0 \quad (mol\ N\ h^{-1}) \tag{21}$$

which can be solved for $[NO]_{cell}$, equivalent to $[NO]_{aq}$ when in steady state.

# References

Al-Attar, S., and de Vries, S. (2015) An electrogenic nitric oxide reductase. *FEBS Lett* **(in press)**.

Bailey, J., Bailey, J., and Ollis, D.F. (1986) *Biochemical Engineering Fundamentals*. New York: McGraw-Hill Science/Engineering/Math.

Bar-Even, A., Noor, E., Savir, Y., Liebermeister, W., Davidi, D., Tawfik, D.S., and Milo, R. (2011) The moderately efficient enzyme: evolutionary and physicochemical trends shaping enzyme parameters. *Biochemistry* **50**: 4402-4410.

Berg, H.C. (1983) *Random Walks in Biology*. New Jersey: Princeton University Press.

Bergaust, L., Shapleigh, J., Frostegård, Å., and Bakken, L.R. (2008) Transcription and activities of $NO_x$ reductases in *Agrobacterium tumefaciens*: the influence of nitrate, nitrite and oxygen availability. *Environ Microbiol* **10**: 3070-3081.

Bergaust, L., Mao, Y., Bakken, L.R., and Frostegård, Å. (2010) Denitrification response patterns during the transition to anoxic respiration and posttranscriptional effects of suboptimal pH on nitrogen oxide reductase in *Paracoccus denitrificans*. *Appl Environ Microbiol* **76**: 6387-6396.

Bergaust, L., van Spanning, R.J.M., Frostegård, Å., and Bakken, L.R. (2012) Expression of nitrous oxide reductase in *Paracoccus denitrificans* is regulated by oxygen and nitric oxide through FnrP and NNR. *Microbiology* **158**: 826-834.

Bouchal, P., Struhárová, I., Budinská, E., Šedo, O., Vyhlídalová, T., Zdráhal, Z. et al. (2010) Unraveling an FNR based regulatory circuit in *Paracoccus denitrificans* using a proteomics-based approach. *Biochim Biophys Acta* **1804**: 1350-1358.

Bowman, L.A.H., McLean, S., Poole, R.K., and Fukuto, J.M. (2011) The diversity of microbial responses to nitric oxide and agents of nitrosative stress: close cousins but not identical twins. *Adv Microb Physiol* **59**: 135-219.

Carr, G.J., and Ferguson, S.J. (1990) The nitric oxide reductase of *Paracoccus denitrificans*. *Biochem J* **269**: 423-429.

de Vries, S., Suharti, and Pouvreau, L.A.M. (2007) Nitric oxide reductase: structural variations and catalytic mechanism. In *Biology of the Nitrogen Cycle*. Bothe, H., Ferguson, S.J., and Newton, W.E. (eds). Amsterdam: Elsevier B. V., pp. 57-66.

Dermastia, M., Turk, T., and Hollocher, T.C. (1991) Nitric oxide reductase: Purification from *Paracoccus denitrificans* with use of a single column and some characteristics. *J Biol Chem* **266**: 10899-10905.

Fujiwara, T., and Fukumori, Y. (1996) Cytochrome *cb*-type nitric oxide reductase with cytochrome *c* oxidase activity from *Paracoccus denitrificans* ATCC 35512. *J Bacteriol* **178**: 1866-1871.

Gates, A.J., Luque-Almagro, V.M., Goddard, A.D., Ferguson, S.J., Roldán, M.D., and Richardson, D.J. (2011) A composite biochemical system for bacterial nitrate and nitrite assimilation as exemplified by *Paracoccus denitrificans*. *Biochem J* **435**: 743-753.

Girsch, P., and de Vries, S. (1997) Purification and initial kinetic and spectroscopic characterization of NO reductase from *Paracoccus denitrificans*. *Biochim Biophys Acta* **1318**: 202-216.

Hassan, J., Bergaust, L.L., Wheat, I.D., and Bakken, L.R. (2014) Low probability of initiating *nirS* transcription explains observed gas kinetics and growth of bacteria switching from aerobic respiration to denitrification. *PLoS Comput Biol* **10**: e1003933.

Hoglen, J., and Hollocher, T.C. (1989) Purification and some characteristics of nitric oxide reductase containing vesicles from *Paracoccus denitrificans*. *J Biol Chem* **264**: 7556-7563.

Kuňák, M., Kučera, I., and van Spanning, R.J.M. (2004) Nitric oxide oscillations in *Paracoccus denitrificans*: the effects of environmental factors and of segregating nitrite reductase and nitric oxide reductase into separate cells. *Arch Biochem Biophys* **429**: 237-243.

Liu, B., Mao, Y., Bergaust, L., Bakken, L.R., and Frostegård, Å. (2013) Strains in the genus *Thauera* exhibit remarkably different denitrification regulatory phenotypes. *Environ Microbiol* **15**: 2816-2828.

Ludwig, J., Meixner, F.X., Vogel, B., and Förstner, J. (2001) Soil-air exchange of nitric oxide: an overview of processes, environmental factors, and modeling studies. *Biogeochemistry* **52**: 225-257.

Lueking, D.R., Fraley, R.T., and Kaplan, S. (1978) Intracytoplasmic membrane synthesis in synchronous cell populations of *Rhodopseudomonas sphaeroides*. Fate of "old" and "new" membrane. *J Biol Chem* **253**: 451-457.

Mania, D., Heylen, K., van Spanning, R.J.M., and Frostegård, Å. (2014) The nitrate-ammonifying and *nosZ*-carrying bacterium *Bacillus vireti* is a potent source and sink for nitric and nitrous oxide under high nitrate conditions. *Environ Microbiol* **16**: 3196-3210.

Medinets, S., Skiba, U., Rennenberg, H., and Butterbach-Bahl, K. (2014) A review of soil NO transformation: associated processes and possible physiological significance on organisms. *Soil Biol Biochem* **80**: 92-117.

Molstad, L., Dörsch, P., and Bakken, L.R. (2007) Robotized incubation system for monitoring gases ($O_2$, NO, $N_2O$, $N_2$) in denitrifying cultures. *J Microbiol Methods* **71**: 202-211.

Müller, C., Rütting, T., Kattge, J., Laughlin, R.J., and Stevens, R.J. (2007) Estimation of parameters in complex $^{15}N$ tracing models by Monte Carlo sampling. *Soil Biol Biochem* **39**: 715-726.

Pan, Y., Ni, B.-J., and Yuan, Z. (2013) Modeling electron competition among nitrogen oxides reduction and $N_2O$ accumulation in denitrification. *Environ Sci Technol Lett* **47**: 11083-11091.

Poling, B.E., Prausnitz, J.M., and O'Connell, J.P. (2000) *The Properties of Gases and Liquids*. New York: McGraw-Hill Education.

Poole, R.K., and Hughes, M.N. (2000) New functions for the ancient globin family: bacterial responses to nitric oxide and nitrosative stress. *Mol Microbiol* **36**: 775-783.

Qu, Z. (2014) Respiratory regulation in *Paracoccus denitrificans* and in soil, implications for $N_2O$ emissions. In *Department of Environmental Sciences*. Ås, Norway: Norwegian University of Life Sciences.

Schlesinger, W.H., and Bernhardt, E.S. (2013) *Biogeochemistry: An Analysis of Global Change*. Oxford: Academic Press.

Sistrom, W.R. (1960) A requirement for sodium in the growth of *Rhodopseudomonas spheroides*. *J Gen Microbiol* **22**: 778-785.

Spiro, S. (2007) Regulators of bacterial responses to nitric oxide. *FEMS Microbiol Rev* **31**: 193-211.

Spiro, S. (2012) Nitrous oxide production and consumption: regulation of gene expression by gas-sensitive transcription factors. *Philos Trans R Soc Lond B Biol Sci* **367**: 1213-1225.

Tarantola, A. (2005) *Inverse Problem Theory and Methods for Model Parameter Estimation*. Philadelphia: Society for Industrial and Applied Mathematics.

Thorndycroft, F.H., Butland, G., Richardson, D.J., and Watmough, N.J. (2007) A new assay for nitric oxide reductase reveals two conserved glutamate residues form the entrance to a proton-conducting channel in the bacterial enzyme. *Biochem J* **401**: 111-119.

van Spanning, R.J.M., Richardson, D.J., and Ferguson, S.J. (2007) Introduction to the biochemistry and molecular biology of denitrification. In *Biology of the Nitrogen Cycle*. Bothe, H., Ferguson, S.J., and Newton, W.E. (eds). Amsterdam: Elsevier B. V., pp. 3-20.

Wilhelm, E., Battino, R., and Wilcock, R.J. (1977) Low-pressure solubility of gases in liquid water. *Chem Rev* **77**: 219-262.

Xu, J., Xu, X., and Verstraete, W. (2000) Adaptation of *E. coli* cell method for micro-scale nitrate measurement with the Griess reaction in culture media. *J Microbiol Methods* **41**: 23-33.

Zacharia, I.G., and Deen, W.M. (2005) Diffusivity and solubility of nitric oxide in water and saline. *Ann Biomed Eng* **33**: 214-222.

# Supporting Information

## Calculation of the *c*Nor molecules per cell in *Pa. denitrificans*

To estimate turnover rates of *c*Nor, we need an estimate of the number of protein molecules per cell. Girsch and de Vries (1997) extracted and purified *c*Nor from anaerobically grown *Paracoccus denitrificans* and obtained a nearly pure fraction (on protein-basis) after hydroxyapatite column separation. Based on the measured activity in this fraction and the fact that the activity of *c*NOR *in vitro* is approx. 50% of that in intact membranes, 18% of the *c*Nor was recovered. Based on the protein content in the pure fraction (4.2 *mg*) and the protein content of the original membrane fraction (2000 *mg*), we find that the membrane protein fraction contains $\frac{\frac{4.2}{0.18}}{2000} = 0.0117$ *g cNor g*$^{-1}$ *membrane proteins*, or 167 *nmol cNor g*$^{-1}$ *membrane proteins* (assuming mol weight of *c*Nor = 70,000).

Assuming that membrane proteins account for $\frac{1}{3}$ to $\frac{1}{2}$ of the total protein pools of bacterial cells, we find that the *c*Nor content per g whole cell protein is 56–84 *nmol cNor g*$^{-1}$ *cell-protein*.

Bergaust et al. (2010, Supplementary Material) measured whole cell protein of *Pa. denitrificans* to be $96\times10^{-15}$ *g cell*$^{-1}$. With 56–84 *nmol cNor g*$^{-1}$ *cell-protein*, we find that the amount of *c*Nor per cell is $5.34–8.02\times10^{-21}$ *mol cell*$^{-1}$ = 3212–4818 *molecules cell*$^{-1}$.

### References

Bergaust, L., Mao, Y., Bakken, L.R., and Frostegård, Å. (2010) Denitrification response patterns during the transition to anoxic respiration and posttranscriptional effects of suboptimal pH on nitrogen oxide reductase in *Paracoccus denitrificans*. *Appl Environ Microbiol* **76**: 6387-6396.

Girsch, P., and de Vries, S. (1997) Purification and initial kinetic and spectroscopic characterization of NO reductase from *Paracoccus denitrificans*. *Biochim Biophys Acta* **1318**: 202-216.

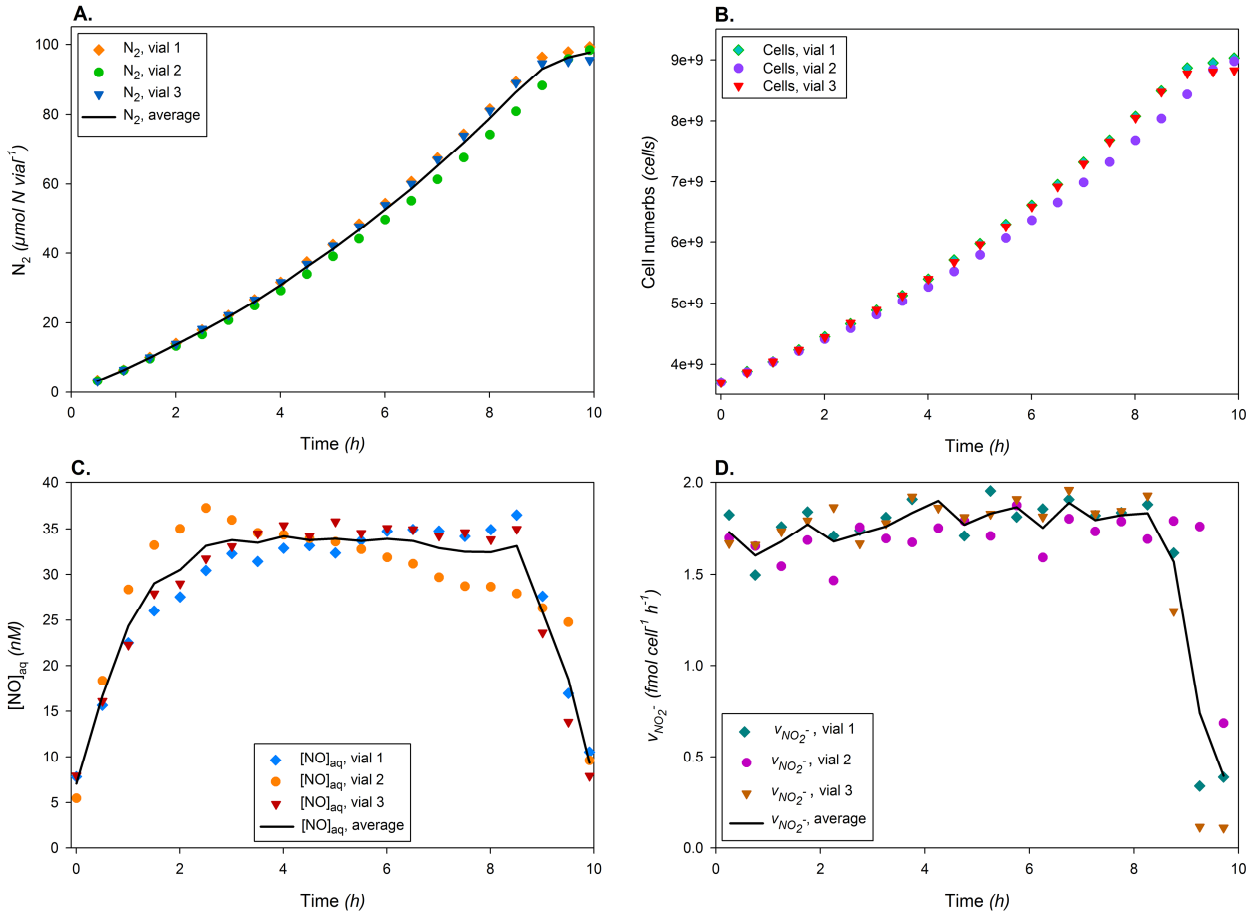


**Figure S1. Cell-specific rates of $NO_2^-$ reduction ($v_{NO_2^-}$).** The measured $N_2$ production (**A**) was used to estimate cell density (**B**) based on previously determined growth yield = $1.79\times10^{13}$ *cells mol$^{-1}$electrons to NO$_x$* (Bergaust et al., 2010). Panel **C** shows the NO concentrations (*nM in the liquid*). For each time increment, the cell specific rates of $NO_2^-$ reduction were calculated (Panel **D**) based on the measured rates per vial and the estimated cell numbers. For all the panels, the individual result for the three replicate vials are shown (line = average). The final cell density, measured by $OD_{660}$ in the individual vials, was within ±7% of that predicted by cumulative electron flow and the growth yield = $1.79\times10^{13}$ *cells mol$^{-1}$electrons.*

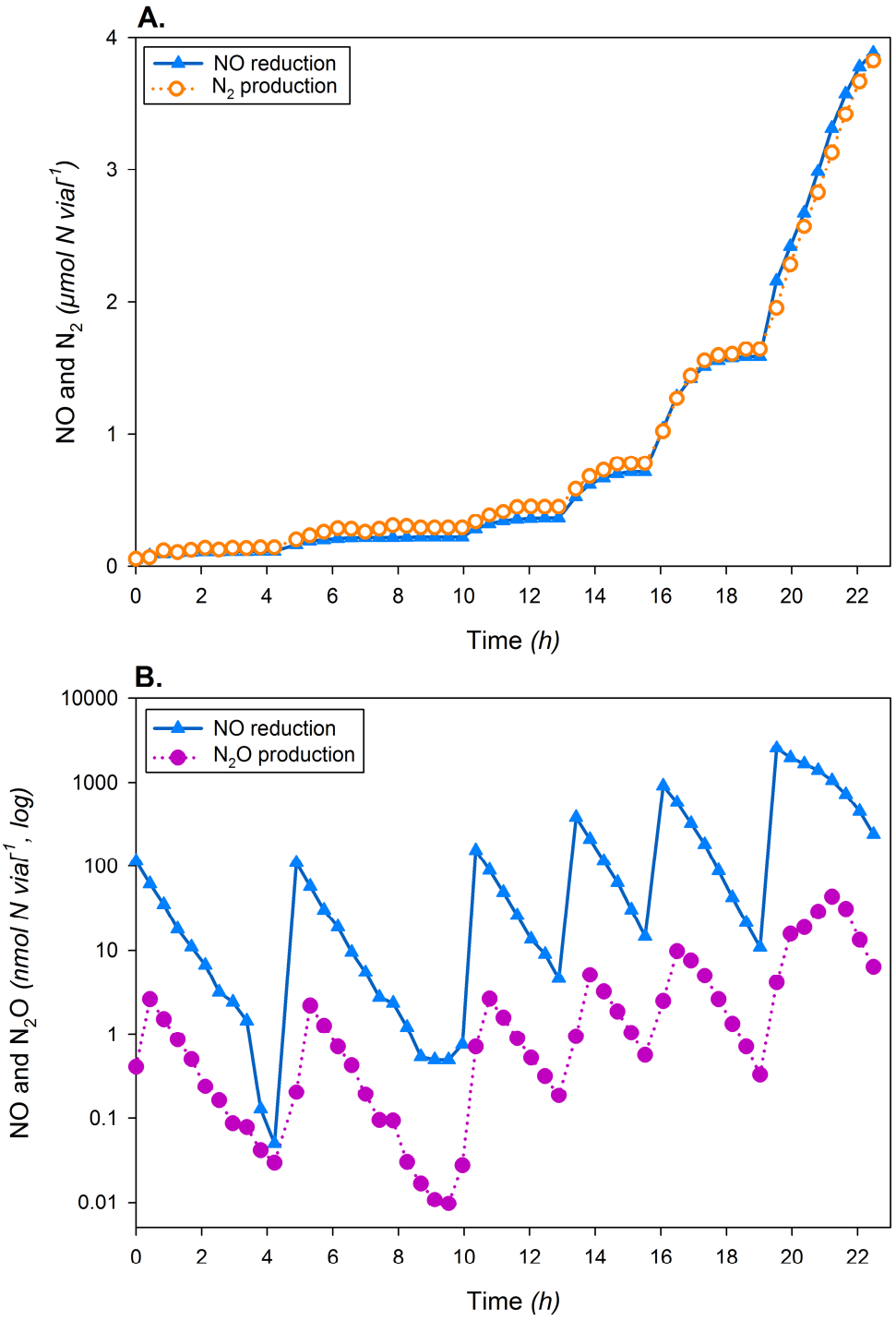


**Figure S2. Recovery of NO-N as $N_2$ (A) and $N_2O$ concentrations throughout the NO reduction assay (B).** Panel **A** shows the cumulative NO reduction and $N_2$ production (*µmol NO* and *$N_2$–N vial$^{-1}$*, i.e., in liquid + headspace), closely matching throughout the incubation. Panel **B** shows the amounts of NO and $N_2O$-N (*nmol N vial$^{-1}$*) throughout the incubation (logarithmic scale). Both the results are for the same vial as shown in Fig. 4 in the manuscript.

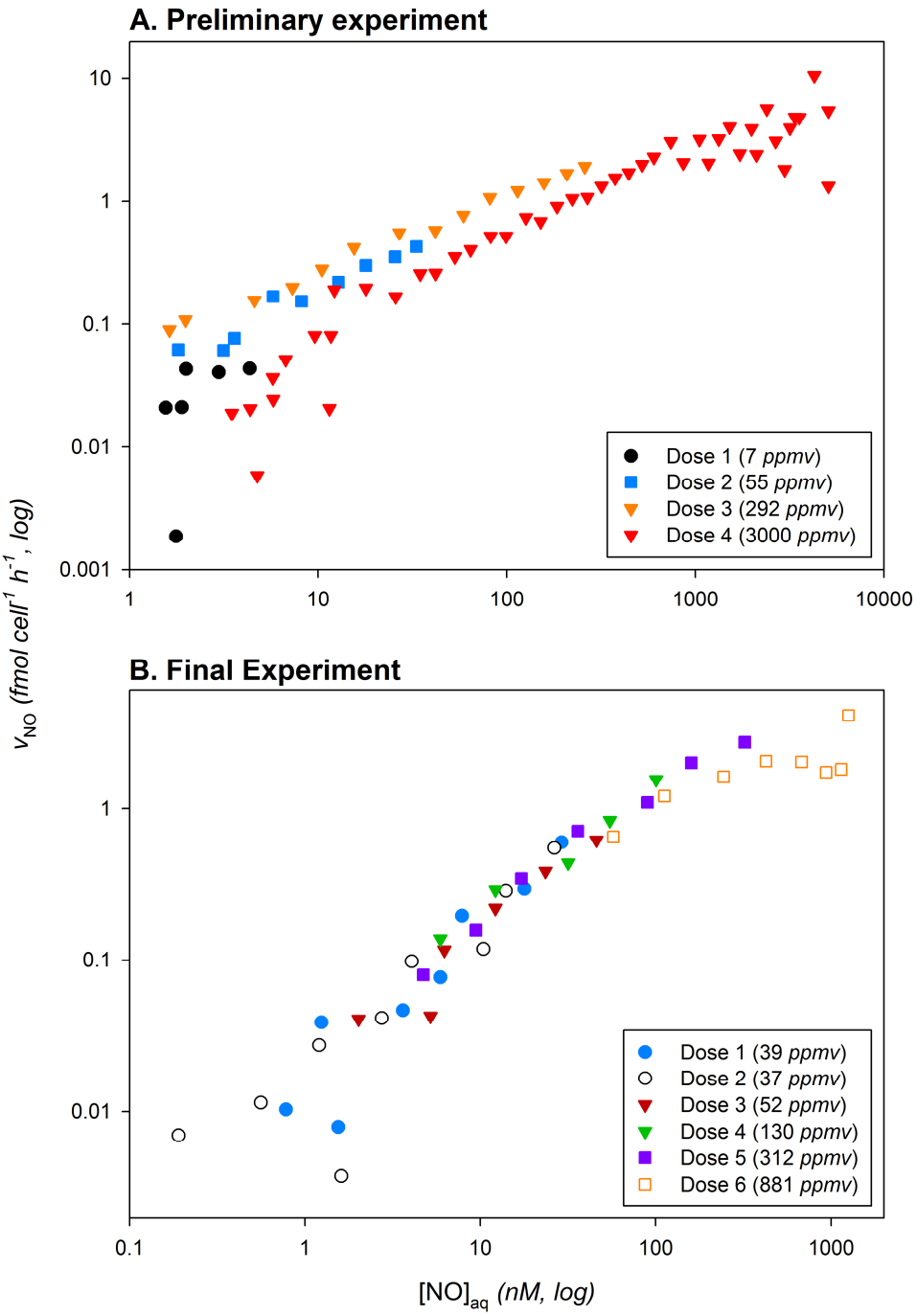


**Figure S3. Inhibition of NO reduction by high NO concentrations.** Panel **A** shows the results for preliminary experiments similar to that shown in Fig. 4, but with higher final doses of NO. The log-log plot shows the cell-specific rates of NO reduction ($v_{NO}$, *fmol cell*$^{-1}$ *h*$^{-1}$) against the NO concentrations in the liquid ([NO]$_{aq}$) for single time increments during depletion of four consecutive doses (7, 55, 292, and 3000 *ppmv*; 1 *ppmv NO in headspace* gives 2.12 *nM in the liquid* when in equilibrium). $v_{NO}$ during depletion of the first three doses shows reasonably

similar concentration dependency, while the cells that had been exposed to the final high dose of NO (*3000 ppmv*; $[NO]_{aq} \approx 6\ \mu M$) had clearly lower rates by a factor of 2–3. In these experiments, OD was measured throughout the experiments, and the cell numbers were found to increase in proportion with the cumulated NO reduction throughout the depletion of the first three doses, but not after the fourth high dose. Thus, growth was evidently permanently impeded by exposure to such high NO concentrations. Panel **B** shows the result for one of the three replicate vials used in the final experiment for determining $K_{mNO}$ and $v_{maxNO}$. In this case, the last high dose (*881 ppmv*; $[NO]_{aq} \approx 1.87\ \mu M$ if in equilibrium) apparently resulted in a more transient depression in NO reduction.

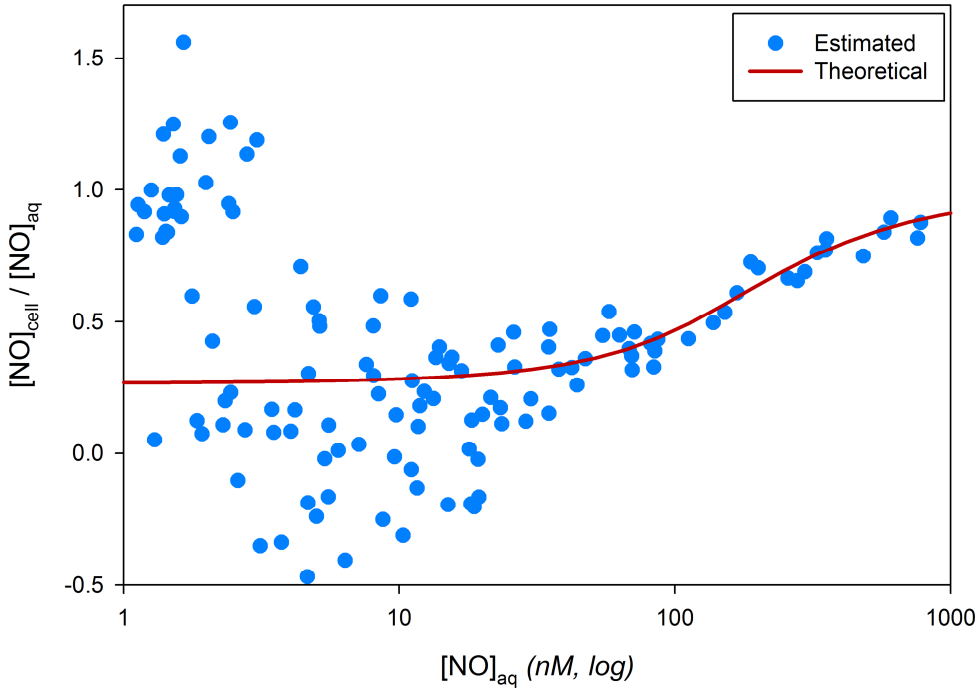


**Figure S4. The relationship between the estimated NO concentration at the cell surface ($[NO]_{cell}$) and that in the bulk liquid ($[NO]_{aq}$).** The panel shows the ratio $\frac{[NO]_{cell}}{[NO]_{aq}}$ plotted against $[NO]_{aq}$ (log scale), together with the theoretical curve for spheres with radius 0.4 $\mu m$, $v_{maxNO}$ = 3.56 *fmol cell*$^{-1}$ *h*$^{-1}$, and $K_{mNO}$ = 34 *nM*. There is good agreement for $[NO]_{aq}$ > 20 *nM*, but for lower concentrations, there is much experimental noise. A negative ratio means that the estimated $[NO]_{cell}$ is negative.

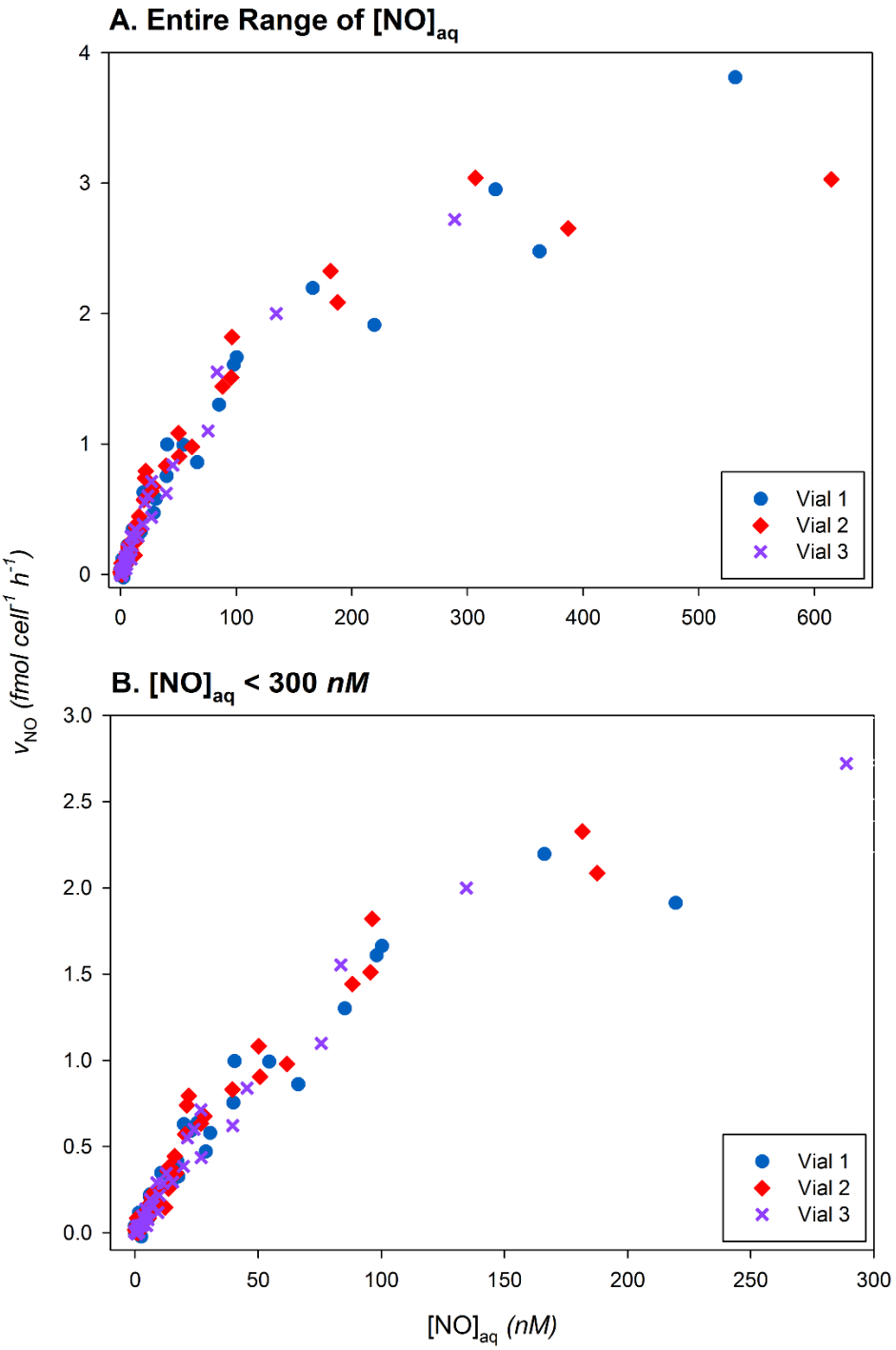


**Figure S5. Estimated cell-specific rates of NO-reduction ($v_{NO}$, *fmol cell*$^{-1}$ *h*$^{-1}$) for individual time increments.** The rates are plotted against the estimated concentration of NO in the aqua ($[NO]_{aq}$). Panel **A** shows the entire range, and Panel **B** shows the results for $[NO]_{LP}$ < 300 *nM*. All data shown are for NO depletion through the first 2–3 injections of NO < 500 *ppmv* (= $[NO]_{aq}$ < 1 $\mu M$). The estimated $v_{NO}$ for $[NO]_{aq}$ > 300 *nM* is more variable than at lower concentrations.

# P A P E R III

**Accepted (minor revision, 5th Sept. 2015), PLOS Computational Biology**

# Transient accumulation of $NO_2^-$ and $N_2O$ during denitrification explained by assuming cell diversification due to stochastic transcription of denitrification genes

**Junaid Hassan*, Linda L. Bergaust, Zhi Qu, Lars R. Bakken**

# Transient accumulation of $NO_2^-$ and $N_2O$ during denitrification explained by assuming cell diversification due to stochastic transcription of denitrification genes

Junaid Hassan[1¶*], Lars R. Bakken[1¶], Zhi Qu[1,#a&], Linda L. Bergaust[2&]

[1] Department of Environmental Sciences, Norwegian University of Life Sciences, Ås, Norway

[2]Chemistry, Biotechnology and Food Science, Norwegian University of Life Sciences, Ås, Norway

[#a]Current address: College of Natural Resources and Environment, Northwest A&F University, Shaanxi, China

*Corresponding author

E-mail: junaid.hassan@nmbu.no (JH)

[¶]These authors contributed equally to this work.

[&]These authors also contributed equally to this work.

## Abstract

Denitrifying bacteria accumulate $NO_2^-$, NO and $N_2O$, the amounts depending on the transcriptional regulation of core denitrification genes in response to $O_2$-limiting conditions. The genes include *nar*, *nir*, *nor* and *nosZ*, encoding $NO_3^-$-, $NO_2^-$-, NO- and $N_2O$ reductase, respectively. We previously constructed a dynamic model to simulate growth and respiration in batch cultures of *Paracoccus denitrificans*. The observed denitrification kinetics were adequately simulated by assuming a stochastic initiation of *nir*-transcription in each cell with an extremely low probability (0.5% $h^{-1}$), leading to product- and substrate-induced transcription of *nir* and *nor*, respectively, via NO. Thus, the model predicted cell diversification: after $O_2$ depletion, only a small fraction was able to grow by reducing $NO_2^-$.

Here, we have developed the model further to simulate batch cultivation with $NO_3^-$, i.e., the $NO_2^-$, NO, $N_2O$ and $N_2$ kinetics, measured in a novel experiment including frequent measurements of $NO_2^-$. *Pa. denitrificans* reduced practically all $NO_3^-$ to $NO_2^-$ before initiating gas production. The $NO_2^-$ production is adequately simulated by assuming stochastic *nar*-transcription, as that for *nirS*, but with a higher probability (0.035 $h^{-1}$) and initiating at a higher $O_2$ concentration.

Our model assumes that all cells express *nosZ*, thus predicting that a majority of cells have only $N_2O$-reductase. This sub-population (A) grows by respiring $N_2O$ produced by the sub-population with $NO_2^-$- and NO-reductase (B). The ratio $\frac{B}{A}$ is low immediately after $O_2$ depletion, but increases throughout the anoxic phase because B grows faster than A. As a result, the model predicts initially low but gradually increasing $N_2O$ concentration throughout the anoxic phase, as observed.

The modelled cell diversification neatly explains the observed denitrification kinetics and transient intermediate accumulations. The result has major implications for understanding the relationship between genotype and phenotype in denitrification research.

## Author Summary

Denitrifiers generally respire $O_2$, but if $O_2$ becomes limiting, they may switch to anaerobic respiration (denitrification) by producing $NO_3^-$-, $NO_2^-$-, NO- and/or $N_2O$ reductase, encoded by *nar*, *nir*, *nor* and *nosZ* genes, respectively. Denitrification causes transient accumulation of $NO_2^-$ and $NO/N_2O$ emissions, depending on the activity of the four reductases. Denitrifiers lacking *nosZ* produce ~100% $N_2O$, whereas organisms with only *nosZ* are net consumers of $N_2O$. Full-fledged denitrifiers are equipped with all four reductases, genetic regulation of which determines $NO_2^-$ accumulation and $NO/N_2O$ emissions. *Paracoccus denitrificans* is a full-fledged denitrifying bacterium, and here we present a modelling approach to understand its regulation. We found that the observed transient accumulation of $NO_2^-$ and $N_2O$ can be neatly

explained by assuming cell diversification: all cells express *nosZ*, while a minority expresses *nar* and *nir+nor*. Thus, the model predicts that in a batch culture of this organism, only a minor sub-population is full-fledged denitrifier. The cell diversification is a plausible outcome of stochastic initiation of *nar* and *nir* transcription, which then becomes autocatalytic by $NO_2^-$ and NO. The findings are important for understanding the regulation of denitrification in bacteria: product-induced transcription of denitrification genes is common, and we surmise that diversification in response to anoxia is widespread.

## Introduction

The dissimilative reduction of nitrate ($NO_3^-$) to nitrite ($NO_2^-$), nitric oxide (NO), nitrous oxide ($N_2O$), and finally to $N_2$ (denitrification) is an indispensable process in the nitrogen cycle, returning N to the atmosphere as $N_2$. However, denitrification significantly leaks the gaseous intermediates NO and $N_2O$, both with serious consequences for the environment. $N_2O$ catalyses depletion of the stratospheric ozone (1) and causes global warming, contributing ~10% to the anthropogenic climate forcing (2). Data suggests that since the 1950s, the atmospheric $N_2O$ has been increasing, and before being photolysed in the stratosphere, the gas persists for an average ~120 years in the troposphere (3). ~70% of global $N_2O$ emissions are tentatively attributed to microbial nitrification and denitrification in soils (4), where denitrification, generally, is considered a more dominant source (5).

### To mitigate $N_2O$ emissions, we need to understand the physiology of denitrifiers.

To devise robust strategies for mitigating global $N_2O$ emissions, a good understanding of its primary source is imperative, i.e., genetics, physiology, and regulatory biology of denitrifiers. Any knowledge of the environmental controllers of $N_2O$ is incomplete without understanding the causal relationships of such controllers at the physiological level (6).

The biogeochemical models developed for understanding the ecosystem controls of denitrification and $N_2O$ emissions treat the denitrifying community of soils and sediments as

a single homogenous unit with certain characteristic responses to $O_2$ and $NO_3^-$ concentrations (6, 7). Natural denitrifying communities, however, are mixtures of organisms with widely different denitrification regulatory phenotypes (8). The regulatory response of such mixtures is not necessarily equal to the 'sum of its components' because there will be interactions, not the least, via the intermediates NO and $NO_2^-$. Hence, it is probably a mission impossible to predict the regulatory responses of complex communities based on their phenotypic composition. Nevertheless, investigations of the regulation in model organisms like *Pa. denitrificans* provide us with essential concepts, enhancing our ability to understand the regulatory responses of mixed communities and to generate meaningful hypotheses. Thus, future biogeochemical models of $N_2O$ and NO emissions are expected to have more explicit simulations of the regulatory networks involved, and a first attempt has recently been published (9).

## Simulating the cell diversification in response to impending anoxia to analyse its implications for $NO_2^-$, $N_2$, and $N_2O$ kinetics

Dynamic modelling has been used to a limited extent to analyse various denitrification phenotypes; for example, to analyse $NO_3^-$ and $NO_2^-$ reduction and gas-kinetic data for individual strains (10) and mixtures of selected phenotypes (11); to model the consequence of competition for electrons between denitrification reductases (12, 13); to investigate the control of $O_2$ on denitrification enzymes and inhibition of cytochrome *c* oxidase by NO in *Agrobacterium tumefaciens* (14); and to examine the effect of copper availability on $N_2O$ reduction in *Paracoccus denitrificans* (15). In our previous model (16), we simulated $O_2$ and $N_2$ kinetics from batch incubations of *Pa. denitrificans* (8, 17) to test if a postulated cell diversification, driven by stochastic initiation of *nirS*, could explain the $N_2$ production kinetics in $NO_2^-$-supplemented media. The available data also contained $NO_3^-$-supplemented treatments, but $NO_3^-$ and $NO_2^-$ were not monitored, and the experiment provided no information about the $N_2O$ kinetics, except that the concentrations were extremely low (below the detection limit of the thermal conductivity detector used). Recently, a neat dataset was generated from batch incubations supplemented with $NO_3^-$, with frequent

measurements of $NO_2^-$ and a more sensitive detection of $N_2O$ by an electron capture detector (18). That encouraged us to extend our previous model and simulate the cell diversification during transition from oxic to anoxic conditions, targeting the regulation of Nar and *c*Nor/NosZ ($N_2O$ emissions) in *Pa. denitrificans*.

## Regulatory network of denitrification in *Paracoccus denitrificans*

*Pa. denitrificans* is a facultative anaerobe capable of reducing $NO_3^-$ all the way to $N_2$:

$$NO_3^- \xrightarrow{\text{nNar}} NO_2^- \xrightarrow{\text{NirS}} NO \xrightarrow{c\text{Nor}} N_2O \xrightarrow{\text{NosZ}} N_2$$

In response to impending anoxic conditions, the organism sustains respiratory metabolism by producing the membrane-bound cytoplasmic nitrate reductase (nNar), cytochrome $cd_1$ nitrite reductase (NirS), cytochrome *c* dependent nitric oxide reductase (*c*Nor), and nitrous oxide reductase (NosZ). Transcription of the genes encoding these reductases (*narG*, *nirS*, *norBC*, and *nosZ*, respectively) are regulated by the FNR-type proteins FnrP, NarR, and NNR. FnrP contains a 4Fe-4S cluster for sensing $O_2$, and NNR harbours a NO-sensing haem; NarR, however, is poorly characterised and is most likely a $NO_2^-$-sensor (19-21). All these sensors remain inactive during aerobic growth conditions (19).

**Transcription of denitrification genes in *Pa. denitrificans*.** FnrP/NarR and NNR facilitate a product-induced transcription of the *nar* and *nirS* genes, respectively (Fig. 1, see $P_1$ and $P_2$): Low oxygen concentration ($[O_2]$) activates the self-regulating FnrP, which induces *nar* transcription in coaction with NarR. The self-regulating NarR is activated by $NO_2^-$ [and/or, probably, by $NO_3^-$ (21)]; thus once a cell starts producing traces of $NO_2^-$, *nar* expression becomes autocatalytic. Transcription of *nirS* is induced by NNR, which is apparently inactivated by $O_2$ (22, 23), but under anoxic/micro-anoxic conditions, NNR is activated by NO. Thus, once traces of NO are produced, the expression of *nirS* also becomes autocatalytic (19, 20). In contrast, *nor* transcription is substrate (NO) induced via NNR while *nosZ* is equally induced by NNR or FnrP (24). High concentrations of NO may constrain *nar* transcription by inactivating FnrP (20) and, like $O_2$, render NosZ dysfunctional by inactivating the $Cu_Z$ subunit

of the reductase (25), but these observations are ignored in our model because *Pa. denitrificans* restrict [NO] to very low levels.

## Entrapment of cells in anoxia: the underlying hypothesis and modelling

Denitrification proteome, once produced in response to an anoxic spell, is likely to linger within the cells under subsequent oxic conditions, ready to be used if anoxia recurs. But the proteome will be diluted by aerobic growth because the transcription of denitrification genes is inactivated under oxic conditions (20). Hence, a population growing through many generations under fully oxic conditions is expected to undertake *de novo* synthesis of denitrification enzymes when confronted with anoxia. Batch cultivations of such aerobically raised *Pa. denitrificans* provided indirect evidence for a novel claim that, in response to anoxia, only a small fraction of the incubated population is able to produce denitrification proteome (8, 17, 26, 27). Our dynamic modelling of Bergaust *et al.'s* (17) $NO_2^-$-supplemented incubations corroborated this, suggesting that a probabilistic function (specific probability = 0.005 $h^{-1}$) resulting in the recruitment of 3.8–16.1% of all cells to denitrification is adequate to explain the measured $N_2$ kinetics (16).

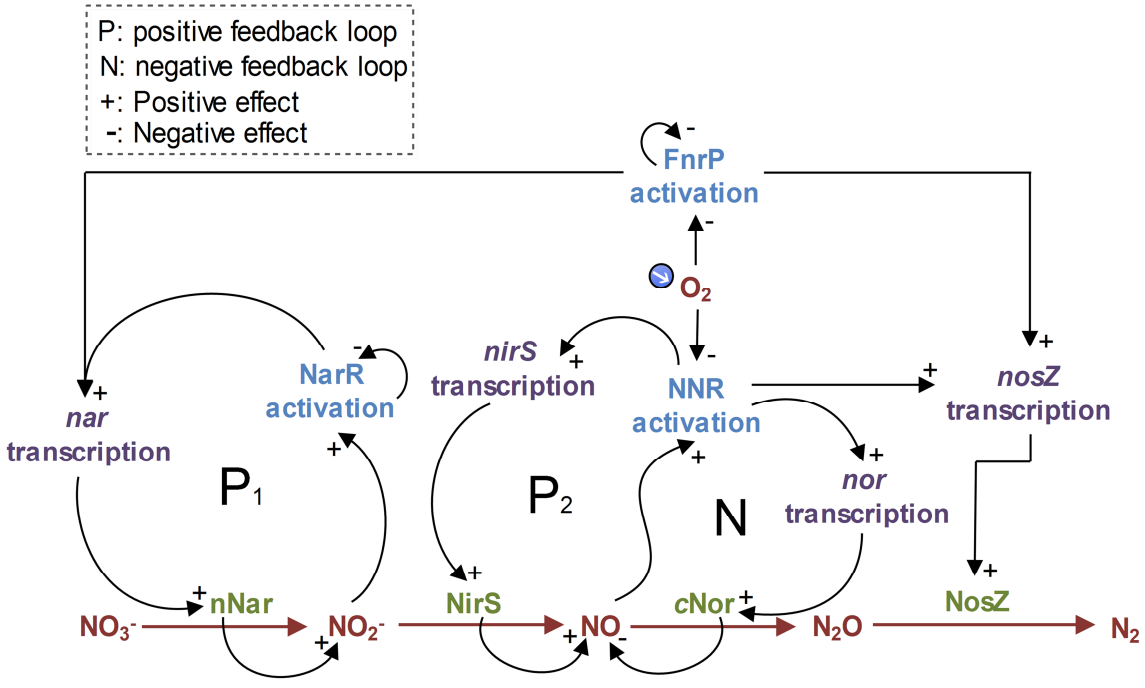


**Fig. 1. Regulatory network of denitrification in *Pa. denitrificans*.** The network is driven by four core enzyme-complexes: nNar (transmembrane nitrate reductase encoded by the *narG*

gene), NirS (cytochrome *cd*$_1$ nitrite reductase encoded by *nirS*), *c*Nor (NO reductase encoded by *norBC*), and NosZ ($N_2O$ reductase encoded by *nosZ*). When anoxia is imminent, the low [$O_2$] is sensed by FnrP, which in some interplay with NarR (a $NO_2^-$ sensor) induces *nar* transcription. NarR is activated by $NO_2^-$; thus once a cell starts producing traces of $NO_2^-$, *nar* expression becomes autocatalytic (see $P_1$). Transcription of *nirS* is induced by NNR (a NO sensor), activated under anoxic/micro-anoxic conditions by NO; thus once traces of NO are produced, the expression of *nirS* also becomes autocatalytic (see $P_2$) (20). The activated $P_2$ will also induce *nor* and *nosZ* transcription via NNR. The transcription of *nosZ*, however, can also be induced equally and independently by FnrP (24).

Our model was based on the hypothesis that the entrapment of a large fraction in anoxia is due to a low probability of initiating *nirS* transcription, which in response to $O_2$ depletion is possibly mediated through a minute pool of intact NNR, crosstalk with other factors (such as FnrP), unspecific reduction of $NO_2^-$ to NO by Nar, and/or through non-biologically formed traces of NO found in a $NO_2^-$-supplemented medium. Regardless of the exact mechanism(s), once *nirS* transcription is initiated, the positive feedback via NO/NNR (Fig. 1, see $P_2$) would allow the product of a single transcript of *nirS* to induce a subsequent burst of *nirS* transcription. The activated positive feedback will also help induce *nor* and *nosZ* transcription via NNR, rapidly transforming a cell into a full-fledged denitrifier. We further hypothesised that recruitment to denitrification will only be possible as long as a minimum of $O_2$ is available because, since *Pa. denitrificans* is non-fermentative, the synthesis of first molecules of NirS will depend on energy from aerobic respiration.

The above hypothesis was modelled by segregating the culture into two pools (subpopulations): one for the cells without ($N_{D-}$) and the other with denitrification enzymes ($N_{D+}$). Initially, all cells were $N_{D-}$, growing by consuming $O_2$. As [$O_2$] fell below a certain threshold, $N_{D-}$ recruited to $N_{D+}$ with a constant probability ($h^{-1}$), assumed to be that of the *nirS* transcriptional activation, and the recruitment halted as $O_2$ was completely exhausted, assuming lack of energy (ATP) for enzyme synthesis.

## Underlying assumptions and aims of the present modelling

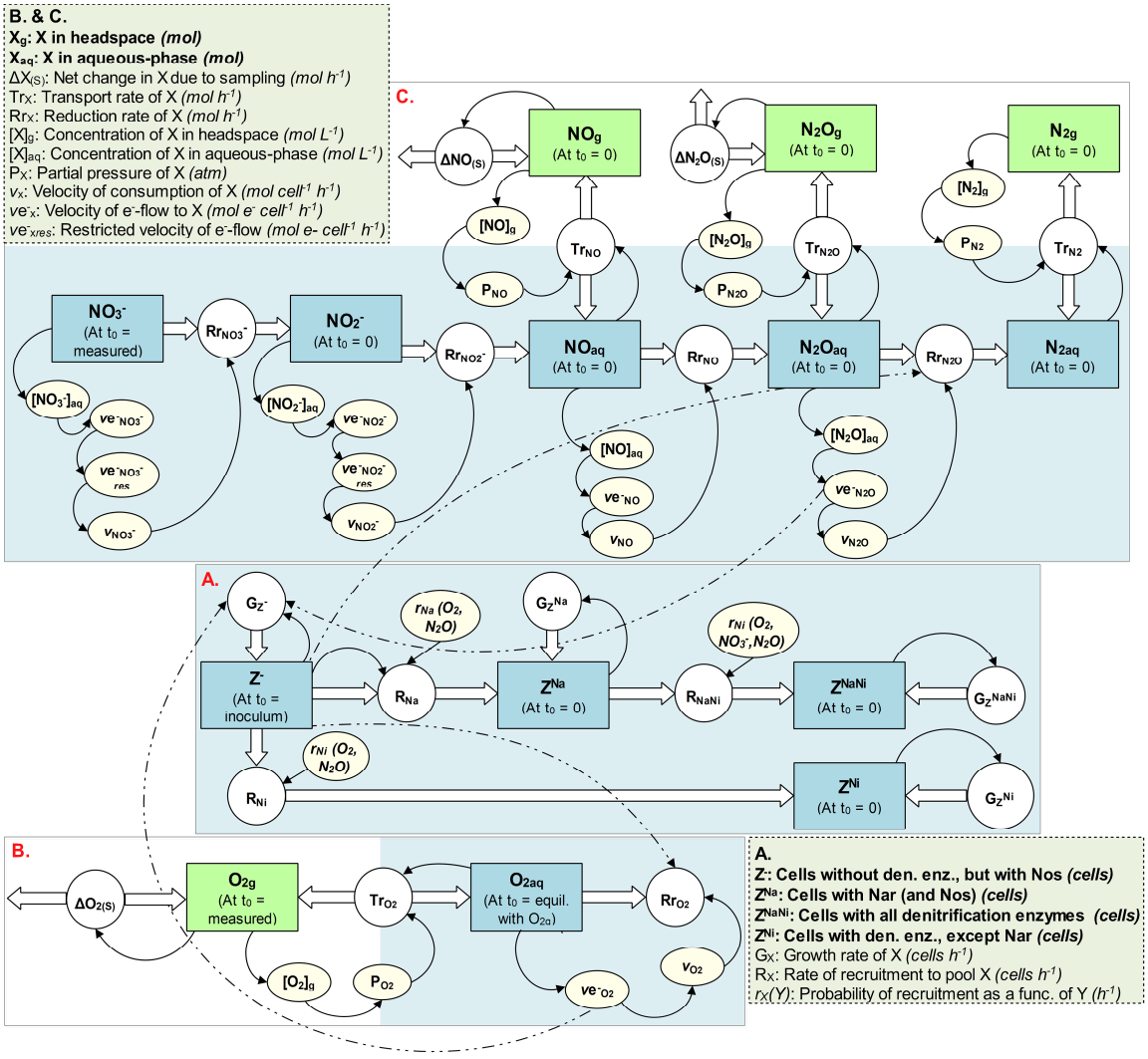


**Fig. 2. A stock and flow diagram illustrating the model's structure. A.** Cell diversification and growth; **B.** $O_2$ kinetics; **C.** Denitrification kinetics. The squares represent the state variables, the circles the rate of change in the state variables, the shaded ovals the auxiliary variables, the arrows dependencies between the variables, and the edges (thicker arrows) represent flows into or out of the state variables. All feedback relationships among the three model sectors could not be shown; however, for illustration the feedback relationships of one sub-population ($Z^-$) are shown (dashed arrows). Within each state variable, $t_0$ refers to its initial value.

The present model is an extension of that developed in Hassan *et al.* (16). Here we have divided the respiring culture into four pools (Fig. 2A):

1. $Z^-$ : cells without Nar, NirS, and *c*Nor
2. $Z^{Na}$: cells with Nar
3. $Z^{NaNi}$: cells with Nar, NirS, and *c*Nor
4. $Z^{Ni}$: cells with NirS and *c*Nor

All these subpopulations are assumed to scavenge $O_2$ (if present) and produce NosZ in response to impending anoxia. The latter because the *nosZ* genes are readily induced by the $O_2$-sensor FnrP (24).

The $Z^-$ pool (Fig. 2A) contains the inoculum that grows by aerobic respiration. As $[O_2]$ falls below a critical threshold (empirically determined, 18), the cells within $Z^-$ are assumed to start synthesising Nar with a certain probability and populate the $Z^{Na}$ pool. The aim is to investigate whether, like for *nirS*, the initiation of *nar* transcription (by some mutually dependent activity of FnrP and NarR) can also be explained as a probabilistic phenomenon, quickly differentiating a cell into a full-fledge $NO_3^-$ scavenger through product ($NO_2^-$) induced transcription via NarR (Fig. 1, see $P_1$). If so, we were interested to estimate what fraction of the cells is required to adequately simulate the measured data ($NO_2^-$ production), aiming at scrutinising the general assumption that all cells in such populations produce Nar in response to impending anoxia.

Next, when $[O_2]$ is further depleted to another critical threshold (18), the $Z^-$ and $Z^{Na}$ cells are assumed to initiate *nirS* transcription with a low per hour probability and, thereby, populate the $Z^{Ni}$ and $Z^{NaNi}$ pools, respectively. As explained above for our previous model, NirS + *c*Nor production is assumed to be *a)* coordinated because the transcription of both *nirS* and *nor* is induced by NO via the NO-sensor NNR (Fig. 1), and *b)* stochastic because the initial transcription of *nirS* (paving the way for the autocatalytic expression of NirS and substrate-induced *nor* transcription) happens in the absence of NO or at too low [NO] to be sensed by NNR.

Synthesis of denitrification enzymes requires energy, which all the subpopulations can obtain by respiration only. Hence, the initiation of the autocatalytic expression of *nar* and *nirS* (i.e., recruitment to $Z^{Na}$ and $Z^{NaNi}/Z^{Ni}$, respectively, Fig. 2A) depends on the availability of the relevant terminal $e^-$-acceptor(s) above a critical concentration to sustain a minimum of

respiration. For $Z^-$, the only relevant $e^-$-acceptors are $O_2$ and the traces of $N_2O$ produced by $Z^{Ni}$ and $Z^{NaNi}$. The same applies For $Z^{Na}$, but in addition, this subpopulation can also obtain energy by reducing $NO_3^-$, if present. In our previous model (16), we assumed that recruitment to denitrification was sustained by energy from $O_2$-respiration only, not $NO_3^-$ because we simulated $NO_2^-$-supplemented treatments and not by $N_2O$ because we naively assumed that the pool of this $e^-$-acceptor was insignificant ($N_2O$ concentrations were below the detection limit of the system used for those experiments). However, the present model assumes that the recruitment from $Z^-$ to $Z^{Na}$ and $Z^-$ to $Z^{Ni}$ is sustained by both $O_2$- and $N_2O$-reduction, and the recruitment from $Z^{Na}$ to $Z^{NaNi}$ is sustained by $O_2$-, $N_2O$- and $NO_3^-$-reduction, when above a critical minimum ($ve^-_{min}$). The default value for $ve^-_{min}$ was set to an arbitrary low value (= 0.44% of maximum $e^-$-flow rate to $O_2$), and we have investigated the consequences of increasing, decreasing, and setting $ve^-_{min}$ = 0.

The expressions of *nar* and *nirS* + *nor* (recruitments to $Z^{Na}$ and $Z^{NaNi}$/$Z^{Ni}$, respectively, Fig. 2A) are modelled as instantaneous discrete-events in each cell, thus ignoring the time-lag from the initiation of gene transcription till the cell is fully equipped with the reductase(s) in question. That is because the lag observed between the emergence of denitrification gene transcripts and the subsequent gas products suggests that the synthesis of denitrification enzymes takes less than half an hour (17, 18), which is negligible for the purposes of our modelling.

The main purpose of the present modelling is to investigate if a full-fledged model including all four functional denitrification reductases could adequately simulate the observed kinetics and stoichiometry of denitrification in a medium supplemented with $NO_3^-$. In particular, we were interested in the $NO_2^-$ kinetics as controlled by *nar*- and *nir* transcription and to test if the peculiar $N_2O$ kinetics (low, but increasing concentrations throughout the anoxic phase) could be explained by our modelled cell diversification.

# Materials and Methods

## An overview of the modelled experiment

**Batch incubation.** Qu *et al.* (18) incubated *Pa. denitrificans* (DSM-413) at 20 °C, using 50 mL Sistrom's (28) medium in 120 mL gas-tight vials. Either succinate or butyrate (5 mM) was used as the main carbon source, enough to secure consumption of all available $e^-$-acceptors. After distribution of the medium, each vial was loaded with a magnetic stirring bar, sterilised through autoclaving, supplemented with 2 mM $KNO_3$, and tightly sealed. To remove $O_2$ and $N_2$ from the headspace, the headspace air was evacuated and replaced by helium (He) through cycles of evacuation and He-filling (He-washing). Some vials were supplemented with oxygen to reach 7 vol.% $O_2$ in headspace (treatment designated 7% $O_2$). The remaining vials received no $O_2$ (designated 0% $O_2$, although there were traces of $O_2$ present, despite the He washing). For each treatment (i.e., C source and initial $O_2$), there were three replicates, and each vial was inoculated with $2.2\times10^8$ aerobically grown cells.

**$NO_2^-$ and gas measurement.** Gases ($CO_2$, $O_2$, NO, $N_2O$, and $N_2$) were monitored by frequent sampling of the headspace, using an improved version of the robotised incubation system described by Molstad *et al*. (29). In short, the system draws gas samples from the headspace (peristaltic pumping) via the septum (pierced by a needle), filling three loops that are used to inject samples to the two GC columns and the chemiluminescence analyser for the determination of NO. The sample drawn is replaced by He (reversing the peristaltic pump), thus securing ~1 atm pressure. The primary improvements of the new system are a more sensitive detection of $N_2O$ (by an electron capture detector), lower sampling volumes (~1 mL), and lower leaks of $O_2$ and $N_2$ through the sampling system (4 nmol $O_2$ and 12 nmol $N_2$ per sampling, which is ~20% of that for the old system).

To extract samples for measuring $NO_2^-$ without tampering the original vials, identical (parallel) vials were prepared for each treatment. Using sterile syringes, samples of 0.1 mL were regularly drawn from the liquid-phase of the parallel vials and immediately analysed for $NO_2^-$.

**The model**

The model is constructed in Vensim DSS 6.2 Double Precision (Ventana Systems, inc. http://vensim.com/) using techniques from the field of system dynamics (30).

**Cell diversification and growth.** The respiring population is divided into four subpopulations, according to their reductases (Fig. 2A): 1) $Z^-$: cells without Nar, NirS, and *c*Nor; 2) $Z^{Na}$: cells with Nar; 3) $Z^{NaNi}$: cells with Nar, NirS, and *c*Nor; and 4) $Z^{Ni}$: cells with NirS and *c*Nor. All the subpopulations are assumed to equally respire $O_2$, if present, and express *nosZ* in response to oxygen depletion (24). $Z^-$ contains the inoculum (= $2.2\times10^8$ cells) that grows by aerobic respiration. As $O_2$ is depleted, the $Z^-$ cells populate the other pools by producing Nar and/or NirS + *c*Nor.

The recruitment from $Z^-$ to $Z^{Na}$ ($R_{Na}$, Fig. 2A) takes place first:

$$R_{Na} = Z^- \times r_{Na}(O_2, N_2O) \quad (1)$$

(cells $h^{-1}$)

where $r_{Na}(O_2, N_2O)$ is a conditional specific probability ($h^{-1}$) for any $Z^-$ cell to initiate *nar* transcription (quickly transforming a cell into a $NO_3^-$ scavenger through autocatalytic gene expression, see Fig. 1, $P_1$):

$$r_{Na}(O_2, N_2O) = \begin{cases} \textbf{IF} & [O_2]_{aq} < [O_2]_{na} \textbf{ AND } \left(ve^-_{O_2} + 0.5 \times ve^-_{N_2O}\right) > ve^-_{min} \\ \textbf{THEN} & r_{Na} \\ \textbf{ELSE} & 0 \end{cases} \quad (2)$$

($h^{-1}$)

where $r_{Na}$ ($h^{-1}$) is a constant specific probability for a cell to initiate *nar* transcription once $O_2$ concentration in the aqueous-phase ($[O_2]_{aq}$, mol $L^{-1}$) falls below a critical concentration ($[O_2]_{na}$), empirically determined as the $[O_2]_{aq}$ (= $4.75\times10^{-5}$ mol $L^{-1}$) at the outset of $NO_2^-$ accumulation in the medium (18). The second condition for a cell to produce first molecules

of Nar is a minimum of $e^-$-flow to an $e^-$-acceptor ( $ve^-_{min}$ , mol $e^-$ $cell^{-1}$ $h^{-1}$), assumed to generate minimum ATP required for protein synthesis. $ve^-_{O_2}$ and $ve^-_{N_2O}$ (mol $e^-$ $cell^{-1}$ $h^{-1}$) are the cell-specific velocities of $e^-$-flow to $O_2$ and $N_2O$, respectively. The latter is weighed down by 0.5 because mole ATP per mole $e^-$ transferred to $NO_x^-$/$NO_x$ is lower for denitrification than for aerobic respiration (17, 20). For a $Z^-$ cell, $ve^-_{NO_2^-}$ and $ve^-_{NO}$ are not considered here, since such a cell is assumed to have no NirS and *c*Nor.

The fraction of the cells that successfully produces Nar ($F_{Na}$) is calculated based on the integral of the recruitment (Eq. 1):

$$F_{Na} = 1 - e^{-r_{Na} \times t_{Na}} \quad (3)$$

(dimensionless)

where $t_{Na}$ is the time-window available for the recruitment. In theory, $t_{Na}$ is the time-period when $[O_2]_{aq} < [O_2]_{na}$ **AND** $(ve^-_{O_2} + 0.5 \times ve^-_{N_2O}) > ve^-_{min}$ (Eq. 2), thus including the recruitment to $Z^{Na}$ after the depletion of $NO_3^-$ (the recruitment based on $ve^-_{N_2O}$ starts after $NO_3^-$ is depleted). However, the recruitment after the $NO_3^-$ depletion would be inconsequential for the simulated (and measured) $NO_2^-$ kinetics. To calculate the functional $F_{Na}$ actually responsible for producing $NO_2^-$, we ignored the $N_2O$-sustained recruitment, thus considering $t_{Na}$ as the time when $[O_2]_{aq} < [O_2]_{na}$ **AND** $ve^-_{O_2} > ve^-_{min}$.

Next, the cells within $Z^{Na}$ and $Z^-$ are recruited to $Z^{NaNi}$ and $Z^{Ni}$ ($R_{NaNi}$ and $R_{Ni}$, respectively, Fig. 2A), as they are assumed to stochastically initiate *nirS* transcription, paving the way for NO/NNR mediated autocatalytic expression of *nirS* + *nor* (Fig. 1). In principle, the rates of both these recruitments are modelled as that of the recruitment from $Z^-$ to $Z^{Na}$ (Eqs. 1–2): *a)* Both trigger as $O_2$ falls below another critical concentration ($[O_2]_{ni}$), low enough to activate NNR to induce *nirS* transcription; $[O_2]_{ni}$ (= $1.16 \times 10^{-5}$ mol $L^{-1}$) is empirically determined as the $O_2$ concentration at the outset of NO accumulation (18). *b)* Both continue as long as a minimum

of $e^-$-flow to the relevant terminal $e^-$-acceptor is possible, sustaining the respiratory metabolism to generate ATP for protein synthesis:

$$R_{NaNi} = Z^{Na} \times r_{Ni}(O_2, NO_3^-, N_2O) \quad (4)$$

(cells $h^{-1}$)

$$r_{Ni}(O_2, NO_3^-, N_2O) =$$
$$\textbf{IF} \quad [O_2]_{aq} < [O_2]_{ni} \ \textbf{AND} \left( ve^-_{O_2} + 0.5 \times ve^-_{NO_3^-} + 0.5 \times ve^-_{N_2O} \right) > ve^-_{min} \quad (5)$$
$$\textbf{THEN} \quad r_{Ni}$$
$$\textbf{ELSE} \quad 0$$

($h^{-1}$)

where $ve^-_{NO_3^-}$ and $ve^-_{N_2O}$ are multiplied with 0.5 as in Eq. 2, and $r_{Ni}$ is a constant specific probability ($h^{-1}$) for the initiation of *nirS* transcription.

The recruitment from $Z^-$ to $Z^{Ni}$ ($R_{Ni}$, Fig. 2A) is modelled as a product of $Z^-$ and a conditional specific probability, $r_{Ni}(O_2, N_2O)$, which is different from Eq. 5 only in that $ve^-_{NO_3^-}$ is omitted, since $Z^-$ do not possess Nar:

$$R_{Ni} = Z^- \times r_{Ni}(O_2, N_2O) \quad (6)$$

(cells $h^{-1}$)

$$r_{Ni}(O_2, N_2O) =$$
$$\textbf{IF} \quad [O_2]_{aq} < [O_2]_{ni} \ \textbf{AND} \left( ve^-_{O_2} + 0.5 \times ve^-_{N_2O} \right) > ve^-_{min} \quad (7)$$
$$\textbf{THEN} \quad r_{Ni}$$
$$\textbf{ELSE} \quad 0$$

($h^{-1}$)

The fraction that successfully produced NirS + *c*Nor ($F_{Ni}$) is calculated based on the integral of $R_{NaNi}$ and $R_{Ni}$:

$$F_{Ni} = \left(1 - e^{-r_{Ni} \times t_{NaNi}}\right) \times F_{Na} + \left(1 - e^{-r_{Ni} \times t_{Ni}}\right) \times \left(1 - F_{Na}\right) \quad (8)$$

(dimensionless)

where $t_{NaNi}$ is the duration of the recruitment from $Z^{Na}$ to $Z^{NaNi}$, i.e., when $[O_2]_{aq} < [O_2]_{ni}$ **AND** $(ve^-_{O_2} + 0.5 \times ve^-_{NO_3^-} + 0.5 \times ve^-_{N_2O}) > ve^-_{min}$ (Eqs. 4–5), $F_{Na}$ is the fraction recruited to the pool of Nar positive cells ($Z^{Na}$, Eq. 3), and $t_{Ni}$ is the duration of the recruitment from $Z^-$ to $Z^{Ni}$, i.e., when $[O_2]_{aq} < [O_2]_{ni}$ **AND** $(ve^-_{O_2} + 0.5 \times ve^-_{N_2O}) > ve^-_{min}$ (Eqs. 6–7).

Each of the populations will grow depending on the rates of $e^-$-flow to the various $e^-$-acceptors they are able to use:

$$G_{Z^-} = Z^- \times \left( Ye^-_{O_2} \times ve^-_{O_2} + Ye^-_{NO_x} \times ve^-_{N_2O} \right) \quad (9)$$

$$G_{Z^{Na}} = Z^{Na} \times \left[ Ye^-_{O_2} \times ve^-_{O_2} + Ye^-_{NO_x} \left( ve^-_{NO_3^- res} + ve^-_{N_2O} \right) \right] \quad (10)$$

$$G_{Z^{NaNi}} = Z^{NaNi} \times \left[ Ye^-_{O_2} \times ve^-_{O_2} + Ye^-_{NO_x} \left( ve^-_{NO_3^- res} + ve^-_{NO_2^- res} + ve^-_{NO} + ve^-_{N_2O} \right) \right] \quad (11)$$

$$G_{Z^{Ni}} = Z^{Ni} \times \left[ Ye^-_{O_2} \times ve^-_{O_2} + Ye^-_{NO_x} \left( ve^-_{NO_2^- res} + ve^-_{NO} + ve^-_{N_2O} \right) \right] \quad (12)$$

(cells $h^{-1}$)

where $Ye^-_X$ (cells $mol^{-1}$ $e^-$ to X = $O_2$ or $NO_x^-/NO_x$) is the growth yield determined under the actual experimental conditions, and $ve^-_X$ (mol $e^-$ $cell^{-1}$ $h^{-1}$) is the cell-specific velocity of $e^-$-flow to X ($O_2$ or $NO_x^-/NO_x$), which depends on the concentration of the $e^-$-acceptor (see Eqs. 17, 20, and 28). For $NO_3^-$ and $NO_2^-$, a restricted velocity ($ve^-_{NO_X^- res}$) is used so that when electrons flow to $O_2$, $NO_3^-$, and $NO_2^-$ simultaneously, the total $ve^-$ per cell does not exceed the maximum electrons that the TCA cycle ($ve^-_{max\,TCA}$) can deliver per hour (see Eqs. 21–22).

**$O_2$ kinetics.** $O_2$ is initially present in the headspace ($O_{2g}$, mol, initialised according to the experiment, see Table 1) but is transported to the liquid-phase ($O_{2aq}$) due to its consumption therein (Fig. 2B). The transport rate ($Tr_{O_2}$) is modelled according to Molstad *et al.* (29):

$$Tr_{O_2} = k_t \left( k_{H(O_2)} \times P_{O_2} - [O_2]_{LP} \right) \quad (13)$$

(mol $h^{-1}$)

where $k_t$ (L $h^{-1}$) is the empirically determined coefficient for the transport of gas between the headspace and the liquid, $k_{H(O_2)}$ (mol $L^{-1}$ $atm^{-1}$) is the solubility of $O_2$ in water at 20 °C, $P_{O_2}$ ($=[O_2]_g \times R \times T$, atm) is the partial pressure of $O_2$ in the headspace, and $[O_2]_{aq}$ (mol $L^{-1}$) is the $O_2$ concentration in the liquid ($[O_2]_{aq} = \frac{O_{2aq}}{Vol_{aq}}$).

**Table 1. Simulated experiment (18).**

| Batch | C-source | $O_{2_g}(t_o)$ (vol.%)* | $NO_3^-(t_o)$ (mM) | Replicates |
|---|---|---|---|---|
| 1 | Butyrate | ~0 | 2 | 3 |
| 2 | Butyrate | 7 | 2 | 3 |
| 3 | Succinate | ~0 | 2 | 3 |
| 4 | Succinate | 7 | 2 | 3 |

* Target values for initial $O_2$ concentrations in the headspace (vol.%). ~0 means that the intended concentration should be zero, but there were detectable traces of $O_2$, despite several cycles of evacuation and He-flushing of the headspace.

In addition, the model simulates the changes in $O_{2g}$ due to sampling. The robotised incubation system used monitors gas concentrations by sampling the headspace, where each sampling alters the concentrations in a predictable manner: a fraction of $O_{2g}$ is removed and replaced by He (dilution), but the sampling also results in a marginal leakage of $O_2$ through the tubing and membranes in the injection system. The net change in $O_{2g}$ ($\Delta O_{2(S)}$) as a result of each sampling is calculated as:

$$\Delta O_{2(S)} = \frac{O_{2leak} - O_{2g} \times D}{t_s} \quad (14)$$

(mol $h^{-1}$)

where $O_{2leak}$ (mol vial$^{-1}$) is the $O_2$ leakage into the headspace, D (dilution) is the fraction of each headspace gas replaced by He, and $t_s$ (h) is the time taken to complete each sampling. $\Delta O_{2(S)}$ is negative if $O_{2g}$ is high and marginally positive at very low oxygen concentrations.

$O_2$ in the liquid-phase ($O_{2aq}$, mol, Fig. 2B) is initialised by assuming equilibrium with $O_{2g}$ at the time of inoculation ($O_{2aq}(t_0) = P_{O_2} \times k_{H(O_2)} \times Vol_{aq}$). The dynamics of $O_{2aq}$ are modelled as a function of transport between the headspace and the liquid ($Tr_{O_2}$, Eq. 13) and its reduction rate ($Rr_{O_2}$, mol h$^{-1}$):

$$\frac{d(O_{2aq})}{dt} = Tr_{O_2} - Rr_{O_2} \tag{15}$$

$$Rr_{O_2} = \left(Z^{-} + Z^{Na} + Z^{NaNi} + Z^{Ni}\right) \times v_{O_2} \tag{16}$$

(mol h$^{-1}$)

where $Z^{-}$, $Z^{Na}$, $Z^{NaNi}$, and $Z^{Ni}$ (cells) are all the sub-populations present (described above); thus, we assume that all cells have the same potential to consume $O_2$. $v_{O_2}$ (mol cell$^{-1}$ h$^{-1}$) is the cell-specific velocity of $O_2$ consumption, obtained by the velocity of e$^-$-flow to $O_2$ $\left(ve^-_{O_2}, \frac{1\ mol O_2}{4\ mol e^-}\right)$, where $ve^-_{O_2}$ is modelled as a Michaelis-Menten function of oxygen concentration:

$$ve^-_{O_2} = \frac{ve^-_{max O_2} \times [O_2]_{aq}}{K_{mO_2} + [O_2]_{aq}} \tag{17}$$

(mol e$^-$ cell$^{-1}$ h$^{-1}$)

where $ve^-_{max O_2}$ (mol e$^-$ cell$^{-1}$ h$^{-1}$) is the maximum velocity of e$^-$-flow to $O_2$ per cell (determined under the actual experimental conditions), $[O_2]_{aq}$ (mol L$^{-1}$) is the $O_2$ concentration in the liquid-phase, and $K_{mO_2}$ (mol L$^{-1}$) is the half-saturation constant for $O_2$ reduction.

**Denitrification kinetics.** The pool of $NO_3^-$ (mol, Fig. 2C) is initialised according to the experiment (Table 1) and that of $NO_2^-$ = 0. The kinetics of these nitrogen oxyanions ($NO_x^-$) are modelled as:

$$\frac{d(NO_3^-)}{dt} = -Rr_{NO_3^-} = -\left(Z^{Na} + Z^{NaNi}\right) \times v_{NO_3^-} \quad (18)$$

$$\frac{d(NO_2^-)}{dt} = Rr_{NO_3^-} - Rr_{NO_2^-} = Rr_{NO_3^-} - \left(Z^{NaNi} + Z^{Ni}\right) \times v_{NO_2^-} \quad (19)$$

(mol $h^{-1}$)

where $Rr_{NO_x^-}$ (mol $h^{-1}$) is the reduction rate, $Z^{Na} + Z^{NaNi}$ (cells) is the total number of cells with Nar, $Z^{NaNi} + Z^{Ni}$ (cells) is the total NirS active population, and $v_{NO_x^-}$ (mol $cell^{-1}$ $h^{-1}$) is the cell-specific velocity of $NO_x^-$ consumption, obtained by the velocity of $e^-$-flow to $NO_x^-$ $\left(\frac{1 \text{ mol } NO_3^-}{2 \text{ mol } e^-} \text{ \& } \frac{1 \text{ mol } NO_2^-}{1 \text{ mol } e^-}\right)$. The latter is modelled as a Michaelis-Menten function of $NO_x^-$ concentration:

$$ve^-_{NO_x^-} = \frac{ve^-_{max NO_x^-} \times [NO_x^-]_{aq}}{K_{mNO_x^-} + [NO_x^-]_{aq}} \quad (20)$$

(mol $e^-$ $cell^{-1}$ $h^{-1}$)

where $ve^-_{max NO_x^-}$ (mol $e^-$ $cell^{-1}$ $h^{-1}$) is the maximum velocity of $e^-$-flow to $NO_x^-$ per cell (determined under the actual experimental conditions), $[NO_x^-]_{aq}$ (mol $L^{-1}$) is the $NO_x^-$ concentration in the aqueous-phase, and $K_{mNO_x^-}$ (mol $L^{-1}$) is the half-saturation constant for $NO_x^-$ reduction.

The velocity of $NO_3^-$ and $NO_2^-$ consumption had to be restricted ($ve^-_{NO_x^- res}$) to ensure that when electrons flow to $O_2$, $NO_3^-$, and $NO_2^-$ simultaneously, the total $ve^-$ per cell does not exceed

an estimated maximum delivery of electrons from the TCA cycle ($ve^-_{maxTCA}$). In competition for electrons, $O_2$ is prioritised (20), followed by $NO_3^-$ and $NO_2^-$, respectively (18):

$$ve^-_{NO_3^-res} = \text{Min}\left(ve^-_{NO_3^-}, \left(ve^-_{maxTCA} - ve^-_{O_2}\right)\right) \quad (21)$$

$$ve^-_{NO_2^-res} = \text{Min}\left(ve^-_{NO_2^-}, \left(ve^-_{maxTCA} - ve^-_{O_2} - ve^-_{NO_3^-res}\right)\right) \quad (22)$$

(mol $e^-$ $cell^{-1}$ $h^{-1}$)

where $ve^-_{NO_3^-res}$ is the realised $e^-$-flow to $NO_3^-$, limited either by available $NO_3^-$ or the availability of electrons (due to competition with $O_2$); $ve^-_{NO_2^-res}$ is the realised $e^-$-flow to $NO_2^-$. Such competition for electrons was not implemented for $ve^-_{NO}$ and $ve^-_{N_2O}$ because at the onset of NO- and $N_2O$ production (hence reduction), the total velocity of $e^-$-flow to all available $e^-$-acceptors (as predicted by the enzyme kinetics alone) never exceeded $ve^-_{maxTCA}$.

Gas consumption and production takes place in the aqueous phase, but the gases are transported between the aqua and the headspace depending on their concentrations in the two phases. Each gas in the aqua, $X_{aq}$ (molN, Fig. 2C), is modelled as a function of production, consumption (not applicable to $N_2$), and the net transport, where $N_2O_{aq}$ and $N_{2aq}$ are initialised with zero, and $NO_{aq}$ is initialised with a negligible $1\times10^{-25}$ mol to avoid division by zero (in Eq. 28).

$$\frac{d(NO_{aq})}{dt} = Rr_{NO_2^-} - Rr_{NO} + Tr_{NO} \quad (23)$$

$$\frac{d(N_2O_{aq})}{dt} = Rr_{NO} - Rr_{N_2O} + Tr_{N_2O} \quad (24)$$

$$\frac{d(N_{2aq})}{dt} = Rr_{N_2O} + Tr_{N_2} \quad (25)$$

(molN $h^{-1}$)

where $Rr_{NO_X}$ (molN $h^{-1}$) is the relevant $NO_x^-/NO_x$ reduction rate, and $Tr_{N_X}$ represents the gas transport rate between the aqua and the headspace (Eq. 29; NB: $Tr_{N_X} < 0$ for the net transport from aqua to the headspace).

The reduction of NO to $N_2O$ ($Rr_{NO}$) and $N_2O$ to $N_2$ ($Rr_{N_2O}$) is modelled likewise as a function of the number of relevant cells and the velocity of $e^-$-flow to NO and $N_2O$ (mol $e^-$ $cell^{-1}$ $h^{-1}$), respectively:

$$Rr_{NO} = \left(Z^{NaNi} + Z^{Ni}\right) \times v_{NO} \quad (26)$$

$$Rr_{N_2O} = \left(Z^{-} + Z^{Na} + Z^{NaNi} + Z^{Ni}\right) \times v_{N_2O} \quad (27)$$

(molN $h^{-1}$)

where $v_{NO}$ and $v_{N_2O}$ are obtained by the velocity of $e^-$-flow to NO and $N_2O$, respectively $\left(1\frac{\text{molN}}{\text{mol e}^-}\right)$. $ve^-_{N_2O}$ is modelled as a Michaelis-Menten function of $[N_2O]$, similarly as that of $O_2$, $NO_3^-$, and $NO_2^-$ (Eqs. 17 and 20), but $ve^-_{NO}$ is modelled assuming a cooperative binding of two NO molecules with *c*Nor to form $N_2O$ (31):

$$ve^-_{NO} = \frac{ve^-_{maxNO}}{1 + K_{2NO}\left(\frac{1}{[NO]_{aq}} + \frac{K_{1NO}}{\left([NO]_{aq}\right)^2}\right)} \quad (28)$$

(mol $cell^{-1}$ $h^{-1}$)

where $ve^-_{maxNO}$ (mol $e^-$ $cell^{-1}$ $h^{-1}$) is the empirically determined maximum velocity of $e^-$-flow to NO per cell, $[NO]_{aq}$ (mol $L^{-1}$) is the NO concentration in the liquid-phase, and $K_{1NO}$ & $K_{2NO}$ (mol $L^{-1}$) are the equilibrium dissociation constants for the *c*Nor/NO- and *c*Nor/$(NO)^2$ complex, respectively.

The transport of $NO_{aq}$, $N_2O_{aq}$, and $N_{2\,aq}$ between the liquid and the headspace (Eqs. 23–25) is modelled as:

$$Tr_N = k_t \times \left( k_{H(N)} \times P_N - [N]_{aq} \right) \quad (29)$$

(molN $h^{-1}$)

where $k_t$ is the empirically determined coefficient for the transport of each gas between the headspace and the liquid, $k_{H(N)}$ (molN $L^{-1}$ $atm^{-1}$) is the solubility of NO, $N_2O$, or $N_2$ in water at 20 °C, $P_N$ ($=[N]_g \times R \times T$, atm) is the partial pressure of each gas in the headspace, and $[N]_{aq}$ (mol $L^{-1}$) represents the concentration of each gas in the liquid-phase.

The amount of NO and $N_2O$ in the headspace ($NO_{x_g}$, molN, Fig. 2C) is a function of transport (Eq. 29) and the disturbance by gas sampling, simulated as discrete events at time-points given as input to the model (equivalent to the sampling times in the experiment):

$$\Delta NO_{x(S)} = \frac{NO_{x_g} \times D}{t_s} \quad (30)$$

(molN $h^{-1}$)

where $\Delta NO_{x(S)}$ is the net change in the amount of $NO_{x_g}$ (molN), D (dilution) is the fraction of each gas replaced by He, and $t_s$ (h) is the time taken to complete each sampling. For $N_2$, the model ignores the sampling loss because the experimental data on $N_2$ production to be compared with the model output are corrected for the sampling disturbance (29). Thus, the model estimates somewhat higher $N_2$ concentrations than that experienced by the organisms, which is acceptable, since the concentration of $N_2$ is unlikely to have consequences for the metabolism.

## Parameterisation

Most of the parameter values used in the model are well established in the literature (see Table 2); however, uncertain parameters include $K_{mO_2}$, $K_{mN_2O}$, $ve^-_{maxO_2}$, and $ve^-_{min}$.

**Table 2. Model parameters.**

| | Description | Value | Units | Reference |
|---|---|---|---|---|
| **Butyrate treatments** | | | | |
| $ve^-_{max\mathrm{TCA}}$ | Max. cell-specific rate of $e^-$-flow from the TCA cycle | $1\times10^{14}$ | mol $e^-$ cell$^{-1}$ h$^{-1}$ | (18) |
| $ve^-_{max\mathrm{O_2}}$ | The maximum cell-specific velocity of $e^-$-flow to $O_2$ | $4.22\times10^{-15}$ | mol $e^-$ cell$^{-1}$ h$^{-1}$ | Optimisation |
| $ve^-_{max\mathrm{NO_3^-}}$ | The maximum cell-specific velocity of $e^-$-flow to $NO_3^-$ | $1\times10^{-14}$ | mol $e^-$ cell$^{-1}$ h$^{-1}$ | (18) |
| $ve^-_{max\mathrm{NO_2^-}}$ | The maximum cell-specific velocity of $e^-$-flow to $NO_2^-$ | $2.65\times10^{-15}$ | mol $e^-$ cell$^{-1}$ h$^{-1}$ | (18) |
| $ve^-_{min}$ | The min. velocity of $e^-$-flow to $O_2/NO_x^-/NO_x$ required for protein synthesis (ATP) | $1.87\times10^{-17}$ | mol $e^-$ cell$^{-1}$ h$^{-1}$ | Assumption |
| $Ye^-_{O_2}$ | The growth yield per mole of electrons transferred to $O_2$ | $2.74\times10^{13}$ | cells (mol $e^-$)$^{-1}$ | (18) |
| $Ye^-_{NO_x}$ | The growth yield per mole $e^-$ to $NO_3^-$, $NO_2^-$, NO, or $N_2O$ | $1.12\times10^{13}$ | cells (mol $e^-$)$^{-1}$ | (18) |
| **Succinate treatments** | | | | |
| $ve^-_{max\mathrm{TCA}}$ | Max. cell-specific rate of $e^-$-flow from the TCA cycle | $9.34\times10^{-15}$ | mol $e^-$ cell$^{-1}$ h$^{-1}$ | (18) |
| $ve^-_{max\mathrm{O_2}}$ | The maximum cell-specific velocity of $e^-$-flow to $O_2$ | $4.42\times10^{-15}$ | mol $e^-$ cell$^{-1}$ h$^{-1}$ | (18) |
| $ve^-_{max\mathrm{NO_3^-}}$ | The maximum cell-specific velocity of $e^-$-flow to $NO_3^-$ | $9.34\times10^{-15}$ | mol $e^-$ cell$^{-1}$ h$^{-1}$ | (18) |
| $ve^-_{max\mathrm{NO_2^-}}$ | The maximum cell-specific velocity of $e^-$-flow to $NO_2^-$ | $2.01\times10^{-15}$ | mol $e^-$ cell$^{-1}$ h$^{-1}$ | (18) |
| $ve^-_{min}$ | The minimum velocity of $e^-$-flow to $O_2/NO_x^-/NO_x$ required for protein synthesis (ATP) | $1.95\times10^{-17}$ | mol $e^-$ cell$^{-1}$ h$^{-1}$ | Assumption |
| $Ye^-_{O_2}$ | The growth yield per mole of electrons transferred to $O_2$ | $4.97\times10^{13}$ | cells (mol $e^-$)$^{-1}$ | (18) |
| $Ye^-_{NO_x}$ | The growth yield per mole $e^-$ to $NO_3^-$, $NO_2^-$, NO, or $N_2O$ | $1.52\times10^{13}$ | cells (mol $e^-$)$^{-1}$ | (18) |
| **Parameters common for both succinate and butyrate treatments** | | | | |
| $[O_2]_{na}$ | The $[O_2]$ in aqua below which Nar production triggers | $5.95\times10^{-5}$ | mol L$^{-1}$ | (18) |
| $[O_2]_{ni}$ | The $[O_2]$ in aqua below which NirS production triggers | $9.75\times10^{-6}$ | mol L$^{-1}$ | (18) |
| $r_{Na}$ | The specific-probability of producing Nar | 0.035 | h$^{-1}$ | Optimisation |
| $r_{Ni}$ | The specific-probability of producing NirS | 0.004 | h$^{-1}$ | Optimisation |
| $ve^-_{max\mathrm{NO}}$ | The maximum cell-specific velocity of $e^-$-flow to NO | $3.56\times10^{-15}$ | mol $e^-$ cell$^{-1}$ h$^{-1}$ | (32) |
| $ve^-_{max\mathrm{N_2O}}$ | The maximum cell-specific velocity of $e^-$-flow to $N_2O$ | $5.5\times10^{-15}$ | mol $e^-$ cell$^{-1}$ h$^{-1}$ | (24) |
| $K_{m\mathrm{O_2}}$ | The half-saturation constant for $O_2$ reduction | $2.25\times10^{-7}$ | mol L$^{-1}$ | Optimisation |
| $K_{m\mathrm{NO_3^-}}$ | The half-saturation constant for $NO_3^-$ reduction | $5\times10^{-6}$ | mol L$^{-1}$ | (33, 34) |
| $K_{m\mathrm{NO_2^-}}$ | The half-saturation constant for $NO_2^-$ reduction | $4.13\times10^{-6}$ | mol L$^{-1}$ | (35, 36) |
| $K_{1\mathrm{NO}}$ | The equilibrium dissociation constant for *c*Nor/NO complex | $8\times10^{-14}$ | mol L$^{-1}$ | (32) |

| | | | | |
|---|---|---|---|---|
| $K_{2NO}$ | The equilibrium dissociation constant for *c*Nor/$(NO)_2$ complex | $34\times10^{-9}$ | mol $L^{-1}$ | (32) |
| $K_{mN_2O}$ | The half-saturation constant for $N_2O$ reduction | $5.93\times10^{-7}$ | mol $N_2O$-N $L^{-1}$ | Optimisation |
| D | Dilution (due to sampling): fraction of $O_2$ replaced by He | 0.015 | – | (18) |
| $k_{H(O_2)}$ | Solubility of $O_2$ in water at 20 °C | 0.001 | mol $L^{-1}$ $atm^{-1}$ | (37) |
| $k_{H(NO)}$ | Solubility of NO at 20 °C | 0.0021 | mol $L^{-1}$ $atm^{-1}$ | (29) |
| $k_{H(N_2O)}$ | Solubility of $N_2O$ at 20 °C | 0.056 | mol $N_2O$-N $L^{-1}$ $atm^{-1}$ | (37) |
| $k_{H(N_2)}$ | Solubility of $N_2$ at 20 °C | 0.0007 | mol $N_2$-N $L^{-1}$ $atm^{-1}$ | (37) |
| $k_t$ | The coeff. for gas transport between headspace and liquid | 3.6 | L $vial^{-1}$ $h^{-1}$ | Measured |
| $O_{2leak}$ | $O_2$ leakage into the vial during each sampling | $2.92\times10^{-9}$ | mol | Measured |
| R | Universal gas constant | 0.083 | L atm $K^{-1}$ $mol^{-1}$ | – |
| T | Temperature | 293.15 | K | (18) |
| $t_s$ | The time taken to complete each sampling | 0.017 | h | (29) |
| $Vol_g$ | Headspace volume | 0.07 | L | (18) |
| $Vol_{aq}$ | Aqueous-phase volume | 0.05 | L | (18) |

**$K_{mO_2}$** (Eq. 17)**.** *Pa. denitrificans* has three haem-copper terminal oxidoreductases (38) with $K_{mO_2}$ ranging from nM to µM (39, 40), so we decided to estimate the parameter value by optimising $K_{mO_2}$ for the low [$O_2$] treatments data. Vensim was used for the optimisation, where $K_{mO_2}$ = $2.25\times10^{-7}$ neatly simulated the $O_2$ depletion for both the succinate- and butyrate-supplemented treatments.

**$K_{mN_2O}$.** *In vitro* studies of NosZ from *Pa. denitrificans* estimate the values for $K_{mN_2O}$ = 5 µM at 22 °C and pH 7.1 (41) and 6.7 µM at 25 °C and pH 7.1 (42). When our model was simulated with $K_{mN_2O}$ in this range, given our empirically estimated $ve^-_{maxN_2O}$ (24), the simulated $N_2O$ reached concentrations much higher than that measured (see Results/Discussion). A more adequate parameter value (= 0.6 µM) was found by optimising $K_{mN_2O}$ in Vensim. The value is within the range determined for soil bacterial communities (43).

$ve^-_{maxO_2}$ (Eq. 17) could be estimated using the empirically determined cell yield per mole of electrons to $O_2$ ($Ye^-_{O_2}$, cells per mol $e^-$) and the maximum specific growth rate (µ, $h^{-1}$):

$ve^-_{max O_2} = \frac{\mu}{Ye^-_{O_2}}$. We are confident about the yields for the two C-substrates used, but the empirically determined μ for the butyrate treatments is suspiciously low (= 0.067 $h^{-1}$), providing $ve^-_{max O_2}$ = 2.45×10$^{-15}$ mol $e^-$ $cell^{-1}$ $h^{-1}$. Simulations with this value grossly underestimated the rate of $O_2$ depletion as compared to that measured, which forced us to estimate the parameter value by optimisation, providing $ve^-_{max O_2}$ = 4.42×10$^{-15}$ and 4.22×10$^{-15}$ mol $e^-$ $cell^{-1}$ $h^{-1}$ for the succinate- and butyrate treatments, respectively. These values give μ = 0.22 and 0.12 $h^{-1}$, respectively: for the succinate treatments, the value is in the same range as that empirically determined (= 0.2 $h^{-1}$); for the butyrate treatments, the value seems more realistic than 0.067 $h^{-1}$.

$\boldsymbol{ve^-_{min}}$ (Eqs. 2, 5, and 7) is the per cell velocity of $e^-$-flow to $O_2$ ($ve^-_{O_2}$) assumed to generate minimum ATP required for synthesising the initial molecules of denitrification enzymes. Since we lack any empirical or other estimations for this parameter, it is arbitrarily assumed to be the $ve^-_{O_2}$ when $[O_2]_{aq}$ reaches 1 nM. At this concentration, $ve^-_{min}$ is determined by the Michaelis-Menten equation $\left( ve^-_{min} = \frac{ve^-_{max O_2} \times [O_2]_{aq}}{(K_{mO_2} + [O_2]_{aq})} \right)$, using $ve^-_{max O_2}$ and $K_{mO_2}$ given above. The values obtained for the succinate- and butyrate-supplemented treatments = 1.96×10$^{-17}$ and 1.87×10$^{-17}$ mol $e^-$ $cell^{-1}$ $h^{-1}$, respectively, which for both the cases is 0.44% of $ve^-_{max O_2}$. To investigate the impact of $ve^-_{min}$ on the model behaviour ($r_{Na}$ and $r_{Ni}$, Eqs. 1–2, 4–5, and 6–7), sensitivity analyses were performed by simulating the model with $ve^-_{min}$ corresponding to $[O_2]_{aq}$ = 5×10$^{-9}$, 5×10$^{-10}$, and 0 mol $L^{-1}$ (see Results/Discussion).

# Results/Discussion

## Low probabilistic initiation of *nar* transcription, resulting in the fraction of the population with Nar < 100%

To test the assumption of a single homogeneous population with all cells producing Nar in response to $O_2$ depletion, we simulated the model with the specific probability for a $Z^-$ cell

to initiate *nar* transcription ($r_{Na}$) = 4 $h^{-1}$, resulting in 98% of the cells possessing Nar within an hour (see Eqs. 1–3). Evidence suggests that less than half an hour is required to synthesise denitrification enzymes (17, 18), but an hour's time is assumed here to allow margin for error. The results show that, for all the treatments, the simulated $NO_2^-$ production (mol $vial^{-1}$) grossly overestimates that measured (Fig. 3).

To find a reasonable parameter value, we optimised $r_{Na}$ for the 0% $O_2$ treatments, so that the simulated $NO_2^-$ production matches that measured. The results (Table 3) suggest that a low probabilistic initiation of *nar* transcription (average $r_{Na}$ = 0.035 $h^{-1}$) is adequate to simulate the measured $NO_2^-$ kinetics (Fig. 3). In the Butyrate, 7% $O_2$ treatment (Fig. 3B), the simulated $NO_2^-$ starts earlier, but the rate of accumulation is similar to that measured.

Once $O_2$ falls below a certain threshold, the production of Nar is assumed to trigger with $r_{Na}$ = 0.035 $h^{-1}$ and last until a minimum of respiration is sustained by the $e^-$-flow to $O_2$ and $N_2O$ ($ve^-_{O_2}$ and $ve^-_{N_2O}$), assumed to fulfil the ATP needs for Nar production (Eqs. 1–2). But the production of Nar sustained by $ve^-_{N_2O}$ was inconsequential for simulating the measured $NO_2^-$ production, since $NO_3^-$ was already exhausted when $N_2O$ started accumulating (i.e., when $ve^-_{N_2O} > 0$). For this reason, the fraction that produced Nar ($F_{Na}$, Eq. 3 and Table 4) is calculated as functional (= 0.23–0.43) and theoretical (= 0.56–0.81), where the first is the fraction actually responsible for $NO_2^-$ production (sustained by $ve^-_{O_2}$), but the latter also incorporates the fraction that produced Nar after the exhaustion of $NO_3^-$ (sustained by $ve^-_{O_2}$ as well as $ve^-_{N_2O}$). The rationale behind calculating the theoretical $F_{Na}$ is the empirical data indicating that Nar transcription is not turned off in response to $NO_3^-$ depletion (18). Although our model cannot test the theoretical $F_{Na}$, but the functional $F_{Na}$ suggests that, contrary to the common assumption, the measured $NO_2^-$ kinetics can be neatly explained by only 23–43.3% of the population producing Nar in response to $O_2$ depletion.

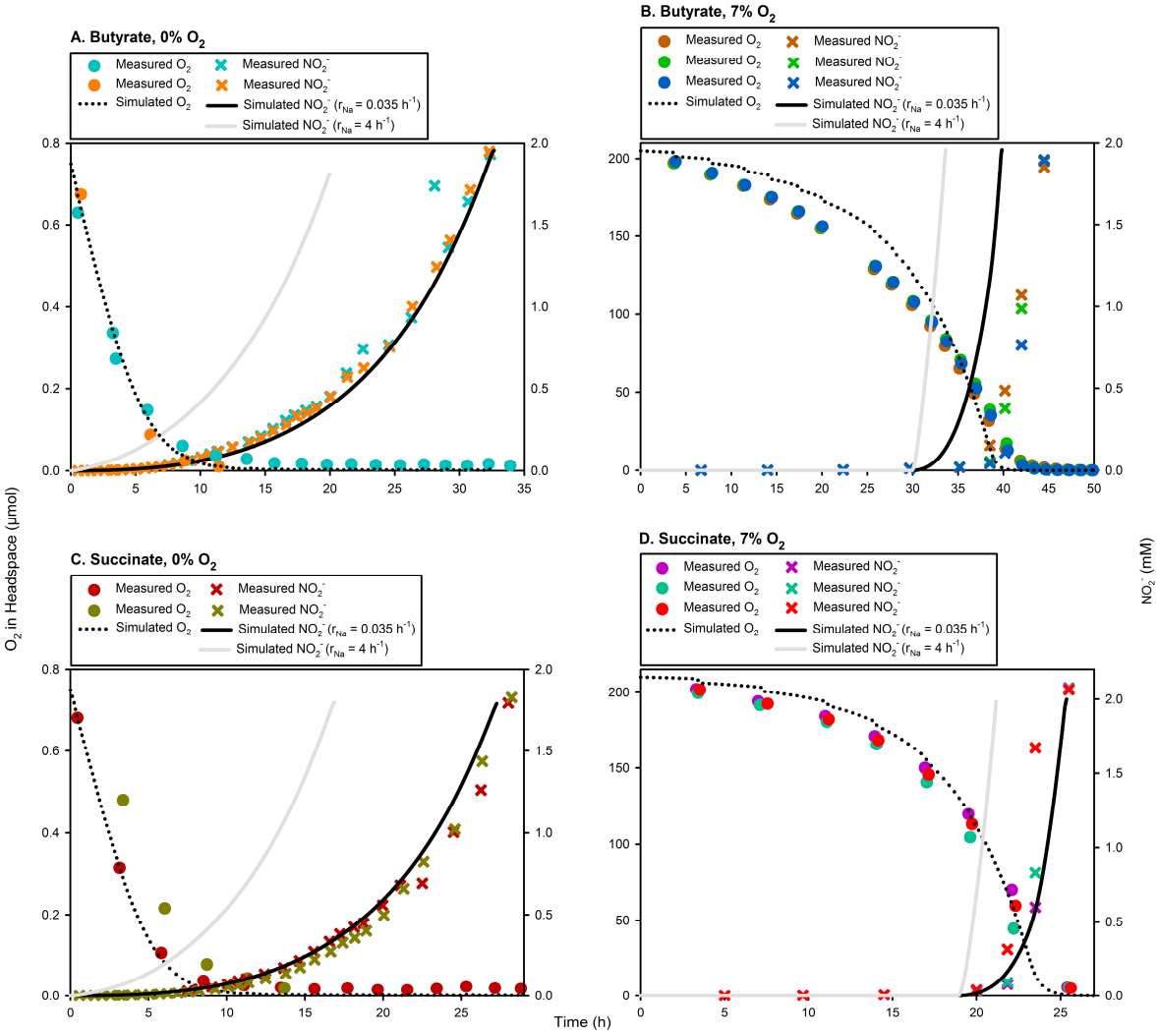


**Fig. 3. Comparison of measured and simulated $NO_2^-$ accumulation assuming definitive versus stochastic initiation of *nar* transcription.** To test the assumption of a single homogeneous population with almost all cells expressing *nar* in response to $O_2$ depletion, we forced our model to achieve 98% Nar-positive cells ($Z^{Na}$) within an hour by setting the specific-probability of initiating *nar* transcription ($r_{Na}$) = 4 $h^{-1}$. This resulted in grossly overestimated rates of $NO_2^-$ accumulation for all treatments (grey curves). In contrast, we simulated the model with $r_{Na}$ = 0.035 $h^{-1}$ obtained through optimisation, resulting in a reasonable agreement with measurements for all treatments, except for an apparent time frameshift for the Butyrate, 7% $O_2$ treatment.

**Table 3. Specific-probability of *nar* and *nirS* transcriptional initiation ($r_{Na}$ and $r_{Ni}$, respectively) estimated for each treatment by optimisation (best match between the simulated and measured data).**

| Batch | C-source | Treatment*: $O_2$ (vol.%), $NO_3^-$ (mM) | Optimal $r_{Na}$ ($h^{-1}$) | Optimal $r_{Ni}$ ($h^{-1}$) |
|---|---|---|---|---|
| **1** | Butyrate | ~0, 2 | 0.041 | 0.005 |
| **2** | Butyrate | 7, 2 | – | 0.004 |
| **3** | Succinate | ~0, 2 | 0.030 | 0.005 |
| **4** | Succinate | 7, 2 | – | 0.003 |
| | | | **Avg. = 0.035** | **Avg. = 0.004** |

* Treatment refers to the C-source, initial oxygen concentration in the headspace (measured as headspace-vol.%), and initial $NO_3^-$ concentration in the medium (mM).

**Table 4. The fraction of the population with Nar ($F_{Na}$) and NirS ($F_{Ni}$) estimated based on the optimal specific-probability of *nar* and *nirS* transcriptional initiation ($r_{Na}$ and $r_{Ni}$), respectively**.

| Batch | C-source | $O_2$ (vol.%), $NO_3^-$ (mM) | Functional $F_{Na}$* (unitless) | Theoretical $F_{Na}$* (unitless) | $F_{Ni}$ (unitless) |
|---|---|---|---|---|---|
| **1** | Butyrate | ~0, 2 | 0.433 | 0.813 | 0.221 |
| **2** | Butyrate | 7, 2 | 0.343 | 0.656 | 0.088 |
| **3** | Succinate | ~0, 2 | 0.357 | 0.803 | 0.206 |
| **4** | Succinate | 7, 2 | 0.230 | 0.564 | 0.077 |

* Functional $F_{Na}$ is the fraction of cells expressing Nar while $NO_3^-$ is still present, while Theoretical $F_{Na}$ is the fraction expressing Nar when including the theoretical recruitment after $NO_3^-$ depletion (supported by energy from $N_2O$ reduction).

## Very low probabilistic initiation of *nirS* transcription

When we optimised the specific probability of *nirS* transcriptional activation ($r_{Ni}$, see Eqs. 4–5 and 6–7) to fit the measured data, the average $r_{Ni}$ = 0.004 $h^{-1}$ (Table 3) adequately simulated the measured $NO_2^-$ depletion and $N_2$ accumulation (Fig. 4). The recruitment to denitrification lasted for 19.5–47.3 h, i.e., the time when [$O_2$] was below a critical concentration and the velocity of $e^-$-flow to $O_2$ and the relevant $NO_x^-/NO_x$ remained above a critical minimum (Eqs. 4–5 and 6–7). The resulting fraction recruited to denitrification ($F_{Ni}$, see Eq. 8 and Table 4) was 0.08–0.18, the bulk of which depended on the $e^-$-flow to $NO_3^-$ and $N_2O$ (instead of aerobic respiration).

To test whether the measured data could be explained without the recruitment sustained by $NO_3^-$ and $N_2O$ respiration, we also simulated the model with the recruitment as a function of $O_2$ alone and re-optimised $r_{Ni}$, which on average increased to 0.012 $h^{-1}$ (providing $F_{Ni}$ = 0.083–

0.35). This was expected since $O_2$ is exhausted rather quickly, shrinking the time-window available for the recruitment. However, the simulations without the recruitment sustained by $NO_3^-$ - and $N_2O$ respiration were less satisfactory: using the average $r_{Ni}$ = 0.012 $h^{-1}$ generally resulted in larger deviations than for the default simulations (S1 Fig.), and the optimal $r_{Ni}$ for individual treatments varied grossly (50% higher values for the ~0% $O_2$ treatments than for the 7% $O_2$ treatments). This contrasts the default simulations, where the optimal $r_{Ni}$ for individual treatment were quite similar.

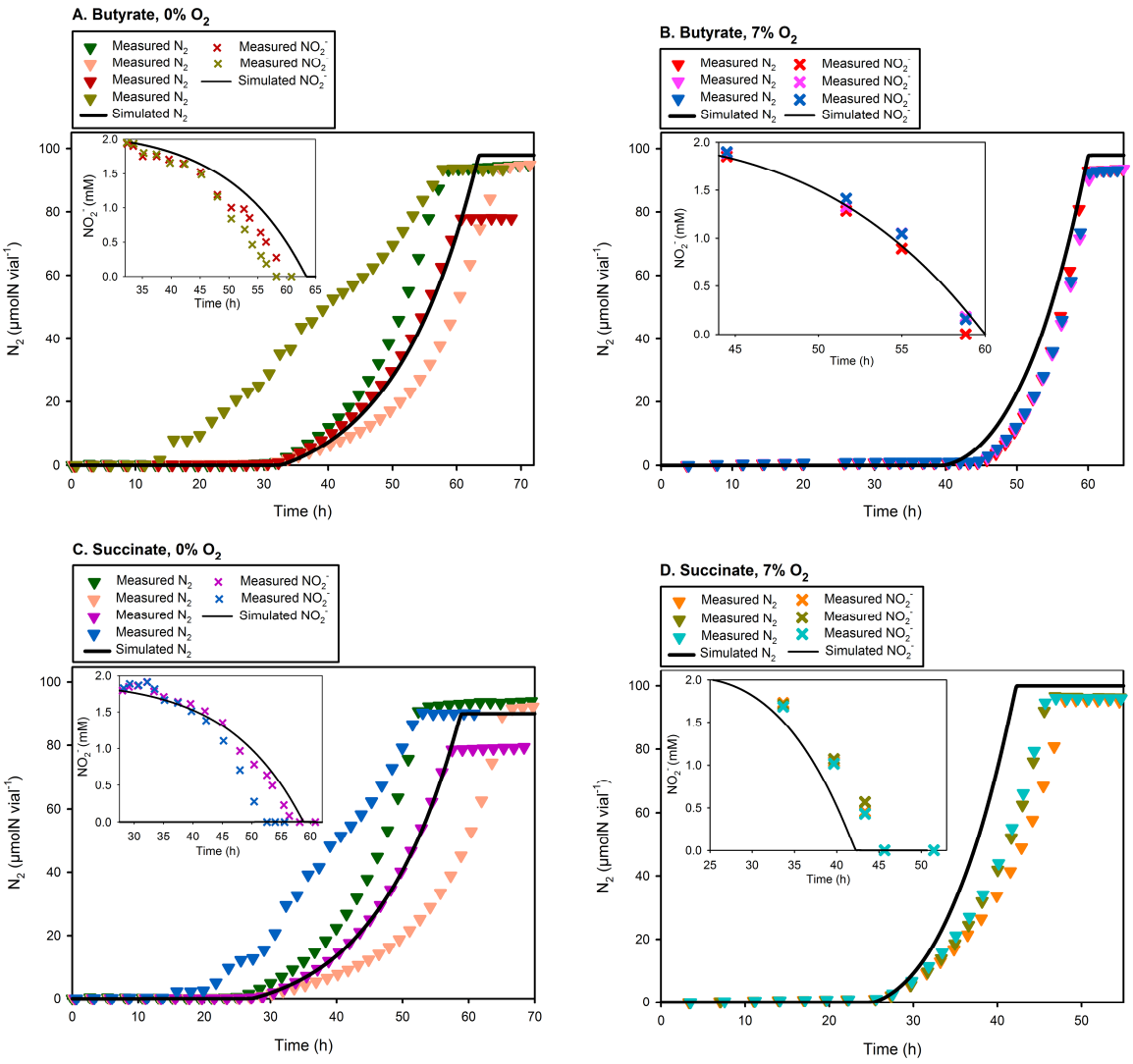


**Fig. 4. Comparison of measured and simulated data assuming stochastic initiation of *nirS* transcription.** Each panel compares $NO_2^-$ depletion (sub-panel) and $N_2$ accumulation (main panel) from three/four replicates of an experimental treatment with simulations. The simulations are carried out with an optimised specific-probability of *nirS* transcriptional

initiation (average $r_{Ni}$ = 0.004 $h^{-1}$, Eqs. 4–5 and 6–7), allowing 7.7–22.1% of the population to produce NirS + *c*Nor (Eq. 8) during the available time-window (= 19.5–47.3 h).

## Sensitivity of $r_{Na}$ and $r_{Ni}$ to $ve^-_{min}$

Recruitment to denitrification (both *nar* and *nirS* transcription) is assumed to continue only as long as the combined $e^-$-flow to $O_2$, $NO_3^-$ and $N_2O$ is greater than $ve^-_{min}$ (Eqs. 1–2, 4–5, and 6–7). To test the model's sensitivity to this parameter, we estimated $r_{Na}$ and $r_{Ni}$ by optimisation for different values of $ve^-_{min}$, relative to the default value = $1.95\times10^{-17}$ mol $e^-$ $cell^{-1}$ $h^{-1}$. For all cases, the model was able to adequately simulate the measured $N_2$ kinetics by moderate adjustments of $r_{Na}$ and $r_{Ni}$. Table 5 shows the average optimal values of $r_{Na}$ and $r_{Ni}$, obtained by fitting simulated $N_2$ kinetics to the data, for different values of $ve^-_{min}$. S2 Fig. shows adequate simulations of measured $N_2$ kinetics assuming $ve^-_{min}$ = 0, with optimised $r_{Na}$ = 0.033 $h^{-1}$ and $r_{Ni}$ = 0.0033 $h^{-1}$. Thus, although assuming $ve^-_{min}$ > 0 appears logical, it is not necessary to explain the measured data.

**Table 5. Estimated $r_{Na}$ and $r_{Ni}$, depending on $ve^-_{min}$.**

| $ve^-_{min}$ (mol $e^-$ cell $h^{-1}$) | Optimal $r_{Na}$ ($h^{-1}$) | Optimal $r_{Ni}$ ($h^{-1}$) |
|---|---|---|
| **5 × Default*** | 0.041 | 0.0062 |
| **Default** | 0.035 | 0.0041 |
| **0.5 × Default** | 0.034 | 0.0035 |
| **0** | 0.033 | 0.0033 |

* Refers to the default value = $1.95\times10^{-17}$ mol $e^-$ $cell^{-1}$ $h^{-1}$.

## $N_2O$ kinetics

To simulate $N_2O$ kinetics, we first used $ve^-_{max N_2O}$ (=$5.5\times10^{-15}$ mol $e^-$ $cell^{-1}$ $h^{-1}$), empirically determined under similar experimental conditions as simulated here (24), and adopted the literature values for $K_{mN_2O}$ (= 5 and 7 µM 41, 42, respectively). But with $K_{mN_2O}$ = 5 µM, the model predicted $N_2O$ accumulation ~10–20 times higher than measured for the ~0% and ~2–3 times higher for the 7% $O_2$ treatments (Fig. 5). This forced us to simulate the model with the parameter value estimated by optimisation, providing the average $K_{mN_2O}$ = 0.6 µM.

The measured $N_2O$ shows a conspicuous increase throughout the entire active denitrification period, and this phenomenon is neatly captured by the model. The reason for this model prediction is that the number of $N_2O$ producing cells ($Z^{NaNi} + Z^{Ni}$, Fig. 2A) is low to begin with compared to the number of $N_2O$ consuming cells ($Z^- + Z^{Na} + Z^{NaNi} + Z^{Ni}$), but the fraction of $N_2O$ producers will increase during the anoxic phase for two reasons: one is the recruitment to $Z^{NaNi}$ & $Z^{Ni}$, another is the fact that the model predicts approximately three times faster cell-specific growth rate for $Z^{NaNi}$ & $Z^{Ni}$ than for $Z^-$ & $Z^{Na}$ ($ve^-_{N_2O}$ is identical for all groups, while $ve^-_{NO_2^-}$ and $ve^-_{NO}$ are both zero for $Z^-$ but for $Z^{NaNi}$ & $Z^{Ni}$, it holds that $ve^-_{NO_2^-} \approx ve^-_{NO} > ve^-_{N_2O}$. To illustrate this phenomenon, we ran the model, assuming that the $Z^-$ & $Z^{Na}$ cells had no $N_2O$ reductase, resulting in *a)* constant $N_2O$ concentration throughout the entire anoxic phase and *b)* much higher $N_2O$ concentrations than measured (Fig 5). The overestimation is a trivial result, easily avoidable by increasing $ve^-_{max N_2O}$ or decreasing $K_{mN_2O}$ moderately. However, the prediction of a constant $N_2O$ concentration is clearly in conflict with the experimental data, and no parameterisation could force the model to reproduce this phenomenon, other than the differential expression of denitrification genes.

Hence, although there is room for further refinements, our default assumption regarding differential expression of NirS and NosZ explains the observed $N_2O$ kinetics: 1) abrupt initial accumulation to very low levels due to recruitment of relatively small numbers to the $N_2O$ producing pools ($Z^{NaNi}$ & $Z^{Ni}$), 2) increasing $N_2O$ concentration due to recruitment and faster cell-specific growth of $Z^{NaNi}$ & $Z^{Ni}$ than that of the cells only consuming $N_2O$ ($Z^- + Z^{Na}$).

This modelling exercise sheds some light on the possible role of regulatory biology of denitrification in controlling $N_2O$ emissions from soils. If all cells in soils had the same regulatory phenotype as *Pa. denitrificans*, their emission of $N_2O$ would probably be miniscule, and soils could easily become strong net sinks for $N_2O$ because the majority of cells would be 'truncated denitrifiers' with only $N_2O$ reductase expressed. It remains to be tested, however, if the regulatory phenotype of *Pa. denitrificans* is a rare or a common phenomenon among full-fledged denitrifiers. We foresee that further exploration of denitrification phenotypes will unravel a plethora of response patterns.

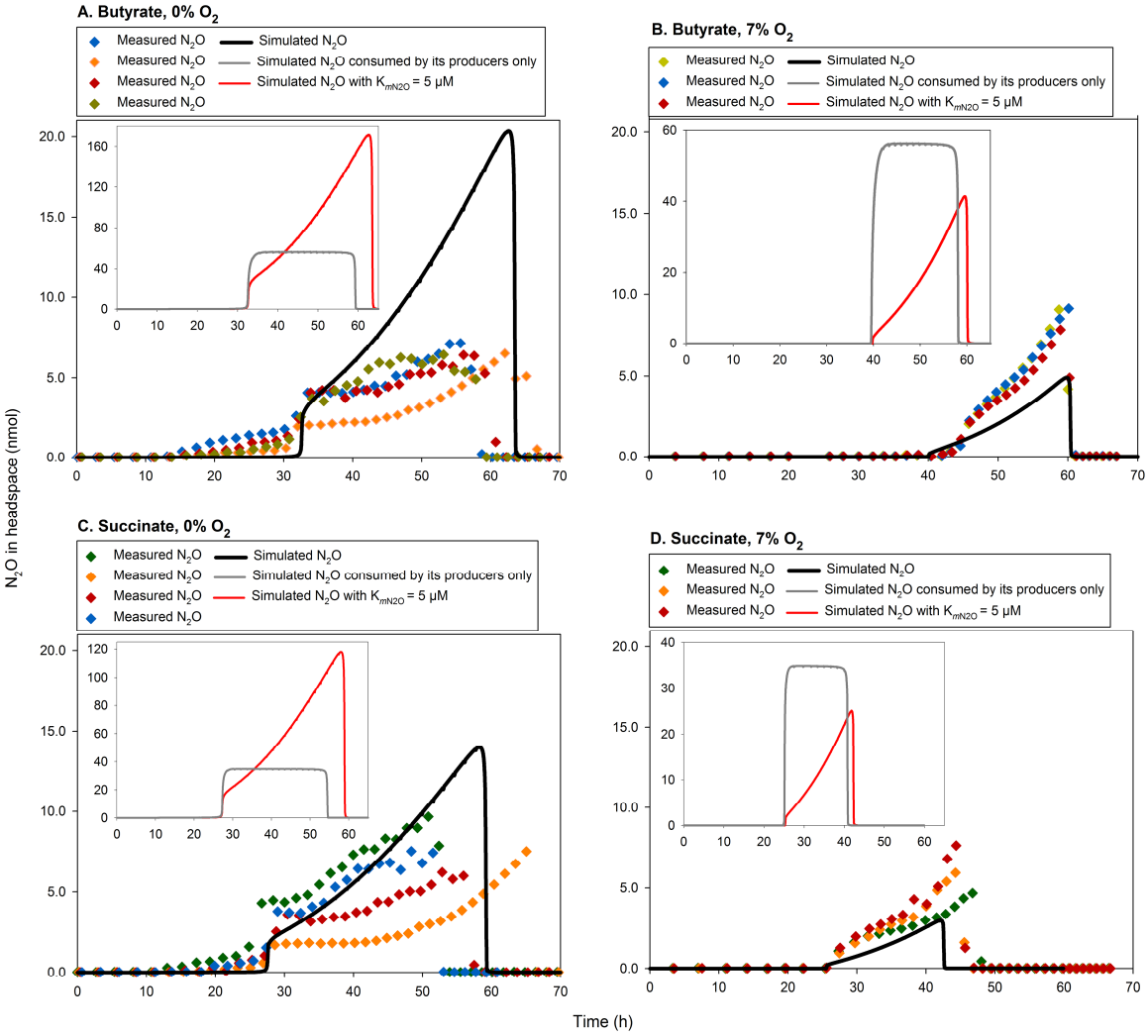


**Fig. 5. Comparison of the measured $N_2O$ with that simulated.** Each main panel (A–D) compares the measured $N_2O$ (single vial results) with the default simulation using the parameter values given in Table 2, i.e. $K_{mN_2O}$ = 0.6 µM (estimated through optimisation) and $ve^-_{maxN_2O}$ = 5.5×10$^{-15}$ mol e$^-$ cell$^{-1}$ h$^{-1}$ (24). In contrast, each inserted panel shows the simulated $N_2O$ assuming 1) $N_2O$ consumption only by the cells producing $N_2O$ ($Z^{NaNi}$ + $Z^{Ni}$), and 2) the literature value for $K_{mN_2O}$ = 5 µM (41). The results show that the measured $N_2O$ kinetics are best explained by assuming its production by a small fraction ($Z^{NaNi}$ + $Z^{Ni}$) and consumption by the entire population ($Z^-$ + $Z^{Na}$+ $Z^{NaNi}$ + $Z^{Ni}$).

## Conclusion

Using dynamic modelling, we have demonstrated here that the denitrification kinetics in *Pa. denitrificans* can be adequately explained by assuming low probabilistic transcriptional activation of the *nar* and *nirS* genes and a subsequent autocatalytic expression of the enzymes. Such autocatalytic gene expressions are common in prokaryotes, rendering a population heterogeneous because of the stochastic initiation of gene transcription, with a low probability (44). For $N_2O$ kinetics, our hypothesis was that *a)* the gas is produced by a fraction of the incubated population that is able to initiate *nirS* transcription with a certain probability, leading to a coordinated expression of *nirS* + *nor* via NO (16), and *b)* $N_2O$ is consumed by the entire population because, in response to anoxia, *nosZ* is readily induced by FnrP (24). Our model corroborated this hypothesis by reasonably simulating the $N_2O$ kinetics with the specific-probability of *nirS* transcriptional activation = 0.004 $h^{-1}$, resulting in 7.7–22.1% of the population producing NirS + *c*Nor (hence $N_2O$), but all cells producing NosZ (hence equally consuming $N_2O$).

## References

1. Ravishankara AR, Daniel JS, Portmann RW. Nitrous oxide ($N_2O$): the dominant ozone-depleting substance emitted in the 21st century Science. 2009;326(5949 ):123-5
2. Bryson Bates, Zbigniew W. Kundzewicz, Shaohong Wu, Nigel Arnell, Virginia Burkett, Petra Döll, et al. Technical paper on climate change and water. Budapest: Intergovernmental Panel on Climate Change 2008 Contract No.: IPCC-XXVIII/Doc.13 (8.IV.2008).
3. Lassey K, Harvey M. Nitrous oxide: the serious side of laughing gas. Water & Atmos. 2007;15(2):10-1.
4. Butterbach-Bahl K, Baggs EM, Dannenmann M, Kiese R, Zechmeister-Boltenstern S. Nitrous oxide emissions from soils: how well do we understand the processes and their controls? Philos Trans R Soc Lond B Biol Sci. 2013;368:20130122.
5. Signor D, Cerri CEP. Nitrous oxide emissions in agricultural soils: a review. Pesq Agropec Trop. 2013;43(3):322-38.
6. Bakken LR, Bergaust L, Liu B, Frostegård Å. Regulation of denitrification at the cellular level – a clue to understanding of $N_2O$ emissions from soils. Philos Trans R Soc Lond B Biol Sci. 2012;367:1226-34.
7. Bakken LR, Dörsch P. Nitrous oxide emission and global changes: modelling approaches. In: Bothe H, Ferguson SJ, Newton WE, editors. Biology of the Nitrogen Cycle. Amsterdam: Elsevier B. V.; 2007. p. 382-95.
8. Bergaust L, Bakken LR, Frostegård Å. Denitrification regulatory phenotype, a new term for the characterization of denitrifying bacteria. Biochem Soc Trans. 2011;39:207-12.
9. Zheng J, Doskey PV. Modeling nitrous oxide production and reduction in soil through explicit representation of denitrification enzyme kinetics. Environ Sci Technol. 2015;49(4):2132-9.

10. Betlach MR, Tiedje JM. Kinetic explanation for accumulation of nitrite, nitric oxide, and nitrous oxide during bacterial denitrification. Appl Environ Microbiol. 1981;42(6):1074-84.
11. Vasiliadou IA, Siozios S, Papadas IT, Bourtzis K, Pavlou S, Vayenas DV. Kinetics of pure cultures of hydrogen-oxidizing denitrifying bacteria and modeling of the interactions among them in mixed cultures. Biotechnol Bioeng. 2006;95(3):513–25.
12. Almeida JS, Reis MAM, Carrondo MJT. Competition between nitrate and nitrite reduction in denitrification by *Pseudomonas fluorescens*. Biotechnol Bioeng. 1995;46(5):476-84.
13. Thomsen JK, Geest T, Cox RP. Mass spectrometric studies of the effect of pH on the accumulation of intermediates in denitrification by *Paracoccus denitrificans*. Appl Environ Microbiol. 1994;60(2):536-41.
14. Kampschreur MJ, Kleerebezem R, Picioreanu C, Bakken L, Bergaust L, de Vries S, et al. Metabolic modeling of denitrification in *Agrobacterium tumefaciens*: a tool to study inhibiting and activating compounds for the denitrification pathway. Front Microbiol. 2012;3.
15. Woolfenden HC, Gates AJ, Bocking C, Blyth MG, Richardson DJ, Moulton V. Modeling the effect of copper availability on bacterial denitrification. Microbiologyopen. 2013;2(5): 756-65.
16. Hassan J, Bergaust LL, Wheat ID, Bakken LR. Low probability of initiating *nirS* transcription explains observed gas kinetics and growth of bacteria switching from aerobic respiration to denitrification. PLoS Comput Biol. 2014;10(11):e1003933.
17. Bergaust L, Mao Y, Bakken LR, Frostegård Å. Denitrification response patterns during the transition to anoxic respiration and posttranscriptional effects of suboptimal pH on nitrogen oxide reductase in *Paracoccus denitrificans*. Appl Environ Microbiol. 2010;76(19):6387-96.
18. Qu Z, Bergaust LL, Bakken LR. Respiratory regulation in *Paracoccus denitrificans* and in soil, implications for $N_2O$ emissions Ås: Norwegian University of Life Sciences; 2014.
19. Bouchal P, Struhárová I, Budinská E, Šedo O, Vyhlídalová T, Zdráhal Z, et al. Unraveling an FNR based regulatory circuit in *Paracoccus denitrificans* using a proteomics-based approach. Biochim Biophys Acta. 2010;1804(6):1350-8.
20. van Spanning RJM, Richardson DJ, Ferguson SJ. Introduction to the biochemistry and molecular biology of denitrification. In: Bothe H, Ferguson SJ, Newton WE, editors. Biology of the Nitrogen Cycle. Amsterdam: Elsevier B. V.; 2007. p. 3-20.
21. Wood NJ, Alizadeh T, Bennett S, Pearce J, Ferguson SJ, Richardson DJ, et al. Maximal expression of membrane-bound nitrate reductase in *Paracoccus* is induced by nitrate via a third FNR-like regulator named NarR. J Bacteriol. 2001;183(12):3606-13.
22. Spiro S. Regulators of bacterial responses to nitric oxide. FEMS Microbiol Rev. 2007;31:193-211.
23. Spiro S. Nitrous oxide production and consumption: regulation of gene expression by gas-sensitive transcription factors. Philos Trans R Soc Lond B Biol Sci. 2012;367:1213-25.
24. Bergaust L, van Spanning RJM, Frostegård Å, Bakken LR. Expression of nitrous oxide reductase in *Paracoccus denitrificans* is regulated by oxygen and nitric oxide through FnrP and NNR. Microbiology 2012;158:826-34.
25. Richardson D, Felgate H, Watmough N, Thomson A, Baggs E. Mitigating release of the potent greenhouse gas $N_2O$ from the nitrogen cycle – could enzymic regulation hold the key? Trends Biotechnol. 2009;27(7):388-97.
26. Bergaust L. Regulatory biology of denitrification in *Agrobacterium tumefaciens* and *Paracoccus denitrificans*; responses to environmental controllers. Ås: Norwegian University of Life Sciences; 2009.
27. Nadeem S, Dörsch P, Bakken LR. The significance of early accumulation of nanomolar concentrations of NO as an inducer of denitrification. FEMS Microbiol Ecol. 2013;83(3):672-84.
28. Sistrom WR. A requirement for sodium in the growth of *Rhodopseudomonas spheroides*. J Gen Microbiol. 1960; 22(3):778-85.
29. Molstad L, Dörsch P, Bakken LR. Robotized incubation system for monitoring gases ($O_2$, NO, $N_2O$, $N_2$) in denitrifying cultures. J Microbiol Methods. 2007;71:202-11.
30. Hannon B, Ruth M. Modeling Dynamic Biological Systems 2nd ed. Ruth M, Hannon B, editors. New York: Springer 2014.

31. Girsch P, de Vries S. Purification and initial kinetic and spectroscopic characterization of NO reductase from *Paracoccus denitrificans*. Biochim Biophys Acta. 1997;1318:202-16.
32. Hassan J. Exploring the regulation of denitrification and NO and $N_2O$ kinetics in *Paracoccus denitrificans* using simulation modelling. Ås: Norwegian University of Life Sciences; 2015.
33. Parsonage D, Greenfield AJ, Ferguson SJ. The high affinity of *Paracoccus denitrificans* cells for nitrate as an electron acceptor. Analysis of possible mechanisms of nitrate and nitrite movement across the plasma membrane and the basis for inhibition by added nitrite of oxidase activity in permeabilised cells. Biochim Biophys Acta. 1985;807(1):81-95.
34. Davies KJP, Lloyd D, Boddy L. The effect of oxygen on denitrification in *Paracoccus denitrificans* and *Pseudomonas aeruginosa*. J Gen Microbiol. 1989;135:2445-245 1.
35. Gates AJ, Luque-Almagro VM, Goddard AD, Ferguson SJ, Roldán MD, Richardson DJ. A composite biochemical system for bacterial nitrate and nitrite assimilation as exemplified by *Paracoccus denitrificans*. Biochem J. 2011;435(3):743-53.
36. Pan Y, Ni B-J, Yuan Z. Modeling electron competition among nitrogen oxides reduction and $N_2O$ accumulation in denitrification. Environ Sci Technol Lett. 2013;47:11083-91.
37. Wilhelm E, Battino R, Wilcock RJ. Low-pressure solubility of gases in liquid water. Chem Rev. 1977;77:219-62.
38. de Gier J-WL, Lübben M, Reijnders WNM, Tipker CA, Slotboom D-J, van Spanning RJM, et al. The terminal oxidases of *Paracoccus denitrificans*. Mol Microbiol. 1994;13(2):183-96.
39. Fukumori Y, Yamanaka T. Two $K_m$ values for cytochrome *c* of $aa_3$-type two-subunit cytochrome *c* oxidase from *Nitrobacter agilis*. FEBS Lett. 1984;170(2):301-4.
40. Pitcher RS, Watmough NJ. The bacterial cytochrome $cbb_3$ oxidases. Biochim Biophys Acta. 2004;1655:388-99.
41. Kristjansson JK, Hollocher TC. First practical assay for soluble nitrous oxide reductase of denitrifying bacteria and a partial kinetic characterization. J Biol Chem. 1980;255:704-7.
42. Snyder SW, Hollocher TC. Purification and some characteristics of nitrous oxide reductase from *Paracoccus denitrificans*. J Biol Chem. 1987;262:6515-25.
43. Holtan-Hartwig L, Dörsch P, Bakken LR. Comparison of denitrifying communities in organic soils: kinetics of $NO_3^-$ and $N_2O$ reduction. Soil Biol Biochem. 2000;32:833-43.
44. Raj A, van Oudenaarden A. Nature, nurture, or chance: stochastic gene expression and its consequences. Cell. 2008;135(2):216-26.

# Supporting Information

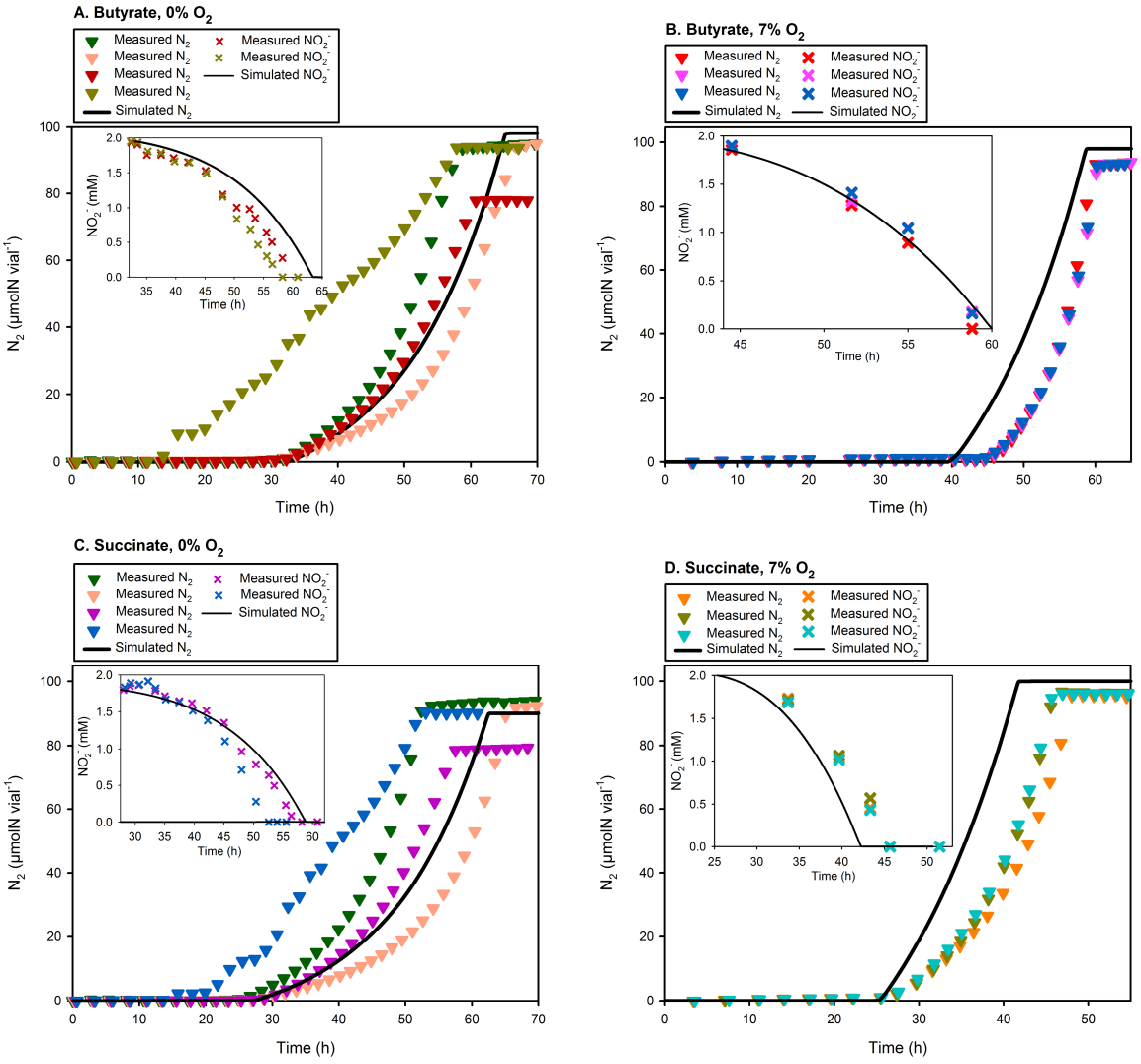


**S1 Fig. Comparison of measured and simulated data assuming stochastic initiation of *nirS* transcription with aerobic respiration being the only energy source for producing NirS + *c*Nor.** In each panel, $NO_2^-$ depletion (sub-panel) and $N_2$ accumulation (main panel) from three/four replicates of an experimental treatment are compared with simulations. The simulations here are to be compared with the default simulations (Fig. 4), run assuming that the coordinated NirS + *c*Nor production (via *nirS* transcriptional activation) is sustained by the energy generated by $O_2$ as well as $NO_3^-$ and/or $N_2O$ reduction. The default simulations provided an average specific-probability of *nirS* transcriptional activation ($r_{Ni}$) = 0.004 $h^{-1}$ (Eqs. 4–5 and 6–7) by optimisation, allowing 7.7–22.1% of the population to produce NirS +

*c*Nor (Eq. 8) in 19.5–47.3 h. To match the measured data here, the average $r_{Ni}$ had to be raised to 0.012 $h^{-1}$, since the time available for the enzyme synthesis shrank (= 3.5–16 h) due to a rapid exhaustion of $O_2$. Comparatively, the assumption that the ATP from $NO_3^-$ and/or $N_2O$ reduction should help cells produce denitrification enzymes seems logically more convincing and better explains the measured data.

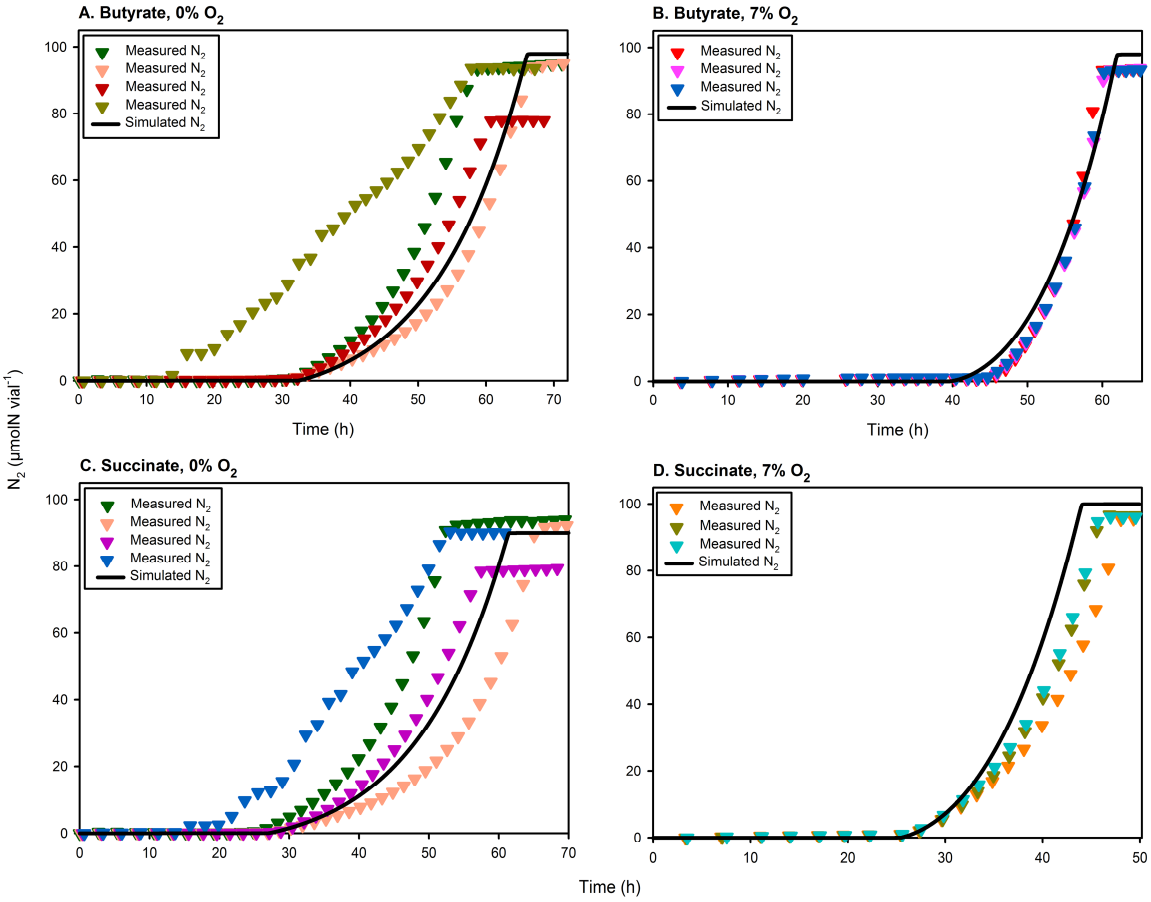


**S2 Fig. Measured vs. simulated $N_2$ kinetics assuming $ve^-_{min}$ = 0.** The default simulations are carried out assuming that for a cell to produce first molecules of Nar and NirS, a minimum of $e^-$-flow to an available $e^-$-acceptor ($ve^-_{min}$, mol $e^-$ $cell^{-1}$ $h^{-1}$) is necessary to generate a minimum of ATP required for protein synthesis (Eqs. 1–2, 4–5, and 6–7). Although assuming $ve^-_{min}$ seems logical, but measured $N_2$ kinetics adequately simulated here with $ve^-_{min}$ = 0 shows that the assumption is not necessary to explain the measured data.